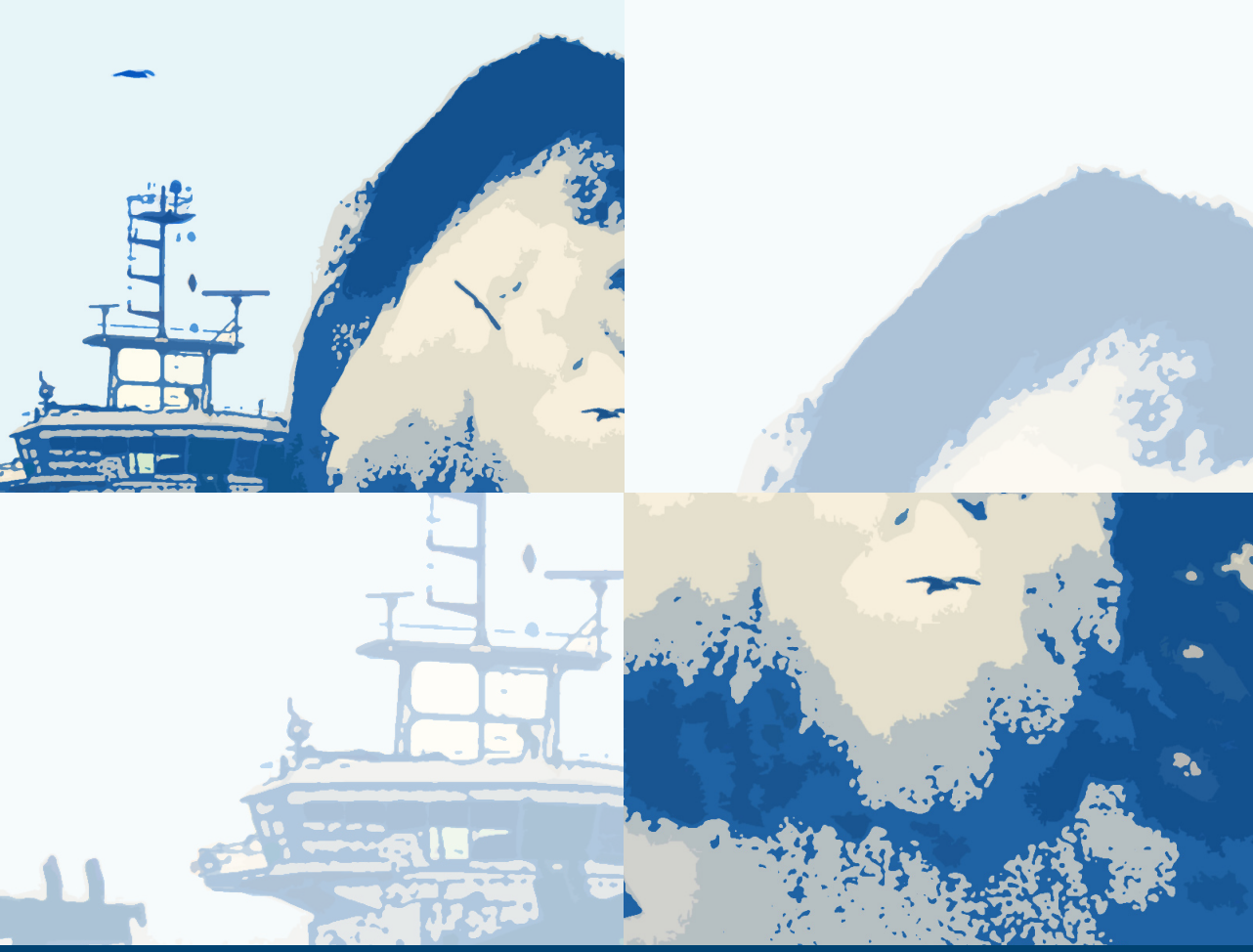

Model-Based Control of Hopper Dredgers

Jelmer Braaksma

Model-Based Control of Hopper Dredgers

Jelmer Braaksma

Cover design: Grietje Huitema

Model-Based Control of Hopper Dredgers

Proefschrift

ter verkrijging van de graad van doctor
aan de Technische Universiteit Delft,
op gezag van de Rector Magnificus prof.dr.ir. J.T. Fokkema,
voorzitter van het College voor Promoties,
in het openbaar te verdedigen op maandag 4 februari 2008 om 10.00 uur
door

Jelmer BRAAKSMA,

elektrotechnisch ingenieur,
geboren te Harlingen.

Dit proefschrift is goedgekeurd door de promotor:
Prof.dr. R. Babuška, M.Sc.

Toegevoegd promotor:
Dr.ir. J.B. Klaassens

Samenstelling promotiecommissie:

Rector Magnificus	voorzitter
Prof.dr. R. Babuška, M.Sc.	Technische Universiteit Delft, promotor
Dr.ir. J.B. Klaassens	Technische Universiteit Delft, toegevoegd promotor
Prof.dr.ir. C. van Rhee	Technische Universiteit Delft
Prof.dr.ir. J. van Amerongen	Universiteit Twente
Prof.dr.ir. R. De Keyser	Universiteit Gent
Prof.ir. W.J. Vlasblom	Technische Universiteit Delft
Ir. C. de Keizer	IHC Systems B.V., Sliedrecht
Prof.dr.ir. B. De Schutter	Technische Universiteit Delft, reservelid

Ir. C. de Keizer heeft als begeleider in belangrijke mate aan de totstandkoming van het proefschrift bijgedragen.

Published and distributed by: J. Braaksma
E-mail: j.braaksma@ihcmerwede.com

ISBN 978-90-9022693-4

Keywords: model predictive control, trailing suction hopper dredger, optimisation.

Printed in the Netherlands

Acknowledgments

I look back on my Ph.D. period with great pleasure. It was great to do the research at the Delft Center for Systems and Control (DCSC). I did not only appreciate the research itself, but also being surrounded by wonderful colleagues. I enjoyed the lunches where we could have interesting discussions and the Friday afternoon drinks. Therefore a word of thanks to all of you who contributed to this experience.

Besides this general word of gratitude, a number of people deserve to be thanked. First of all, I thank my promotor Robert Babuška and my supervisors Ben Klaassens and Cees de Keizer for their excellent supervision. Combined they have all the properties I needed to make this Ph.D. research successful. I have not only appreciated your high quality feedback, but also your mental support and non-technical discussions. Robert, your enthusiasm and commitment kept me on track. Your knowledge and creative ideas inspired me in the research. Ben, I will miss our discussions, but also the less serious conversations. Thank you for being my mental coach! Cees, your solid background in control for the dredging process has helped me to get grip on the problem. Thank you for your continual confidence in me.

I thank IHC Systems B.V. and SenterNovem who provided the financial support for giving me this opportunity and future opportunities. I thank Jacco Osnabrugge for his feedback on my research and introducing me into the world of hopper dredgers with a trip to Marseille.

I have greatly appreciated and benefited from the cooperation and feedback received from DEME and MTI. Not only did they supplied the data, I also received useful feedback from the 'field' in the form of discussions and information. In particular from MTI, I want to thank Kees van den Berg for proofreading my thesis, furthermore, I thank Mario Alvarez Grima, Ton de Gruijter and Sergio Ooijens for their efforts.

I am grateful and have really enjoyed working with my collegues at DCSC, of whom I in particular thank Domenico Belomo, Monique van den Berg, Sjoerd Dietz, Rogier Ellenbroek, Redouane Hallouzi, Diederick Joosten, Rudy Negenborn, Marcel Oosterom, Justin Rice and Kim van Schagen for sharing enjoyable times. Also I thank my student Dongzi Wangli for his contribution to my work. Marc van Agthoven, thank you for your feedback on my thesis.

I acknowledge the efforts of the members of my Ph.D. committee and their constructive remarks on my research. I thank Abe Bonnema and Rogier Ellenbroek for their willingness of being my paranymphs. Also, I am grateful for the love and support of my family. Finally, Grietje thank you so much for your love, support and patience throughout these years.

Delft, February 2008
Jelmer Braaksma

Contents

Summary xi

Samenvatting xv

1 Introduction 1
- 1.1 System Description . . . 2
- 1.2 Control of the Hopper Dredger . . . 5
- 1.3 Scope and Approach of the Thesis . . . 6
- 1.4 Research Goals . . . 6
- 1.5 Outline of the Thesis . . . 7

2 Trailing Suction Hopper Dredger 9
- 2.1 Introduction . . . 9
- 2.2 Ship Type . . . 11
- 2.3 Hopper . . . 13
  - 2.3.1 Inlet System . . . 13
  - 2.3.2 Overflow Weirs . . . 14
  - 2.3.3 Sensors and Automation . . . 14
  - 2.3.4 Hopper Test Rig . . . 16
- 2.4 Excavation System . . . 18
  - 2.4.1 Drag Head . . . 18
  - 2.4.2 Swell Compensator . . . 19
  - 2.4.3 Pump and Pipe . . . 20
  - 2.4.4 Sensors and Automation . . . 21
- 2.5 Power Train . . . 23
- 2.6 Propulsion System . . . 24
- 2.7 Economical Loading: Tangent Method . . . 24
- 2.8 Data . . . 26

3 Modelling the Trailing Suction Hopper Dredger Dynamics 27
- 3.1 An Overview of the Overall Model . . . 28
- 3.2 Hopper Model . . . 30
  - 3.2.1 Mass-Balance Equations . . . 31
  - 3.2.2 Overflow Rate . . . 33
  - 3.2.3 Overflow Density . . . 34
  - 3.2.4 Soil-Type-Dependent Parameters . . . 39

3.3 Drag-Head Model . . . 39
3.3.1 Drag-Head Production Model . . . 41
3.3.2 Drag-Head Cutting Force Model . . . 42
3.4 Pump-Pipeline Model . . . 45
3.4.1 Pump Model . . . 47
3.4.2 Pipeline Model . . . 48
3.4.3 Static Head Loss . . . 50
3.4.4 Pressure Loss of the Drag Head . . . 51
3.4.5 Soil-Dependent Parameters . . . 51
3.5 Power Train Model . . . 51
3.6 Ship Motion Model . . . 54
3.6.1 Forward Motion Model . . . 54
3.6.2 Draught Model . . . 55
3.7 Concluding Remarks . . . 56

4 Parameter Estimation and Model Calibration 57
4.1 Parameter Estimation . . . 58
4.1.1 Off-line Estimation . . . 58
4.1.2 On-line Estimation . . . 61
4.1.3 Performance Measures . . . 63
4.2 Data for Calibration . . . 63
4.3 Hopper Model . . . 65
4.3.1 Results for Data Set A . . . 70
4.3.2 Results for Data Set B . . . 72
4.4 Drag-Head Model . . . 77
4.5 Pump-Pipeline Model . . . 80
4.5.1 Off-line Estimation . . . 83
4.5.2 On-line Estimation . . . 83
4.5.3 Off-line Parameter Estimation . . . 85
4.5.4 Adaptive Parameter Estimation of Pump Process . . . 86
4.6 Power Train Model . . . 89
4.7 Ship Model Including Trail Force Model . . . 91
4.8 Concluding Remarks . . . 94

5 Optimal Control for Hopper Loading 97
5.1 Conventional Control of the Trailing Suction Hopper Dredger . . . 97
5.2 Optimisation Problem . . . 98
5.2.1 Model Construction . . . 99
5.2.2 Optimisation Setup . . . 103
5.3 Benchmark . . . 104
5.3.1 Hopper Process . . . 104
5.3.2 Overall Process . . . 105
5.4 Dynamic Optimisation . . . 105
5.4.1 Dynopt . . . 106
5.4.2 Model Predictive Control . . . 108
5.5 Optimisation of the Hopper Process . . . 111
5.5.1 Dynamic Optimisation with Time Discretisation . . . 112

5.5.2 Model Predictive Control . . . 118
5.6 Optimisation of the Overall Process with MPC . . . 126
5.6.1 Comparison of MPC with Data . . . 127
5.6.2 MPC for Two Soil Types . . . 129
5.7 Concluding Remarks . . . 135

6 Simulation Scenarios **137**
6.1 Power Limitation . . . 137
6.1.1 Ship Configuration . . . 137
6.1.2 Parameters and Soil Type . . . 138
6.1.3 Comparison . . . 139
6.1.4 Simulation Results . . . 140
6.2 Parameter Uncertainty . . . 145
6.2.1 Parameter Mismatch . . . 145
6.2.2 On-line Parameter Estimation and Adaptation . . . 148
6.2.3 Soil Type Estimator . . . 152
6.3 Concluding Remarks . . . 154

7 Conclusions **155**
7.1 Thesis Contributions . . . 156
7.2 Conclusions . . . 157
7.2.1 Model and Parameter Estimation . . . 157
7.2.2 Controller and Performance . . . 158
7.3 Recommendations . . . 160

A Pump-Pipeline Model **163**

B Calibrated Parameters **167**

C Automatic Black-Box Modelling for the Drag Head Process **169**

D Soil-Type-Dependent Parameters **171**

Glossary **177**

Summary

The trailing suction hopper dredger (TSHD) is a ship that excavates sand and sediment from the bottom while sailing. It trails a drag head over the bottom that breaks the coherence of the sand with water jets and teeth. A centrifugal pump aspirates a mixture of sand and water and transports this to a hold, the so-called hopper. The hopper is equipped with an overflow weir that discharges excess water and low-density mixture back to the sea. Because of this the dredger can continue dredging while coarse sand settles at the bottom of the hopper and water with fine sand flows overboard. As soon as the hopper is filled with sufficient sand, the pipe and drag head are pulled in and the ship sails to the discharge location. At this location the material is discharged by opening the bottom doors or by pumping the material out through the pipeline. After discharging, the ship sails to the dredging area and the process starts over again.

The modern TSHDs are advanced ships that are equipped with many automation systems that can be controlled with integrated computer systems from the bridge. From the operators it is expected that they generate the right set-points for all these systems. The latest ships are designed such that one operator is responsible for controlling the complete ship. This can only be achieved with a high degree of automation. The determination of the set points is not unambiguous, since vital information, which is necessary to make a correct decision, is not always at hand.

The subject of this thesis is a control strategy that strives to optimise the dredging process operation. This control system must take into account all the subjects that influence the performance of the TSHD. Whereas the consequences of the control actions are only observable in the performance at the end of the cycle, a control strategy has been chosen which is based on model predictive control (MPC).

Five processes influence the performance of the dredging process: the hopper sedimentation process, the drag-head excavation process, the pump and pipeline process, the power-train process and the sailing process. These systems are coupled, and it is of vital importance that all these systems are incorporated when optimising the overall system. Furthermore, it is necessary to incorporate the constraints of the system, such as the available power and the limited available inlet pressure of the pump.

Given these properties, MPC is very suitable for this application, because it is able to predict the systems behaviour that affects the performance. The process consists of a cycle, and it is not until the end of the cycle that the performance can be evaluated. In particular the sedimentation process in the hopper can not be observed by the operator; therefore, he will not and can not incorporate this in the determination of his strategy. By predicting which behaviour affects the performance, MPC can incorporate this behaviour.

The goal of this thesis is to investigate to what degree does an advanced integral control approach improve the performance. To achieve this goal, models have been derived for numerical simulation of the behaviour of the process. The following steps have been taken to achieve this goal:

- Modelling of the systems behaviour for the purpose of simulation and for designing the controller. On the one hand, this model is used to test the MPC and to analyze which factors are important when optimising the performance. On the other hand, this model forms part of the MPC for the online prediction of the objective function. This objective function quantifies what the optimal and desired behaviour is.

- Validation of the model using data from measurements and calibration of the soil-type-dependent parameters. For the calibration process two methods can be distinguished: off-line and online. The off-line method uses data of a complete cycle. The method is particular suitable for validating the models. The parameters are calibrated with data from a complete cycle. Then these parameters are used in the model to predict the outputs of the other cycles using open-loop simulation. If the parameters do not vary much during the dredging process, this method can be used online as well. Data of the last cycle are then used to calibrate the parameters in the model that is used for prediction in the current cycle. However, if the parameters vary too much, they must be estimated online with the use of adaptive estimation techniques.

- Nonlinear programming, where both the differential equations and the objective function are discretised with respect to time, is used for analysis of the influence of the sedimentation process in the hopper on the performance. This method takes the constraints into account. Then a MPC is designed and applied to the overall process. For this controller two scenarios are used to analyze its behaviour. One scenario is used to see how the MPC controls the system in case of power limitation and a trade-off is made when dividing the power over the systems. The other scenario is utilised to investigate the effect of the parameter uncertainty on the performance of the MPC and how the MPC reacts if the process parameters vary during operation.

The models derived for the sedimentation process, the pump and pipeline system, and the power train show sufficient accuracy for the use in the MPC. The validation shows that the models are able to predict the behaviour of the process. Also, they are computational fast so that they are applicable for on-line use in the MPC. However, two models, the black-box drag-head model and the ship/cut-force model, need to be developed further, because the ship/cut-force model is not sufficiently accurate and for the black-box drag-head model it is uncertain if it can be applied under new conditions.

The optimisation of only the sedimentation process clearly shows that this process is an important part of the optimisation of the overall process. This is demonstrated by comparing the optimised strategy with a scenario that purely optimises the incoming production without taking into account the sedimentation process. The analysis shows that this scenario is only optimal for sand material with a grain size larger than 0.3 mm. When dredging finer sand, the sedimentation process should be taken into account

when optimising. When the sand becomes finer, the incoming flow-rate should be reduced, assuming that incoming density increases at the same time. This correlation was found in the data sets. The improvement in terms of production per time unit compared with the non-optimised scenario varies between 2% for coarse sand up to 22% for fine sand. This analysis involves the complete dredging cycle with a total sailing and discharge time of 3.5 h.

The simulation of the overall process with the five subsystems and the use of the MPC shows the same behaviour as described above, but this system takes much more important details into account, such as the vacuum limitation at the pump inlet and the power limitations. The flow rate is controlled by varying the diesel engine speed (the diesel engine drives the pump), the ship speed is controlled by the pitch angles of the propellers and the incoming density is regulated with the water valve on the drag head.

The MPC strategy is compared with a strategy in which the diesel engine speed is nominal, a strategy which is often used in practice. The MPC strategy shows that this is in most cases suboptimal. The reduction of the pump speed results in an improvement of the cycle production rate, a reduction of the overflow losses and a reduction of the power usage. The improvement compared with the scenario varies between 7% for coarse sand up to 21% for fine sand.

The MPC outperforms the benchmark in case of a power limiting scenario. It reduce the demanded pump power, so more power is available for the propulsion. The ship can maintain its optimal speed and an improvement of 20% is achieved, calculated in production per time unit. Also, the overflow losses are reduced by the MPC.

J. Braaksma

Samenvatting

De sleephopperzuiger is een schip dat al varend zand en ander sediment opzuigt van de bodem. Over de bodem wordt een sleepkop getrokken die de grond loswoelt met waterjets en messen. De centrifugaalpomp zuigt vervolgens een mengsel van zand en water op en transporteert dit naar een opslagtank in het schip, de zogenaamde beun. In de beun bevindt zich een overstortsysteem, dat overtollig water en de fijne zandfractie terug laat stromen naar het oppervlaktewater. Hierdoor kan de sleepzuiger doorbaggeren, terwijl het zand met de grote korrels naar de bodem van de beun zinkt, en water met zand dat niet bezinkt stroomt overboord. Zodra de beun gevuld is met voldoende zand, worden de zuigbuis en sleepkop binnengehaald en vaart het schip naar de stortlocatie. Op deze locatie wordt het materiaal gelost door middel van het openen van de bodemdeuren, of met de pomp door een leiding geperst. Na het lossen vaart het schip weer naar de baggerlocatie en begint het proces opnieuw.

De moderne sleephopperzuigers zijn geavanceerde schepen met een grote hoeveelheid automatiseringssystemen die vanaf de brug door middel van geïntegreerde computersystemen worden bestuurd. Er wordt van de operators verwacht dat zij de juiste setpoints genereren voor al deze systemen. De allerlaatste schepen worden zelfs zo ingericht dat alles bediend kan worden door één operator. Dit is alleen mogelijk bij een grote mate van automatisering. Het bepalen van de setpoints is niet eenduidig doordat vitale informatie voor het nemen van de juiste beslissing ontbreekt. Veelal zijn de optimale setpoints afhankelijk van de grondsoort. Deze informatie is niet altijd aanwezig.

Het onderwerp in dit proefschrift is een regelstrategie die streeft naar een optimale bedrijfsvoering onder de hierboven beschreven veranderde omstandigheden. Deze moet rekening houden met alle facetten die het functioneren van de sleephopperzuiger beïnvloeden. Aangezien de gevolgen van bepaalde regelakties pas aan het einde van de baggercyclus in de performance tot uiting komen, wordt van de regelalgoritmen voorspellend gedrag geëist. Wij stellen daarom voor om een op model gebaseerde voorspellende regeltechniek ("model predictive controller", MPC) te gebruiken.

In het baggerproces zijn er vijf verschillende systemen de performance beïnvloeden: de beun, de sleepkop, de pomp en pijplijn, het aandrijfsysteem en het schip. Deze systemen zijn aan elkaar gekoppeld en kunnen daarom niet afzonderlijk geoptimaliseerd worden. Het is daarom van vitaal belang dat al deze systemen meegenomen worden in de optimalisatie. Daarnaast moet er rekening gehouden worden met de beperkingen van het systeem, zoals bijvoorbeeld het beperkte vermogen en de beperkte vacumdruk van de pomp. MPC is, gelet op deze eigenschappen van het systeem, uitermate geschikt om de performance te optimaliseren.

Het tweede aspect dat MPC uitermate geschikt maakt, is haar mogelijkheid om

het gedrag dat de performance beïnvloedt te voorspellen. Omdat het proces uit een cyclus bestaat, is de uiteindelijke performance pas aan het einde van een dergelijke cyclus bekend. Met name het bezinkgedrag in de beun kan operator niet observeren, en daarom kan en zal hij dit niet meenemen in het bepalen van zijn strategie. Door te voorspellen welk gedrag de performance beïnvloedt, kan er in de MPC wel rekening mee worden gehouden.

Het doel van dit proefschrift is om te onderzoeken in hoeverre een op dit model gebaseerde voorspellende regeltechniek in staat is om de performance van het baggerproces van de sleephopperzuiger te verbeteren. Dit is gedaan aan de hand van modellen en numerieke simulatie van het procesgedrag. Daartoe zijn in dit proefschrift de volgende stappen ondernomen:

- Modellering van het systeemgedrag met een dynamisch model. Enerzijds is dit model gebruikt om de MPC regelaar te testen en te analyseren welke factoren belangrijk zijn voor de optimalisatie van de performance. Anderzijds vormt dit model een onderdeel van de MPC regelaar ten behoeve van een online voorspelling van de doelfunctie. Met de doelfunctie wordt gekwantificeerd wat optimaal en gewenst is.

- Validatie van de modellen aan de hand van de gemeten data en calibratie van de parameters, die afhankelijk zijn van de grondsoort. In het calibratieproces onderscheiden we twee methoden: offline en online. De offline methode gebruikt de data van een complete cyclus. Deze methode wordt met name gebruikt om de modellen te kunnen valideren. Hiertoe worden de parameters gekalibreerd met data van één cyclus. Deze parameters worden vervolgens gebruikt in het model om met open-lus simulatie het gedrag van de andere cycli te voorspellen. Wanneer blijkt dat de desbetreffende parameters niet veel variëren tijdens het baggerproces kan deze methode ook online worden toegepast. Dan kunnen de data van de vorige cyclus gebruikt worden voor de calibratie van het model dat gebruikt wordt voor de voorspelling van het gedrag van de huidige cyclus. Echter wanneer de parameters te veel variëren, moeten de parameters online worden gekalibreerd met behulp van adaptieve schatters.

- Met behulp van niet-lineair programmeren, waarbij zowel het dynamische model als de doelfunctie naar de tijd is gediscretiseerd, is eerst een analyse gedaan naar optimalisatie van alleen het bezinkproces in de beun. Hierbij wordt rekening gehouden met de beperkingen van het systeem. Vervolgens is er een MPC regelaar ontwikkeld die is toegepast op het totale systeem. Voor de MPC regelaar zijn er een tweetal scenario's genomen om het gedrag te analyseren van het MPC systeem. Hierbij is gekeken wat een MPC regelaar doet in het geval dat het vermogen beperkt is en er afwegingen gemaakt moeten worden in de regelstrategie. Daarnaast is geanalyseerd, met behulp van een scenario, wat de invloed van parameteronzekerheid is op de performance en hoe de MPC regelaar reageert wanneer de procesparameters variëren tijdens het baggerproces.

De modellen die zijn afgeleid voor het bezinkgedrag, het pomp- en pijpsysteem en het aandrijfmodel, zijn voldoende nauwkeurig voor het gebruik in de MPC regelaar. De validatie laat zien dat de modellen in staat zijn het gedrag te voorspellen. Daarnaast zijn ze snel genoeg voor de online toepassing in de MPC regelaar. Echter

twee modellen, het black-box sleepkopmodel en het scheeps/snijkrachtmodel moeten verder ontwikkeld worden, omdat voor het scheeps/snijkrachtmodel de nauwkeurigheid te wensen overlaat en het voor het black-box sleepkopmodel onzeker is of dit model onder nieuwe omstandigheden even goed werkt.

De optimalisatie van het bezinkproces in de hopper laat duidelijk zien dat dit proces een belangrijk onderdeel is voor de optimalisatie van het gehele baggerproces. Dit is aangetoond door de geoptimaliseerde strategie te vergelijken met een scenario waarbij alleen de ingaande productie maximaal is, zonder rekening te houden met het bezinkproces. De analyse laat zien dat dit scenario alleen optimaal is bij een korrelgrootte van 0.3 mm en groter. Bij fijner zand moet wel degelijk het bezinkproces worden meegenomen in de optimalisatie. Naar mate het zand fijner wordt, moet het ingaande debiet worden verlaagd, waarbij wordt aangenomen dat de dichtheid hierdoor toeneemt. Deze correlatie was sterk aanwezig in de beschikbare data. De verbetering vergeleken met het scenario dat zonder behulp van de optimalisatie behaald wordt ligt tussen 2% voor fijn zand en 22% voor grof zand. Deze analyse neemt de gehele cyclus in ogenschouw waarbij de totale vaar- en lostijd 3.5 uur is.

De simulaties van de MPC regelaar laten hetzelfde gedrag zien als hierboven beschreven, maar dit systeem neemt nog meer belangrijke details mee, zoals de beperkingen van het vacuüm en de vermogensbeperking. Het debiet wordt nu tijdens de simulaties door middel van de dieseltoeren geregeld, de scheepssnelheid door de pitchhoeken van de schroef en de ingaande dichtheid door de waterflap op de sleepkop. De MPC strategie wordt vergeleken met de strategie waarbij de dieseltoeren nominaal zijn, een strategie die men vaak in de praktijk tegenkomt. De MPC strategie laat zien dat dit niet altijd optimaal is. Het terugregelen van de pompsnelheid leidt tot een verbetering van het sedimentatieproces, een verhoogde cyclusproductie, een vermindering van de overvloeiverliezen en vermindering van het opgenomen vermogen. De verbetering vergeleken met het scenario varieert tussen 7% voor grof zand en 21% voor fijn zand.

De MPC regelaar presteert veel beter dan de benchmark in een vermogensbeperkte situatie. Door in deze situatie het opgenomen pompvermogen te reduceren, is er meer vermogen beschikbaar voor de voortstuwing. Hierdoor kan het schip de optimale snelheid blijven behouden. Het scenario laat zien dat een verbetering van 20% in productie per tijdseenheid gehaald kan worden. Daarnaast reduceert de MPC regelaar de overvloeiverliezen.

J. Braaksma

1

Introduction

The trailing suction hopper dredger (TSHD) plays a crucial role in large-scale land reclamation projects. Without the hopper dredger, projects such as Chek Lap Kok airport in Hong Kong, Singapore's port and Dubai's land reclamation would not be feasible. The enormous scale increase during the years, from the Maasvlakte with 450 million m^3 of sand in 1964 to the Dubai islands with a total projected fill volume of all projects combined of 2.4 billion m^3 (de Jong et al., 2005), requires jumbo dredgers with capacities up to 33000 m^3, which is an equivalent of 1650 truckloads.

One of the characteristics of the TSHD is the dredging cycle. The hopper dredger sails to an area with suitable sand that can be excavated from the bottom with a drag head (see Fig. 1.1). It starts filling the onboard cargo hold, the so-called hopper. In this hopper, a separation process takes place where the sand settles at the bottom and excess water flows overboard. Once the hopper is full with sediment, the ship sails to the discharge location where the unloading takes place by either opening the bottom doors or pumping the material out of the hopper by the dredge pumps.

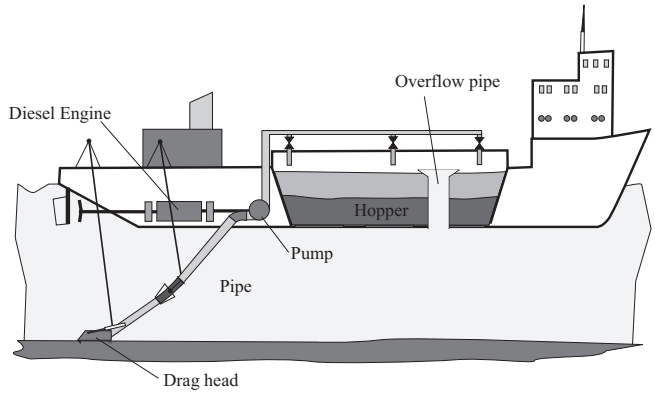

Figure 1.1: A schematic drawing of a hopper dredger.

Two processes dominate the operation of the TSHD. The excavation process determines the amount of sand entering the hopper and the sedimentation process determines the efficiency of separation of sand and water in the hopper. In general, part of

the sand does not settle inside the hopper, but flows overboard through the overflow. This overflow loss prolongs the dredging cycle, increases the cost and can possibly have a negative impact on the environment.

A major constraint to this dredging process is the total installed power, which determines the maximum sailing velocity and pump power. Ship builders strive for a balance between the installed power and hopper capacity. Heavier and larger engines leave less room for hopper space and less weight for mixture in the hopper. Other constraints can be the vacuum limitation at the inlet of the dredge pump and the maximum allowable draught.

Optimisation of the dredging performance demands an integral approach that takes the dredging cycle, the excavation, the sedimentation process and the constraints into account. To date, research has focused on single processes at a time (de Bree, 1977; Miedema, 1987; Matoušek, 1997; van Rhee, 2002). However, to optimise the overall dredging performance, all processes have to be taken into account. Moreover, advanced control techniques are not yet commonly applied on board of hopper dredgers.

Historical Overview

Even though the first centrifugal pumps were introduced in 1680 (Encyclopedia Britannica, 2007), they were not used for dredging until around 1857 (Bos, 1974). Until then the dredged material was transported mechanically, for example, with buckets. The centrifugal pump marked a new era of hydraulic transport of sand and water in the dredging industry. It was a Dutch invention to equip the stationary dredger "Adam I" with a hold: the hopper (de Koning, 1978). This sea-going ship sailed to the dredging area where it filled the hopper. During dredging, it was stationary and attached to anchors. After filling the hopper, the ship sailed to a discharge area and unloaded the material. An important improvement came with the TSHDs which were built in Europe after 1960 (de Koning, 1978). These dredgers were based on developments that started in 1902 by the US Army Corps of Engineers, who did extensive research on drag heads and swell compensators. Before 1960, the dredgers in Europe were mostly stationary, which disrupted the shipping traffic substantially due to the anchors and lines. Advantages of the TSHD are less disruption of the shipping traffic, it is capable of working under rough sea conditions and can cover a large work area.

1.1 System Description

The TSHD has several important components, which are briefly described in this section.

Drag Head

Typical of a TSHD is the drag head that breaks the coherence of the sand at the bottom. In the beginning, drag heads accomplished this by an erosion process and the pressure difference over the drag head. The pump and pipe aspirate water and the resulting flow erodes the sand underneath the drag head. Only very low mixture densities result from the erosion process alone (Vlasblom, 2003). Water jets increase the production of the drag head by breaking the coherence of the sand and forming

a mixture. These jets are located at the front of the drag head, as shown in Fig. 1.2. Teeth installed on the drag head cut sand or cohesive soils such as clay. The latest development is to also install jets in the teeth of the drag head for cutting (Vandycke et al., 2005; Vercruijsse et al., 2005). The cutting forces (Miedema, 1987) are delivered by the thrust force of the ship's propellers. Hydraulic cylinders regulate the excavation depth by adjusting the visor angle. When the pressure drop over the drag head becomes too large, the water valve can be opened to reduce this pressure drop. This prevents the pump from cavitating.

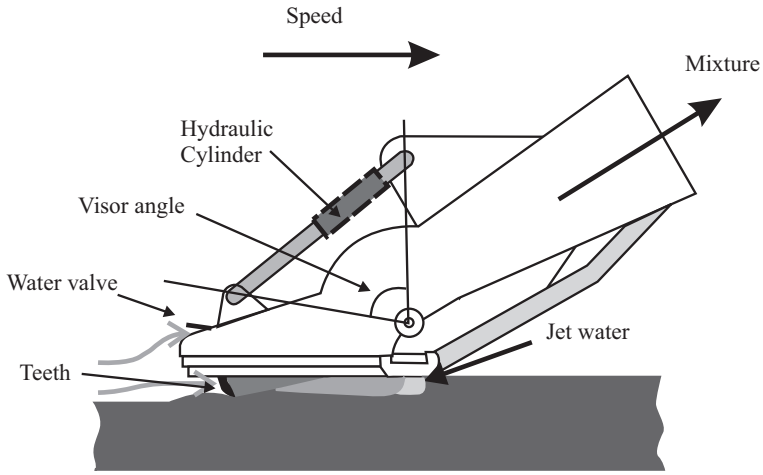

Figure 1.2: A drag head with jet system and teeth.

Centrifugal Pump

The centrifugal pump and pipeline system transports the mixture of soil and water formed in the drag head to the hopper. The mixture enters the pump near the axis of the impeller that throws the mixture out into the pump casing. The mixture leaves the pump through the discharge pipe. The pump creates pressure in the hydraulic system to transport the mixture from the bottom to the hopper. If the impeller has more blades, the efficiency increases. However, more blades decrease the clearance for debris and rock which might enter the pump. Therefore, a trade-off between efficiency and clearance is made in the design of the dredge pump. When the incoming liquid contains too much vapour or gas, the pump starts cavitating.

Suction Pipe

The TSHD is equipped with one or two suction pipes. Throughout this thesis a ship configuration with one suction pipe is considered, unless otherwise stated. The suction pipe connects the drag head to the hull inlet, from where another pipe is connected to the dredge pump. The suction pipeline consists of three or more sections to give the drag head enough degrees of freedom in following the bottom profile. Three gantries are installed to move the suction pipe overboard and inboard. The drag head gantry

and middle gantry set the angles of the pipeline. An elbow gantry places the suction pipe in front of the hull inlet. Fig. 1.3 shows the drag head, pump and pipe assembly.

Swell Compensator

Swell compensators maintain the contact between the drag head and the bottom, regardless of irregularities of the bottom of the area to be dredged and motion of the ship. They use hydraulic cylinders to tension the drag head cables. The operators regulate the pressure in the cylinders so that the vertical force of the drag head can be adapted to the soil type.

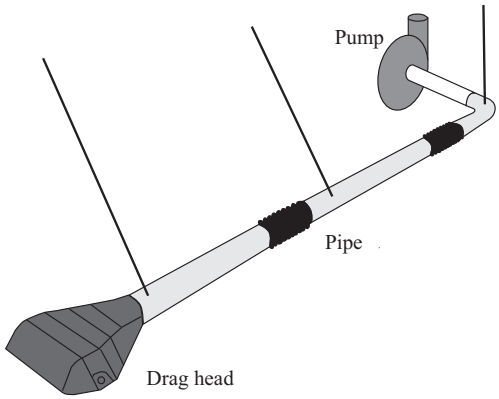

Figure 1.3: The drag head, pump and pipeline assembly.

Hopper

The hopper is a large storage tank in which the sand settles. A diffuser distributes the mixture coming from the pump over the width of the hopper, so that the incoming mixture velocity is lowered. Coarser grains settle at the bottom of the hopper where they form a sand bed, while lighter grains remain in suspension (see Fig. 1.4). During loading, the mixture level in the hopper rises until it reaches the overflow weir through which excess water or mixture is discharged overboard.

Overflow Weir

Most modern dredgers are equipped with an overflow weir which is adjustable in height. The operators use the overflow weir to control the volume of the mixture in the hopper. The increasing load in the hopper leads to an increasing draught of the ship. Once the ship reaches the maximum allowable draught, an automatic controller or the operators lower the overflow height. This allows the TSHD to continue dredging while maintaining the maximum draught. However, the density of the material which flows overboard (overflow losses) increases with time. If the dredging continues too long, almost all the excavated material flows directly overboard through the overflow. To prevent this from happening, the operators must decide when to stop dredging.

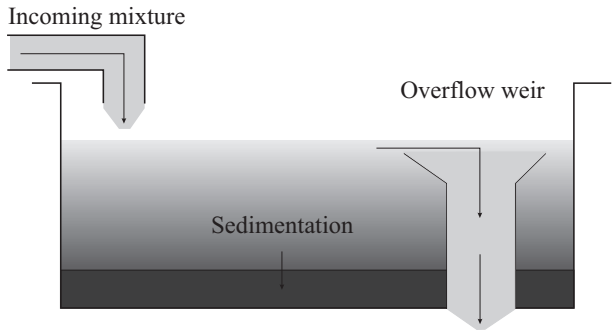

Figure 1.4: The hopper sedimentation process.

Dredging Cycle and Optimal Dredging Time

The whole dredging cycle consists of four phases: (1) dredging, (2) sailing to a discharge area, (3) discharge and (4) sailing back to the dredge area. Although phases 2/4 do not contribute to the total amount of material in the hopper, they are important for the dredging strategy. First of all, an important decision in the strategy is the stopping time for the dredging process. The stopping time is determined by the soil type and other material properties. For coarse sand, the overflow losses are marginal and the dredging continues until the hopper is full. For finer sand material, the overflow losses will be significant and the dredging continues until the best economical time. The optimal stopping time is influenced by the total sailing and discharging time. The longer the sailing distance and/or discharge time, the more economical it is to continue dredging and fill the hopper (IHC Holland, 1991).

1.2 Control of the Hopper Dredger

The modern TSHD is a complex system with several automation systems. Every subsystem is equipped with its own local control system, such as a diesel fuel rack controller, a pump controller, etc. The operators determine the set-points for each system on consoles on the bridge. These consoles communicate the set-points to the local controllers via a field bus.

From interviews with operators it is understood that for many controllers it is unclear how the set-points should be chosen and what their effect is on the dredging performance. Most of the set-points are set to their default values. The dredging equipment is very expensive and operators do not like to experiment with it. Furthermore, the strong coupling between the systems and always changing environment makes it a very complicated system to control. It is often hard to differentiate between the effect caused by the operator strategy and by the disturbances of the environment. It takes years of experience to understand the complete process. Often the dredging process operators are not experienced enough to fully utilise the systems potential. A solution to this is an operator advisory system or an optimal control system.

One of the first ideas on advising the operator how to optimise the dredging cycle has been based on an analogue computer (Knust, 1973). The method calculates the

volume of dry sand in the hopper online and displays it to the operator. Also, the production per time unit is calculated by dividing this volume by the cycle time. This method is now implemented on every modern dredger (IHC Holland, 1991). Nowadays, modern communication systems allow for remote monitoring of the hopper dredger (Hahlbrock and Freese, 1998).

The next step is a system that advises the operators on which set-points should be chosen. One of the first attempts was a system based on the concepts of artificial intelligence (Kurita et al., 1992; Ikeda et al., 1995). A system has been implemented on the "Seiryu Maru" dredger, based on fuzzy reasoning to incorporate expert knowledge into the control system. Later this system was installed on its successor, the "Hakusan" (Morita et al., 2002). The first drawback of this system is that it is completely based on expert knowledge, which, to my knowledge, is not available in the literature. Usually this knowledge is neither available from the crew. The second drawback is that it is a fixed system based on a small number of tests and soil conditions. As the soil conditions vary continuously, it is very hard to find general rules for controlling the hopper dredger for every soil type. Even if this is possible, it does not guarantee that the ship performs optimally in every situation and under varying conditions. Therefore, I propose here to use an adaptive control technique that tries to maximise the performance for varying operating conditions without using expert knowledge.

1.3 Scope and Approach of the Thesis

This thesis focuses on the control aspects of the TSHD. Choices for the system design have a large influence on the achievable control performance. Therefore, an integrated approach of the system design and control design is beneficial. Currently, these choices are based on operational aspects of the hopper dredger, such as average sailing distance, type of work, maximum draught and many more. However, since the TSHDs are often deployed in projects with objectives different from the designed objective, and the design choices are permanent and not easily adapted, the system design is considered fixed. The control design, on the other hand, is more flexible and can be adjusted to changing operating conditions. Therefore, it is assumed that improving the control design will lead to improvement in the performance.

The objective of this research is to show that an advanced control technique that uses an integral system approach is able to improve the performance. Simulations of the whole system are based on first-principle models. These models are validated with data from a real ship and a test rig. The data are obtained from a TSHD with hopper capacity of 13700 m^3 and one suction pipe. The test rig is a scale model of the hopper for validation of the hopper sedimentation model. To obtain the soil dependent parameters, we use a data-driven estimation approach.

1.4 Research Goals

During the last decade, substantial research has been done on several processes that are important for the TSHD. However, not much effort went into the investigation of improving the performance by means of controlling the TSHD. Therefore, the aim of this study was to find an answer to the following question:

- To what degree does an advanced integral control approach improve the performance?

To answer this question several research topics have to be defined. First of all, for the purpose of simulation and control design, a model must be derived. This will be a control oriented model which should be computationally fast. As speed is usually achieved at the cost of accuracy, we need to validate the model and test its accuracy. Then a controller is designed and finally the improvement that can be achieved is investigated. To summarise, the following research topics are addressed in this thesis:

- Development of a model for simulating the TSHD and for optimising its performance. This performance is defined with an objective function and depends on the objectives. In this thesis we consider one objective which is based on the production rate of the complete dredging cycle.
- Investigation of the model accuracy to verify whether the developed models are suitable for control.
- Development of a controller to optimise the performance of a TSHD under different circumstances. This controller must find the control signals that optimise the given objective.
- Investigation of the improvement obtained with the model based control techniques.

1.5 Outline of the Thesis

The four research topics are described in four chapters. In Chapter 2, detailed background information on the TSHD is given. The chapter describes the components of the TSHD and provides the necessary background information for the other chapters. Readers who are familiar with the TSHD process can skip this chapter.

Chapter 3 describes the model which has been developed with the aim to optimise the dredging performance. The total model is subdivided into five parts and a model of each part is derived. One of the main reasons to split the model is that there are many possible configurations of a TSHD. By making the model modular it can be applied to all configurations with only minor adjustments.

Chapter 4 gives the results of the validation of the model and the calibration of the parameters. It describes the methods which are used and the simulation results. The models consist of soil-type-dependent parameters that may vary during operation. The first approach that is shown is calibrating the parameters on data from a complete cycle. Then, given these parameters, the model predicts the behaviour of the other cycles (off-line estimation). This approach will show us if the models have sufficient accuracy. However, this approach is only useful on-line in the situation where the parameters do not vary rapidly during the process and the soil type is the same everywhere in the dredging area. If this assumption is not valid, the parameters must be adapted on-line during operation. Eventually for implementation of model based control on board of the TSHD all the soil-dependent parameters must be adapted on-line. In this thesis this on-line adaptation is only developed for the parameters of the pump and pipeline.

Chapter 5 gives details on how much improvement can be made by using optimal control strategies under varies circumstances. Also in this chapter, an optimising controller is derived. Simulations of two scenarios are given in Chapter 6. One scenario simulates a TSHD that has limited power available and the other scenario shows the effects of uncertainties in the parameters used in the controller. The thesis ends with the conclusions and recommendations as given in Chapter 7. Additional background information is given in the Appendices.

2

Trailing Suction Hopper Dredger

This chapter starts with describing the work method of the trailing suction hopper dredger (TSHD), the dredging cycle. Then, based on the dredging cycle, the most economical method of loading is determined. Finally, all the components on board of the TSHD that play a role in its performance are described.

Figure 2.1: The TSHD, busy rain-bowing.

2.1 Introduction

The TSHD has a broad application area, ranging from maintenance dredging of waterways and harbours to excavating sand for land reclamation. At first the hopper was

only used for deepening and maintaining the waterways. Nowadays, hopper dredgers are involved in land-reclamation projects, gravel excavation (specialised ship) and in making trenches and pits for the offshore industry.

In this thesis we consider only the excavation of sand, but the hopper can also be used for silt, clay, gravel and even rock materials. Although, clay may cause problems such as congestion in the drag head or it can stick inside the hopper.

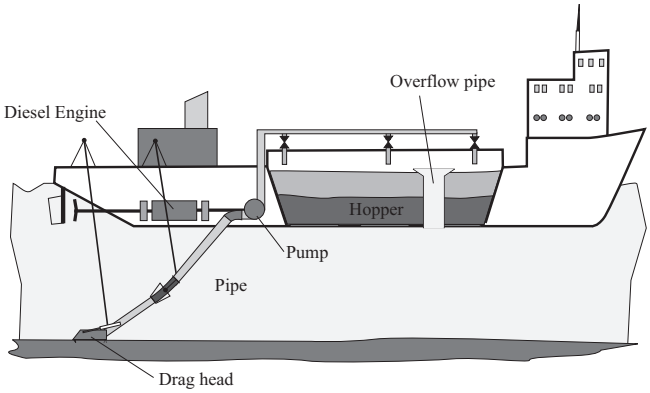

Figure 2.2: A schematic drawing of a hopper dredger.

The hopper dredger operates in cycles. Each cycle consists of dredging, sailing to the discharging area, discharging the material and sailing to the dredging area. Fig. 2.3 schematically shows the phases of the cycle. Note that the figure does not show an empty ship that sails back to the dredging area. When the hopper dredger arrives at the dredging area, the ship navigator reduces the speed of the ship to approximately 1.5 m/s. In the meantime, the dredging process operator starts lowering the suction pipe overboard and, when the drag heads are a few metres above the sand bed, the centrifugal pumps. Then the drag heads are lowered to the bottom of the sea and the mixture starts flowing from the drag head into the hopper through a pipeline.

The level of the mixture in the hopper rises until it reaches the overflow weir. For non-settling or poorly settling materials, such as silt, the dredging process stops at this point. For sand and gravel, the dredging continues while excess water or low-density mixture flows out of the hopper through the overflow weirs. This phase is called the constant volume phase. As long as the incoming density is higher than the outgoing density, the mass in the hopper increases. For a ship with a fixed overflow system, the process continues until the ship reaches its maximum allowable draught. A ship with an adjustable overflow system maintains the maximum allowable draught by lowering the overflow weir, and so discharging more water/light weight mixture. The total mass in the hopper remains constant and, therefore, this phase is called the constant-tonnage phase. The dredging stops either when the hopper is full, i.e., the overflow weir height is equal to the sand bed height, or when it is not economically efficient to continue dredging.

After the dredging has been stopped, the ship sails to the discharge area. There are three ways of discharging the hopper content (see the three bottom panels of Fig. 2.3). The simplest method is by opening the bottom doors in the hopper. The material

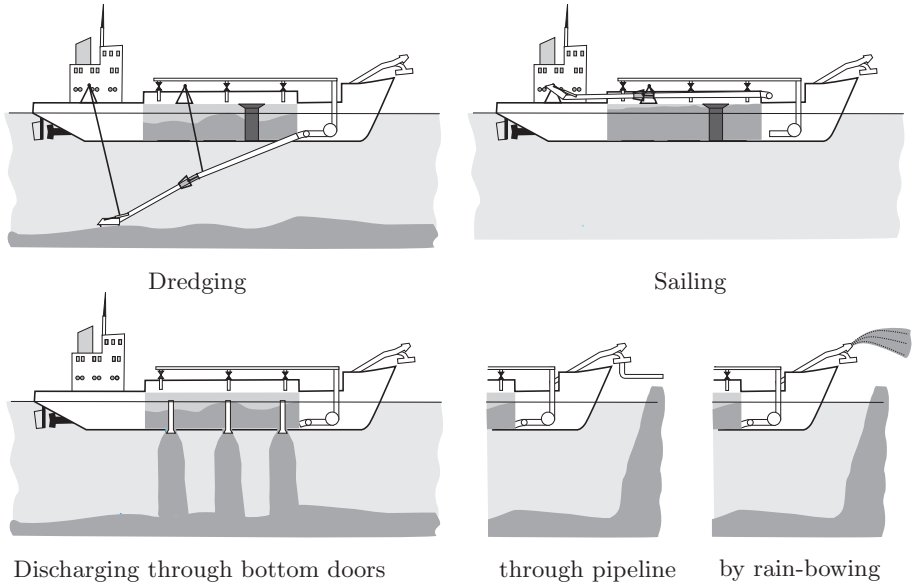

Figure 2.3: The dredging cycle.

flows out naturally through the bottom doors. The operator closes the doors when there is almost no sand left in the hopper. The dredge pump can be used to discharge the remaining water.

The second method of discharging is through a shore connection. Usually, a floating pipeline is connected to the pump-pipeline system of the ship. The dredger uses the sand pump to discharge the material through the pipeline. If the TSHD is equipped with two pumps, they can be used in series for pumping the material over a long distance. Water jets are used to fluidise the material in the hopper. Usually this is done in one section at the time. In the bottom of the hopper, a so-called self-emptying channel is used for discharging the material from the hopper. By opening the valves in this channel and pumping water through the channel, the material is transported out of the hopper and discharged through a pipeline (see the bottom middle panel of Fig. 2.3).

The last method of discharging is similar to the second method. The material is sprayed into the air (shown in the bottom right panel of Fig. 2.3). This so-called rain-bowing is commonly used for beach nourishment and land reclamation. When all the material has been discharged, the TSHD sails to the dredging area and the next cycle starts.

2.2 Ship Type

This section describes the TSHD configuration that is used throughout this thesis. TSHDs are mostly custom-built ships. Thus, there are many types, each with different configuration and/or dimensions. It is impossible to investigate all these configurations in this study. The ship which is used in this thesis as the subject for optimisation is

shown in Fig. 2.4. This choice is determined by the data sets we have available of this type of ship. However, the methods that will be derived in this thesis will also be applicable in other ship configurations.

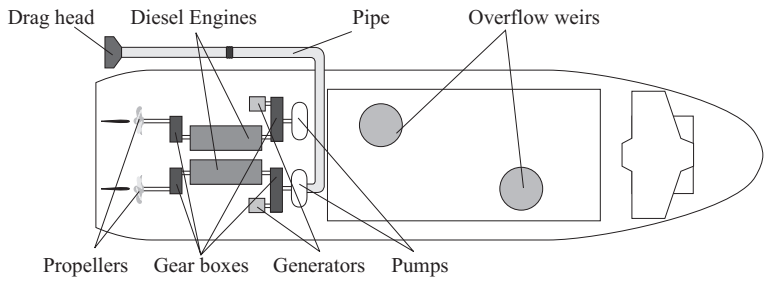

Figure 2.4: A schematic drawing of a TSHD.

This ship has a hopper capacity of 13700 m^3. It is equipped with two main diesel engines each with a power of 5760 kW. Its overall length is 142.8 m, its width is 26.8 m and the maximum draught is 9.82 m. It can reach a maximum speed of 8.1 m/s (15.7 knots) when loaded and it can dredge down to a depth of 30 m. The dredger is equipped with one suction pipe with a diameter of 1.20 m. It has one onboard dredge pump and an additional pump for discharging the material through a pipeline. Each of the main engines drives from its aft a four-blade 4.4 m propeller, through a reduction gearbox, and from its forward end a pump, also through a reduction gearbox. Furthermore, each engine feeds a 2950 kW AC generator. These generators provide the power for the electric motors that drive the jet pumps and the 525 kW bow thrusters, as well as the auxiliaries, hydraulics, lighting, etc. See Tab. 2.1 for an overview of this configuration. In this thesis a total sailing and discharging time of 3.5 hours is considered.

Table 2.1: Ship configuration used throughout this thesis.

Description	Value	Unit
Length	142.8	m
Width	26.8	m
Maximum draught	9.82	m
Hopper capacity	13700	m^3
Loading capacity	21000	ton
Suction pipe diameter	1.2	m
Nr of pumps	2 (1 for dredging)	-
Nr of pipes	1	-
Propeller diameter	4.4	m
Max speed loaded	8.1	m/s

2.3 Hopper

The main function of the hopper is the temporal storage of sand for transportation to the discharge area. The hopper has an approximately rectangular shape and is located in the middle of the ship. A hopper dredger is usually equipped with one hopper. The hopper is equipped with on or two overflow weirs. The height of these weirs can be adjusted with hydraulic cylinders. When fully loaded, the draught of the ship has reached its maximum, which is indicated on the hull by the so-called dredge mark.

2.3.1 Inlet System

The inlet system feeds the material into the hopper without introducing excessive turbulence, which would have a negative effect on the sedimentation process. The inlet system has several inlet points to divide the material in case of coarse sand evenly in the hopper. This avoids that all the material settles at one end of the ship. In Fig. 2.5, two inlets can be distinguished that span the width of the hopper, one in the middle and one at the back. The third inlet point is not visible in the figure.

Figure 2.5: An example of a hopper.

2.3.2 Overflow Weirs

The overflow weir is a system to discharge the excess water and low-density mixture. During filling of the hopper with a mixture of water and sand, the mixture level rises until it reaches the overflow height. Thereafter, the filling continues while the low-density mixture of water and sand flows out. Grains that do not settle fast enough leave the hopper through the overflow.

Figure 2.6: Overflow weir.

When the draught of the ship is at its maximum, i.e., at its dredge mark, the ship continues loading while lowering the adjustable overflow (see Fig. 2.6). The total mass in the hopper remains the same, but the density in the hopper increases. The dredging is stopped according to the economical loading principle, as explained in Section 2.7. This method is called the constant-tonnage loading system.

In another loading strategy the operators adjust the level to the height up to which they want to fill the hopper and leave it in that position until the sand bed in the hopper has reached the overflow height. Then the loading stops and the ship sails to the discharge area to unload the material.

2.3.3 Sensors and Automation

The hopper system is equipped with several sensors and a constant-tonnage loading controller. The sensors are used to calculate the important variables for process monitoring and control, such as the total hopper volume V_t, the total hopper mass m_t, the tons of dry solids TDS and the height of the overflow weir h_o.

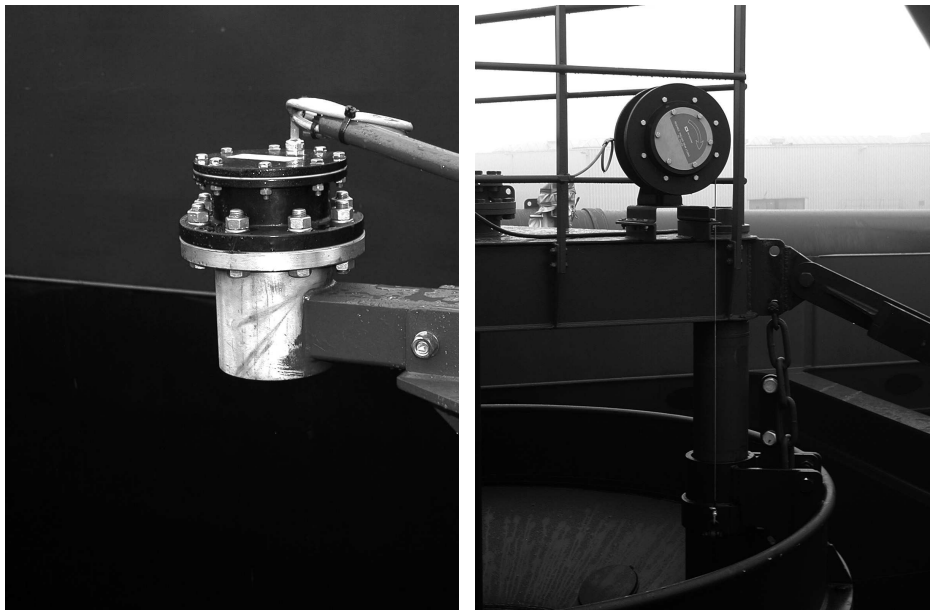

(a) Hopper mixture level sensor. (b) Overflow height sensor.

Figure 2.7: Sensors in the hopper.

Mass of Hopper Content

The mass in the hopper is derived from the draught of the ship. The draught is a function of the ship mass. The hopper mass is derived by subtracting the mass of an empty ship from the mass of a full ship.

There are four pressure sensors in the bottom of the hull to calculate the draught, list and trim. The total mass of the ship is derived from these measurements. List depends on the roll angle of the ship and trim on pitch angle. They are expressed in meters. From the total mass, the mass of the hopper content m_t is calculated by correcting for the mass of the empty ship and ballast tanks:

$$m_t = m_{sh} - m_b - (m_{sh0} - m_{b0}),$$

where m_{sh} is the total mass of the ship, m_b the mass in the ballast tanks, m_{sh0} the total mass of the ship during calibration and m_{b0} the mass in the ballast tanks during calibration.

Volume of Hopper Content

The hopper volume is determined by the mixture height sensors located above the hopper (see Fig. 2.7(a)). The volume is calculated from the mixture height measurements, the geometric shape of the hopper, the trim and list of the ship.

The hopper volume can be calculated as follows:

$$V_t = f(\varphi, \upsilon, h_t),$$

where $f(\varphi, \upsilon, h_t)$ is a given nonlinear function, h_t the mixture height in the hopper, υ the list and φ the trim.

Tons of Dry Solids

At the end of the dredging cycle the hopper is filled with a mixture of sand and water. Usually the customer only pays for the amount of solid material, referred to as the ton of dry solids (TDS). The TDS is calculated from the mass m_t and volume V_t of the total material inside the hopper. The TDS is calculated using the following equation:

$$\text{TDS} = \frac{(m_t - V_t \rho_w)\rho_q}{\rho_q - \rho_w}, \tag{2.1}$$

where the density of the sand particle (quartz) is ρ_q and of water ρ_w.

Draught Control/Constant Tonnage Controller

The height of the overflow weir is measured with a position sensor, see Fig. 2.7(b). The mixture level and, thus, the hopper volume are regulated by controlling the overflow height. Ships that are equipped with an adjustable overflow are often also equipped with a constant-tonnage loading controller. This is a PI-controller that lowers the overflow weir automatically when the draught of the ship is at the dredge mark (maximum mass allowed in the hopper). In this phase, the volume of the mixture in the hopper is reduced, but the total mass remains constant.

2.3.4 Hopper Test Rig

Part of the available data has been obtained on a test rig. This data set is from a study on sand sedimentation in the hopper, which was performed at MTI in Kinderdijk (Ooijens et al., 2001). Fig. 2.8 shows a schematic of this test rig, developed at MTI, Kinderdijk for research on sand sedimentation. The system contains three main components: a test hopper for the experiments, a settling tank, and a storage and mixing hopper (not shown in figure). Water jets are installed in the storage hopper to fluidise the sand. The sand is then transported to the test hopper by opening valves in the self-emptying canal underneath the storage hopper. The mixture inlet discharges the sand water mixture into the test hopper where sand is sedimented. When the water level reaches the overflow system the material flows out of the hopper and it is pumped into the settling tank.

The main dimensions and specification of the hopper test rig are given in Tab. 2.2. The rig is a scaled-down version of the ship named "Antigoon". For information on validation and comparison of the test rig data and the ship data, the reader is referred to (Ooijens et al., 2001). During the tests the following measurements were performed:

1. Flow rate into the hopper.
2. Flow rate out of the hopper located in the return pipe.

3. Density of the flow into the hopper.
4. Density of the flow out of the hopper in the return pipe.
5. Flow rates of the jet system.
6. Heights of the overflows.
7. Level of the mixture in the hopper.

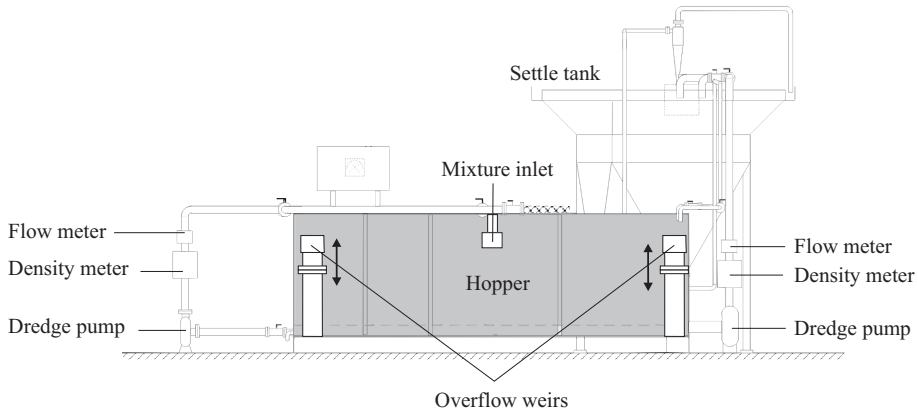

Figure 2.8: The hopper test rig "Schanulleke". Reprinted from (Ooijens et al., 2001), with permission.

Apart from these measurements, additional measurements were done inside the mixture to investigate the sedimentation process. Two sensor poles, positioned at different locations, measured the density of the mixture at 12 discrete levels with Conductivity Concentration Meters (CCMs). A radioactive concentration sensor was used to measure the density, at another location. Finally the mixture velocity was measured at three levels in one location by electromagnetic velocity meters. This last measurement is not used in this research.

Table 2.2: Main dimensions and specifications of the test hopper rig.

Description	Value	Unit
Length	11.34	m
Width	2.04	m
Max flow-rate	0.10	m^3/s
Overflow height	$1.40 \cdots 2.40$	m
Grain size (d_{50})	100	μm
Max input density	1600	kg/m^3

2.4 Excavation System

The excavation system has several important components (see Fig. 2.9). The soil is excavated by the drag head and transported through the suction pipe to the pump. The pump creates a flow to transport the mixture from the bottom of the sea to the hopper. Winches are used to lower and raise the drag head and the suction pipe that usually consists of three parts. The swell compensator tensions the drag-head cable. This system allows the drag head to operate in seas with swell. This system also compensates for irregularities of the bottom of the sea.

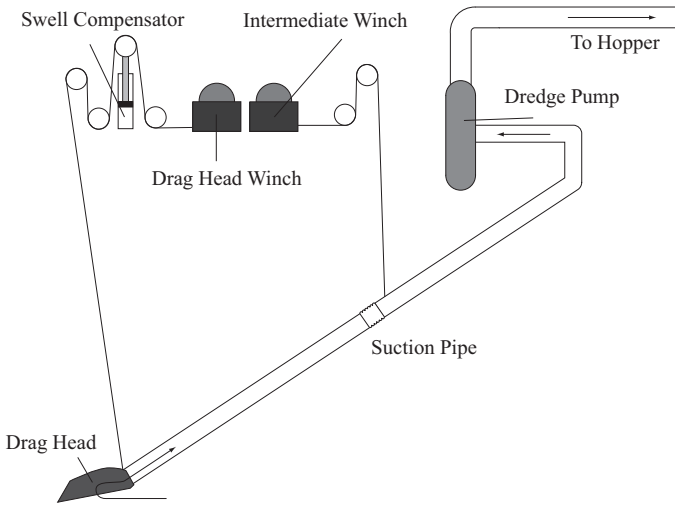

Figure 2.9: The excavation system of the TSHD.

2.4.1 Drag Head

The production level of the head is determined by three processes: cutting the sand, erosion due to the water flow and eroding by jetting. Several different drag heads are used in dredging. Two commonly used drag heads are the IHC drag-head and the California drag-head (see Fig. 2.10). A distinction can be made between so-called passive and active drag-heads. A passive drag-head has a loose visor that can follow the profile of the bottom. The visor can also be fixed so that it has a fixed angle with the lower suction pipe.

The active head has hydraulic cylinders (see Fig. 2.11), to control the visor angle relative to the lower suction pipeline. The visor angle is the angle between the lower suction pipeline and the visor. These cylinders can be pressure controlled (loose mode) or position controlled (fixed mode). In the pressure-controlled mode, the visor exerts an adjustable force on the bottom such that the visor follows the bottom unevenness. When the visor is position controlled, the dredging process operator sets a cutting height for the visor. The visor angle is controlled such that a layer of material is excavated by the drag head. If the angle is increased too much, the front of the head rises above the sand and the production drops, as a lot of water is aspirated.

(a) The Dutch drag-head or IHC drag-head. (b) The California drag-head.

Figure 2.10: The two most commonly used drag heads.

A drag head can be equipped with water jets. A jet pump inside the ship pumps water to the jet nozzles at high pressure. The nozzles on the drag head break the coherence of the sand. If the vacuum of the pump becomes too high, the water valve opens and water is added to the drag head. This prevents the pump from cavitating.

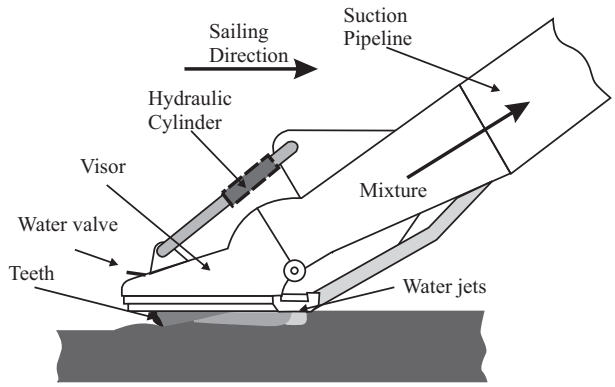

Figure 2.11: An active California drag-head.

2.4.2 Swell Compensator

The swell compensator is a hydraulic piston that tensions the hoist cable (see Fig. 2.12). Its main goal is to maintain contact between the drag head and the seabed while the ship is moving due to swell and in case of bottom irregularities. Once the drag head touches the bottom, the piston moves up and tensions the cable. The tension force can be regulated to control the force that the drag head applies to the bottom. The force supplied by the swell compensator is twice the force acting on the drag head. Softer soils, such as mud and silt, require a lower downward force than sand.

Figure 2.12: Swell compensator.

2.4.3 Pump and Pipe

The pump in the TSHD is a centrifugal pump that consists of a rotating impeller in a pump housing (see Fig. 2.13). The impeller is either powered directly by the diesel engine or by an electric motor. Usually the pump is located inside the ship, but to dredge at very large depths the pump can also be located in the suction pipe. In this case the pump is powered by an electric motor.

The impeller has several curved blades. Rotating the impeller accelerates the mixture inside the pump. The created vacuum sucks up the mixture of sand and water that is excavated by the drag head. This vacuum is limited by the vapour pressure of the mixture. If the absolute pressure at the inlet becomes too low, the mixture starts to evaporate and bubbles occur at the inlet. These bubbles increase in size as they travel through the pump. This effect, called cavitation, is reducing the pump efficiency and increases wear and tear in the pump.

The suction pipe usually consists of two sections and is lowered and raised by winches (see Fig. 2.9). The suction pipe has a larger diameter than the pressure part of the pipe after the pump. In the pressure section there are two important sensors mounted, a mixture velocity sensor and density sensor. These sensor measurements provide information on the incoming production to the operators.

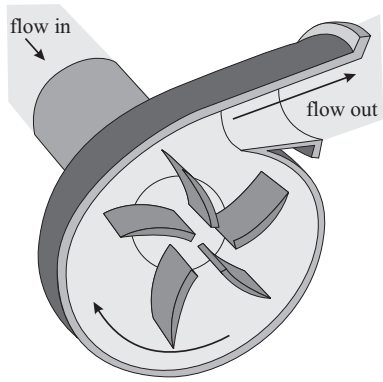

Figure 2.13: The Centrifugal dredge pump.

2.4.4 Sensors and Automation

Incoming Mixture Density

The incoming mixture density is measured using a radioactive source placed on the discharge pipe directly above the pump and, if possible, in a vertical piece of the pipe. Several types of detectors are used, such as a Geiger-Müller tube, scintillation counter and ionisation chamber. The first type has an accuracy of up to 5% and the second type and third type can reach an accuracy of up to 1 or 2%.

The material is assumed to be homogenous over the pipe diameter. Therefore, the density measurements are performed in a vertical pipe if possible. In a horizontal pipe heavy sand settles at the bottom of the pipe, leading to a non-homogenous density pattern. Other reasons for a reduction in accuracy are:

- Pipe-wall thickness, due to wear the pipe wall gets thinner, which lead to less absorption of the radiation.
- Degeneration of the radioactive source. Although software is used to compensate, this leads to uncertainties in the measurements.
- Slip of sand in tube. Due to gravity and friction effects, heavy sand may have a lower velocity than the mixture in the tube. This means that the average delivered density in the hopper is lower than the measured density. The coarser the sand, the higher the slip factor is.

The first two effects are compensated by automatic calibration when pumping water.

Incoming Mixture Velocity/Flow rate

Mixture velocity is usually measured with Electromagnetic Flow (EMF) meters. Although the name suggests that the flow is measured it is actually the velocity that is measured. Electric coils are used to generate a magnetic field in the tube. Perpendicular to the induced field, two electrodes (on each side of the tube) measure a voltage.

This voltage is proportional to the velocity. Modulation techniques are used to obtain a proper signal-to-noise ratio. The measured voltage is given by the following equation:

$$U = kB\tilde{v}d_p,$$

where k is a constant, B the magnetic field strength, $\tilde{v}$ average velocity and d_p the pipe diameter. Once the velocity is known, the flow is calculated as follows:

$$Q_i = \frac{1}{4}\pi d_p^2 \tilde{v}$$

Pump Control

The pump controller is used to control the flow rate through the pipe line by varying the pump speed. To maintain a constant flow rate, the pump controller increases the pump speed when the density increases and lowers the pump speed when the density decreases. Therefore, hoisting the drag head will not lead to an increasing flow rate. Overload and excessive fuel rate are avoided. The pump controller is used by experienced operators at the end of the dredging cycle to reduce the inflow velocity, in order to minimise the overflow losses.

Drag Head Control

An active drag head has several actuators that are used for control. There is a hydraulic actuator that controls the visor angle. Moreover, a water valve is installed for creating a bypass for the inflowing water. The water valve is opened when the pressure at the pump inlet becomes too low and the manometric head of the pump drops.

The drag head is controlled either manually or automatically. In manual mode, the operator controls the visor angle by pressing buttons or using levers. A controller can regulate the visor angle to control the excavation depth or it can regulate the pressure of the hydraulic actuators of the visor. In automatic mode, a constant visor force is applied on the bottom. This way the visor follows the contour of the bottom.

Automatic Drag head Winch Control

The Automatic Drag head Winch Control (ADWC) controls the winches to maintain a certain geometric configuration of the pipe. There are several set-points which define the area in which the drag head is allowed to move. If the drag head violates these limits, it is hoisted to prevent that the pipe damages.

Automatic Light Mixture Overboard

The Automatic Light Mixture Overboard (ALMO) system operates a valve behind the dredge pump. If the density of the mixture is lower than a certain threshold, this valve is opened and the mixture flows overboard instead of in the hopper. This prevents the low-density mixture to dilute the hopper content when dredging silt. The ALMO can also be used to redirect the incoming flow overboard when the flow rate is higher than a certain threshold. A high flow rate can lead to large turbulence and a reduced settling performance in some cases.

2.5 Power Train

The total available power is divided over three main processes: dredge pumps, jet pumps and the propulsion system. The latter can be divided into power for the main propulsion and the lateral bow thrusters. There are a variety of possible power configurations. Dredging companies have their own preference of what configuration is best.

A commonly used configuration is the direct-drive system (see Fig. 2.14). The diesel engines drive the dredge pumps, as well as the propulsion of the ship. When the diesel engine speed is controlled to control the pump speed, the propeller rotational velocity, as well as the generator speed, is varying. This limits the controllability, since the generator grid frequency must stay within limits to avoid damage to the electrical appliances.

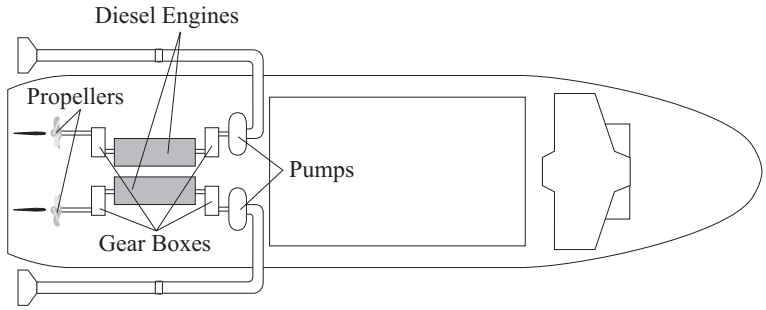

Figure 2.14: Diesel direct configuration.

The second configuration is the hopper dredger with submerged pumps (see Fig. 2.15). For suction depths more than 30 m, the submerged pump is commonly used. A submerged pump allows for higher incoming densities. Especially at large suction depths this is economically attractive. A diesel engine drives the propeller and a generator for driving the electric motors of the submerged pumps. This configuration does have one or two inboard pumps (not shown) to pump the material ashore.

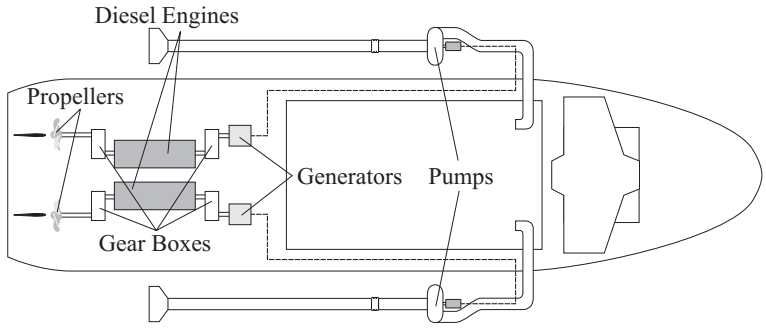

Figure 2.15: Underwater pump configuration.

In the all-electric ship, all power consumers are powered by an electric motor.

The two diesel engines drive the generators (see Fig. 2.16). This is the most flexible configuration for optimal power distribution. This configuration is more expensive than the other two.

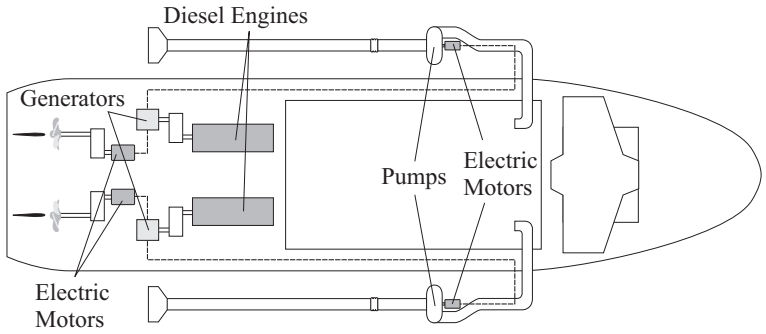

Figure 2.16: All electric configuration.

2.6 Propulsion System

The most commonly used propulsion system for a hopper dredger is a propeller with variable blade pitch. The hopper is usually equipped with two propellers. Each propeller is powered by a diesel engine or an electric motor. For the diesel-driven propellers, the thrust force is controlled by adjusting the pitch of the propeller blades. The shaft rotational velocity can be controlled between 70% and 100% of the maximum diesel engine speed to control the pumps. Besides the main propulsion system the ship is equipped with lateral thrusters for accurate positioning and complicated manoeuvres.

2.7 Economical Loading: Tangent Method

The subject of economic loading involves the complete dredging cycle. Near the end of the dredging, the overflow losses increase rapidly. This can be unattractive from an economic point of view or it can be environmentally unfriendly in case fine grained sediment is discharged into the surface water. In this situation the ship uses up fuel while the sand mass in the hopper only increases marginally. A method has been developed to assist the operators in deciding when to stop dredging, the so-called tangent method.

The amount of sand in the hopper can be expressed in Tons of Dry Solids (TDS). This is the mass of sand when all the water is removed. During loading of the hopper, the amount of sand increases. When the mixture level in the hopper reaches the overflow, a mixture of water and sand flows overboard. Usually these overflow losses increase towards to the end of the dredging cycle. The overflow losses can become as high as the incoming production rate, so that the mass of sand remains constant in the hopper.

From the TDS, the production per time unit is calculated by dividing the TDS in the hopper by the total cycle time. Graphically this is done by drawing a line from the point when the dredging has stopped in the previous cycle to the TDS value at that moment. The gradient of this line represents the production per time unit for at that moment for the complete cycle. For the most economical loading this gradient is maximum (IHC Holland, 1991). The time corresponding to that situation is the optimum dredging time.

To illustrate the tangent method, two effects that affect the optimal dredging time are illustrated in Fig. 2.17 and Fig. 2.18. First, the effect of the soil type will be described and then the influence of the sailing and discharge time.

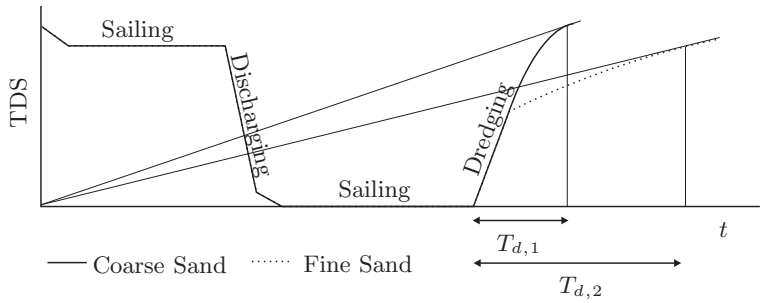

Figure 2.17: The dependence of the optimal dredging time on soil type.

A TSHD encounters different soil types while dredging. Each soil type exhibits a different sedimentation behaviour in the hopper. Coarse sand will settle faster than fine sand. Consequently, when the overflow phase starts, more grains will be in suspension for fine sand than for coarse sand. Therefore, the overflowing mixture has a higher density with fine sand than with coarse sand. Fig. 2.17 shows the two TDS graphs of the two soil types. The TDS graph of fine sand has a sharp bend as result of the overflowing sand mass. Therefore, the filling of the hopper takes more time and the dredging time increases. A line is drawn from the point where the previous dredging cycle has stopped. The optimal dredging time is where the tangent line touches the TDS graph. For coarse sand the optimal dredging time is much shorter. The ideal stopping time for coarse sand is $T_{d,1}$ and for fine sand it is $T_{d,2}$.

Off-line this analysis is straightforward, but on-line it is not. Due to measurement noise and uncertainties in the measurements or due to a temporary reduction in incoming density, the gradient of the line may decrease. An operator can falsely interpret this phenomenon and, incorrectly draw the conclusion that the optimal dredging time has been reached.

Fig. 2.18 shows the influence of the sailing time on the optimal stopping time. For a longer sailing time, $t_{sail,2}$ instead of $t_{sail,1}$, the optimal stopping time increases from $T_{d,1}$ to $T_{d,2}$. Again, this is demonstrated in the figure by the tangent line method. A line is drawn from the moment the dredging has stopped in the previous cycle, t_1 for the short cycle and t_2 for the long cycle, to the TDS curve of the current cycle. For a longer sailing time, the tangent point t_2 will be right of t_1 and, according to the tangent line, the optimal stopping time increases from $T_{d,1}$ to $T_{d,2}$.

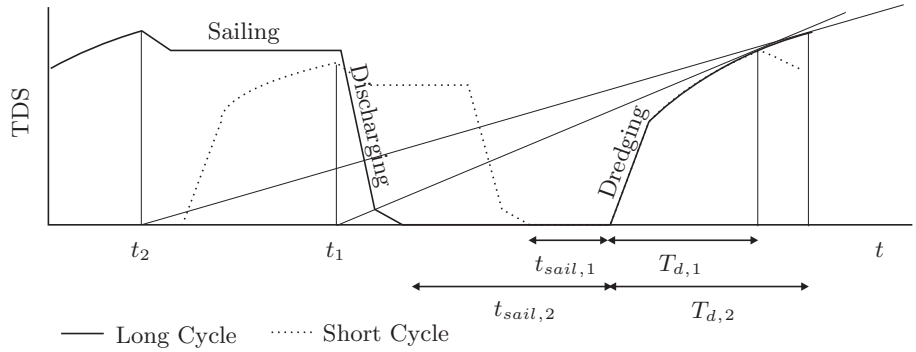

Figure 2.18: Dependence of the optimal dredging time on the sailing and discharging time.

2.8 Data

For this project, three different data sets are available. Two of the data sets are measured on board of a TSHD and one is measured on a test rig.

The first data set, hereafter called data set A, was obtained on a test rig at MTI, focussing in detail on the important processes in the hopper with regard to the sedimentation process. The data contain information from sensors measuring inside the mixture of the hopper, used for the validation of the hopper model, discussed in sections 3.2 and 4.3

The second data set, data set B, was measured on a ship with one suction pipe that was excavating sand for land reclamation. These measurements were taken using the standard data acquisition protocol used on board. After studying this data set it turned out that not all measurements relevant for our research have been recorded. For example, the operator set-points are not stored. Therefore, in a third measurement, data set C, all the relevant variables were measured. This time the project was not land reclamation, but maintenance dredging in a large waterway. Since our focus is on optimisation of sand production, this project is not particularly suitable and the data from many dredging cycles have been discarded, because the dredged material of those cycles is not sand. Nevertheless, this data set is suitable for our investigation on ship motion and power consumption.

3

Modelling the Trailing Suction Hopper Dredger Dynamics

In the previous chapter we have seen the system overview of the trailing suction hopper dredger (TSHD) and defined our objective to improve the system performance with use of an advanced control technique. To apply the theory of advanced control, we must derive a model for the hopper dredger. This is a control-oriented model for the use of control design and system simulation. The total system consists of several smaller subsystems, each with its own function. A detailed model description of each of these smaller systems is presented in this chapter. Parts of this chapter have been published in (Braaksma, Klaassens, Babuška and de Keizer, 2007a).

There is a large variety of models available from the literature, each describing a part of the TSHD process. Some areas are covered very well, such as the hopper sedimentation process and pump-pipeline behaviour, but for a part of the system, such as the drag-head excavation process, there are hardly any models available. The models described in the literature have not been developed for control and process optimisation. Moreover, there have been only a few studies investigating the interaction of the processes and an optimal control strategy for the dredging process. The aim of this study is to develop a control-oriented model that covers the whole process of the TSHD for optimising the performance. For the unknown parts of the system, either black-box models or simple physical models are developed. These models capture the main dynamic behaviour of the system.

In literature, the focus of modelling has always been on isolated parts of the total system (Camp, 1946; de Bree, 1977; Miedema, 1987; Matoušek, 1997; van Rhee, 2002). However, the interaction between the subsystems is very important for optimal control of the total process. The influence of a particular subsystem on the performance is not constant and may vary over time. Moreover, for every soil type this relation is different.

The main reasons for modelling the total dredging process are:

- Controller testing: the model is developed for testing and validation of the control strategies.
- Model-based control: it is possible to develop a model predictive controller (MPC) that uses an internal model to optimise the performance.

- Estimation of unmeasured variables, such as the sand bed mass in the hopper (i.e., the model is used to derive an observer or virtual sensor).

The models of the dredging process, available in the literature, are detailed and sometimes based on partial differential equations (PDEs) (van Rhee, 2002). This modelling approach leads to complicated models with many parameters which are dependent on soil type and on uncertain influences, such as the grain-size distribution and in situ soil conditions. On a laboratory scale, these models perform very well, because the parameters can be obtained from on-line and off-line measurements, and the soil type and also the grain size distribution are known (Miedema, 1987; Vlasblom and Miedema, 1995; Matoušek, 1997; van Rhee, 2002). Unfortunately these parameters are not known in practice. Moreover, if such data are available from a survey it is still uncertain how to interpolate between the surveyed locations of the dredging area.

For model-based control it is required that the process is modelled such that the parameters can be obtained from on-line measurements. The requirements for the models, therefore, are the following:

- Accuracy: for on-line optimisation, a certain accuracy is required, but accuracy is usually achieved at the cost of computational time. Model-based optimisation techniques use a model to compute the best strategy. This requires many model simulations. For on-line applications the time for computing the control inputs is limited. Therefore, models for the use of on-line control should be fast. The models should be as accurate as possible within the constraints on computational time and parametrisation.

- Complexity and parametrisation: the most accurate models are based on PDEs. With increasing complexity, however, the computational effort also increases. We should find models with the least computational effort but still capture the most dominant effects which are important for the optimisation. Often it is possible to approximate the system with a 1-D description, that captures the effect in the direction that is dominant in the production. For the ship model this is the forward speed, for example.
  The dredging process is characterised by a changing environment. When the soil parameters change, the dynamic behaviour of all the systems changes. Therefore, the soil-type-dependent parameters must be adapted on-line during the process. The models should have as few parameters as possible and the model structure should be such that these parameters can be estimated from the measured data.

- White box versus black-box modelling: related to the previous requirement, physical models tend to become very complex and have a large number of parameters. Moreover, some parts of the system are not very well understood and, therefore, not modelled in the literature. In summary, the total model will be a combination of white box physical models and black-box data-driven models.

3.1 An Overview of the Overall Model

Functionally, the model of the overall dredging process can be divided into five parts: the power train model, the ship motion model, the drag head model, the pump-pipeline model and the hopper model, as shown in Fig. 3.1. The five functions are:

- Powering: a diesel engine powers the power consumers and distributes this power via the power train. The main power consumers are propellers/bow thrusters, dredge pumps and water jet pumps.
- Sailing: the ship movement is controlled by the propellers, the bow thrusters and the rudders.
- Transport: the excavated material in the drag head is transported by the pump and pipeline into the hopper.
- Excavating: the material is excavated by the drag head.
- Storage: the material is stored temporarily in the hopper where the sedimentation takes place.

Fig. 3.1 shows the interconnections of the sub-models. Each section in this chapter describes one block, as denoted in the figure below. For example, the hopper model describes the relation of the input variables: incoming flow rate Q_i, incoming density ρ_i and the set-point for overflow height h_o, to the output variables: total hopper mass m_t and total hopper volume V_t. Besides the interconnecting variables, there are internal state variables in the blocks, such as the mass of the sand bed m_s in the hopper model.

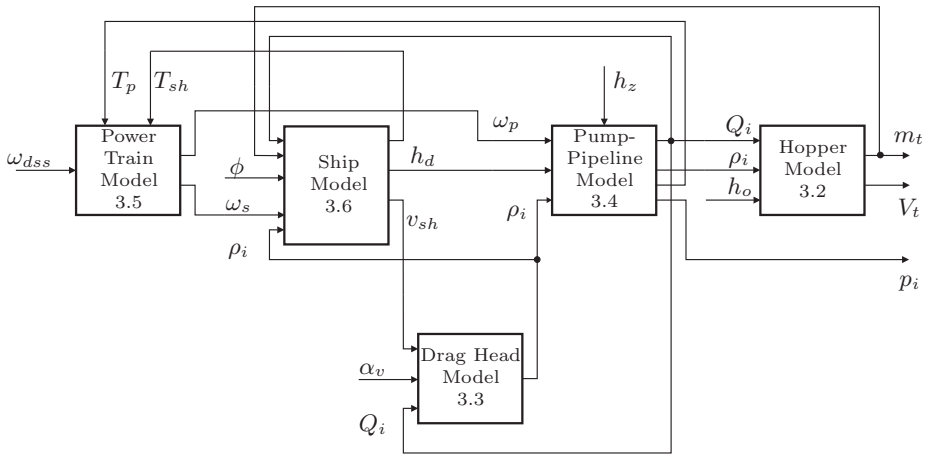

Figure 3.1: Block scheme of the overall process model.

Before going further into the details of the model, each sub-model will be described briefly. The power train model receives a set-point for the diesel engine speed (ω_{dss}). The actual speed is determined by the dynamics of the system, which are influenced by the torques of the pump (T_p) and the propeller (T_{sh}). The diesel engine speed is reduced in two gear-boxes, one for the pump speed (ω_p) and one for the propeller speed (ω_s).

The ship's forward speed (v_{sh}) is controlled by the pitch angle of the propellers (ϕ). The pitch angle and the rotational velocity of the propeller determine the thrust force. This force is related to the amount of excavated material; thus, the ship model

has the density of the drag head and the flow rate as input. The draught of the ship (h_d) depends on the mass in the hopper m_t.

The flow rate in the pump and pipeline is controlled by the pump speed ω_p. The pressure drop in the pipeline depends on the density in the pipe and pump (ρ_i), the pump position under the water level (related to h_d) and on the dredging depth (h_z). The absolute pressure at the inlet of the pump is given by p_i. A water valve α_v, located on the drag head can be used to dilute the mixture in the drag head. This control variable is used to lower the density to avoid the pump from cavitating, when inlet pump pressure is near its allowed minimum.

3.2 Hopper Model

Prior to stating the modelling problem, see Fig. 3.2, we briefly describe the loading process of the hopper. This process shows three different phases:

- In the first phase, the height of the hopper content (h_t) is lower than the height of the overflow weir (h_o, see Fig. 3.3 for the definition of the symbols).
- The second phase starts when the mixture level in the hopper has reached the overflow weir. The overflow weir height and, thus, the volume remain constant and, therefore, this phase is called the constant-volume phase. Typically, water or low-density mixture is flowing overboard in this phase.
- The third phase starts when the ship has reaches its maximal draught. The overflow weir is automatically lowered such that a constant hopper mass is maintained. This phase is called the constant-tonnage phase and the overflow losses are typically bigger than in the constant-volume phase. This phase ends when the losses become so high that it is no longer economically feasible to continue dredging.

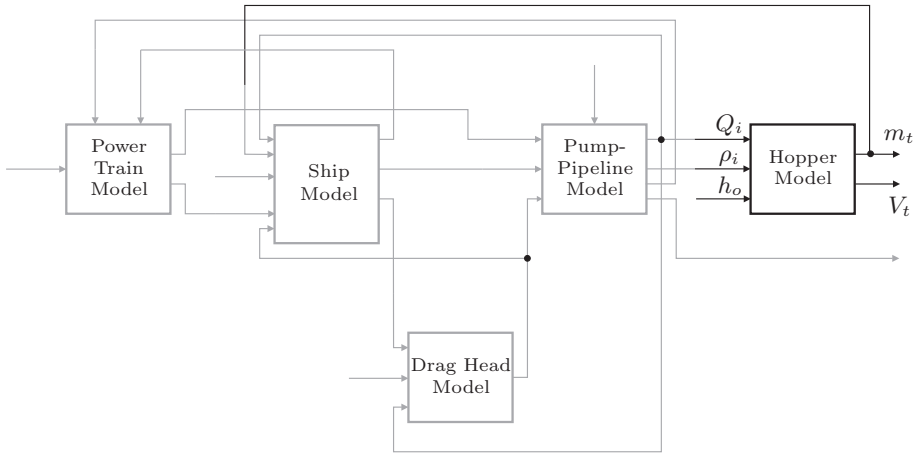

Figure 3.2: A block diagram of the total process model, where the hopper model is highlighted.

From the drag head a mixture with flow rate Q_i and density ρ_i flows into the hopper and forms a mixture with an average density ρ_m. The sand settles with a flow rate Q_s at the bottom of the hopper where a sand bed forms with height h_s and density ρ_s (see Fig. 3.3). In the second and the third phase, mixture from the top layer is discharged through the overflow with flow rate Q_o. In the beginning, the density ρ_o is low and, thus, the losses, but as the sand bed grows, the losses become bigger. These losses can become as high as the incoming mass. The loading stops when it is not economically feasible to continue. The sedimentation rate and overflow losses depend heavily on the type of soil and can be affected by the incoming flow rate Q_i and density ρ_i.

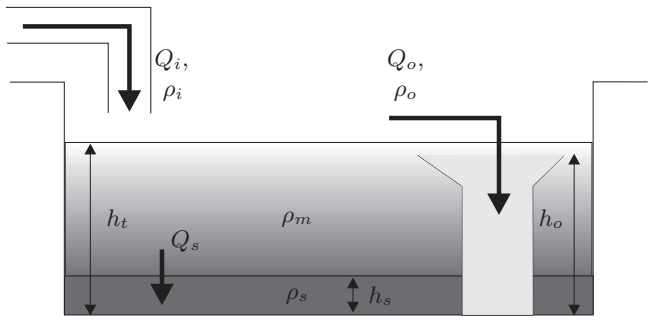

Figure 3.3: The sedimentation process in the hopper.

In the literature, a number of sedimentation models have been proposed (Camp, 1946; Yagi, 1970; Ooijens, 1999; van Rhee, 2002). These models, however, cannot be used for real-time control or optimisation of the dredging process. The reason is that they are based on detailed modelling of the physical phenomena and therefore contain too many uncertain parameters. Moreover the computation time is often too large for the use in the optimisation algorithms. Therefore, it is proposed here to use simplified and computationally efficient models for our model-based controller. On the other hand the detailed models are useful for simulating the process and for testing the model-based control techniques, but in this thesis the process model and the model in the model-based controller are in the same model set.

3.2.1 Mass-Balance Equations

The model has three state variables: the total mass in the hopper (m_t), the total volume of the mixture in the hopper (V_t) and the mass of the sand bed (m_s). The sedimentation dynamics are described by the following differential equations:

$$\begin{aligned} \dot{V}_t &= Q_i - Q_o \\ \dot{m}_t &= Q_i\rho_i - Q_o\rho_o \\ \dot{m}_s &= Q_s\rho_s\,. \end{aligned} \tag{3.1}$$

The first two equations represent the volume and mass balance, respectively. The third equation gives the rate of sand sedimentation, where Q_s is the sand flow rate from the mixture layer to the sand bed layer and ρ_s is the sand bed density.

Gravity is the driving force of the sedimentation flow Q_s. A single grain settles with a velocity v_{s0}, but particles in a dense suspension have a lower settling velocity. Based on experiments, Richardson and Zaki (1954) suggested an expression for the actual settling velocity:

$$v_s = v_{s0}(1 - C_m)^{\beta}\,, \tag{3.2}$$

where

$$C_m = \frac{\rho_m - \rho_w}{\rho_q - \rho_w}$$

is the volumetric concentration of the mixture, with ρ_m the mixture density, ρ_w the density of water and ρ_q the density of sand (quartz). The parameter β depends on the particle Reynolds number and v_{s0} is the undisturbed settling velocity of a grain. Both parameters are soil type dependent.

The sedimentation process exhibits a discontinuity in density and velocity at the sand bed height $h_s(t)$, called a shock front. The evolution of the sand bed layer across the shock front follows from the conservation of mass:

$$\frac{\partial}{\partial t}\iiint_V \rho\, dV = \iint_A \rho v_s\, dS\,,$$

where V is the control volume, A the area through which mass is flowing in or out of the control volume and v_s the settling velocity of the particles. In our 1D case, this equation simplifies to, (van Groesen and Molenaar, 2007):

$$\frac{d}{dt}\int_0^b \rho(h)\, dh = [\rho(h)v_s(h)]_0^b\,, \tag{3.3}$$

where the density $\rho(h)$ and the velocity $v_s(h)$ are functions of the height h and b is a point well above the sand bed height h_s. Splitting the integral at the left-hand side, we obtain:

$$\frac{d}{dt}\int_0^b \rho(h)\, dh = \frac{d}{dt}\left\{\int_0^{h_s(t)} \rho(h)\, dh + \int_{h_s(t)}^b \rho(h)\, dh\right\} = (\rho_s - \rho_m)\frac{dh_s}{dt}\,. \tag{3.4}$$

The right-hand side of equation (3.3) is:

$$[\rho(h)v_s(h)]_0^b = \rho_s \cdot 0 - (-\rho_m v_s + \rho_w v_s)\,. \tag{3.5}$$

The first term is zero because the velocity of the particles in the sand layer is zero. The second term $-\rho_m v_s$ is the mass flux of the particles settling in the mixture. The third term $\rho_w v_s$ is the mass flux of water flowing upward as a result of the settling of the particles.
Combining (3.4) and (3.5) gives the following expression:

$$(\rho_s - \rho_m)\frac{dh_s}{dt} = (\rho_m - \rho_w)v_s\,. \tag{3.6}$$

Substituting (3.2) into (3.6) leads to:

$$\frac{dh_s}{dt} = v_{s0}\frac{\rho_m - \rho_w}{\rho_s - \rho_m}\left(\frac{\rho_q - \rho_m}{\rho_q - \rho_w}\right)^{\beta}\,. \tag{3.7}$$

Near the sand bed erosion takes place. According to van Rhee (2002) the erosion is a function of the shields parameter θ, with: $\theta = kv_{local}^2$, with k some constant. The erosion depends on the local flow-velocity v_{local}. This local flow-velocity is caused by density currents above the sand bed. In our 1-D approximation this local horizontal flow-velocity is not modelled or known. Therefore, we assume uniform flow velocity distribution, which means that the horizontal flow velocity s_0 in the hopper is equal over the height:

$$s_0 = \frac{Q_o}{W_{sh} h_m} ,$$

where W_{sh} is the width of the hopper and $h_m = h_t - h_s$ the mixture height. The erosion factor becomes:

$$\mu = \min \left(\frac{Q_o^2}{(k_e h_m)^2}, 1 \right) , \tag{3.8}$$

with k_e the erosion factor which is dependent on the soil type and the width W_{sh}. The sedimentation rate of the sand bed is modified to include the erosion effect as follows:

$$\frac{dh_s}{dt} = (1-\mu) v_{s0} \frac{\rho_m - \rho_w}{\rho_s - \rho_m} \left(\frac{\rho_q - \rho_m}{\rho_q - \rho_w} \right)^{\beta} .$$

Finally the expression for the sand flow rate follows from $Q_s = A \frac{dh_s}{dt}$:

$$Q_s = A(1-\mu) v_{s0} \frac{\rho_m - \rho_w}{\rho_s - \rho_m} \left(\frac{\rho_q - \rho_m}{\rho_q - \rho_w} \right)^{\beta} , \tag{3.9}$$

where A is the hopper area.

3.2.2 Overflow Rate

The volume of material in the hopper is given by the volume balance (see (3.1)). The incoming flow rate fills the hopper until the level reaches the height h_o of the overflow weir. From that moment mixture flows out of the hopper with a flow rate Q_o. This flow rate is modelled as follows (Franzini, 1997):

$$Q_o = k_o \max(h_t - h_o, 0)^{\frac{3}{2}} , \tag{3.10}$$

where k_o is a parameter depending on the overflow weir shape and circumference.

Modern dredgers are often equipped with a constant tonnage controller. This controller lowers the overflow height as the maximum draught of the ship has been reached. In this way the maximum draught is maintained and the dredging can continue. During this phase the hopper mass stays constant, but the density in the hopper increases. The overflow is controlled by a PI controller with an anti-windup element. This is modelled as follows:

$$\begin{aligned} \dot{h}_i &= \frac{k_{pc}}{\tau_c}(m_{t,max} - m_t) - k_{ac}(h_{i2} - h_o) \\ h_{i2} &= h_i + k_{pc}(m_{t,max} - m_t) \\ h_o &= \min(\max(h_{i2}, h_{o,min}), h_{o,max}) , \end{aligned} \tag{3.11}$$

where h_{ci} is the output of the integrator, k_{pc} the P-gain, τ_c the integration time constant, $m_{t,max}$ the maximum allowed mass in the hopper, k_{ac} the anti-windup gain, $h_{o,min}$ the minimum height of the overflow weir and $h_{o,max}$ the maximum height of the overflow weir.

3.2.3 Overflow Density

An accurate prediction of the overflow density ρ_o requires a model of the density profile in the mixture above the sand bed. The density is a decreasing function of the height above the sand, but the exact form of this function is uncertain and varies with time. Three models are proposed in this section: a linear model, an exponential model and a piece-wise constant (water-layer) model.

Linear Model

This model assumes that the mixture density (ρ_m) decreases linearly in the upward direction. Under this assumption, the general density ($\rho(h)$) of a particular height h above the hopper bottom is given by:

$$\rho(h) = \max\big(\rho_s - k_{\rho_l}(h - h_s), \rho_w\big)\,. \tag{3.12}$$

The only parameter in this equation is the slope $k_{\rho l}$. It can be determined uniquely by considering the fact that the average mixture density ρ_m,

$$\rho_m = \frac{m_t - m_s}{V_t - \frac{m_s}{\rho_s}} = \frac{\rho_s(m_t - m_s)}{V_t\rho_s - m_s}\,, \tag{3.13}$$

must be equal to the average of the density profile (3.12):

$$\rho_m = \frac{1}{h_m}\int_{h_s}^{h_t} \max\big(\rho_s - k_{\rho_l}(h - h_s), \rho_w\big)\mathrm{d}h\,, \tag{3.14}$$

with $h_m = h_t - h_s$. To solve (3.14) for $k_{\rho l}$, one needs to distinguish the two situations depicted in Fig. 3.4.

The height h in the hopper is given on the x-axis and the density ρ on the y-axis. The top panel shows three layers in the hopper. The sand bed at the bottom with density ρ_s for $0 \le h < h_s$, the mixture layer with density decreasing over the height for $h_s \le h < h_x$ and a water layer with density ρ_w for $h_x \le h < h_t$. In this situation the average mixture density ρ_m is so low that the mixture only reaches the height h_x. The integral in (3.14) then equals to:

$$\rho_m = \frac{1}{h_m}\left(\rho_w h_m + \frac{1}{2}h_x(\rho_s - \rho_w)\right)\,,$$

from which we can express:

$$h_x = \frac{2h_m(\rho_m - \rho_w)}{\rho_s - \rho_w}\,, \tag{3.15}$$

and compute the slope as:

$$k_{\rho_l} = \frac{\rho_s - \rho_w}{h_x} = \frac{(\rho_s - \rho_w)^2}{2h_m(\rho_m - \rho_w)}\,. \tag{3.16}$$

The bottom panel of Fig. 3.4 shows the situation that there is no water layer. In this case the linear density gradient spans the complete mixture height. The indicated

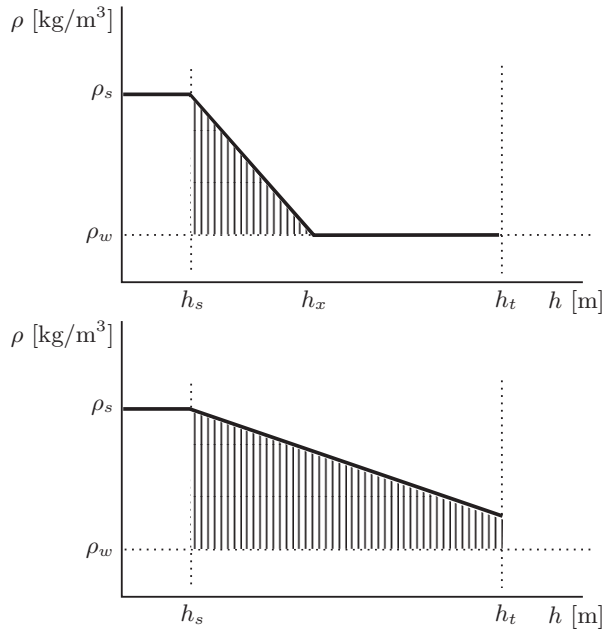

Figure 3.4: Two different situations with the linear density profile: top, mixture layer with water layer on top; bottom, $\rho_m > \frac{1}{2}(\rho_w + \rho_s)$.

triangle spans the entire mixture layer. The substitution $h_x = h_m$ into (3.15) gives the limit condition for ρ_m:

$$\rho_m = \frac{1}{2}(\rho_w + \rho_s)\,. \tag{3.17}$$

If $\rho_m > \frac{1}{2}(\rho_w + \rho_s)$, the integral in (3.14) includes the trapezoid, as shown in the bottom panel of Fig. 3.4. The slope becomes:

$$k_{\rho_l} = \frac{2(\rho_s - \rho_m)}{h_m}\,. \tag{3.18}$$

Combining equations (3.16) and (3.18) yields the final equation for the slope:

$$k_{\rho_l} = \begin{cases} \frac{2(\rho_s-\rho_m)}{h_m} & \text{for} \quad \rho_m > \frac{1}{2}(\rho_w + \rho_s) \\ \frac{(\rho_s-\rho_w)^2}{2h_m(\rho_m-\rho_w)} & \text{otherwise.} \end{cases} \tag{3.19}$$

The overflow density is obtained by substituting $h = h_o$ into (3.12):

$$\rho_o = \max\left(\rho_s - k_{\rho_l}(h_o - h_s), \rho_w\right)\,. \tag{3.20}$$

Equations (3.19) and (3.20) constitute the linear model for the overflow density ρ_o.

Exponential Model

This model assumes an exponentially decreasing function of the height above the sand layer, see Fig. 3.5. This model consists of two layers. A sand-bed layer with density ρ_s for $0 \leq h < h_s$ and a mixture layer with an exponentially decreasing density for $h_s \leq h < h_t$. In the limit with $h \to \infty$ the density goes to $\rho \to \rho_w$.

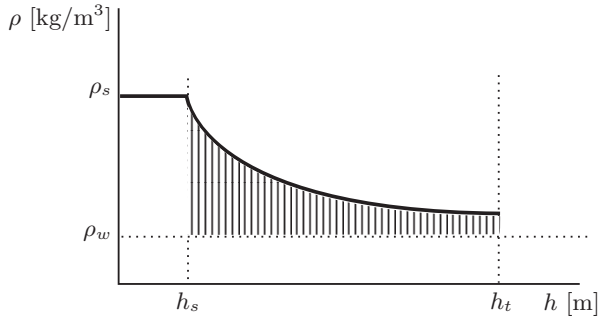

Figure 3.5: Density profile of the exponential model.

The density $\rho(h)$ at height h is given by:

$$\rho(h) = \rho_w + (\rho_s - \rho_w)e^{-k_{\rho_e}(h-h_s)}\,. \tag{3.21}$$

The coefficient k_{ρ_e} can again be determined uniquely by considering the fact that the average mixture density ρ_m (3.13) must equal the average of the exponential profile:

$$\rho_m = \frac{1}{h_m}\int_{h_s}^{h_t} \rho_w + (\rho_s - \rho_w)e^{-k_{\rho_e}(h-h_s)}\mathrm{d}h\,.$$

Computing the integral, we obtain the equation:

$$\rho_m = \frac{\rho_s - \rho_w + \rho_w k_{\rho_e} h_m - (\rho_s - \rho_w)e^{-k_{\rho_e} h_m}}{h_m\, k_{\rho_e}}\,,$$

that can be rearranged as:

$$1 - ak_{\rho_e} = e^{bk_{\rho_e}}\,, \tag{3.22}$$

with

$$a = \frac{h_m(\rho_m - \rho_w)}{\rho_s - \rho_w} \quad \text{and} \quad b = -h_m\,.$$

Although this equation cannot be directly solved for $k_{\rho e}$, through algebraic manipulation we can change it into the form $y = xe^x$, of which solution is $x = W(y)$, where W is Lambert's W function (Corless et al., 1996).

To solve, first one has to multiply both sides of (3.22) by $\frac{b}{a}e^{\frac{b}{a}-bk_{\rho_e}}$ to obtain the following equation:

$$(\frac{b}{a} - bk_{\rho_e})e^{(\frac{b}{a}-bk_{\rho_e})} = \frac{b}{a}e^{\frac{b}{a}}\,,$$

which solution is:

$$\frac{b}{a} - bk_{\rho_e} = W\left(\frac{b}{a}e^{\frac{b}{a}}\right)\,.$$

Finally express k_{ρ_e}:

$$k_{\rho_e} = \frac{1}{a} - \frac{1}{b} W\left(\frac{b}{a} e^{\frac{b}{a}}\right)$$

and substitute back for a and b:

$$k_{\rho_e} = \frac{1}{h_m}\left[\frac{\rho_s - \rho_w}{\rho_m - \rho_w} + W\left(\frac{\rho_s - \rho_w}{\rho_w - \rho_m} e^{\frac{\rho_s - \rho_w}{\rho_w - \rho_m}}\right)\right]. \tag{3.23}$$

As Lambert's W function only depends on one variable ρ_m, it can be easily approximated by a polynomial, in order to reduce the computation time. To make the approximated function independent of the parameters ρ_s and ρ_w, define:

$$f(k) = W\left(-\frac{1}{k} e^{-\frac{1}{k}}\right),$$

where $k = \frac{\rho_m - \rho_w}{\rho_s - \rho_w}$ and $k \in (0, 1]$. Function $f(k)$ can be accurately approximated by a 12th-degree polynomial:

$$f_p(k) = p_0 + p_1 k + \cdots + p_{12} k^{12},$$

where the coefficients are found by least-squares fitting. The overflow density is obtained by substituting $h = h_o$ into (3.21):

$$\rho(h) = \rho_w + (\rho_s - \rho_w) e^{-k_{\rho_e}(h - h_s)}. \tag{3.24}$$

Equations (3.23) and (3.24) constitute the exponential model for the overflow density ρ_o.

Water-Layer Model

The density profile above the sand layer is approximated by a two-layer (piece-wise constant) model (Fig. 3.6). This model assumes that a thin water layer is formed on top of the mixture soup layer (van Rhee, 2002; Ooijens, 1999). This layer is formed by an upward flow of water which is caused by the settling of the grains. The displacement of a volume of grains downwards invokes the same volume of water flowing in the opposite direction.

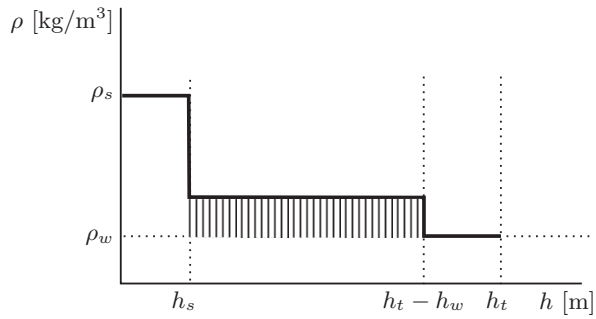

Figure 3.6: Density profile of the water-layer model.

The overflow rate (Q_o) is the sum of the water flow (Q_w) and the mixture soup flow (Q_{ms}) (see Fig. 3.7). We assume that Q_w flowing out of the hopper equals the upward water flow at the bed height. The positive flow Q_w is directed upward and the flow of the solids is directed downwards (see Fig. 3.7). The water flow is equal to the flow of the solids through the mixture:

$$Q_w = Q_{solids}\,,$$

where Q_{solids} is the volumetric flow of the grains (solids) in the mixture. Note that Q_{solids} is different from Q_s, because Q_s is the sand flow rate relative to the sand bed and, because this bed is rising, Q_s is different from Q_{solids}. The flow of solids through an area in the hopper is given by:

$$Q_{solids} = A_s v_s = AC_{ms} v_s\,,$$

where A_s is the cross-section area of the grains and C_{ms} is the volumetric concentration of the soup. Using (3.2), this leads to the following expression for the water flow Q_w:

$$Q_w = A(1-\mu)v_{s0}\frac{\rho_m - \rho_w}{\rho_q - \rho_w}\left(\frac{\rho_q - \rho_m}{\rho_q - \rho_w}\right)^{\beta}. \tag{3.25}$$

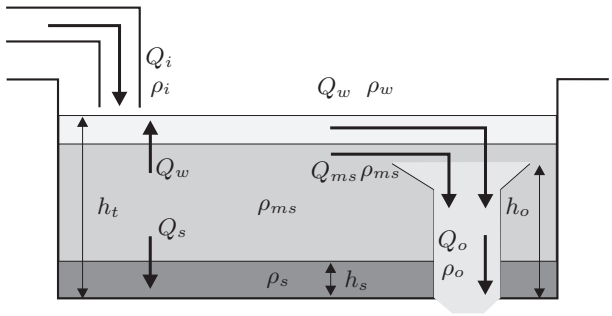

Figure 3.7: A schematic of the water-layer model.

For small Q_o, only pure water from the water layer is flowing out at the overflow. However, when $Q_o > Q_w$ the sand/water mixture flow becomes non-zero:

$$Q_{ms} = \max(Q_o - Q_w, 0)\,. \tag{3.26}$$

The outgoing density ρ_o is given by the mixing the two flows:

$$\rho_o = \frac{\rho_{ms}Q_{ms} + \rho_w Q_w}{Q_{ms} + Q_w}\,. \tag{3.27}$$

The density of this mixture soup can be computed as $\rho_{ms} = (h_m\rho_m - h_w\rho_w)/(h_m - h_w)$. However, as the water-layer height h_w is not known, an additional assumption must be made. We assume that the water layer is very thin and, hence, the mixture soup density ρ_{ms} approximately equals the total mixture density ρ_m, i.e., there is ideal

mixing, which can also be observed in Fig. 8.7 of (van Rhee, 2002). Substituting $\rho_{ms} = \rho_m$ into (3.27), the overflow density is given by:

$$\rho_o = \frac{(\rho_m - \rho_w)Q_{ms}}{Q_{ms} + Q_w} + \rho_w \,. \tag{3.28}$$

Equations (3.25), (3.26) and (3.28) constitute the water-layer model for the overflow density ρ_o.

The three proposed models are calibrated in Chapter 4. Which model performs best is determined based on the calibration and validation results. The best model is used for the control design and in the simulation model.

3.2.4 Soil-Type-Dependent Parameters

The hopper model has four parameters that depend on the type of soil and, therefore, are variable (see Tab. 3.1). The other parameters can be obtained off-line which are not discussed in this thesis.

Table 3.1: Summary of parameters that need to be calibrated with data.

Parameter	Description
ρ_s	Sand-bed density in hopper
v_{s0}	Undisturbed settling velocity
k_e	Erosion pickup flux coefficient
β	Exponent in settling equation based on particle Reynolds number

The next chapter discusses the parameter estimation problem and shows the calibration results, as well as the validation results.

3.3 Drag-Head Model

The drag head is the suction mouth of the hydraulic system that, together with the pump, aspirates a mixture of water and soil. It is used to break the coherence of various soil types. This is done erosive, mechanically or both.

Sand consolidates over time, as the grains are packed together under the influence of gravity and water pressure. The drag head fluidises sand by injecting water under high pressure, and cuts a sand layer if the drag head is equipped with teeth. Sand and water form a mixture in the drag head and are aspirated by the pump (see Fig. 3.8). The resulting water flow, due to the dredge pump, also erodes the grains at the bottom for some additional production. Water can be added into the drag head by opening the water valve to dilute the mixture.

Teeth are mounted on the drag head for the excavation of hard packed sand or cohesive material. These teeth cut a layer of sand that enters the drag head. This cutting process may cause large cutting forces, especially in case of fine and hard-packed sand (Miedema, 1987; Miedema, 1994). Underwater cutting of sand results in the phenomenon which is called dilatancy. During this process the pore volume of the

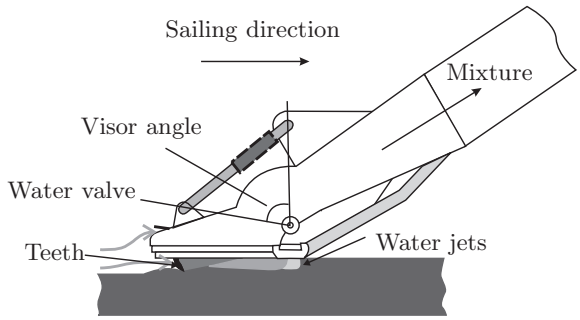

Figure 3.8: Schematic of the drag head.

sand increases at the shear line (see Fig. 3.9). The grains are rearranged and after cutting the pores are filled with more water. This means that water flows though the sand to the shear line during this cutting. When water flows through packed sand there must be a pressure difference. This pressure difference increases the cutting forces.

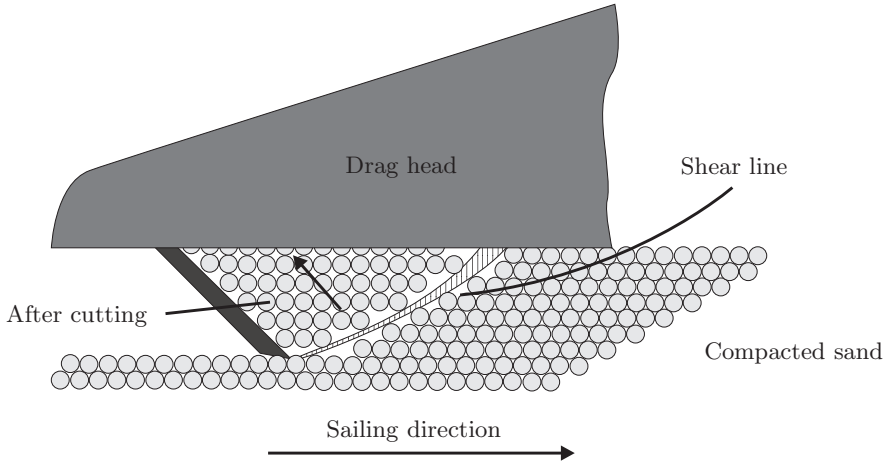

Figure 3.9: Cutting sand

The purpose of the drag-head model is to describe two phenomena:

- The drag head models the production rate which depends on the relevant (control) variables, such as the ships speed, flow rate and water valve angle. Since the pump is used to control the flow rate, the drag-head model must describe the incoming density to predict the incoming production.
- The cutting forces, playing a significant role in the ship's dynamics. High cutting forces require a large propulsion power and this reduces the power available for the pumping process.

The relation of this model to the other models is illustrated in Fig. 3.10.

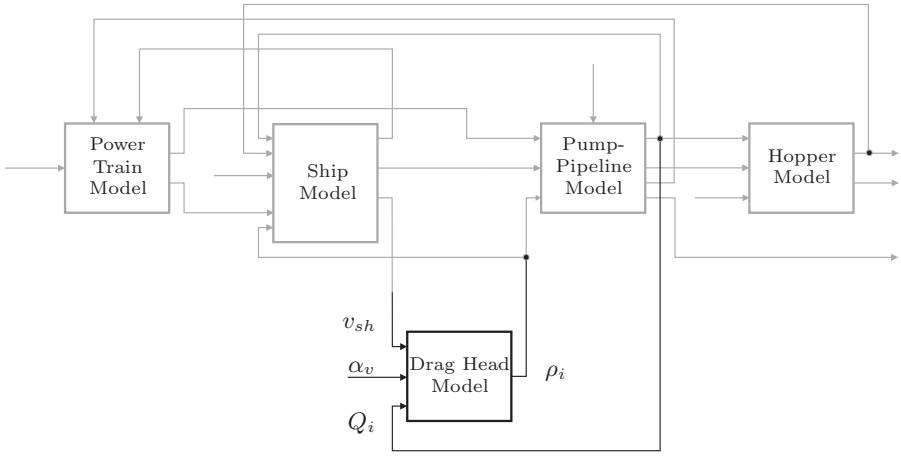

Figure 3.10: A block diagram of the overall process model, where the drag head model is highlighted.

3.3.1 Drag-Head Production Model

The production of the drag head depends on the incoming flow rate and the incoming density. The flow rate of the pump can be controlled by varying the pump speed. Therefore, to simulate the incoming production in the drag head this model should predict the density of the material entering the drag head (ρ_i). The mixture formation in the drag head is a complex process for which not many models are available in the literature (Yagi and Okayama, 1975; Slotta and Heydarpour, 1989; Miedema, 1995). A physical model would have many soil-dependent parameters, such as permeability and in situ density, which are unknown. Moreover, it is unclear how jetting, cutting and eroding interact with each other. Therefore, we decided to use a black-box modelling approach that automatically determines which variables are important for predicting the drag-head density.

There are many data-driven black-box modelling approaches (Ljung, 1987; Sjoberg et al., 1995; Vandewalle and Suykens, 1998). We use a nonlinear data-driven approach that uses a large data set with the measured variables and analyses these with an algorithm that builds polynomial models (Maertens et al., 2005). These models are calibrated on the data. Here follows a description of the conditions under which this model was created:

- The drag head which is used is an uncontrolled drag head with a loose visor.
- The excavated material is coarse sand.
- The water jets are turned on.
- The pump speed is kept constant, so there was no flow control.
- The ship's speed was manually adjusted by an operator. This causes fluctuations in the ship speed between 0.5 m/s and 2 m/s.

- For part of the dredging cycle, the pump inlet pressure is close to the vapour pressure, in particular in the beginning of the dredging process. This means that in these parts the vacuum limitation plays an important role in the excavation process.

From the total data set a subset of variables is chosen that are related to the drag head excavation process. A genetic algorithm searches the large solution space of possible models and selects the best models for the prediction. Variables which have small correlation with the predicted incoming density are excluded from the model and only those variables remain that best predict the density. A detailed description of the procedure is given in Appendix C. This automatic black-box modelling approach, applied by Wangli (2006) results in the following model for the density:

$$\rho_i = -a_{dh} Q_i^2 + b_{dh} v_{sh} + c_{dh} \,, \tag{3.29}$$

where a_{dh}, b_{dh} and c_{dh} are positive coefficients.

This black-box data-driven model must be used with care. It is uncertain if the model is valid under other conditions than those mentioned on the previous page. This means that if the conditions change, not only the parameters change, but also the structure of this model changes. In the first case the parameters should be adapted, but in the second case a new model should be created by repeating the modelling method on the new data set.

The derived model shows that the drag head density is negatively correlated with the flow rate. The flow rate has the largest effect on the density. The sensitivity of the incoming density for the ship speed varies between cycles. It should also be noted that the model is dependent on the type of drag head and the control mode of the drag head. Furthermore, if a variable, such as the water jet flow rate, is kept constant, the method is not able to find that particular correlation, should it exist.

As described above we assumed an uncontrolled drag head; however, the drag head is equipped with a water inlet valve. By opening this valve the incoming density is reduced. This is used to prevent the pump from cavitating. It is assumed that the density in the drag head equals the water density when the valve is fully opened ($\alpha_v = 0$). When the valve is closed ($\alpha_v = 1$), the drag head acts as given in equation (3.29). We postulate that the incoming density can be varied between ρ_w and ρ_i as follows:

$$\rho_i = \alpha_v(-a_{dh} Q_i^2 + b_{dh} v_{sh} + c_{dh}) + (1 - \alpha_v)\rho_w \,, \tag{3.30}$$

where $0 \leq \alpha_v \leq 1$ is the normalized water valve angle for manipulating the incoming density.

3.3.2 Drag-Head Cutting Force Model

The drag-head cutting force model simulates the forces that arise when cutting water-saturated sand. The cutting takes place with a row of teeth mounted on the drag head (see Fig. 3.11). These cutting forces have been studied by Miedema (1987). Because there are unknown parameters and variables it is necessary to make the following assumptions before this model can be derived:

- The teeth are fully injected in the sand if the excavation height is larger than the cutting height, i.e., $h_e > h_c$.

- The spillage of the drag head is neglected, which means that all the excavated material is aspirated in the drag head.
- The in situ density ρ_{si} is assumed to be known.
- The water jets have no influence on the cutting force.
- The heel of the drag head is always in contact with the bottom.

These assumptions are very strict and perhaps not valid in practice; therefore, this model needs improvement in further research if it is to be used in control applications. The model will not consider the vertical force balance, only the horizontal. The fourth item is only true if the amount excavated sand is higher than the jet-production. Unfortunately, the jet production is unknown and therefore this assumption is necessary.

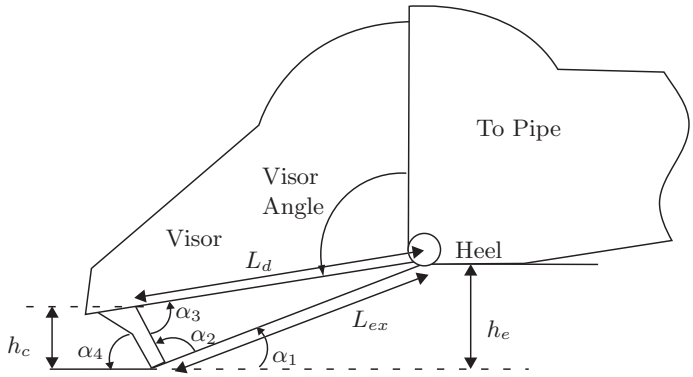

Figure 3.11: The geometry of the drag head for calculating the cutting forces.

There are two possible regimes for the cutting process (Miedema, 1987), non-cavitating cutting and cavitating cutting. For non-cavitating cutting the equation is:

$$F_{cn} = k_c v_{sh} h_c^2 \,,$$

where k_c is the cutting force coefficient for non-cavitating cutting, v_{sh} the ships speed and h_c the cutting height, see Fig. 3.11. For cutting in the cavitating regime the equation is:

$$F_{cc} = k_{ccav}(h_z + 10)h_c \,,$$

where k_{ccav} is the cutting force coefficient for cavitating cutting and h_z the dredging depth. The overall cutting forces are given by the following equation:

$$F_c = \min(F_{cn}, F_{cc}) \,. \tag{3.31}$$

The cutting height h_c depends on the visor angle (see Fig. 3.11). This visor angle is derived from the excavation height (h_e), that is calculated from the mass balance.

If we assume that there is no spillage during excavation and that all excavated sand is aspirated in the drag head, the excavated production rate is:

$$P_d = W_d v_{sh} C_{si} h_e \rho_q \,,$$

where W_d is the width of the drag head, C_{si} the in situ volumetric concentration, h_e the excavated height and ρ_q the density of the sand quartz. Since we assume that there is no spillage, all the sand enters the drag head together with a certain amount of water.
Then, the production rate in the pipeline is given by:

$$P_{in} = C_d Q_i \rho_q \,,$$

where C_d is the incoming volumetric concentration of solids and Q_i the flow rate. Using $P_{in} = P_d$, the following relation for the excavated height can be derived:

$$h_e = \frac{Q_i C_d}{C_{si} W_d v_{sh}} \,, \tag{3.32}$$

where W_d the width of the drag head. By substituting the concentrations:

$$C_d = \frac{\rho_i - \rho_w}{\rho_q - \rho_w} \qquad\qquad C_{si} = \frac{\rho_{si} - \rho_w}{\rho_q - \rho_w}$$

in (3.32), the excavation height becomes:

$$h_e = \frac{Q_i(\rho_i - \rho_w)}{(\rho_{si} - \rho_w) W_d v_{sh}} \,,$$

where ρ_{si} is the in situ density, ρ_i the incoming density in the drag head (calculated in the drag-head model, see Section 3.3), ρ_w the density of water and ρ_q the density of the sand quartz.

Using the sine and cosine rules the angles α_1 and α_2 can be derived from the excavation height, as shown below. The angle α_3 is blade angle.

$$\alpha_1 = \arcsin\left(\frac{h_e}{L_{ex}}\right) \tag{3.33}$$

$$\alpha_2 = \arccos\left(\frac{L_d^2 - L_{th}^2 - L_{ex}^2}{-2 L_{th} L_{ex}}\right) \,, \tag{3.34}$$

with:

$$\alpha_4 = \pi - \alpha_2 - \alpha_1 \tag{3.35}$$

and

$$L_{ex} = \sqrt{L_{th}^2 + L_d^2 - 2 L_{th} L_d \cos(\alpha_3)} \,,$$

where L_d is the distance from the visor rotation point to the teeth connection point, L_{th} the length of the teeth and L_{ex} the distance from the visor rotation point to the tips of the teeth.

For the cutting height two regimes can be identified. If the excavation height h_e is larger than h_c the complete blade is injected in the sand, but if the excavation height

is smaller only part of the blade is injected. In the latter case the cut height equals the excavation height. This results in the following equation for the cut height:

$$h_c = \min(L_{th} \sin(\alpha_4), h_e) \,.$$

The soil-type-dependent parameters of the drag-head model that must be calibrated are summarised in Tab. 3.2

Table 3.2: Summary of the parameters that need to be calibrated with data.

Parameter	Description
a_{dh}	Drag-head density dependence on flow rate
b_{dh}	Drag-head density dependence on ship's speed
c_{dh}	Drag-head density constant
k_c	Cutting force coefficient for non-cavitating cutting
k_{ccav}	Cutting force coefficient for cavitating cutting

3.4 Pump-Pipeline Model

The pump speed (ω_p), coming from the power train model (see Fig. 3.12), determines the pump head, i.e., differential pressure, to control the flow rate in the pipeline. The following disturbances affect this process:

- The density of the mixture has two effects: it changes the hydraulic friction in the pipeline and it changes the pump head that the pump delivers.
- Particle size, the smaller the grain size, the more the delivered pump pressure increases. The pump head is the total pressure difference that the pump supplies to the hydraulic system.
- The draught of the ship influences the static head loss in the pipeline.

The pump pressure accelerates the mixture of water and sand which is formed in the drag head. The mixture is transported through the pipe to the inlet of the hopper. In the pump pipeline model, it is assumed that the slip factor is one, i.e., the grains travel as fast as the water. For a short pipeline on board of the hopper dredger this assumption is justified, because there is enough turbulence to keep the grains in suspension.

The pump-pipeline dynamics are influences by several disturbances. The density in the pipeline influences the hydraulic friction. Moreover, the pressure loss in the pipeline is influenced by the draught of the ship and the dredging depth. Also, the pump pressure is influenced by the varying density of the mixture in the pump.

The pump-pipeline dynamics have been studied extensively (Durand and Condolios, 1952; Fürböter, 1961; Jufin and Lopatin, 1966; de Bree, 1977; Wilson, 1992; Miedema, 1996; Matoušek, 1997). The pump-pipeline model must predict the flow rate Q_i, based on the pump speed ω_p for a given density ρ_i (see Fig. 3.13 for a schematic of

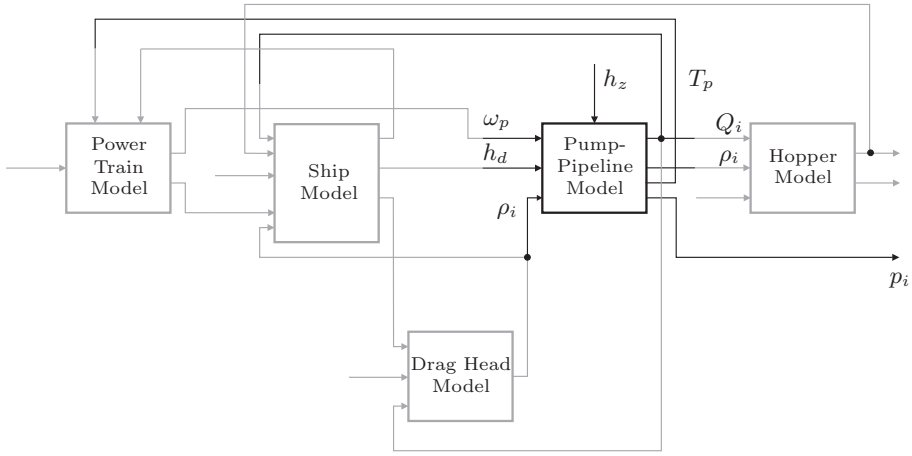

Figure 3.12: A block diagram of the overall process model, where the pump-pipeline model is highlighted.

the pump-pipeline system). The equations for the pump-pipeline model are as follows:

$$\dot{Q}_i = \frac{A_p}{\rho_i L_p}(\Delta p_{man} - \Delta p_{loss} - \Delta p_s - \Delta p_d)\,, \tag{3.36}$$

where Δp_{man} is the manometric head pressure that the pump delivers to accelerate the mixture (Section 3.4.1), Δp_{loss} the hydraulic friction loss (Section 3.4.2), Δp_s the static head loss (Section 3.4.3), Δp_d the pressure loss over the drag head (Section 3.4.4), A_p the average area of the pipeline, L_p the pipeline length and ρ_i the density drag head, pipe and pump.

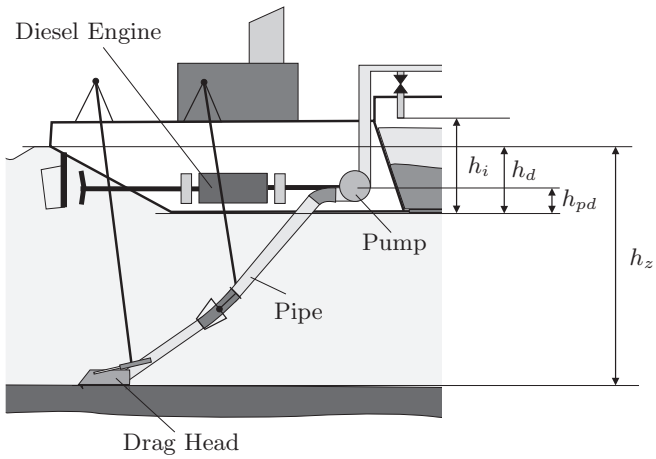

Figure 3.13: Definitions of the heights used to calculate static head loss.

The transport delay is neglected here. This delay depends on the average flow velocity and the length of the suction pipe. For this ship the delay is estimated to be

approximately 8 s, i.e., 2 samples in the data. We can neglect this, since the sample time constant (60 s) of the MPC is expected to be 8-times this value.

3.4.1 Pump Model

The pump delivers the pressure in the hydraulic system. The dredge pump is a centrifugal pump, which consists of an impeller rotating inside a pump housing. The pump model predicts the pressure Δp_{man} delivered to the mixture flow rate, see (3.36), based on the pump speed ω_p and other variables such as the mixture density ρ_i in the pump, flow rate Q_i and soil type. The characteristic of an ideal pump with constant speed, based on Euler's derivation, is given in Fig. 3.14(a).

This model describes the ideal behaviour of a pump, for which the following two assumptions are made:

1. The pump has an infinite number of infinitely small blades, which means that all the streamlines are parallel to the blades and the rotational velocity of all the fluid particles is the same as for the blades.

2. There are no friction losses and momentum losses.

An actual pump suffers from losses such as impact losses and internal friction losses. Moreover, some of the assumptions in Euler's model are not valid. This is illustrated in Fig. 3.14(b).

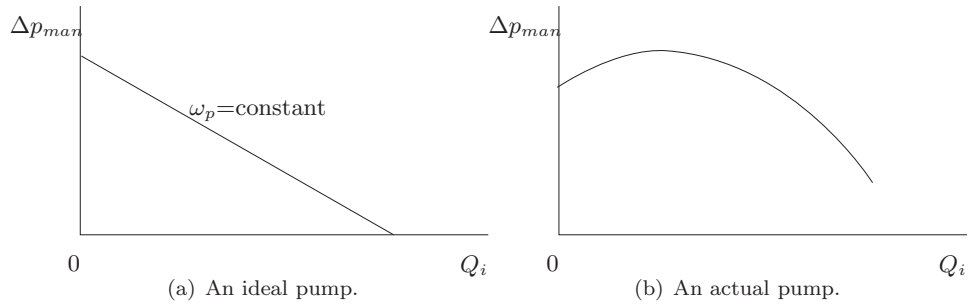

(a) An ideal pump. (b) An actual pump.

Figure 3.14: Pump characteristics.

This model is obtained by curve fitting a polynomial function to data from a pump test. The resulting model incorporates the impact losses of mixture flowing into the pump housing, friction losses and losses due to a finite number of impeller blades. The model for pumping water is the following:

$$\Delta p_{manw} = c_{0n}\omega_p^2 - c_{1n}\omega_p Q_i - c_{2n}|Q_i|Q_i\,, \tag{3.37}$$

where c_{0n}, c_{1n} and c_{2n} are pump coefficients given by the pump manufacturer.

The power is expressed by:

$$P_w = c_{0p}\omega_p^3 + c_{1p}\omega_p^2 Q_i + c_{2p}\omega_p Q_i^2 + c_{3p}Q_i^3\,,$$

where c_{0p}, c_{1p}, c_{2p} and c_{3p} are pump coefficients that are given by the pump manufacturer. Stepanoff experimentally derived the effects of solids with a certain particle

diameter on the pump head. The pump model must be corrected for this so-called solids effect as follows (Miedema, 1996):

$$\Delta p_{man} = \Delta p_{manw}(1 + \frac{\rho_q - \rho_w}{\rho_w}\gamma C_t)\,,$$

where γ is a coefficient that models the solids effect, which depends on the grain size. This solids effect depends on the grain size, i.e., the pump head is higher for mixtures of sand with small grain sizes and lower for large grain sizes. The pump power when pumping mixture is the following, (Braaksma, Osnabrugge, Babuška, de Keizer and Klaassens, 2007):

$$P_p = \frac{\rho_m}{\rho_w} P_w\,,$$

Given this equation, the demanded pump torque is calculated using $P_p = T_p\omega_p$ as follows:

$$T_p = \frac{P_p}{\omega_p}\,.$$

3.4.2 Pipeline Model

The pipeline model describes the pressure drop due to the hydraulic friction of water or mixture with the pipeline wall. For a detailed derivation of the pipeline hydraulic friction model the reader is referred to Appendix A. The pressure drop depends on the flow regime, i.e., laminar or turbulent. For dredging sand this regime is turbulent (Matoušek, 2001). For this regime, the hydraulic friction increases quadratically with the increase in flow velocity.

The friction coefficient (Darcy-Weisbach) depends on the roughness of the pipe, the pipe diameter and the Reynolds number of the flow. The Moody diagram in Fig. D.1 in Appendix D shows how this coefficient is determined. The parameters pipeline roughness and Reynolds number of the flow are not available on-line; thus, we estimate the Darcy-Weisbach coefficient from data in the next chapter. The Moody diagram is given to verify if these estimates result in realistic values. For the dredging process this coefficient ranges between 0.010 and 0.015. The pressure loss for water is calculated as follows:

$$\Delta p_{lossw} = \lambda_f \frac{8\rho_w |Q_i| Q_i}{\pi^2 d_p^5} L_p = \lambda_f a_p |Q_i| Q_i\,,$$

where λ_f is the Darcy-Weisbach friction coefficient, L_p the pipeline length, d_p the pipeline diameter and a_p is given by:

$$a_p = \frac{8\rho_w L_p}{\pi^2 d_p^5}\,.$$

When sand particles are present in the liquid, the pressure drop increases. This solids effect has been described by various empirical models. One of these models that is very suitable for our application, because it has only one parameter to calibrate, is the Führböter model. The pressure drop in a pipeline with mixture is given by:

$$\Delta p_{loss} = \lambda_f a_p |Q_i| Q_i + \frac{S_{kt} b_p C_t}{Q_i}\,, \tag{3.38}$$

with

$$b_p = \rho_w g A_p L_p = \rho_w g \frac{d_p^2 \pi}{4} L_p \,,$$

where S_{kt} is the parameter for the solids effect, which depends on the grain size diameter of the sand in the mixture. There is a correlation between the average grain diameter and the value for S_{kt} which is given in Appendix D, Fig. D.2. This graph is only shown to calculate the grain diameter afterwards, as the parameter S_{kt} will be calibrated using the data given in the next chapter.

Parts of the dredge pipelines are inclined, parts are vertical and the rest horizontal. This affects the solids effect in the pipe. A vertical pipeline, which carries a Newtonian mixture (such as sand), has no solids effect ($b_p = 0$). A horizontal pipeline is described by (3.38), but an inclined pipeline has a reduced solids effect. A general model for a pipeline is given by Worster and Denny (1955):

$$\Delta p_{loss} = \lambda_f a_p |Q_i| Q_i + \frac{S_{kt} b_p C_t}{Q_i} \cos(\alpha_p) \,,$$

where α_p is the angle of the pipeline. The dredging pipeline of the ship consists of several sections with different angles, diameters and lengths. Moreover, the angle of the suction pipeline varies and depends on draught and the dredging depth. The total pressure loss of the pipeline is given by:

$$\Delta p_{loss} = \sum_{j=1}^{N_p} \left(\lambda_f a_j |Q_i| Q_i + \frac{S_{kt} b_j C_t}{Q_i} \cos(\alpha_{pj}) \right) \tag{3.39}$$

$$\Delta p_{loss} = \lambda_f |Q_i| Q_i \sum_{j=1}^{Np} a_j + \frac{S_{kt} C_t}{Q_i} \sum_{j=1}^{Np} b_j \cos(\alpha_{pj}) \tag{3.40}$$

$$a_j = \frac{8 \rho_w L_{pj}}{\pi^2 d_{pj}^5} \tag{3.41}$$

$$b_j = \rho_w g A_{pj} L_{pj} = \rho_w g \frac{d_{pj}^2 \pi}{4} L_{pj} \,, \tag{3.42}$$

where N_p is the number of different pipeline sections, j the pipeline section index, L_{pj} the length of section j, d_{pj} the diameter of section j, α_{pj} the angle of section j and A_{pj} the area of pipeline section j.

The suction pipe on a TSHD is under an angle. This angle is varying in time due to changes in dredging depth and draught, therefore the summation in the second term of (3.40) is time varying. This part of which the angle varies can be written as an addition term.
So for the complete ship configuration equation is given by:

$$\Delta p_{loss} = \lambda_f Q_i^2 k_1 + \frac{S_{kt}}{Q_i} C_t k_2 \cos(\alpha_t) + \frac{S_{kt}}{Q_i} C_t k_3 \,,$$

with α_t the angle of the suction pipe with the horizon and k_1, k_2 and k_3 are constant parameters depending on the complete pipeline configuration.

For simplicity it is assumed that the suction pipe is always straight, than this angle is the following:

$$\alpha_t = \arccos\left(\frac{h_z - h_d}{L_{pi}}\right),$$

where h_z is the dredging depth, h_d the draught of the ship, L_{pi} the length of the suction pipe line (only the part of the pipeline outside the hull).

Minor Losses

The pressure losses described here are derived for straight pipelines. All the losses that come from bends, valves T-joints, etc., are modelled as so-called minor losses and added to the total loss equation. As the parameter λ_f and S_{kt} are calibrated with data in this thesis, these minor losses can be incorporated into the equation for the losses. These parameters will become larger than what would be expected from the theory, but this simplifies the equations and reduces the amount of parameters to be estimated on-line, which is one of the modelling objectives.

3.4.3 Static Head Loss

The hopper dredger excavates sand from the bottom of the sea which is then aspirated into the hopper inlet. The static head must be delivered by the dredge pump. This head losses can be divided in two parts, the head loss of the under water part and the head loss of the part which is above the water level. There are two variables that affect the static head loss:

- Dredging depth h_z, affecting the underwater part of the losses.
- Draught of the ship h_d: during dredging the draught increases due to the loading of the hopper. Therefore, the height of the mixture inlet above the water level decreases and, consequently, the static head loss decreases.

The static head loss for the whole pipeline is then given by the following equation:

$$\Delta p_s = (\rho_{pi} - \rho_w) h_z g + \rho_{pi}(h_i - h_d) g\,,$$

where h_i is the distance from the ship's keel to the pipe inlet in the hopper, ρ_{pi} the average density in the pipeline, g the gravitational acceleration, h_z the dredging depth and h_d the draught. For the definitions of the heights, see Fig. 3.13.

Cavitation

The absolute pressure at the inlet of the dredge pump is limited by the vapour pressure of the liquid. Cavitation occurs when the liquid starts boiling which introduces bubbles into the pump.

The cavitation process is not explicitly modelled, but it should be avoided when optimising the performance. The model predictive controller will treat the absolute inlet pressure as a constraint during the optimisation. In the control strategy cavitation will be avoided by reducing the incoming density when necessary.

The absolute inlet pressure is:

$$p_i = p_{atm} + \rho_w g h_z - \Delta p_{s,s} - \Delta p_{loss,s} - \Delta p_d \,,$$

where $\Delta p_{loss,s}$ is the hydraulic friction loss of the total suction pipeline in front of the pump, $\Delta p_{s,s}$ the static loss in the suction pipeline, p_{atm} the atmospheric pressure and Δp_d the pressure loss over the drag head. The static head loss at the inlet of the pump is given by:

$$\Delta p_{s,s} = \rho_{pi} g (h_z - (h_d - h_{pd})) \,,$$

where h_{pd} is the vertical distance of the pump centre from the keel.

3.4.4 Pressure Loss of the Drag Head

The pressure loss over the drag head is difficult to model, because it depends on several variables, not all of which are known. A reasonably accurate model for the pressure drop that does not depend on unknown variables is given by:

$$\Delta p_d = k_{ld} \frac{1}{2} \rho_i v |v| \,,$$

where k_{ld} is drag head loss coefficient, ρ_i the density in the drag head and v the flow velocity. The equation also includes the pressure drop as result of accelerating the mixture. This equation, in terms of the flow rate Q_i, given that $v = Q_i / A_p$, is

$$\Delta p_d = k_{ld} \frac{1}{2} \rho_i \frac{Q_i |Q_i|}{A_p^2} \,.$$

3.4.5 Soil-Dependent Parameters

The parameters of Tab. 3.3 are the soil-dependent parameters of the pump-pipeline model. Technically, λ_f is not soil type dependent but it is unknown beforehand. The parameter depends on the roughness of the pipe and it takes the minor losses into account. Therefore this parameter is also calibrated in Chapter 4 with the data.

Table 3.3: Summary of parameters that need to be calibrated with data.

Parameter	Description
γ	Solids effect pump
S_{kt}	Solids effect pipeline
λ_f	Darcy-Weisbach friction coefficient

3.5 Power Train Model

The power train system of a hopper dredger consists of a diesel engine, pump, propeller and generator. The power is distributed mechanically via a shaft, electrically with cables or hydraulically with oil in pipes. In the diesel-direct configuration, which is considered in this thesis, the pump and the propeller are connected by shafts and

gearboxes. Power can also be distributed by converting it into electric power and back to mechanical power by a generator and an engine. The advantage is a flexible distribution of the power and optimal use of the diesel engine's best efficiency point. The disadvantage is that there is generally more power loss due to the conversions from mechanical to electrical power and vice versa. The diesel-direct system has less power loss under nominal operating conditions, but a poorer performance when controlling the pump speed.

In general, a ship is equipped with two symmetrical power trains, each driving the power consumers on its own side of the ship. Thus, the starboard engine drives the starboard propeller and starboard dredge pump and the port-side engine drives the port-side propeller and pump. However, for a one pipe ship the power trains are asymmetrical. Only one side powers the dredge pump.

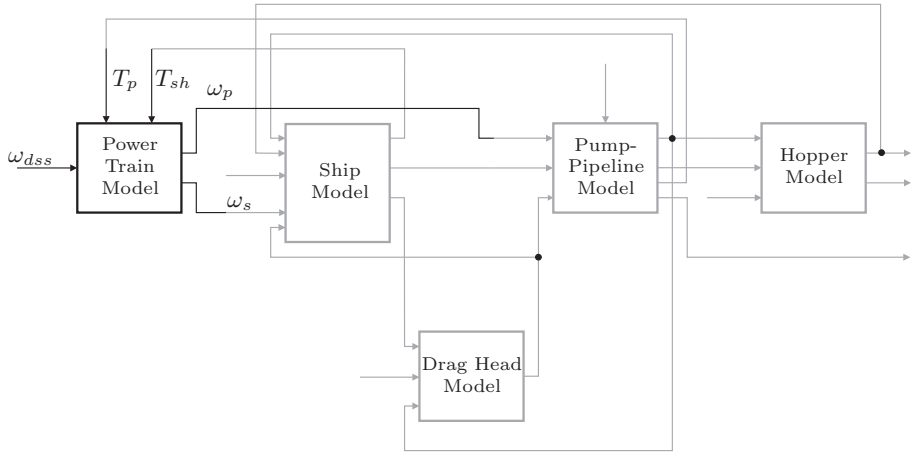

Figure 3.15: A block diagram of the overall process model, where the power train model is highlighted.

The model described here is based on the model of Izadi-Zamanabadi and Blanke (1999) and simulates the rotational velocity of the pump and the propeller shaft, based on the set-point for the diesel engine angular velocity (see Fig. 3.15). The equations of motion reduced to the diesel engine shafts are:

$$
\begin{aligned}
I_d\dot{\omega}_{dp} &= T_{dps} - k_{fr}\omega_{dp} - T_{shp} - T_{auxps} \\
I_d\dot{\omega}_{ds} &= T_{dsb} - k_{fr}\omega_{ds} - T_p - T_{shs} - T_{auxsb}\,,
\end{aligned}
$$

with

ω_{dp}	Port side diesel engine angular velocity
ω_{ds}	Starboard diesel engine angular velocity
k_{fr}	Friction coefficient
I_d	Combined inertia of the power train
T_{dps}	Diesel engine torque of port side engine
T_{dsb}	Diesel engine torque of starboard engine
T_{shp}	Port side propeller torque
T_{shs}	Starboard propeller torque
T_{auxps}	Port side auxiliary torque and generator torque
T_{auxsb}	Starboard auxiliary torque and generator torque
T_p	Pump torque .

The 'governor' of the diesel engine is a PI-controller (Izadi-Zamanabadi and Blanke, 1999) including an anti-windup system to prevent a large value building up in case of saturation. The output of the governor is the fuel index which has an output range between the lower bound Y_{lb} and the upper bound Y_{ub}. The controller is modelled as follows:

$$\dot{Y}_{is} = \frac{k_r}{\tau_i}(\omega_{dss} - \omega_{ds}) - k_{aw}(Y_{PIbsb} - Y_{PIsb})$$

$$Y_{PIbsb} = Y_{is} + k_r(\omega_{dss} - \omega_{ds}) \tag{3.43}$$

$$Y_{PIsb} = \min(\max(Y_{PIbsb}, Y_{lb}), Y_{ub})\,, \tag{3.44}$$

where ω_{dss} is the set-point for the diesel-engine angular velocity, k_r the P-gain, *taui* the time constant of the integrator and k_{aw} the anti-windup parameter.

Physical constraints limit the fuel index as follows:

$$y_{max,s} = \begin{cases} 1, & \text{if } \omega_{ds} \geq 0.8\,\omega_{d,max} \\ \frac{1.5}{\omega_{d,max}}\omega_{ds} - 0.2, & \text{if } 0.4\,\omega_{d,max} < \omega_{ds} < 0.8\,\omega_{d,max} \\ 0.4, & \text{if } \omega_{ds} \leq 0.8 \end{cases} \tag{3.45}$$

$$Y_s = \min(Y_{PIsb}, y_{max,s})\,, \tag{3.46}$$

where $\omega_{d,max}$ is the maximum allowed diesel-engine angular velocity and Y_s the actual fuel index of the starboard engine.

We neglect the diesel-engine dynamics and model the engine as a perfect torque generator:

$$T_{dsb} = k_t Y_s\,,$$

where k_t is the diesel engine gain. The diesel torque drives the shaft which is connected to three gear boxes, one for the propeller, one for the generator and one for the dredge pump. The drive-shaft equations are:

$$\omega_p = \omega_d N_p$$
$$\omega_s = \omega_d N_s\,,$$

where N_p is the gear ratio from the diesel engine to the pump and N_s the gear ratio from the diesel engine to the propeller.

In this thesis a diesel-direct configuration is considered, see Fig. 3.16.

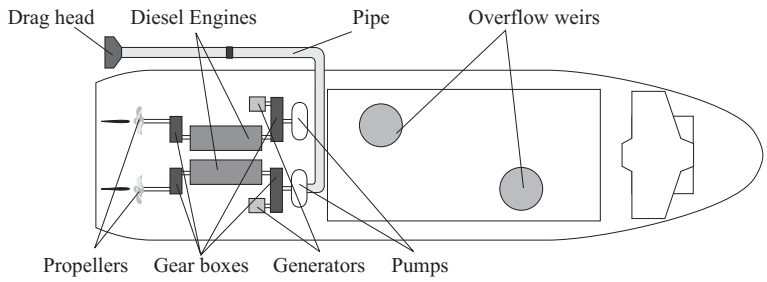

Figure 3.16: Diesel-direct configuration.

3.6 Ship Motion Model

For the ship motion model a 1D approximation is chosen, because the drag-head production only depends on the forward speed of the ship. The other degrees of freedom of the ship motion do not contribute to the production. The ship propellers have a variable blade pitch that regulates the thrust force.

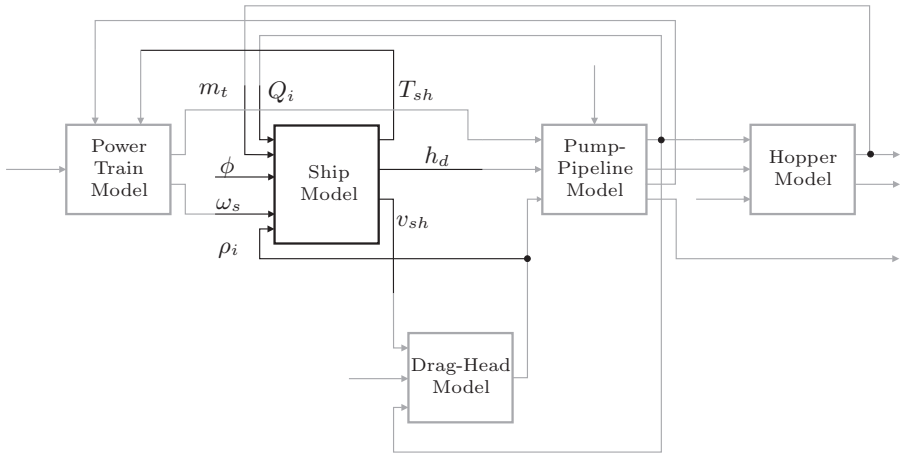

Figure 3.17: A block diagram of the overall process model, where the ship model is highlighted.

3.6.1 Forward Motion Model

The equation for the forward ship's speed (v_{sh}) is based on the Newton's Second Law of motion:

$$(m_{se} + m_t)\dot{v}_{sh} = F_{th} - F_d - F_c\,, \tag{3.47}$$

where F_{th} is the thrust force of the propeller blades, F_d the drag resistance force, F_c the cutting force of the drag head (see equation (3.31)), m_{se} the mass of the empty

ship, m_t the mass of the hopper content (which increases during dredging) and v_{sh} the ship's speed. In deriving equation (3.47) we neglect the time derivative of the mass because this term is very small. The thrust force is given by (Sørensen and Ådnanes, 1997):

$$F_{th} = k_f \omega_{pp}^2 \phi_p^{\frac{3}{2}} + k_f \omega_{ps}^2 \phi_s^{\frac{3}{2}} ,$$

where k_f is the pitch to thrust force gain, ω_{pp} the port-side propeller shaft speed, ω_{ps} the starboard propeller shaft speed, ϕ_p the port-side pitch of propeller blades and ϕ_s the starboard pitch of the propeller blades. The combined ship's drag force of the hull, pipeline and drag head is given by the following equation:

$$F_d = k_d |v_{sh}| v_{sh} ,$$

where k_d is the drag coefficient. This coefficient is variable with time, because of the draught varying with time and the disturbances caused by irregularities of the bottom of the sea. The torques of the two propellers are the following:

$$\begin{aligned} T_{shp} &= k_T \omega_{pp}^2 \phi_p^{\frac{3}{2}} \\ T_{shs} &= k_T \omega_{ps}^2 \phi_s^{\frac{3}{2}} \\ T_{sh} &= \begin{bmatrix} T_{shp} \\ T_{shs} \end{bmatrix} , \end{aligned}$$

where k_T is the torque gain of the propellers.

3.6.2 Draught Model

The draught of the TSHD is variable and depends on the hopper mass m_t (see Fig. 3.17). It suffices to use a linear approximation to model this:

$$h_d = f(m_t) \approx a_d m_t + b_d , \tag{3.48}$$

where h_d is the ships draught, needed for the pump-pipeline model (see Fig. 3.1). The parameters a_d and b_d are constant parameters that must be calibrated, where b_d is the draught of the ship if the hopper is empty and a_d relates the hopper mass to the draught.

The soil-type-dependent parameters of the ship model that are calibrated in Chapter 4 are summarised in Tab. 3.4.

Table 3.4: Summary of parameters that need to be calibrated with data.

Parameter	Description
	Ship Motion Model
k_d	Friction coefficient total drag force 1

3.7 Concluding Remarks

In this chapter, the total system model that is used to simulate and predict the behaviour of the total dredging process is described. The goal of this model is not to describe the behaviour of every subsystem on a microscopic level, but to describe the behaviour that is important for optimisation, taking all interactions of the subsystems into account.

The models stated here all include soil-type-dependent parameters. In the next chapter these parameters will be calibrated with the use of data from measurements. Furthermore, the models will also be validated. The validation results of the hopper sedimentation model will show which of the three models, as presented in Section 3.2.3, for the density profile in the hopper performs best.

All sub-models, except the drag-head production model, are derived from physical modelling. The drag-head production model is derived by means of a data-driven black-box technique, described in Appendix C. In the next chapter the simulation results and validation results of this model are presented. Such a black-box model must be used with care, since there are no guarantees that it is valid on other data sets. Therefore, this model is only valid under the circumstances given in this chapter.

4

Parameter Estimation and Model Calibration

The previous chapter described a model for the application of control for the complete trailing suction hopper dredger (TSHD) process. It consists of five parts: a hopper sedimentation model, a drag-head model, a pump-pipeline model, a power train model and a ship model. This complete model will be used in a model predictive controller (MPC) which will be presented in the next chapter. The performance the MPC depends on the accuracy of the model. Parameters that are dependent on soil type must be estimated based on data, since the model will be used on-line as part of the MPC. In this chapter, the performance of the models is analysed to verify if they are suitable for model predictive control. Parameters that are based on the structure of the ship are calibrated off-line and are not discussed in this thesis.

Estimating the soil-type-dependent parameters is a challenging task, since the measurements are noisy and uncertain. Especially the parameters of the hopper sedimentation model are difficult to estimate, since there are no sensors in the hopper mixture that measure the sand-bed height.

There are several strategies for calibrating the soil-dependent parameters:

- Measure all the detailed soil parameters, such as grain-size distribution, and calculate all the parameters using empirical relations from literature.
- Calibrate manually, based on expert knowledge and physical insight.
- Use measurements to obtain the parameters for a given model structure by means of optimisation that minimises the prediction error.
- Use measurements to obtain both the model structure and parameters at once (black-box modelling) by minimising the prediction error.

For automatic calibration, the first two strategies are not suitable. As the model structure of a large part of the system is known, the third strategy is used to calibrate the parameters. For the drag-head model, the model structure is unknown and the fourth method is applied.

Apart from the calibration of the parameters, the models must be validated. Chapter 3 proposes three alternatives for the hopper model. In this chapter the validation

results decide which model is most suitable for predicting the hopper process behaviour.

Three data sets (A, B and C) are available for calibration and validation. Two data sets are measured on board of a TSHD (data sets B and C) and one data set is measured on a test rig of a scaled-down hopper (data set A) and will be used for validation of the hopper sedimentation process. The other two data sets are used for calibrating and validating all the models. Parts of this chapter have been published in (Braaksma, Klaassens, Babuška and de Keizer, 2007a).

4.1 Parameter Estimation

This chapter discusses two main approaches to estimate parameters: off-line estimation and on-line estimation. Off-line estimation is applied to validate the models. The parameters are calibrated with data from a complete cycle. The parameters are then fixed and the model is used to predict the behaviour of the other dredging cycles. The prediction performance gives a measure of the validity of the particular model and its ability to generalise the dredging behaviour. Of course, if the parameters vary significantly between cycles, the prediction performance also deteriorates. Therefore, this validation is only applied to one data set (data set A, B or C) at a time.

If it turns out that the method described above results in an accurate prediction, this off-line method can also be used on-line as follows. Once a complete dredging cycle is finished, the data of this cycle are used to update the parameters in the prediction model. This model, including the estimated parameters, is used in the next cycle for the prediction. However, if this prediction method is not sufficiently accurate, because of the changing soil conditions, one must use an on-line estimation method that adapts the parameters continuously during the dredging process. At every control sampling instance the parameters are updated and a new prediction is made.

The off-line estimation is applied to all the models that contain soil-dependent parameters. In this thesis only the on-line estimation method for the pump-pipeline process is presented. Solving the on-line estimation problem for the other models will be a part of future research.

4.1.1 Off-line Estimation

The goal of the method presented here is to automatically estimate the parameters without exact knowledge of the soil type. The modelling goal is to predict the performance-related system outputs for an operator or a controller to optimise the dredging strategy. The quality of the model is dependent on the prediction error J. If we assume that the model structure is correct, the prediction error only depends on the parameter vector $\boldsymbol{\theta}$. The parameters which minimise the prediction error $J(\boldsymbol{\theta})$ are the best approximation to the real parameters.

The procedure is schematically shown in Fig. 4.1. The model predicts an output variable $\hat{y}$ based on the inputs u. This output is compared to the measured variable y. The prediction error J is used in the optimiser to correct the parameter vector $\boldsymbol{\theta}$. This procedure is repeated until a stopping criterion is met. Mathematically this

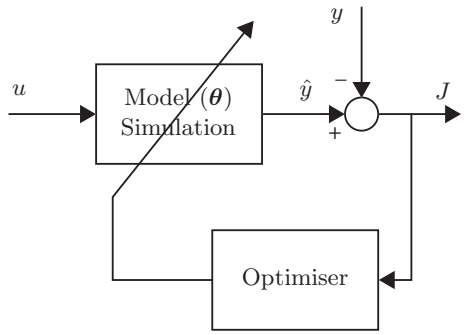

Figure 4.1: Schematic of the parameter estimation.

problem is written as follows:

$$\begin{aligned} \boldsymbol{\theta} &= \arg\min_{\boldsymbol{\theta}} J(\boldsymbol{\theta}) \\ &\text{subject to} \\ &\boldsymbol{\theta}_{min} \leq \boldsymbol{\theta} \leq \boldsymbol{\theta}_{max}, \end{aligned} \tag{4.1}$$

where $\boldsymbol{\theta}$ is the parameter vector that is bounded by its minimum $\boldsymbol{\theta}_{min}$ and maximum $\boldsymbol{\theta}_{max}$. These bounds are introduced to restrict the parameter search space and to keep the model within its feasible region.

For some of the model outputs, the prediction error is nonlinear in the parameters. This leads to a parameter estimation problem that has to be solved by nonlinear optimisation. Several nonlinear global optimisation methods are available, such as multi-start local optimisation, random search, simulated annealing, genetic algorithms and direct search methods. Finding a global minimum is computationally expensive and is, in general, not guaranteed.

When the nonlinear optimisation is sufficiently smooth, Newton's method can be used to solve it. For this method a local gradient and Hessian must be calculated. This method is not suitable for optimisation if the nonlinear function J that must be minimised has one of the following properties (Wright, 1996):

- Calculation of J is very computationally expensive.
- Exact first partial derivatives of J cannot be calculated.
- Numerical approximation of the gradient of J is very expensive or slow.
- Values of J are noisy.

In this practical problem it is not necessary to have a highly accurate solution, because of the errors and uncertainties of the model and the data. Moreover, it is undesirable to gain this accuracy at high computational cost. Our aim is to quickly find a solution.

The best choice for minimising the cost function with the above properties is a direct search method, such as pattern search. This method uses only function values and does not use the gradient. Here we use the pattern search method based on

the original algorithm presented in Hooke and Jeeves (1961), which is a direct search method available in Matlab and extended to cope with bound constraints (Lewis and Torczon, 1999). Other examples of direct search methods are coordinate search with fixed step sizes (Davidon, 1991), evolutionary operation (Box, 1957) and simplex-based direct search methods (Spendley et al., 1962).

Nonlinear optimisation may result in a local minimum or have multiple solutions. For testing purposes, the optimisation algorithm is repeated and for each trial the initial guess of the parameters is randomly chosen in the interval $[\boldsymbol{\theta}_{min}\ \boldsymbol{\theta}_{max}]$. After all trials, the variances of the estimated parameters indicate the sensitivity of the parameters with respect to the predicted variable. Sometimes the estimated parameter clips one of the limits, which (as the limits are chosen very carefully) might indicate that this parameter has a negligible effect on the predicted variable. The estimation procedure is as follows:

1. Select the data of one complete dredging cycle.
2. Repeat the following calibration algorithm for N_a times:
   (a) Randomly choose the initial guess $\boldsymbol{\theta}_{init} \in [\boldsymbol{\theta}_{min}\ \boldsymbol{\theta}_{max}]$.
   (b) Run nonlinear optimisation, to find $\boldsymbol{\theta}_{final}$ and the corresponding J.
   (c) Store the results.
3. Select the $\boldsymbol{\theta}_{final}$ that has the smallest J .
4. Calculate statistical information, such as the standard deviation of $\boldsymbol{\theta}$.
5. Use the optimal $\boldsymbol{\theta}$ and simulate all the other cycles; compare the simulation results with the measurements for validation purposes.

The model is implemented as a set of nonlinear differential equations in Matlab/Simulink. Simulink uses a numerical Ordinary Differential Equation (ODE) solver. A typical characteristic of the TSHD model is that it is a very stiff model. It means that the model is a combination of very slow dynamics (sedimentation process) and very fast dynamics (pump and excavation process). For efficient simulation of such a system, we make use of a stiff solver, such as the solver ODE23tb (available in Matlab) which is by far the fastest solver for this application. The optimisation algorithm simulates the complete dredging process and then calculates the cost function. This simulation procedure is as follows.

1. Initialise parameters other than $\boldsymbol{\theta}$.
2. Initialise $\boldsymbol{\theta}$ coming from the optimisation algorithm.
3. Create the inputs for the simulation $\boldsymbol{u}$.
4. Calculate and initialise the initial states of the integrators in the model.
5. Simulate the model from the start until the end of the dredging process, using an ODE solver and store the output $\hat{y}(k)$ for $k = 0, 1, \cdots, N$.
6. Calculate the cost function $J = \frac{1}{N} \sum_{k=0}^{N} (\hat{y}(k) - y(k))^2$.

Pattern Search

The pattern search algorithm searches for the minimum value of $J(\boldsymbol{\theta})$ by varying $\boldsymbol{\theta} = [\theta_1, \theta_2, \cdots, \theta_K]^T$. The algorithm starts at an initial point $\boldsymbol{\theta}$ in the K-dimensional space. The transition from one point to another is called a *move*. A move is called a success when the value for $J(\boldsymbol{\theta})$ decreases, otherwise it is called a failure.

- Pattern search is a direct search method, which means that it does not calculate or estimate the gradient.
- The algorithm uses pattern vectors to define the search directions in the K-dimensional space. These can be fixed or randomly selected at each iteration.
- The mesh size defines the search distance from the current optimal point at each iteration. This size is doubled if a new point is found with a lower value for $J(\boldsymbol{\theta})$ and halved in all other cases.
- The objective function $J(\boldsymbol{\theta})$ is evaluated, where lower is better.
- The algorithm stops when a stopping criterion is met, e.g., the mesh size is smaller than the predefined minimum mesh size.

Least-Squares

If the parameter estimation problem is linear in the parameters, the estimation is solved with a least-squares algorithm. This section discusses the normal least-squares procedure for off-line estimation of the parameters and the recursive least-squares procedure which is suitable for on-line estimation. Mathematically we try to solve:

$$A\hat{\boldsymbol{\theta}} = \boldsymbol{y}\,, \tag{4.2}$$

where a matrix A contains the measured input variables, $\boldsymbol{y}$ is the measured output variable that the model predicts and $\hat{\boldsymbol{\theta}}$ the parameters to be estimated. Since A is not square in general, this is solved by computing the pseudo-inverse:

$$\hat{\boldsymbol{\theta}} = (A^T A)^{-1} A^T \boldsymbol{y}\,,$$

Sometimes the estimation problem is ill-conditioned then the solution can more reliably calculated through a QR-factorisation of A (Lay, 1997), i.e.,

$$\hat{\boldsymbol{\theta}} = R^{-1} Q^T \boldsymbol{y}\,.$$

4.1.2 On-line Estimation

For the on-line estimation two methods have been implemented. A recursive least squares algorithm is used if the model is linear in the parameters and a particle filter it is a nonlinear estimation problem.

Recursive Least-Squares

The least-squares method described above is used to estimate the parameters once all the data of the complete cycle are gathered. It is also possible to start estimating the parameters as soon as the data is measured and estimate the parameters recursively with the following recursive equation (Young, 1984):

$$\hat{\boldsymbol{\theta}}_k = \hat{\boldsymbol{\theta}}_{k-1} - P_k(\boldsymbol{x}_k \boldsymbol{x}_k^T \hat{\boldsymbol{\theta}}_{k-1} - \boldsymbol{x}_k y_k)\,,$$

with

$$P_k = P_{k-1} - P_{k-1}\boldsymbol{x}_k \left(1 + \boldsymbol{x}_k^T P_{k-1} \boldsymbol{x}_k\right)^{-1} \boldsymbol{x}_k^T P_{k-1}\,,$$

where $\boldsymbol{x}_k$ is the vector with measurements and k the time index. When the parameters vary with time the recursive algorithm can be adapted such that it tracks the varying parameters. This behaviour is obtained by "forgetting" past measurements. There are several implementations available for forgetting the measurements, such as a moving rectangular window and an exponential data weighting function. The implementation for the exponential data weighting function is the following:

$$\hat{\boldsymbol{\theta}}_k = \hat{\boldsymbol{\theta}}_{k-1} - P_k(\boldsymbol{x}_k \boldsymbol{x}_k^T \hat{\boldsymbol{\theta}}_{k-1} - \boldsymbol{x}_k y_k) \tag{4.3}$$

$$P_k = \frac{1}{\alpha}(P_{k-1} - P_{k-1}\boldsymbol{x}_k \left(\alpha + \boldsymbol{x}_k^T P_{k-1} \boldsymbol{x}_k\right)^{-1} \boldsymbol{x}_k^T P_{k-1})\,, \tag{4.4}$$

where $\hat{\boldsymbol{\theta}}_k$ is the parameter vector to be estimated at time k, α the forgetting factor, y_k the to be predicted variable and $\boldsymbol{x}_k$ the vector with variables measured at time k.

Particle Filter

The particle filter uses a probabilistic model that is based on state equations and specifies the probability density functions (PDFs) for the state transition and the measurements function. The objective is to recursively construct the posterior PDF of the state given the measured output, with the following two-stage strategy:

1. In the prediction stage the state-transition model predicts the state PDF one step ahead (the PDF obtained is called the prior).

2. In the update stage the latest measurement is used to correct the prior using the Bayes rule. The PDF obtained after the update is called the posterior PDF.

Particle filters approximate the PDF with N random samples, called particles. Each particle has an associated weight and the weights of all particles sum up to 1. At time k, the prior is represented by N particles and their weights. To approximate the posterior, new particles are generated. Particles are drawn from a (chosen) importance density function which here is equal to the state-transition PDF. Then the weights are updated using the current measurement. The state estimate is now computed as the weighted mean of the particles. For all the details, the reader is referred to Babuška et al. (2006).

4.1.3 Performance Measures

Two performance indices are defined to evaluate the performance of the models. The optimisation algorithm for finding the soil-dependent parameters uses the sum of squares as minimisation criteria. Although this performance index can be used for evaluating the model performance, another performance index is defined, variance-accounted-for (VAF). For a noisy signal the sum of squares can indicate that a perfect model is not performing well. The VAF is less sensitive to this and gives a better model judgement in case of noisy signals.

Variance-Accounted-For

The VAF weights the variance of the residual with the variance $\mathrm{var}(\boldsymbol{y})$ of the measured signal $\boldsymbol{y}$. The maximum VAF is 1, but for an inaccurate model the VAF can even become negative.

$$\mathrm{VAF} = 1 - \frac{\mathrm{var}(\boldsymbol{y} - \hat{\boldsymbol{y}})}{\mathrm{var}(\boldsymbol{y})}\,, \tag{4.5}$$

where $\boldsymbol{y}$ is the measured data and $\hat{\boldsymbol{y}}$ the predicted data.

Sum of Squares

Sum of Squares is applied as performance evaluation (cost function) for the minimisation of the prediction error in the nonlinear calibration procedure. This cost function is minimised by the pattern search algorithm to calibrate the parameters that cannot be calculated directly from the data with a linear least-squares technique. The sum of squares is defined as follows:

$$J(\boldsymbol{\theta}) = \frac{1}{N}\sum_{k=1}^{N}(\hat{y}(k,\boldsymbol{\theta}) - y(k))^2\,,$$

where k is the time index of the sampled data, $\boldsymbol{\theta}$ the parameter to be estimated, $\hat{y}(k,\boldsymbol{\theta})$ the predicted data, $y(k)$ the measured data and N the number of samples.

4.2 Data for Calibration

For the calibration and validation of the models, three data sets are used; one (data set A) is measured on a test rig and two sets (data set B and C) on a hopper dredger. Each data set is different with respect to the measured variables and to the circumstances. Therefore, not all sets are suitable for the calibration of each model. An overview of the three data sets is given in Tab. 4.1.

Data set A is measured on a test rig with a hopper capacity of 40 m^3. The test rig is described in Section 2.3.4. This data set is used for the validation of the hopper model and evaluate the performance of the three hopper models.

Data set B is measured on board of a hopper dredger during a land reclamation project. The sand type is medium sand and the average grain size approximately 0.4 mm. Unfortunately, this set does not contain all the necessary measurements for calibrating the ship model and power-train model.

Table 4.1: Overview of the three data sets

Data Set	A	B	C
Origin	Test rig	Ship	Ship
Hopper capacity [m^3]	40.6	13700	13700
No. of measured variables	45	73	154
Diameter of grains [mm]	0.140	0.4	0.3
Sand type	fine sand	medium sand	medium sand/silt
For models	Hopper	Hopper Pump-pipeline Drag head	Power train Ship motion Drag head

Data set C is measured on the same TSHD as data set B using another measurement protocol. The goal was to measure the set-points to the system, as well as the important variables for the optimisation and calibration of the models. Unfortunately, the set was measured during maintenance dredging which resulted in many short cycles, without an overflow phase. This makes this set less suitable for calibrating the hopper model, but still suitable for calibrating the power train model and the ship model.

The test rig data shows what is happening inside the hopper, such as the density profile. This is done with poles using Conductivity Concentration Meters (CCM poles). These poles measure the density at every 12.5 cm in height with the use of conductivity sensors. Furthermore, the output density and output flow are measured.

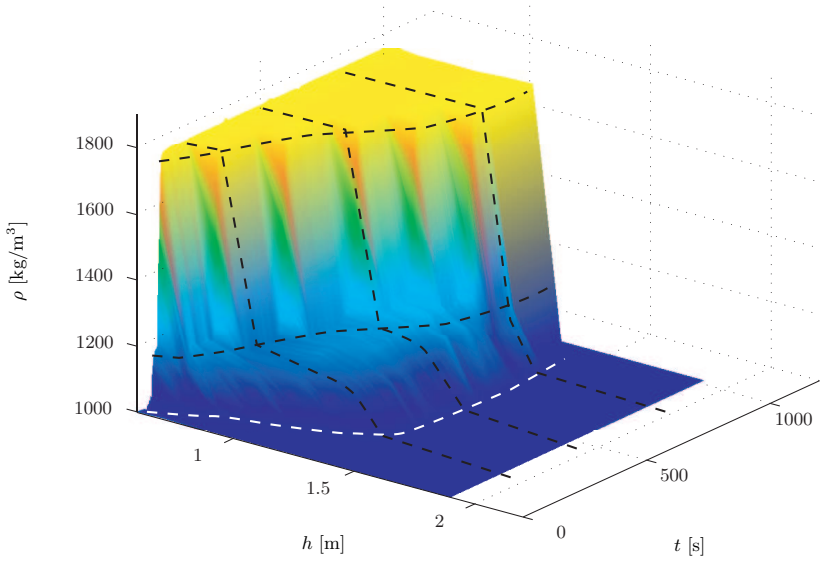

Figure 4.2: Surface plot of the measured data on the test rig (data set A).

The measured data of one of the CCM poles is shown in Fig. 4.2. At $t = 0$ s the

hopper content is only water, so that each sensor measures a density of 1000 kg/m^3. A sand bed is formed at the bottom when the hopper is loaded with mixture. The height of this sand bed grows as indicated in Fig. 4.2. The sand bed has a density of approximately 1780 kg/m^3. The density gradient shows a steep drop above the sand bed and is more or less constant over the height. On top of the mixture forms a small water layer (see Fig. 4.2). The mixture density remains approximately constant over time while the sand bed grows.

In Fig. 4.3 the measurement of the lowest sensor on CCM pole 1 is shown. It is assumed that the density above 1700 kg/m^3 is sand bed. This means that in Fig. 4.3 the bed height is 0.4 m at $t = 95$ s (recall that the sensor is mounted at 0.4 m level). The CCM poles have 12 sensors distributed over the height, so the bed height can be measured at a maximum of 12 discrete events.

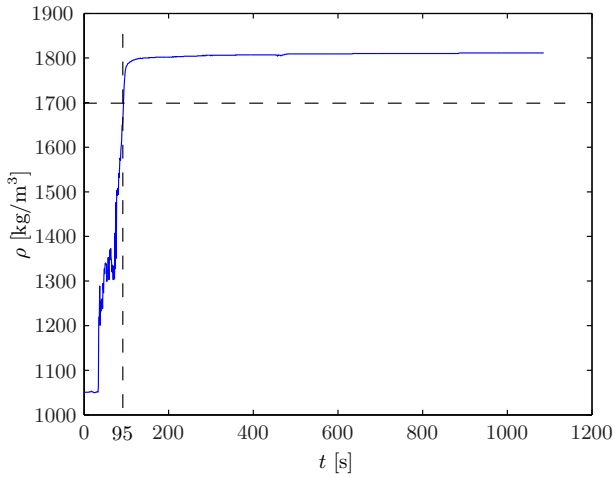

Figure 4.3: Measurement of lowest density sensor on CCM pole 1.

4.3 Hopper Model

The hopper model contains soil-type-dependent parameters. Often the soil type is not exactly known and varies from place to place. The parameters must be calibrated on-line to predict the sedimentation process in the hopper. This is done by estimating the parameters from the available measurements on board of the dredger. First the hopper model is calibrated on the test rig (data set A) to investigate the performance and then the model is calibrated and validated on the actual ship data (data set B).

The signals available for estimation are the total mass in the hopper (m_t) and total volume (V_t). The model equations show that the total volume is not dependent on one of the four soil-type dependent parameters. The total mass in the hopper (m_t) depends on the outgoing density (ρ_o). This outgoing density depends on the four soil-type-dependent parameters, the undisturbed settling velocity v_{s0}, the erosion factor k_e, the parameter β, which is dependent on the Reynolds number of the particle,

and sand bed density in the hopper ρ_s. Therefore, the mass is used to calibrate the parameters.

From the estimation experiences, it turns out that some of these parameters are hard to estimate with only the measurement of the mass of the hopper content m_t. The total mass has a small sensitivity for some of these parameters. It is, therefore, desirable to select only those parameters which have the largest influence on the overflow density and, thus, on the total mass. The parameters which have little sensitivity are kept constant during the estimation of the parameters. The values with little sensitivity are calculated with empirical relations available from the literature.

Sensitivity Analysis

Sensitivity analysis is performed to investigate which parameters can be estimated from the available data. Analytically, this is very hard to do, due to the nonlinearities in the model. Therefore, the sensitivity analysis is performed by numerically simulating the dredging cycle for different values of the parameters. Every trial consists of two simulations where the parameter under investigation is set to either its minimum value or its maximum value. During the trial all other parameters are kept constant (see Fig. 4.4, for the results of 4 trials). The band shows the upper and lower limit of the mass in the hopper. If this band is large the sensitivity for the parameter is high.

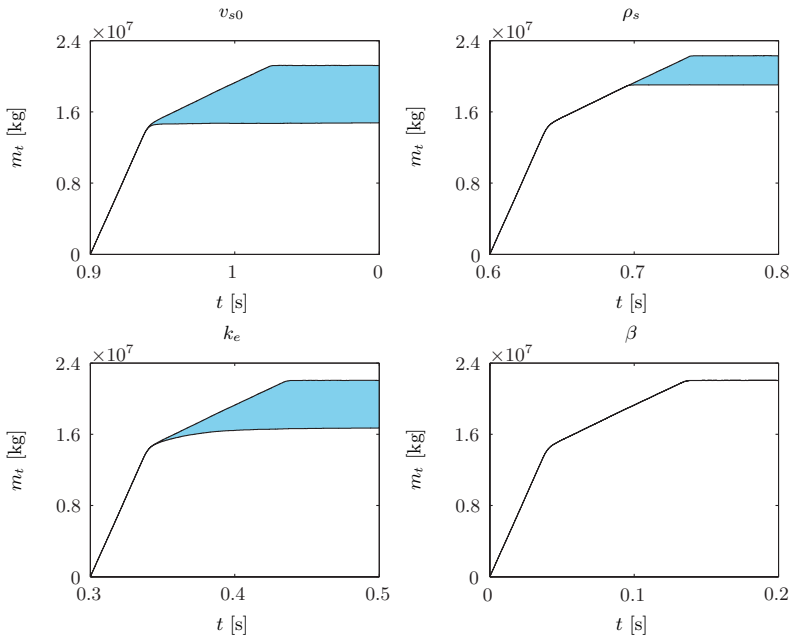

Figure 4.4: Signal range of m_t when varying one parameter. Top left, $v_{s0} \in [0.1, 400]$; top right, $\rho_s \in [1900, 2100]$; bottom left, $k_e \in [1, 25]$; bottom right, $\beta \in [3.5, 5]$.

Fig. 4.4 shows the ranges for varying one parameter while keeping the others con-

stant. A larger band indicates a higher sensitivity. This means that the undisturbed settling velocity and the erosion coefficient have the highest sensitivity and the hindered settling coefficient β has hardly any effect on the hopper mass.

The sensitivity of a variable can depend on the parameter values of the other variables. To determine the sensitivity, a grid is defined in the parameter space. In each trial another grid point is chosen while the parameter under investigation is varied. For every parameter five values are defined and for each grid point two simulations are performed, one simulation with the minimum value of the parameter and one simulation with the maximum value of the parameter. In total 1000 simulations and 500 trials have been performed.

A summary of these results is presented in Tab. 4.2. The values in the table present the RMS value of one trial. The RMS-value is a measure of the sensitivity. The higher it is, the higher the sensitivity of that particular parameter. The Min column gives the values for the trial with the minimum RMS values, and the Max column the RMS values of the trial with the maximum RMS values.

Table 4.2: Parameter sensitivity in RMS value.

Parameter	Min [kg]	Max [kg]
v_{s0}	$1.7 \cdot 10^6$	$5.1 \cdot 10^6$
ρ_s	$9.4 \cdot 10^5$	$1.5 \cdot 10^6$
k_e	$2.6 \cdot 10^6$	$2.6 \cdot 10^6$
β	$7.1 \cdot 10^3$	$7.1 \cdot 10^3$

The column with the min values gives the best indication on the sensitivity. The erosion parameter k_e is the most sensitive parameter, followed by undisturbed settling velocity v_{s0} and the sand bed density ρ_s. The hindered settling coefficient β is the least sensitive. It is therefore decided to exclude this parameter from the automatic calibration process, since it does not influence the hopper mass much.

Tab. 4.2 shows that the sensitivity of a parameter depends on the values of the other parameters, because the minimum values and maximum values differ for parameters v_{s0} and ρ_s. The total estimation problem of the soil-dependent parameters is summarised on the next page.

System of equations:

$$\dot{V}_t = Q_i - Q_o \tag{4.6}$$
$$\dot{m}_t = Q_i\rho_i - Q_o\rho_o \tag{4.7}$$
$$\dot{m}_s = Q_s\rho_s \tag{4.8}$$
$$\dot{h}_i = \frac{k_{pc}}{\tau_c}(m_{t,max} - m_t) - k_{ac}(h_{i2} - h_o) \tag{4.9}$$
$$h_{i2} = h_i + k_{pc}(m_{t,max} - m_t) \tag{4.10}$$
$$h_o = \min(\max(h_{i2}, h_{o,min}), h_{o,max}) \tag{4.11}$$
$$Q_s = A(1 - \min\left(\frac{Q_o^2}{(k_e h_m)^2}, 1\right))v_{s0}\frac{\rho_m - \rho_w}{\rho_s - \rho_m}\left(\frac{\rho_q - \rho_m}{\rho_q - \rho_w}\right)^{\beta} \tag{4.12}$$
$$Q_o = k_o \max(h_t - h_o, 0)^{\frac{3}{2}} \tag{4.13}$$
$$\rho_o = f(V_t, m_t, m_s, h_o), \text{ with} \tag{4.14}$$
$$f(\cdot) = \begin{cases} \rho_o = \max\left(\rho_s - k_{\rho_l}(h_o - h_s), \rho_w\right), & \text{linear model} \\ \rho_o = \rho_w + (\rho_s - \rho_w)e^{-k_{\rho_e}(h - h_s)}, & \text{exponential model} \\ \rho_o = \frac{(\rho_m - \rho_w)Q_{ms}}{Q_{ms} + Q_w} + \rho_w & \text{water layer model} \end{cases} \tag{4.15}$$

Available measurements:

Q_i	flow rate of incoming mixture in hopper
Q_o	flow rate outgoing mixture in hopper (only available in data set A)
ρ_i	incoming mixture density in the hopper (only available in data set A)
ρ_o	density of outgoing mixture in the hopper
m_t	total mass in the hopper (only available in data sets B and C)
V_t	total volume of mixture in the hopper
h_s	sand bed height in the hopper (only available in data set A)
h_o	height of the overflow weir

Parameters to be estimated:

v_{s0}	undisturbed settling velocity
ρ_s	sand bed mass
k_e	erosion parameter

Cost function:

for test rig:

$$J(\boldsymbol{\theta}) = \frac{a}{N_1}\sum_{k=1}^{N_1}(\hat{\rho}_o(k, \boldsymbol{\theta}) - \rho_o(k))^2 + \frac{1-a}{N_2}\sum_{k'=1}^{N_2}(\hat{h}_s(k', \boldsymbol{\theta}) - h_s(k'))^2 \tag{4.16}$$

for ship:

$$J(\boldsymbol{\theta}) = \frac{1}{N}\sum_{k=1}^{N}(\hat{m}_t(k, \boldsymbol{\theta}) - m_t(k))^2 \tag{4.17}$$

The model consists of three differential equations, i.e., (4.6), (4.7) and (4.8). Furthermore, the model consists of several nonlinear algebraic equations, equations (4.12)-(4.14). The measurements available for this model are presented in the overview.

It is not possible to estimate the parameter by a linear least-squares technique and, therefore, the nonlinear estimation technique described in Section 4.1.1 is used. This technique, pattern search, minimises an objective function. For the hopper model two objective functions have been defined, one for data set A (4.16) and one for data set B (4.17). The estimation problem for the test rig (data set A) differs from the estimation problem on the ship data (data set B), see the available measurements. For the test rig, there is no total mass measurement m_t, but there is a measurement of the sand bed height h_s and density ρ_o. Since the model should predict the sand bed height and the overflow density, the error between the sand bed height h_s and the density ρ_o is minimised simultaneously, see (4.16). The parameter a defines the relative importance of the two measurements. The cost function for the ship data is given by (4.17).

To predict the overflow density, we propose three alternatives: the linear model, the exponential model and the water-layer model, see (4.15). The estimation and validation experiments are performed for each of these three models to determine the performance and validity of the models.

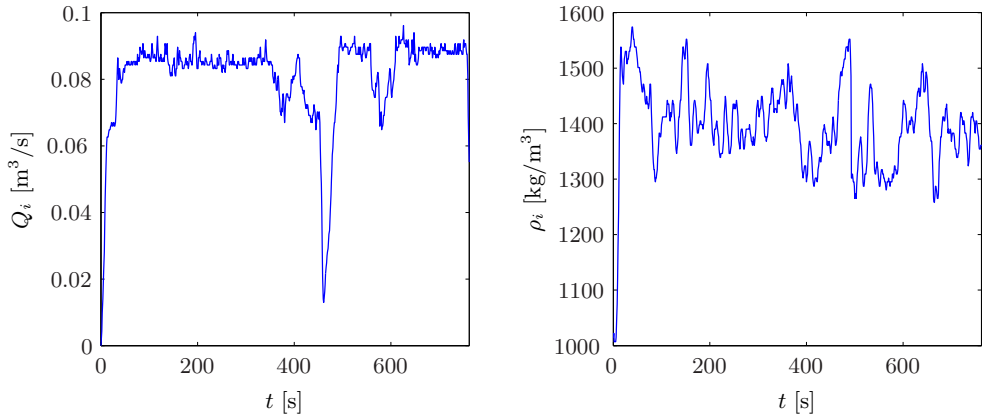

Figure 4.5: Measured inputs of the hopper test rig

Parameter Calibration and Validation Based on Data Set A from Test Rig

To investigate the performance the models are first calibrated and validated with data set A from the test rig (see Section 2.3.4). The following measurements are available from the test rig data (data set A):

- inlet pipe: flow-rate Q_i and density ρ_i, see Fig. 4.5
- hopper: height of the hopper content h_t and height of the overflow weir h_o
- overflow weir: density ρ_o and flow-rate Q_o
- inside mixture: CCMs measure the mixture density at discrete heights with a spacing of 20 cm and a radioactive concentration fork measures the density at one location. The height of this fork can be varied with time.

These CCM density measurements are not very accurate, but sufficient to indicate the height of the sand bed h_s. For one loading cycle, approximately fourteen measurements of the bed height are obtained. Note that there is no hopper mass measurement available in the test rig.

The cost function of (4.16) is minimised, where N_1 is the number of samples of the first criterion, N_2 is the number of samples of the second criterion, $\boldsymbol{\theta} = [v_{s0}\, k_e\, \rho_s]^T$ is the parameter vector, a is a weight, $\rho_o(k, \boldsymbol{\theta})$ and $h_s(k', \boldsymbol{\theta})$ are the model outputs from the ODE solver and the hat symbol $\hat{}$ denotes a measured variable.

Note that the number of measurement samples of ρ_o and h_s is different. The ρ_o is measured with a sample rate of one second and there are approximately $N_1 = 800$ measurements taken in each cycle. The bed height h_s is limited to $N_2 = 24$ samples due to the discrete placement of the CCM sensors. In practice there are at most 14 samples to work with.

The optimisation algorithm is repeated 30 times, where the parameters are randomly initialised within the ranges of Tab. 4.3. After this procedure, the run that has the smallest cost J is selected. The resulting parameters for each model are given in Tab. 4.3.

Parameter Calibration and Validation Based on Data Set B from Ship

On the actual ship the following quantities are measured:

- In the inlet pipe: the density ρ_i and the flow-rate Q_i, see Fig. 4.6.
- In the hopper: the height h_t and the height of the overflow weirs h_o.
- In the hull: the draught of the ship with pressure sensors, from these the hopper mass m_t is derived.

The density ρ_o and the flow-rate Q_o are not measured, because no sensors are installed in the overflow weirs. The measurement of the total mass is used to validate the prediction of ρ_o.

The parameter β has very little effect on the total mass, as shown with the sensitivity analysis; therefore, this parameter is kept constant at $\beta = 4$. The initial bed height h_{s0} is calculated from the initial mass and volume. If we assume that initially the hopper load is composed of a sand layer with the density ρ_s and a water-layer, the mass of the sand layer and the initial bed height are given by:

$$m_s(0) = \rho_s \left(\frac{m_t(0) - V_t(0)\rho_w}{\rho_s - \rho_w} \right) \qquad h_{s0} = \frac{m_s(0)}{\rho_s A}\,, \tag{4.18}$$

where A is the area of the hopper.

4.3.1 Results for Data Set A

This section presents the parameter estimation results of the test rig data, data set A. The calibration of the parameters is performed 30 time for each of the three models. In each trial the parameters are initialised within the ranges denoted in Tab. 4.3. After the trials, the results of the trial is selected that has the lowest value for J.

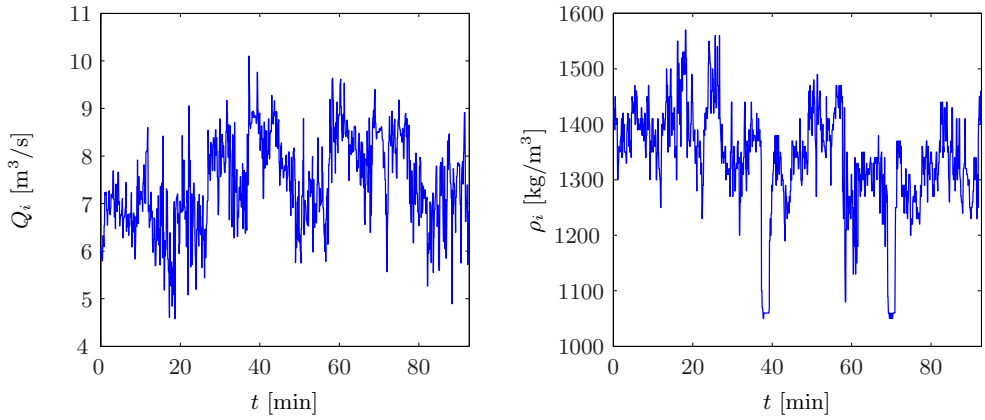

Figure 4.6: Measurements for the calibration (cycle 9), left: incoming flow-rate, right: incoming density.

Table 4.3: Results of the parameter estimation of the test rig data.

			Model		
Parameter		Range	Exponential	Linear	Water layer
v_{s0}	[mm/s]	[0.1, 400]	7.7	6.1	14.0
k_e	[m^2/s]	[0.01, 1]	0.15	0.17	0.14
ρ_s	[kg/m^3]	[1750, 1875]	1780	1750	1839
J	[-]		1.5	3.1	2.0

The simulation results for the output density ρ_o are compared with the data in right panel of Fig. 4.7. The figure shows small differences between the three models, but the exponential model has the smallest error with the data. The water-layer model overestimates the density in the beginning and the linear model does this at the end of the process.

The predicted bed height of each model is compared with the measured bed height (circles in left panel of Fig. 4.7). All three models show a good prediction of the bed height. The results of the parameter calibration are summarised in Tab. 4.3. The estimated parameters of the linear and the exponential model are very similar, but the water layer-model shows different values for v_{s0} and ρ_s. The mean particle size of the sand loaded in the hopper is between 0.11 and 0.16 mm. For this particle size, according to Budryck, the undisturbed settling velocity is between 8 and 16 mm/s. Tab. 4.3 shows that the parameter v_{s0} is 7.7 mm/s for the exponential model, 6.1 mm/s for the linear model and 15 mm/s for the water layer model. Both the linear and exponential model estimate an undisturbed settling velocity that is twice as low as the water-layer model.

The performance J of the three models is similar for the test rig data, but the exponential model is the best model and the linear model the worst model. These results do not give a definite answer to the question which model should be chosen for our application.

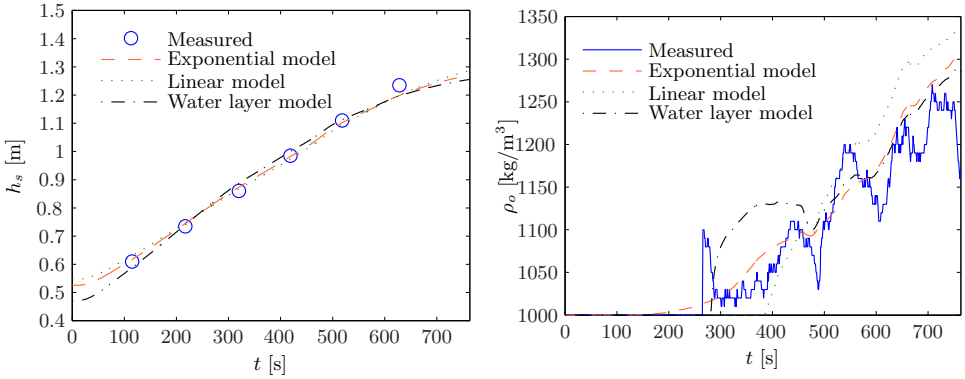

Figure 4.7: Simulated model outputs compared with data: left: h_s, right: ρ_o.

4.3.2 Results for Data Set B

This section describes the results for data set B, measured onboard a TSHD. Here the results for three cycles are shown, see Appendix B for the results of the other cycles. For each model 100 optimisation runs are performed on each cycle, where the parameters are randomly initialised within the ranges

$$\begin{aligned} v_{s0} &\in [1\ 400] && \text{mm/s} \\ k_e &\in [0.1\ 25] && - \\ \rho_s &\in [1900\ 2100] && \text{kg/m}^3\,. \end{aligned}$$

The parameter ranges are wider than for data set A, because there is more uncertainty in what the parameters should be. Moreover, the scale of the system is different which means that the range for k_e is changed. The optimal parameters are given by the median values of the 100 runs. For all cycles and models, an optimal parameter vector $\boldsymbol{\theta}$ is found. This vector is used to validate the models by predicting the total mass of the other cycles than the training cycle.

The estimated parameters

The estimated parameters that are found using the optimisation strategy, are presented in Tab. 4.4. As for data set A, the water layer model parameters differ from the parameters of the exponential and the linear model. Again, the undisturbed settling velocity v_{s0} is larger for the water layer model than for the other two. Also the sand density is slightly higher for the water layer model. The cost function shows that the water layer model has the best accuracy and the linear model the worst accuracy.

These results show that the linear model is the least accurate. The water-layer and the exponential model have an accuracy of the same order of magnitude. The validation results must show which model performs best.

Table 4.4: Calibrated parameters of the three models, a selection of three cycles (data set B).

(a) Exponential model.

Cycle	v_{s0} [mm/s]	k_e [m^2/s]	ρ_s [kg/m^3]	J [-]
5	40	25	1990	$6.7{\cdot}10^{-4}$
8	38	25	1970	$1.4{\cdot}10^{-3}$
9	41	10	1970	$6.7{\cdot}10^{-4}$

(b) Linear model.

Cycle	v_{s0} [mm/s]	k_e [m^2/s]	ρ_s [kg/m^3]	J [-]
5	0.039	25	1970	$2.4{\cdot}10^{-3}$
8	0.038	25	1950	$3.8{\cdot}10^{-3}$
9	0.039	25	1970	$2.3{\cdot}10^{-3}$

(c) Water layer model.

Cycle	v_{s0}	k_e	ρ_s	J
5	0.050	5.4	2030	$2.3{\cdot}10^{-4}$
8	0.044	5.4	1990	$3.0{\cdot}10^{-4}$
9	0.046	4.9	2000	$1.9{\cdot}10^{-4}$

The Validation results

The training results as well as the validation results of three cycles are summarised in Tab. 4.5. The index j is for the training cycle and index i for the validation cycle, i.e., the parameters are estimated with data of cycle j and then simulated with data of cycle i. Therefore, the diagonal presents the training results for $j = i$, and the off-diagonal elements the validation results. The values in the table represent the least-squares error and, thus, a smaller value indicates better model performance.

Table 4.5: Least-squares error of the training (j) and validation cycles (i).

(a) Exponential model.

i	j		
	5	8	9
5	$6.7{\cdot}10^{-4}$	$4.6{\cdot}10^{-3}$	$1.2{\cdot}10^{-3}$
8	$1.1{\cdot}10^{-3}$	$1.4{\cdot}10^{-3}$	$1.2{\cdot}10^{-3}$
9	$7.7{\cdot}10^{-4}$	$1.8{\cdot}10^{-3}$	$6.7{\cdot}10^{-4}$

(b) Linear model.

i	j		
	5	8	9
5	$2.4{\cdot}10^{-3}$	$4.1{\cdot}10^{-3}$	$3.0{\cdot}10^{-3}$
8	$2.8{\cdot}10^{-3}$	$3.8{\cdot}10^{-3}$	$2.5{\cdot}10^{-3}$
9	$2.4{\cdot}10^{-3}$	$4.0{\cdot}10^{-3}$	$2.3{\cdot}10^{-3}$

(c) Water layer model.

i	j		
	5	8	9
5	$2.3{\cdot}10^{-4}$	$7.5{\cdot}10^{-4}$	$7.2{\cdot}10^{-4}$
8	$7.3{\cdot}10^{-4}$	$3.0{\cdot}10^{-4}$	$1.9{\cdot}10^{-4}$
9	$7.9{\cdot}10^{-4}$	$3.0{\cdot}10^{-4}$	$1.9{\cdot}10^{-4}$

The cost function of the water layer model has an average of $2.4{\cdot}10^{-4}$, compared with $2.8{\cdot}10^{-3}$ for the linear model and $9.1{\cdot}10^{-4}$ for the exponential model. This means

that the validation results show that the water-layer model has the best performance. This data set shows a bigger difference in performance than data set A. The values for the validation data of each model are in the same order of magnitude which indicates that the model does not over fit the data.

Simulation outputs

In Fig. 4.8 the output density of the three models is compared with the output density calculated from the measured data. This calculation is done by differentiating the mass and volume balances; therefore, the calculated output density is very noisy. A noncausal filter is used to smoothen the data with a cut-off at 0.001 Hz. This estimate is based on the discretised equation (3.1):

$$\bar{Q}_{o,k} = Q_{i,k} - \frac{1}{T_s}(V_{t,k+1} - V_{t,k}) \tag{4.20}$$

$$\bar{\rho}_{o,k} = \frac{(Q_{i,k}\rho_{i,k} - \frac{1}{T_s}(m_{t,k+1} - m_{t,k}))}{\bar{Q}_{o,k}}. \tag{4.21}$$

Here, the bar denotes that the variable is calculated, index k denotes the discrete time step and T_s is the sample time.

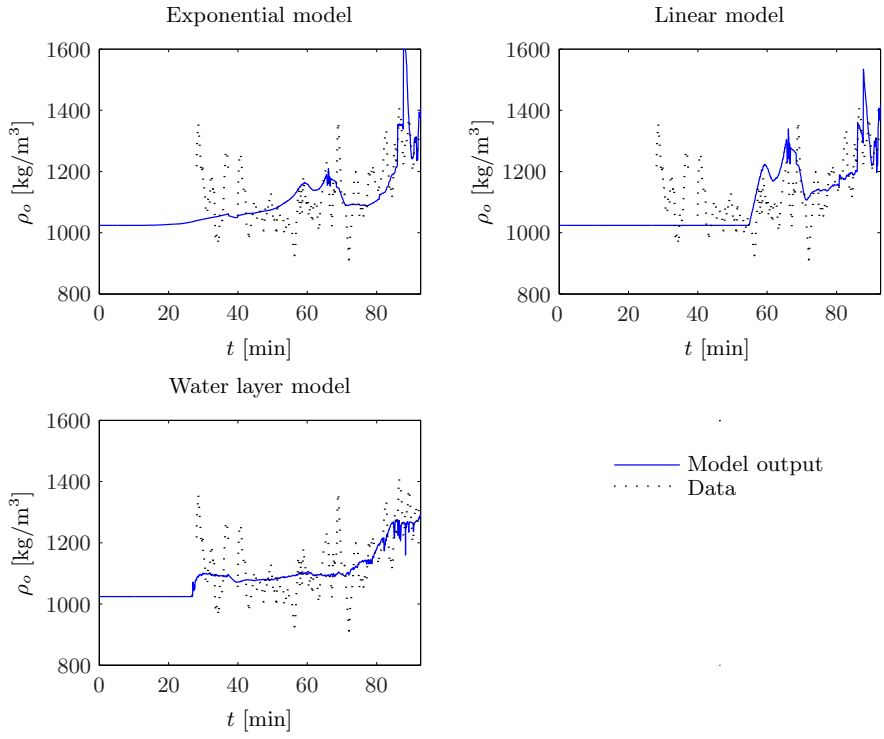

Figure 4.8: Model output density of cycle 9 compared with calculated ρ_o.

The linear model underestimates the density at the beginning of the overflow phase and compensates this by overestimating the density later. The exponential model shows similar behaviour, but not as extreme as the linear model. The water layer model first predicts a constant output density and at the end of the cycle an increasing trend. The models predict a much smoother trend for the outgoing density than the calculated density.

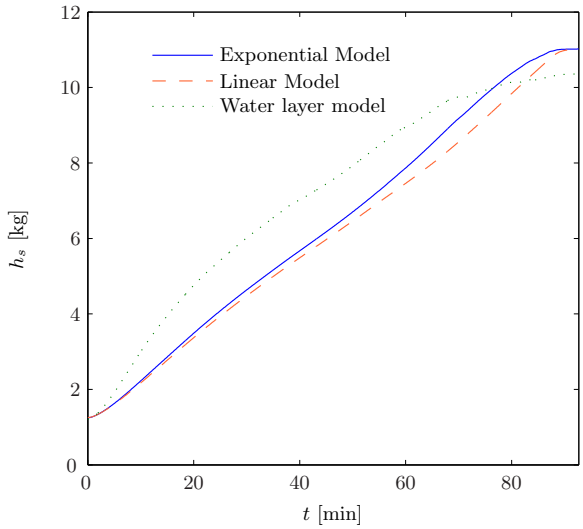

Figure 4.9: Sand bed height of cycle 9 for the three models

The predicted bed height of the water layer model compared with the other two models is different (see Fig. 4.9). This was not the case in data set A, where the three models showed similar predictions of the bed height. The linear and exponential model show similar behaviour, but the water layer model shows a much faster increase of bed height in the beginning of the cycle. Clearly, the increase in hopper size enlarges the difference between the models. The model structure for the sedimentation flow rate towards the bed is the same for all three models. In the pre-overflow phase the incoming mass is the same and, thus, the mixture density in the hopper. The only differences between the models in the pre-overflow phase are the parameters. These differences result in different sand bed behaviour. For the water-layer model it is expected that the bed rises faster, since the estimated undisturbed settling velocity is higher. Due to the integrating effect of the sand-bed model the difference increases.

Fig. 4.10 shows the simulation results of the three models compared with data. The left column in the figure displays the training results of cycle 8 and the right column figures displays the validation results of cycle 9, with the parameters estimated in cycle 8. The panels show the total hopper mass m_t from the moment the overflow phase begins. Before this phase, the data are not interesting because the simulation output is equal to the data. The simulation data show that the exponential and linear model underestimate the output density and, consequently, overestimate the total hopper mass.

The water-layer model shows a much better fit for the training data (left column). The exponential model gives a reasonable prediction after $t = 60$ min, but overall the water layer model performs much better. Clearly, the linear model is not suitable for estimation of the hopper process, because of the large prediction error. Note that the mass increases again in the hopper after $t = 75$ min, when the operators turn off the constant-tonnage loading system.

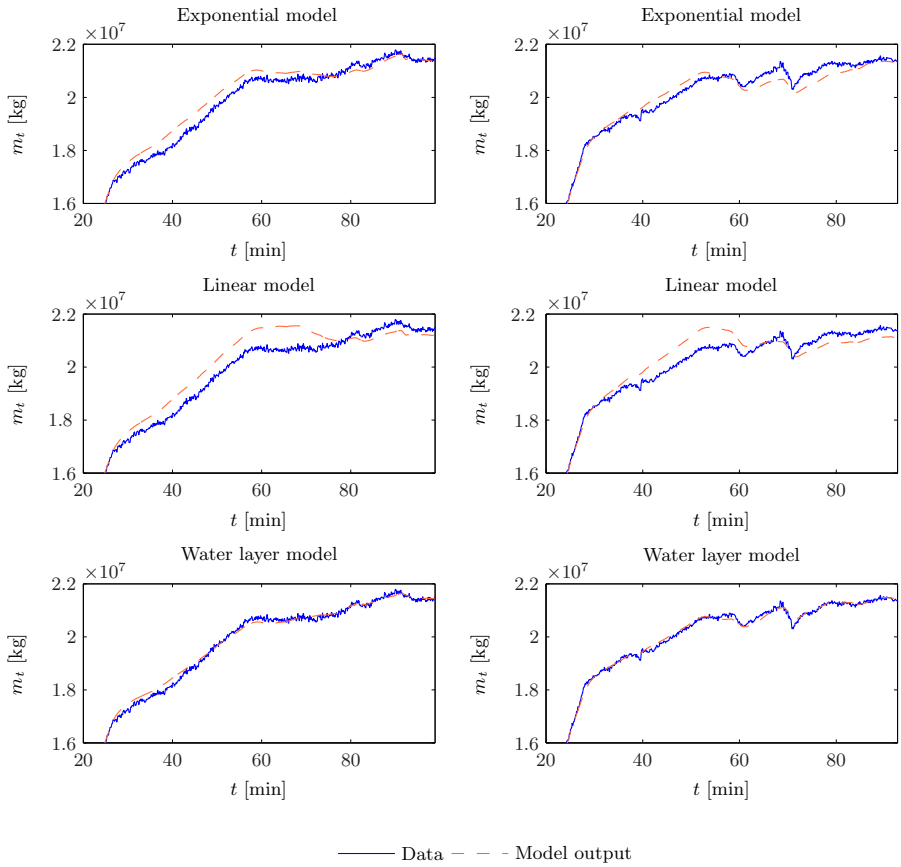

Figure 4.10: Total mass m_t in hopper: top, exponential model; middle, linear model; bottom, water layer model; left, training results; right, validation results.

The right-hand panels of Fig. 4.10 present the validation results. Again, the water layer model performs best; in fact, the performance is equal to the training data, suggesting that the model is suitable for the optimisation strategy in the next chapter. It also indicates that it is possible to use the parameters estimated in a previous cycle to predict the behaviour of the next cycle. The other two models perform worse in the validation cycle, which is consistent with the results of Tab. 4.5. We conclude that the water-layer model is most suitable for use in the optimisation strategy described in the next chapter.

4.4 Drag-Head Model

The drag-head model contains three parameters (a_{dh}, b_{dh} and c_{dh}) that need to be estimated. This is done by a linear-least squares algorithm because the estimation problem is linear in the parameters. The parameters can be directly calculated from the data by using least-squares estimation. First a brief overview of the estimation problem is presented.

System of equations:

$$\rho_i = -a_{dh} Q_i^2 + b_{dh} v_{sh} + c_{dh} \tag{4.22}$$

Available measurements:

Q_i	incoming mixture flow-rate in hopper
ρ_i	incoming mixture density at the pump
v_{sh}	ship's speed

Parameters to be estimated:

a_{dh}, b_{dh}, c_{dh}	parameters in the drag head density model

Fig. 4.11 shows the measured flow-rate and ship speed of cycle 1 that are used to predict the incoming density into the drag head.

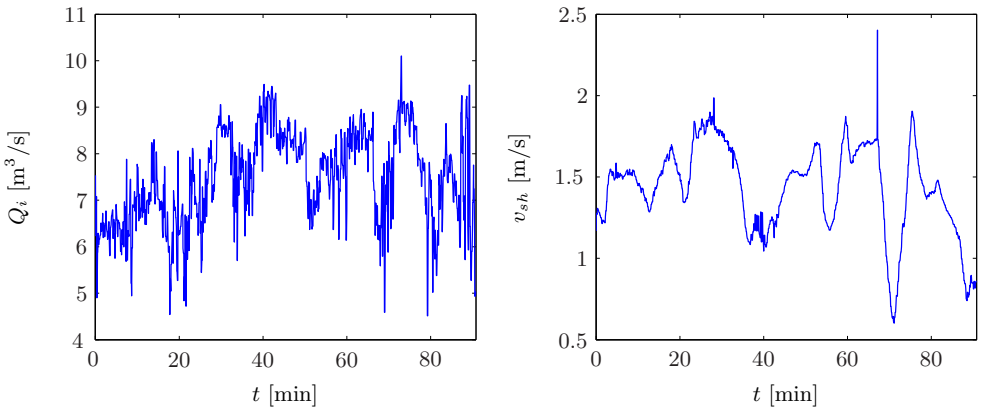

Figure 4.11: Measurements for the calibration (cycle 1), left: incoming flow-rate, right: ship's speed.

The model estimates the density in the drag head. The density is measured right after the pump. This means that the density in the drag head ρ_i is measured with a transport delay at the pump. In the modelling of the previous chapter this delay was neglected. This is justified since the model will be used in a MPC with a sample time which is much longer than the delay. To accurately calibrate the model, this delay has to be incorporated.

The model in terms of the measured variables is:

$$\rho_i(k) = \rho_{i,meas}(k+\tau) = -a_{dh}Q_i^2(k) + b_{dh}v_{sh}(k) + c_{dh}\,,$$

where k is the time index and τ the delay in samples. The parameters are calculated with the least-squares estimation (see (4.2)). For on-line calculation, however, $\rho_{i,meas}(k+\tau)$ is not known, and then the following relation is used:

$$\rho_i(k-\tau) = \rho_{i,meas}(k) = -a_{dh}Q_i^2(k-\tau) + b_{dh}v_{sh}(k-\tau) + c_{dh}\,.$$

The delay is found by estimating the parameter for different values of the delay, $\tau = 0, 1, 2, \cdots, 9$. For all the delays VAF values are calculated and the delay with the highest VAF value is chosen. The best prediction of the density is found for the delay $\tau = 3$.

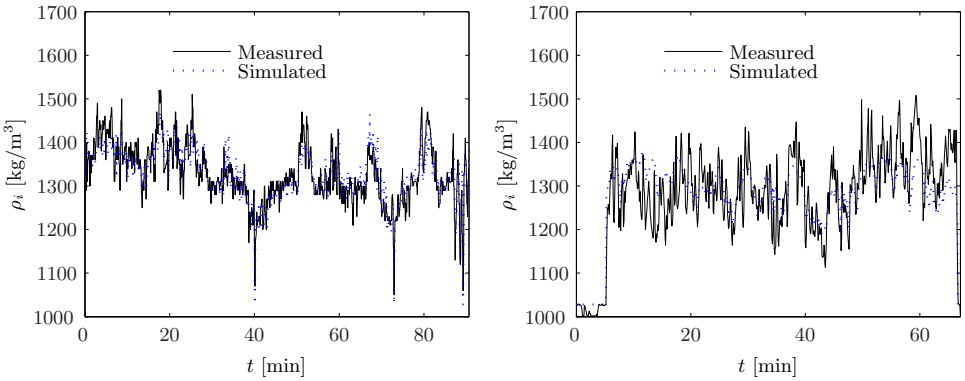

Figure 4.12: Plot of the simulated and measured density ρ_i of the drag head; left, cycle 1 (dataset B); right, cycle 12.

The validation is performed by estimating the parameters in one cycle and simulating the other cycles, i.e., these parameters are calibrated with data of the first cycle and used to optimise the second cycle and so on. Fig. 4.12 shows the simulated and measured density of the drag head of cycle 1 of data set B. This figure illustrates that the fit is very good, which is also shown by the VAF of 0.81 (see Tab. 4.6).

In this table 5 cycles are summarised. The table also shows the standard deviation (Std) of the parameters, which is in most cases less than 10% of the value. On average the estimation performance of the model with data from data set C is not as good as with data from data set B, see Tab. 4.7. The average dredged density for data set C is lower than for data set B. Therefore, the values for the parameters a_{dh} and c_{dh} are smaller in data set C.

The model validation results for data sets B and C are summarised in Tab. 4.8. The estimated parameters of one cycle are used to predict the behaviour in the other cycles. In this table the index i stands for the training cycle and the index j for the validation cycle. The first row shows VAF values of parameters estimated in the first cycle and simulated in the other cycles. On the diagonal are the VAF values of the training data. The other values show the validation results.

Table 4.6: Summary of calibration results for parameters a_{dh}, b_{dh} and c_{dh} on the first five dredging cycles of data set B.

No.	a_{dh}		b_{dh}		c_{dh}		VAF
	Mean	Std	Mean	Std	Mean	Std	
1	3.38	0.08	91	4.17	1388	7.57	0.82
2	3.09	0.07	96	4.70	1363	7.35	0.80
3	2.73	0.06	38	4.33	1393	3.54	0.84
4	4.86	0.12	101	6.24	1462	7.69	0.77
5	3.91	0.10	76	5.96	1435	11.06	0.71

Table 4.7: Summary of calibration results for parameters a_{dh}, b_{dh} and c_{dh} on the first five dredging cycles of data set C.

No.	a_{dh}		b_{dh}		c_{dh}		VAF
	Mean	Std	Mean	Std	Mean	Std	
12	1.63	0.18	93.18	11.12	1217.01	15.83	0.73
13	2.03	0.16	109.49	9.47	1185.42	17.14	0.76
14	2.35	0.15	55.63	10.04	1281.34	15.11	0.72
15	3.06	0.10	77.55	6.02	1258.38	10.46	0.73
16	2.28	0.15	112.93	8.98	1191.46	13.28	0.74

Tab. 4.8 shows that, although the prediction performance is lower for the validation cycles, the accuracy is still high for the results of data set B. The VAF values for data set C are, in general, lower than for data set B. The VAF values for the training cycles are of the same order of magnitude as for validation cycles for both data sets, meaning that the model is useful for predicting the density within one dredging project. These results are improved further by applying a recursive least-squares algorithm (Wangli, 2006) with a forgetting factor.

Table 4.8: Validation results drag head model in VAF: training cycle (i), validation cycle (j).

(a) Data set B.

i	j				
	1	2	3	4	5
1	0.82	0.80	0.80	0.73	0.72
2	0.82	0.80	0.81	0.70	0.71
3	0.78	0.77	0.84	0.71	0.68
4	0.74	0.68	0.58	0.77	0.68
5	0.81	0.78	0.75	0.77	0.72

(b) Data set C.

i	j				
	12	13	14	15	16
12	0.73	0.75	0.71	0.66	0.72
13	0.72	0.76	0.71	0.68	0.74
14	0.72	0.73	0.72	0.71	0.71
15	0.69	0.73	0.70	0.73	0.71
16	0.72	0.75	0.71	0.70	0.74

Ship speed

In data set B and C there is a correlation with the ships speed. To show this, we compare the VAF values for the density model with and without a linear relation with the ships speed in Tab. 4.9. The correlation between the ship speed and the incoming density varies from cycle to cycle. If the values for the VAF are approximately the same, the correlation with the ships speed is weak. For cycles where this is the case the parameter b is also smaller and sometimes even negative.

Table 4.9: Comparison of VAF between the density model with and without the ships speed.

(a) Data set B.

Cycle	With v_{sh}	Without v_{sh}
1	0.82	0.74
2	0.80	0.72
3	0.83	0.82
4	0.77	0.73
5	0.71	0.66

(b) Data set C.

Cycle	With v_{sh}	Without v_{sh}
11	0.73	0.68
12	0.76	0.66
13	0.72	0.71
14	0.73	0.69
15	0.74	0.62

4.5 Pump-Pipeline Model

The pump-pipeline model contains two soil-type dependent parameters: S_{kt} and γ and one parameter that is unknown beforehand λ_f. There are several sensors installed in the pump-pipeline system (see Fig. 4.13), which can be used for the calibration. The difference in pressure over the drag head Δp_d is measured (see right panel of Fig. 4.14), the inlet pressure at the pump p_{mi} and the discharge pressure at the outlet of the pump p_{mo}. With the use of the inlet and discharge pressure, the manometric head that the pump delivers Δp_{man} is calculated, see (4.28). This calculation takes the position h_{mo} of the discharge pressure sensors relative to the pump centre into account. The estimation problem of this model is summarised on the next page.

Moreover, the draught h_d and the dredging depth h_z (see Fig. 4.15), the density in discharge pipe ρ_i (see right panel of Fig. 4.14) and the incoming flow-rate Q_i are available as measurement or derived from measurements. With these measurements the estimation problem can be spit in two. The pump solids effect γ is directly calculated from measurements, see (4.24), with the use of the linear least squares technique, described in Section 4.1.1. For the calculation of the other two parameters: S_{kt} and λ_f; the differential equation of (4.23) must be used. Since differentiating the noisy signal Q_i is not an option, this calibration problem is tackled with the pattern-search method of Section 4.1.1.

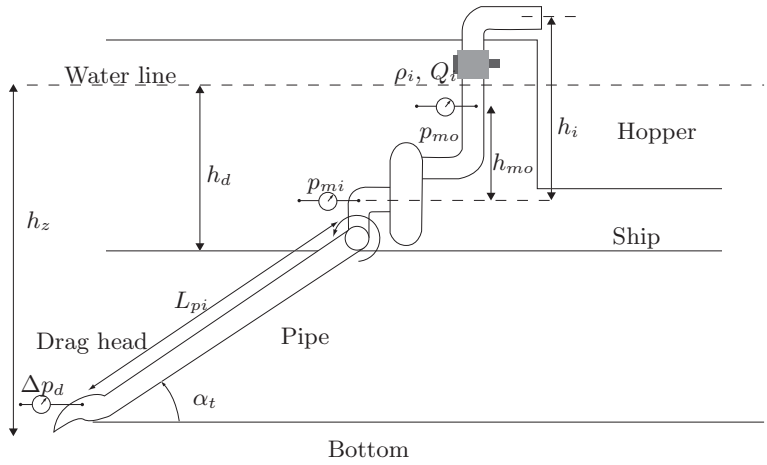

Figure 4.13: Overview pressure measurements and position of the meters.

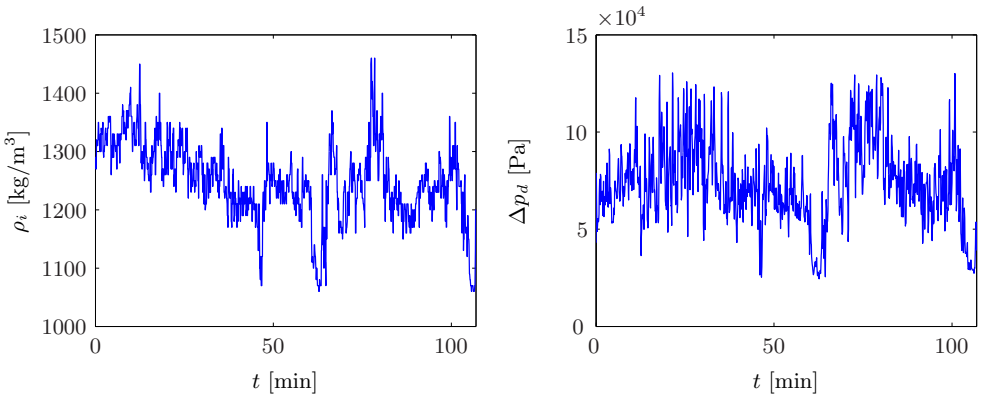

Figure 4.14: Measurements for the calibration (cycle 3), left: incoming density, right: pressure drop over drag head.

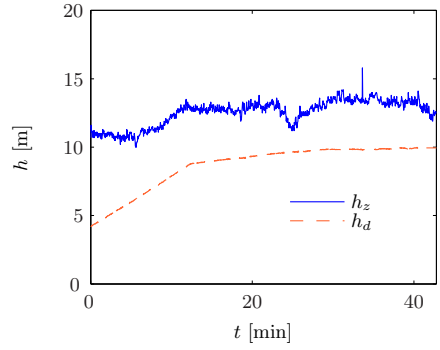

Figure 4.15: Dredging depth and draught measurement of cycle 3

System of equations:

$$\dot{Q}_i = \frac{A_p}{\rho_i L_p}(\Delta p_{man} - \Delta p_{loss} - \Delta p_s - \Delta p_d) \tag{4.23}$$

$$\Delta p_{man} = (c_{0n}\omega_p^2 - c_{1n}\omega_p Q_i - c_{2n}|Q_i|Q_i)\left(1 + \gamma\frac{\rho_i - \rho_w}{\rho_w}\right) \tag{4.24}$$

$$\Delta p_{loss} = \lambda_f Q_i^2 k_1 + \frac{S_{kt}}{Q_i}\frac{\rho_i - \rho_w}{\rho_q - \rho_w}\frac{h_z - h_d}{L_{pi}}k_2 + \frac{S_{kt}}{Q_i}\frac{\rho_i - \rho_w}{\rho_q - \rho_w}k_3 \tag{4.25}$$

$$\Delta p_s = (\rho_i - \rho_w)h_z g + \rho_i(h_i - h_d)g \tag{4.26}$$

$$\tag{4.27}$$

Measured signals:

Q_i	incoming mixture flow-rate in hopper
p_{mi}	pump inlet pressure
p_{mo}	pump outlet pressure
Δp_d	pressure drop over the drag head
ω_p	pump rotational velocity
ρ_i	incoming mixture density in the hopper
h_d	ship's draught
h_z	dredging depth

Calculated signals:

$$\Delta p_{man} = p_{mo} - p_{mi} + h_{mo} g \rho_i \tag{4.28}$$

Parameters to be estimated:

S_{kt}	transport factor in Führböter hydraulic friction model
λ_f	Darcy-Weisbach friction coefficient
γ	solid effect on the pump behaviour

$$\boldsymbol{\theta}_1 = [S_{kt}\, \lambda_f]^T$$

$$\theta_2 = \gamma$$

Cost function:

$$J(\boldsymbol{\theta}_1) = \frac{1}{N_1}\sum_{k=1}^{N_1}(\hat{Q}_i(k, \boldsymbol{\theta}_1) - Q_i(k))^2 \tag{4.29}$$

The pump and pipeline dynamics are fast compared to the other processes, such as the hopper sedimentation process. Variation in the soil type has an immediate effect on the behaviour. First, the parameters are calculated with the off-line method described in Section 4.1.1. These calibrated parameters are used for validation of the models. Thereafter, the parameters are calibrated with the on-line methods described Section 4.1.2 to investigate if the on-line methods improve the prediction performance.

Also, it is verified if a changing soil type can be estimated from the data measured.

4.5.1 Off-line Estimation

Pump Solids Effect

The parameter for the solids effect of the pump is a linear least-squares problem. To solve this problem, equation (4.24) is rearranged as follows:

$$\frac{\rho_i - \rho_w}{\rho_w}\gamma = \frac{\Delta p_{man}}{(c_{0n}\omega_p^2 - c_{1n}\omega_p Q_i - c_{2n}|Q_i|Q_i)} - 1\,,$$

which gives the following least-squares problem:

$$A = \frac{\boldsymbol{\rho_i} - \rho_w}{-\rho_w} \qquad \boldsymbol{y} = \frac{\boldsymbol{\Delta p_{man}}}{(c_{0n}\boldsymbol{\omega_p}^2 - c_{1n}\boldsymbol{\omega_p Q_i} - c_{2n}\boldsymbol{Q_i}^2)} - \mathbf{1} \qquad \theta_2 = \gamma\,,$$

where $\boldsymbol{\Delta p_{man}}$ is the pump head, calculated from the discharge pressure measurement p_{mo} and the inlet pressure measurement p_{mi} (see (4.28)). The math operators are again calculated element-wise, including the square operator ^{2}, and $\mathbf{1}$ is the unity column vector.

Pipeline Pressure Loss

The remaining two parameters, S_{kt} and λ_f, are estimated using the nonlinear optimisation technique by minimising the cost function (4.29). The suction pipe is simulated as one rigid pipe, as shown in Fig. 4.13. Data set B is used for the calibration of the parameters.

4.5.2 On-line Estimation

For the on-line estimation of the pump and pipeline model, two methods are used, recursive least-squares and the particle filter.

Pump Solids Effect

The on-line estimation of the parameter for the pump solids effect γ is calculated using the recursive least-squares algorithm of Section 4.1.2, as this parameter is linear in the parameters (see (4.24)). Instead of using data of a complete dredging cycle as in Section 4.5.1, the parameter is updated with every sampling. Since this parameter varies as the ship sails through the dredging area, the algorithm uses a forgetting factor. This problem is parameterised as follows:

$$x_k = \frac{\rho_{i,k} - \rho_w}{\rho_w} \tag{4.30}$$

$$y_k = \frac{\Delta p_{man,k}}{(c_{0n}{\omega_{p,k}}^2 - c_{1n}\omega_{p,k}Q_{i,k} - c_{2n}{Q_{i,k}}^2)} - 1 \tag{4.31}$$

$$\theta_{2,k} = \gamma_k\,. \tag{4.32}$$

The parameter $\theta_{2,k}$ is calculated at every time step k with equations 4.3 and 4.4

There are situations in which prediction of this parameter is not useful; for example, when the pump is cavitating or in the case that there is only water in the pipeline. In case of a cavitating pump the pump efficiency drops. As a result the solids effect parameter decreases, not due to a change in soil type, but because of cavitation.

When pumping water the sensitivity of the solids effect parameter in the measurement is zero. Therefore, it is useless to adapt the parameter while pumping of water. When either situation occurs the algorithm freezes the parameter and no update takes place.

Pipeline Pressure Loss

For the particle filter, it is necessary to write down the system equations in a discretised state space form. The equation of the pump-pipeline model is discretised using the Euler method:

$$Q_{i,k+1} = Q_{i,k} + \frac{T_s A_p}{\rho_{i,k} L_p}(\Delta p_{man,k} - \Delta p_{loss,k} - \Delta p_{s,k} - \Delta p_{d,k})\,,$$

where T_s is the sampling period, k the time index, Q_i the flow rate, A_p the average area of the pipeline, ρ_i the density in the pipe and the pump, L_p the length of the total pipe, Δp_{man} the pump pressure supplied, Δp_s the static pressure loss, Δp_d the pressure loss over the drag head and Δp_{loss} the pressure loss caused by friction:

$$\Delta p_{loss,k} = \lambda_f Q_{i,k}^{\,2} k_1 + \frac{S_{kt,k}}{Q_{i,k}} \frac{\rho_{i,k} - \rho_w}{\rho_q - \rho_w} \frac{h_{z,k} - h_{d,k}}{L_{pi}} k_2 + \frac{S_{kt,k}}{Q_i} \frac{\rho_{i,k} - \rho_w}{\rho_q - \rho_w} k_3\,,$$

where λ_f is the Darcy-Weisbach friction coefficient, k_1, k_2 and k_3 are constant coefficients, S_{kt} is the transport factor, ρ_w the density of water, h_z is the dredging depth, h_d is the draught of the ship, L_{pi} is the length of the suction pipe and ρ_q the density of sand quartz. Then, the state equation is augmented with a random-walk model for the parameter S_{kt}:

$$S_{kt,k+1} = S_{kt,k} + \epsilon_k\,,$$

where ϵ_k is the noise term. The particle filter assumes the most general, nonlinear state space model:

$$x_{k+1} = f(x_k, u_k, \epsilon_x) \tag{4.33}$$

$$y_k = f(x_k, \epsilon_{y_k})\,, \tag{4.34}$$

where ϵ_x is the state transition noise and ϵ_{y_k} is the output noise. In our case the augmented state, input and output vectors of the system are given by:

$$\boldsymbol{x} = \begin{pmatrix} Q_i \\ S_{kt} \end{pmatrix}, \quad \boldsymbol{u} = \begin{pmatrix} \Delta p_{man} \\ \Delta p_s \\ \Delta p_d \\ \rho_i \\ h_z \\ h_d \end{pmatrix}, \quad y = \begin{pmatrix} Q_i \end{pmatrix}.$$

4.5.3 Off-line Parameter Estimation

In off-line parameter estimation, the data of a complete cycle are available for calibration. Data set B is used, i.e., there are 11 cycles. First the parameter θ_2 is directly calculated with the least-squares technique. Then, this parameter is used in the complete pump-pipeline model to calibrate the other two parameters of $\boldsymbol{\theta}_1$ with the nonlinear optimisation technique. This last procedure is repeated 100 times for the reason explained in Section 4.1.1.

Table 4.10: Summary of calibration results for S_{kt} on the first five dredging cycles.

	S_{kt} [m/s]		γ [-]		λ_f [-]		VAF	
Range:	$0 \cdots 4$		$-1 \cdots 2$		$0 \cdots 1$			
Cycle	Median	Std	Mean	Std	Median	Std	Q_i	Δp_{man}
1	1.91	0.17	0.37	0.007	0.010	0.0014	0.72	0.50
2	1.54	0.13	0.25	0.011	0.011	0.0012	0.59	0.14
3	2.07	0.15	0.21	0.010	0.009	0.0016	0.65	0.38
4	1.10	0.28	0.32	0.007	0.013	0.0017	0.61	0.56
5	1.60	0.16	0.26	0.006	0.011	0.0013	0.71	0.61

The two parameters are randomly initialised for each run within the following ranges: $S_{kt} \in [0, 4]$ and $\lambda_f \in [0, 1]$. The results of 5 cycles are stored and summarised in Tab. 4.10. This table shows the median value and the standard deviation for parameters S_{kt} and λ_f of the 100 trials. Also, the table shows the least-squares results and the standard deviation of the parameter γ.

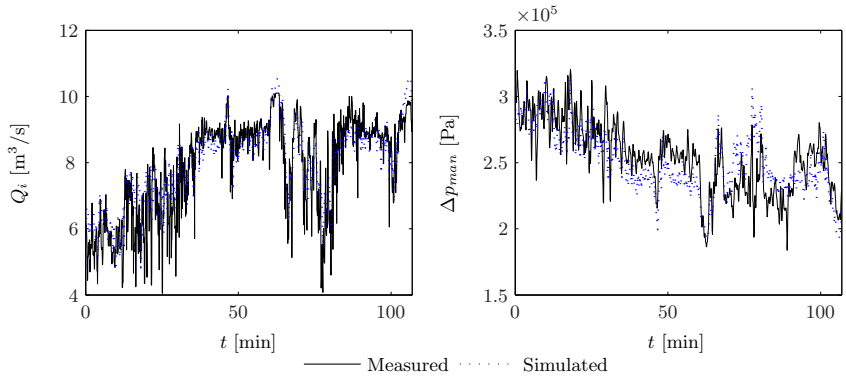

Figure 4.16: Model output and measurement of pump-pipeline system for cycle 3.

Fig. 4.16 shows the simulated and measured variables Q_i and Δp_{man} for cycle 3. The results show that VAF = 0.65 for the estimate of Q_i and VAF = 0.38 for Δp_{man}. The performance of the model varies between the cycles. Fig. 4.16 shows one of the cycles for which the model perform well and Fig. 4.17 shows a cycle for which the model performs the worst. Here the VAF values are 0.49 for Q_i and 0.21 for Δp_{man}.

The results for the first five cycles are summarised in Tab. 4.10.

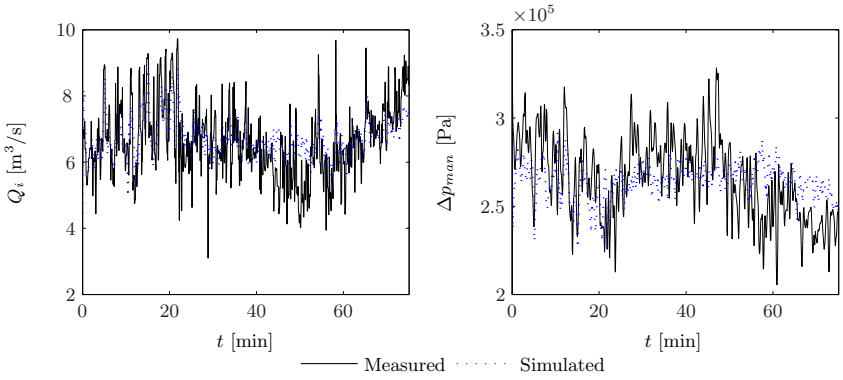

Figure 4.17: Model output and measurement of pump-pipeline system for cycle 11.

The standard deviation of the parameters in Tab. 4.10 is small, which indicates that the estimation procedure performs adequately. There is no indication that the optimisation ends in a local minimum. The parameter λ_f, representing the hydraulic pressure gradient for water, is in the expected range of $0.009 \cdots 0.015$.

To validate the model the following experiment has been performed. The parameters, found during the calibration on the training data set, are used to evaluate the prediction performance on the other cycles. The performance criteria that is used, is the VAF of the flow-rate Q_i, because that is the model output of the pump-pipeline model. The validation results are shown in Tab. 4.11. The prediction results depend heavily on the training data. For example, the data of cycle 3 and 7 perform poorly in predicting the other cycles, because the circumstances are different. The other eight training cycles perform almost equally well. The performance of the training data set is in the same order of magnitude as the validation results. This indicates that there is no over fitting. Moreover, it is clear that in some cycles the model is less accurate (cycle 11).

The pump-pipeline model and, in particular, the pump model are more sensitive to the grain size diameter of the sand. This is shown by the poor performance of the pump model in terms of VAF, see Tab. 4.10. Therefore, training the parameters on one cycle and using them in the other is not possible when the sand types differ too much. This is illustrated by the validation results of training cycles 3 and 7. In the next section, to improve the pump model performance, the parameter γ is made adaptive.

4.5.4 Adaptive Parameter Estimation of Pump Process

This section describes the estimation results of two adaptive parameter estimation techniques recursive least squares for linear problems and particle filtering for nonlinear problems.

Table 4.11: Validation results of the pump-pipeline model.

i	j										
	1	2	3	4	5	6	7	8	9	10	11
1	0.72	0.59	0.61	0.56	0.70	0.56	0.55	0.59	0.64	0.63	0.49
2	0.72	0.59	0.60	0.57	0.70	0.56	0.54	0.59	0.65	0.64	0.49
3	-4.66	-5.70	0.65	-6.78	-2.99	-2.61	-2.87	0.54	0.45	-0.44	-5.13
4	0.69	0.56	0.51	0.61	0.67	0.51	0.44	0.59	0.69	0.65	0.48
5	0.72	0.59	0.60	0.57	0.70	0.56	0.54	0.59	0.65	0.63	0.49
6	0.72	0.59	0.62	0.55	0.70	0.56	0.55	0.59	0.63	0.63	0.49
7	0.70	-0.52	0.65	0.45	0.66	-2.59	0.57	0.56	0.54	-1.28	0.45
8	0.71	0.58	0.57	0.59	0.69	0.54	0.50	0.59	0.68	0.65	0.49
9	0.68	0.55	0.49	0.61	0.66	0.50	0.42	0.59	0.69	0.65	0.48
10	0.70	0.57	0.53	0.60	0.68	0.53	0.47	0.59	0.69	0.65	0.49
11	0.71	0.58	0.57	0.58	0.70	0.55	0.51	0.59	0.67	0.64	0.49

Table 4.12: Results in VAF for the adaptive estimation. As reference the VAF of the off-line strategy of Tab. 4.10 is given. N_p is the number of prediction samples ahead.

Cycle	Reference	Train	$N_p = 1$	$N_p = 12$	$N_p = 50$	$N_p = 100$
1	0.50	0.76	0.75	0.68	0.66	0.59
2	0.14	0.68	0.67	0.60	0.49	0.42
3	0.38	0.78	0.77	0.72	0.63	0.58
4	0.56	0.78	0.77	0.70	0.56	0.45
5	0.61	0.77	0.76	0.70	0.66	0.60

Recursive Least-Squares

The pump parameter γ determines the behaviour of the pump when dredging solids. The value of the parameter depends on the average grain size of the mixture in the pump. As we have seen in the previous section this parameter is linearly dependent on the measured variables and can be calculated by a linear least-squares algorithm. To make this adaptive, the most obvious choice is to use a recursive least-squares algorithm (see Section 4.1.2).

The VAF results are given in Tab. 4.12. The forgetting factor α is set to 0.96. In the second column, the VAF of the previous section is given as reference. The third column shows the training results. The VAF is improved significantly. The other columns show the applicability of the estimation by giving the prediction results. The parameter is kept constant for N_p samples to predict Δp_{man}. The one-step-ahead prediction has almost the same performance as the training results. The larger the prediction horizon the poorer the performance. For a prediction horizon of 12 (60 s), the performance is reasonably good with a VAF between 0.6 and 0.70. The last two columns give the prediction results for a substantial amount of time, which shows that the prediction performance deteriorates.

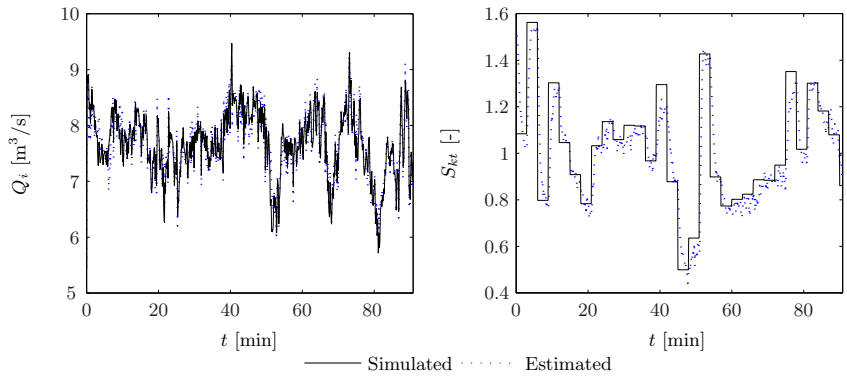

Figure 4.18: Simulation results, solid line is the simulation output and dotted line is the estimation by the particle filter.

Particle Filter

The particle filter is tuned on the pump model by supplying the measured signals $\boldsymbol{u}$ of the data set B to the model and varying the parameter S_{kt} with time. Thereafter, the simulated flow rate Q_i is used to estimate this parameter.

The parameter is randomly varied as band-limited white noise with a sample time of 3 min (see Fig. 4.18). The simulated data has a sample time of 1 s and the number of particles is chosen to be 100. A zero mean Gaussian noise is chosen with the following standard deviations: $\sigma(\epsilon_x) = [0.021\ 0.1001]^T$ and $\sigma(\epsilon_y) = 1$. These standard deviations are chosen experimentally.

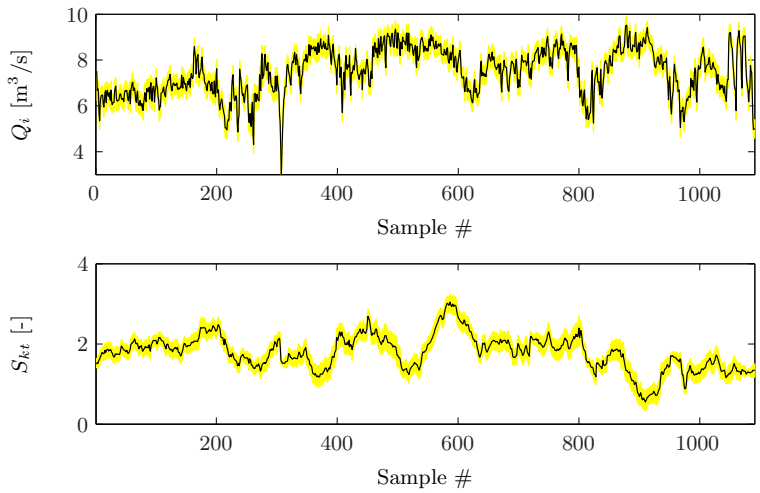

Figure 4.19: Estimation of S_{kt} with a particle filter. Black lines indicate the estimated value, grey lines the variance.

Fig. 4.18 shows the tracking result of the particle filter for the changing parameter in the right-hand panel and simulated and estimated flow rate in the left-hand panel. The filter is tuned by making a trade-off between tracking speed and noise. If the filter is tuned to track the parameter very fast, the signal of the estimated S_{kt} becomes very noisy, which is undesirable.

We use data set B to demonstrate the particle filter on data set B. The first step is to estimate the parameter S_{kt} based on data, and to do this for all the cycles. Fig. 4.19 shows the estimation result for cycle 1. The top panel shows the estimated flow rate in the solid line and in gray the variance of the estimate. The bottom panel shows the result for the estimated parameter S_{kt}. The sample time is 5 s. If the value of S_{kt} increases, this means that the grain size increases. The average value is approximately 1.8, corresponding to a grain size of 0.8 mm, according to equation (D.8). The estimated value of 1.8 is very close to the value estimated with the method described in Section 4.5.3, where $S_{kt} = 1.9$ was estimated. The use of the particle filter is further illustrated in Section 6.2.2.

4.6 Power Train Model

The ship is equipped with two power trains. The port-side engine propels the port-side propeller and a generator for electric power, and the starboard engine powers the starboard propeller, a generator and the dredge pump. The electric power is mostly used for driving the jet pumps, the bow thrusters and the auxiliaries.

System of equations:

$$I_d\dot{\omega}_{dp} = T_{dps} - k_{fr}\omega_{dp} - T_{shp} - T_{auxps} \tag{4.35}$$

$$I_d\dot{\omega}_{ds} = T_{dsb} - k_{fr}\omega_{ds} - T_p - T_{shs} - T_{auxsb} \tag{4.36}$$

$$\dot{Y}_{ip} = \frac{k_r}{\tau_i}(\omega_{dps} - \omega_{dp}) - k_{aw}(Y_{PIbps} - Y_{PIps}) \tag{4.37}$$

$$\dot{Y}_{is} = \frac{k_r}{\tau_i}(\omega_{dss} - \omega_{ds}) - k_{aw}(Y_{PIbsb} - Y_{PIsb}) \tag{4.38}$$

$$Y_{PIbps} = Y_{ip} + k_r(\omega_{dps} - \omega_{dp}) \tag{4.39}$$

$$Y_{PIbsb} = Y_{is} + k_r(\omega_{dss} - \omega_{ds}) \tag{4.40}$$

$$Y_{PIps} = \min(\max(Y_{PIbps}, Y_{lb}), Y_{ub}) \tag{4.41}$$

$$Y_{PIsb} = \min(\max(Y_{PIbsb}, Y_{lb}), Y_{ub}) \tag{4.42}$$

$$y_{max,p} = f(\omega_{dp}), \text{ see (3.45)} \tag{4.43}$$

$$y_{max,s} = f(\omega_{ds}), \text{ see (3.45)} \tag{4.44}$$

$$Y_p = \min(Y_{PIps}, y_{max,p}) \tag{4.45}$$

$$Y_s = \min(Y_{PIsb}, y_{max,s}) \tag{4.46}$$

$$T_{dps} = k_t Y_p \tag{4.47}$$

$$T_{dsb} = k_t Y_s \tag{4.48}$$

$$T_{shp} = k_T(\omega_{dp}N_s)^2\phi_p^{\frac{3}{2}} \tag{4.49}$$

$$T_{shs} = k_T(\omega_{ds}N_s)^2\phi_s^{\frac{3}{2}} \tag{4.50}$$

$$P_p = \frac{\rho_m}{\rho_w}(c_{0p}(\omega_{ds}N_p)^3 + c_{1p}(\omega_{ds}N_p)^2 Q_i + c_{2p}\omega_{ds}N_p Q_i^2 + c_{3p}Q_i^3) \tag{4.51}$$

$$T_p = \frac{P_p}{\omega_{ds}N_p} \tag{4.52}$$

Available measurements:

ω_{pp}	rotational velocity of port-side propeller shaft
ω_{ps}	rotational velocity of starboard propeller shaft
ϕ_p	propeller pitch port side
ϕ_s	propeller pitch starboard
Q_i	incoming mixture flow-rate
ρ_i	density in drag head, pipe and pump
h_z	dredging depth
v_{sh}	ship's speed
m_t	mass of hopper content

Parameters to be Calibrated:

k_T	torque gain of the shrews
T_{auxps}	torque of port-side auxiliaries
T_{auxsb}	torque of starboard auxiliaries

For the calibration of the model the fuel-rack measurement is used, which is only available in data set C. This fuel rack ranges from 0 to 1, where 1 equals maximum fuel injection. When the engine reaches maximum fuel injection, it enters the constant torque regime. This means that when the load is increased even more the speed of the engine drops and the torque remains approximately constant. During the constant torque regime the fuel injection remains at its maximum level.

The model of the power train contains no soil-dependent parameters; therefore, it is not necessary to use automatic calibration for this model. The model is calibrated manually without the use of an optimisation algorithm.

In Fig. 4.20, a comparison between the measured and simulated fuel index for the starboard and the port-side engine is shown. The port-side engine only powers the port-side propeller and the auxiliaries. The starboard engine powers the starboard propeller and the dredge pump, therefore this signal is much noisier due to the stochastic disturbances, caused by the pump torque.

The parameter k_T is manually calibrated on the port-side power train. This parameter only influences the amplitude of the port-side fuel rack. The torque T_{auxps} is calibrated on the bias of the fuel rack. The same value of k_T is used for the starboard propeller. So for the starboard side only the torque T_{auxsb} needs to be calibrated using the bias of the starboard fuel rack.

Given the maximum diesel engine power $P_{max,full}$ and nominal diesel engine angular velocity $\omega_{d,max}$, the engine gain k_t is calculated as follows:

$$k_t = \frac{P_{max,full}}{\omega_{d,max}}\,.$$

The friction coefficient k_{fr} is chosen such that with nominal diesel engine angular velocity the friction loss is 10% of the maximum power.

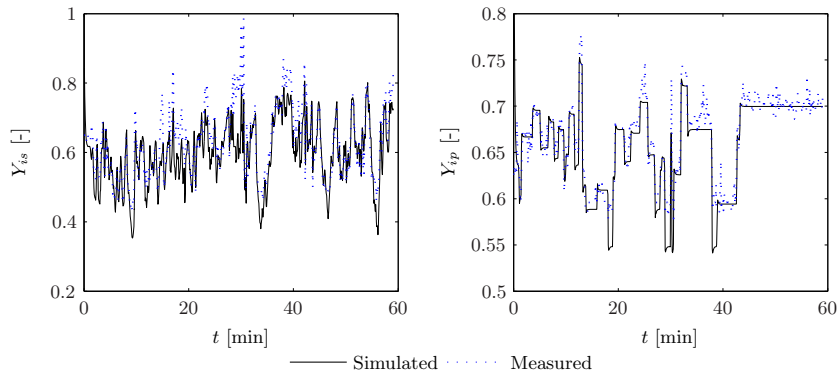

Figure 4.20: Model output and measurement of power train model for cycle 12, data set C.

Sometimes the real fuel index is higher than the modelled fuel index. This is caused by unmodelled power consumers, such as the bow thrusters. These signals are not in the data set; thus, it is not possible to take them into account.

4.7 Ship Model Including Trail Force Model

This section presents the calibration of the ship model, which simulates the forward motion. This is calibrated using numerical simulation of the model and a nonlinear optimisation for determining the parameters. Fig. 4.21 shows the propeller pitches of port-side and starboard of cycle 12 which are used for the estimation of the parameters.

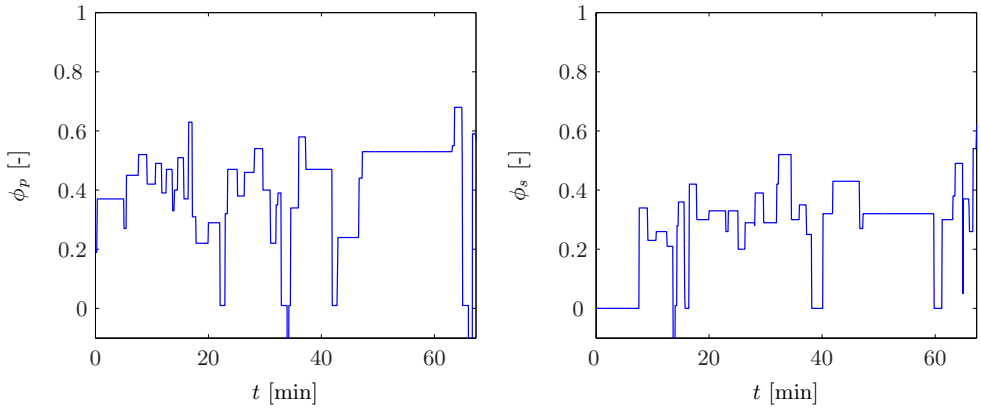

Figure 4.21: Measurements of port-side and starboard propeller pitch (cycle 12)

Three parameters must be calibrated for the ship model. These parameters determine the drag friction of the ship, pipe and drag head and the cutting forces.

System of equations:

$$\dot{v}_{sh} = \frac{1}{m_{se} + m_t}(F_{th} - F_d - F_c) \tag{4.53}$$

$$F_{th} = k_f \omega_{pp}^2 \phi_p^{\frac{3}{2}} + k_f \omega_{ps}^2 \phi_s^{\frac{3}{2}} \tag{4.54}$$

$$F_d = k_d |v_{sh}| v_{sh} \tag{4.55}$$

$$F_c = \min(k_c v_{sh} h_c^2, k_{ccav}(h_z + 10)h_c) \tag{4.56}$$

$$h_e = \frac{Q_i(\rho_i - \rho_w)}{(\rho_{si} - \rho_w) W_d v_{sh}} \tag{4.57}$$

$$h_c = \min(L_{th} \sin(\alpha_4), h_e) \tag{4.58}$$

$$\alpha_4 = f(h_e), \text{ see(3.34)- (3.35)} \tag{4.59}$$

$$\tag{4.60}$$

Available measurements:

ω_{pp}	rotational velocity of port-side propeller shaft
ω_{ps}	rotational velocity of starboard propeller shaft
ϕ_p	propeller pitch port side
ϕ_s	propeller pitch starboard
Q_i	incoming mixture flow-rate
ρ_i	density in drag head, pipe and pump
h_z	dredging depth
v_{sh}	ship's speed
m_t	mass of hopper content

Parameters to be Estimated:

k_c	cutting force coefficient non-cavitating cutting
k_{ccav}	cutting force coefficient cavitating cutting
k_d	friction coefficient total drag force

Cost function:

$$J(\boldsymbol{\theta}) = \frac{1}{N_1} \sum_{k=1}^{N_1} (\hat{v}_{sh}(k, \boldsymbol{\theta}) - v_{sh}(k))^2 \tag{4.61}$$

We use data set C for the estimation of the parameters since this is the only data set with the propeller pitch measurements. The model is tested in five cycles, see Tab. 4.13(a) for the estimation results.

As discussed in Section 3.6, there are two cutting regimes, i.e., non-cavitating cutting and cavitating cutting. This means only one part of the cutting model is active at a particular time (see (4.56)). If during the complete cycle the cutting regime is cavitating cutting, the non-cavitating model part is not active and, thus, the

parameter k_c cannot be estimated. This is one of the reasons that the value for k_c is so high in cycle 14 and 15, compared with the other cycles.

Table 4.13: Estimation and validation results.

(a) Estimated parameters for the ship model.

Cycle No.	k_{ccav}	k_c	k_d	J
12	$1.00{\cdot}10^5$	$1.28{\cdot}10^7$	$7.66{\cdot}10^4$	0.16
13	$9.12{\cdot}10^4$	$1.25{\cdot}10^7$	$7.75{\cdot}10^4$	0.16
14	$3.65{\cdot}10^4$	$5.44{\cdot}10^8$	$1.85{\cdot}10^5$	0.23
15	$6.23{\cdot}10^4$	$5.44{\cdot}10^8$	$1.13{\cdot}10^5$	0.19
16	$6.32{\cdot}10^4$	$1.02{\cdot}10^7$	$1.29{\cdot}10^5$	0.20

(b) Validation results of the ship model.

i	j				
	12	13	14	15	16
12	0.16	0.18	0.26	0.23	0.24
13	0.17	0.16	0.27	0.21	0.24
14	0.28	0.27	0.24	0.24	0.22
15	0.23	0.20	0.27	0.19	0.23
16	0.21	0.21	0.24	0.21	0.19

First data of a cycle is used to calibrate the parameters. This procedure is repeated several times; the initial guess for the parameters is chosen at random. The calibrated parameters of the best run are presented in Tab. 4.13(a). The result for cycle 16 is given in Fig. 4.22. The left-hand panel shows the model output and the measured ship speed and the right-hand panel the corresponding scatter plot. These results show a satisfactory accuracy.

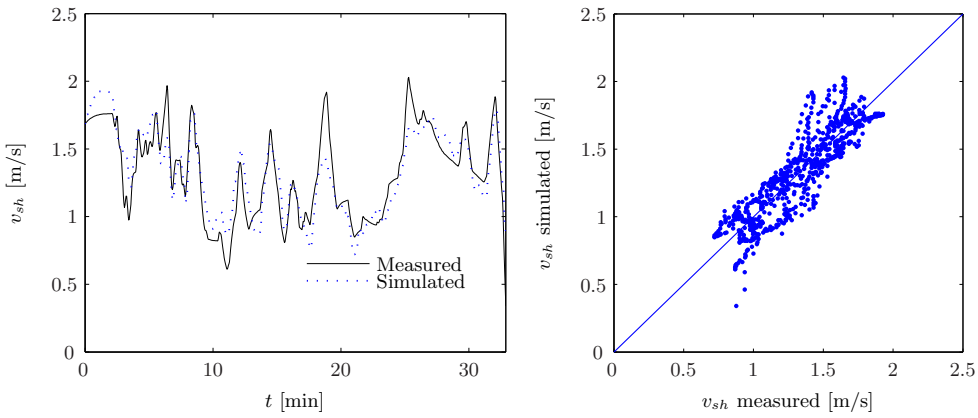

Figure 4.22: Model output and measurement of ship model for cycle twelve.

Fig. 4.23 shows the comparison of the simulated ship speed with the ship speed measured in cycle 13, using parameters calibrated with data of cycle 12. The results are comparable with the training results of Fig. 4.22. A summary of the validation results is presented in Tab. 4.13(b). The row index i is the training cycle and the column index j is the validation cycle. This means the diagonal represents the training results and the off-diagonal elements the results of the validation results. The values in the matrix represent the cost function J of equation (4.61).

There is a large variance in the estimated parameters, see Tab. 4.13(a). This may be the result of changing soil conditions such as permeability, compactness and grain size or due to unmodelled dynamics. This is plausible since the proposed model is a crude simplification of the total complex behaviour. Unfortunately, there was no data available which included the measured trail force and there are a lot of parameters unknown. These facts limit the possibility to do extensive research on validation and modelling of the sailing model. However, despite these limitations, the model shows sufficient similarities with the data to be useful in our application.

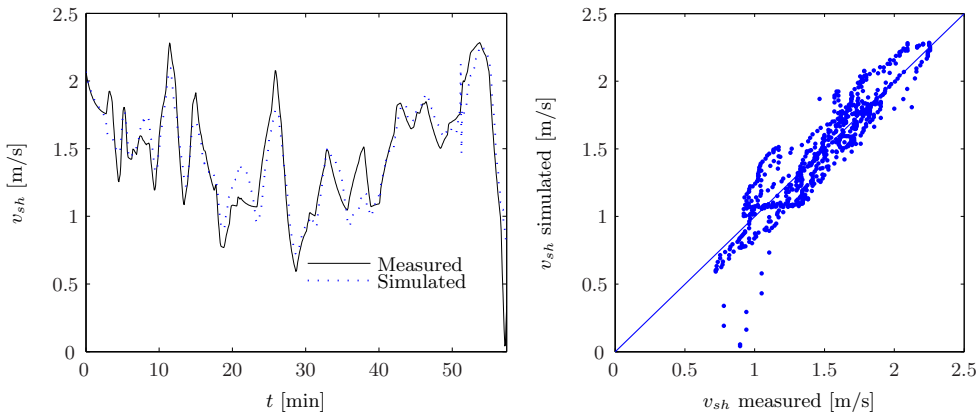

Figure 4.23: Validation of ship model on cycle 13, parameters trained on cycle 12.

4.8 Concluding Remarks

This chapter showed the calibration results and validation results of the five models discussed in Chapter 3. Some of the parameters are calculated directly from the data by means of a linear least-squares technique. This can be converted to an adaptive recursive least-squares technique if the parameter varies in time, e.g., for the pump model parameter γ. The nonlinear parameter estimation problem is tackled by numerical integration of the differential equations and minimising a cost function based on the sum of squares. An optimisation technique called pattern search is used for minimising the cost function.

One parameter, the exponent (β) in the hopper model, is very hard to estimate, because the cost function to be minimises is not sensitive for this parameter. This is caused by the fact that the parameter has no significant influence on the behaviour of

the process. We will use a value taken from literature, see (D.7) in Appendix D.

The internal behaviour of the hopper is only visible in the measurement when a mixture of sand and water is flowing out. In the first phase of the loading or in case only water is flowing out through the overflow weir, the parameters cannot be identified using the estimation algorithms of this chapter. However, the validation results showed that it is possible to estimate the parameters on the data of the previous cycle and use these to predict the behaviour of the next cycle. Another workaround in these situations is to use the parameter estimation in the pump-pipeline process. An average grain size can be estimated from pump-pipeline parameters. From this grain size it is possible to calculate the corresponding hopper parameters, using, for example, empirical relations from the literature.

The calibration of the parameters in the drag-head model with Data set B showed that the variation in the parameters per cycle is not much. The validation results show that the model is able to predict the incoming density of a cycle based on the parameter estimation of the a previous cycle. For data set C the performance of the model is not as good as for data set B. Part of the behaviour of this model is caused by the pump and its vacuum limitations; therefore, there exists a large correlation with the flow rate. The ship speed is also influencing the incoming density especially in data set B, but the influence of the ship speed is much weaker in data set C. In several cycles, the effect of the ship speed is negligible.

The pump-pipeline system is equipped with sufficient sensors to obtain good estimates of the parameters. This can be seen in the relatively small standard deviation of the parameters obtained. The solids effect in the pump cannot be estimated accurately enough with one parameter for the complete cycle. This is solved by using an adaptive least-squares filter to update the parameters. This gives reasonably good predictions for the minute ahead, which will be sufficient since this will be the controller sample time.

The predicted ship speed shows enough similarities with the data to be applicable in our application. However, the calibrated parameters for the trail force vary a lot between cycles. This is caused by changing soil conditions, such as the grain size and permeability, and unmodelled dynamics. If the data used to estimate do not contain enough information, it is difficult to estimate the parameters for non-cavitating cutting and cavitating cutting. This problem must be addressed in future research, as our data set is not suitable to be used in improvement of the models, since there are too many uncertainties and too many unknowns.

Now that the parameters have been calibrated and the models have been validated, in the next chapter we will concentrate on optimising the dredging performance.

5

Optimal Control for Hopper Loading

In the previous two chapters a complete model has been derived and validated with measured data. This model can now be used for designing and testing a controller. This chapter addresses the optimisation of the dredging process by finding an optimal control strategy. Optimal control of a nonlinear system is a complicated issue. The optimal control can be formulated as a constraint based optimisation. This subject has been treated in the classical theory of Optimal Control as developed between 1955 and 1970 (Bellman, 1957; Pontryagin et al., 1962; Canon and Eaton, 1966; Tabak and Kuo, 1969). The solution to the optimal control problem is known and obtained using the Hamilton-Jacobi-Bellman equation. Unfortunately, in most cases it is virtually impossible to solve the optimal control problem analytically. In practice these problems are solved by numerical techniques.

This chapter describes two optimisation techniques: dynamic optimisation with time discretisation (Dynopt) (see Section 5.4.1) and model predictive control (MPC, see Section 5.4.2). Once the techniques have been introduced, first, we show the optimisation of hopper sedimentation/drag-head process in Section 5.5 and then the optimisation of the overall process in Section 5.6. Parts of this chapter have been published in (Braaksma, Klaassens, Babuška and de Keizer, 2007b) and (Braaksma, Osnabrugge, Babuška, de Keizer and Klaassens, 2007).

5.1 Conventional Control of the Trailing Suction Hopper Dredger

Currently, the control system of the trailing suction hopper dredger (TSHD) consists of several local controllers. Each of these controllers influences a small part of the total system. Set-points for the controllers are often determined by the operators. This is not an easy task, because of the complexity of the whole system and the interaction between the local systems. Moreover, varying soil conditions require constant adjustment of these local set-points. In practice, most of the set-points are kept constant, whereas only a few are manually adjusted by operators. Although the ship is equipped with a flow controller and speed controller, in our data set these are not used during the dredging. An interview with the crew revealed that they do not use the controllers because it is unclear how to operate them and what the set-points should be. The

following observations from the data sets were made:

- The ship's speed is manually controlled and, therefore, varies substantially, between 0.35 m/s and 2.0 m/s.

- The pump speed, in fact the diesel engine speed, is kept at its maximum (nominal) speed. One reason for this is to have the maximum power available.

- The ship uses a constant tonnage loading system, which lowers the overflow height as soon as the maximum draught is reached.

To conclude, the controllers are designed from a local perspective and it is unclear how to determine the optimal set-points for these controllers individually in order to achieve global optimal performance. Only experienced operators are able to accomplish this. Therefore, we propose a control methodology that takes all the important processes into account and optimises the overall performance. The approach in this thesis is based on the MPC method, which optimises an objective function with the use of an internal model. The MPC method is especially suitable for this task since it respects constraints. For a TSHD, it is very important, that the system operates within its safety limits. Moreover, the overall performance is optimised taking all the important aspects into account.

5.2 Optimisation Problem

Before designing the controller that optimises the dredging performance, we state the general optimisation problem. The formulation starts with the choice of the objective for the optimisation. For the TSHD, this objective depends on the type of dredging work and the aim of the project. In this thesis, we focus on maximising the production of sand. There are more options, such as optimising the profit, but such an objective function includes uncertain parameters such as fuel cost and the market value of a cubic metre of sand.

The dredging cycle is a process consisting of dredging, sailing to the discharging area, discharging and sailing back to the dredging area. As demonstrated in Section 2.7, the economical loading depends on the sailing and discharge time. To incorporate this, the following objective for the optimisation problem is postulated:

$$J = \frac{\mathrm{TDS}(T_d)}{t_{dis} + t_{sail} + T_d}\,, \tag{5.1}$$

where $\mathrm{TDS}(T_d)$ is the amount of sand in the hopper expressed in tons of dry solids (see (2.1)) time at the end of the dredging cycle, T_d is the time for dredging, t_{dis} is the time for discharging and t_{sail} is the time for sailing. To generalize this objective

function, we introduce the state vector for the total model:

$$\boldsymbol{x}(t) = \begin{pmatrix} x_1(t) \\ x_2(t) \\ \vdots \\ x_{10}(t) \end{pmatrix} = \begin{pmatrix} V_t(t) \\ m_t(t) \\ m_s(t) \\ h_{ci}(t) \\ Q_i(t) \\ v_{sh}(t) \\ \omega_{dp}(t) \\ \omega_{ds}(t) \\ Y_{ip}(t) \\ Y_{is}(t) \end{pmatrix},$$

where m_s is the mass of the sand bed in the hopper, m_t the total mass in the hopper, V_t the total volume in the hopper, h_{ci} the output of the integrator of the constant tonnage controller, Q_i the incoming flow rate, v_{sh} the ships speed, ω_{dp} the port-side diesel engine speed, ω_{ds} the starboard diesel engine speed, Y_{ip} the output of the integrator in the port-side fuel rack controller and Y_{is} the output of the integrator in the starboard fuel rack controller. Given the state vector, the objective function becomes:

$$J(\boldsymbol{x}(T_d), T_d) = \frac{(x_2(T_d) - x_1(T_d)\rho_w)}{t_{dis} + t_{sail} + T_d} \frac{\rho_q}{\rho_q - \rho_w} \tag{5.2}$$

which we will call the *cycle production rate*. The optimisation problem is to maximise the objective function by finding the optimal input trajectories and the optimal dredging time subject to the constraints. These constraints consist of equality constraints in the form of the state equations and inequality constraints. There are inequality constraints for the inputs such as the input limits and for the states such as for example the maximum allowable mass in the hopper. Mathematically, this is formulated as follows:

$$\max_{T_d, \boldsymbol{u}(t)} J(\boldsymbol{x}(T_d), T_d) \tag{5.3}$$

subject to

$$\begin{aligned} &\dot{\boldsymbol{x}}(t) = f(\boldsymbol{x}(t), \boldsymbol{u}(t), t) \\ &g(\boldsymbol{u}(t), t) \geq 0 \\ &h(\boldsymbol{x}(t), t) \geq 0, \end{aligned} \tag{5.4}$$

where $\boldsymbol{x}(t)$ are the system state trajectories, $\boldsymbol{u}(t)$ the system inputs trajectories, f the nonlinear system equations described in Chapter 3 and g and h are constraint functions. Note that the control inputs, as well as the dredging time T_d, are the degrees of freedom for the optimisation.

5.2.1 Model Construction

Several configurations are considered for the optimisation problem in this chapter. We start by analysing a simple model that simulates the hopper process and excavation process and end with analysing the complete model.

Three configurations are considered:

1. A simplified system with only a hopper model and a drag-head model.
2. The same system as 1, but with two dredging pipes.
3. The complete ship with all the models described in Chapter 3 with one dredging pipe.

Hopper Process with One Dredging Pipe

Before discussing the optimisation of the complete TSHD the optimisation methods are first demonstrated on a simple representation of the TSHD. We call this configuration the hopper process, since this process plays the central role. The system combines the drag-head model of Section 3.3 and the hopper model of Section 3.2 (water layer model). The drag-head model is used here to constrain the incoming density. Without the drag-head model all combinations of flow and density would be possible, which is not a realistic view of reality. Note that this system has no pump model and sailing model, which means that it does not take effects such as cavitation and power consumption into account.

Given this model structure (Fig. 5.1) the inputs of the system are incoming flow rate into the hopper, overflow height and ship speed. According to the black-box drag-head model, the density of the drag head depends linearly on the ship's speed (see equation (3.29)) and quadratically with the flow-rate (negatively correlated). In this benchmark we are not interested in optimizing the ship speed, therefore, this speed is chosen at a value of 1.5 m/s. The data show that this is a realistic value.

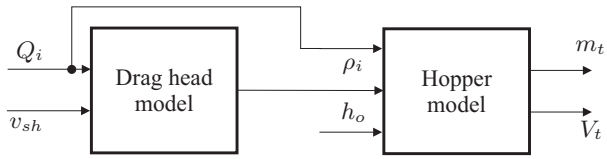

Figure 5.1: Block diagram of the hopper process.

The outputs of the system are determined by the objective function discussed in Section 5.2 and the constraints. For this system there are several constraints. First of all, the control inputs flow rate Q_i and the overflow height h_o are limited by their minimum and maximum value. The flow velocity in the suction pipe must be higher than the critical velocity to prevent sedimentation of sand in the pipe. Furthermore, the maximum flow rate is determined by the pump capacity. The overflow height is constrained by its physical limitation of a minimum and maximum height. There is another constraint for the hopper process, the maximum allowable draught, which is translated to a maximum allowable mass m_t of sand and water in the hopper. Mathematically the constraints are given by:

$$m_t < m_{t,max} \tag{5.5}$$

$$Q_{i,min} \leq Q_i \leq Q_{i,max} \tag{5.6}$$

$$h_{o,min} \leq h_o \leq h_{o,max}\,. \tag{5.7}$$

The hopper process is modelled in Section 3.2 and has three states, with the following structure:

$$\begin{aligned} \dot{V}_t &= Q_i - Q_o \\ \dot{m}_t &= Q_i \rho_i - Q_o \rho_o \\ \dot{m}_s &= Q_s \rho_s \,. \end{aligned} \tag{5.8}$$

The inputs such as the incoming flow rate Q_i and the overflow height h_o are chosen as subject for this optimisation. The incoming density is modelled by the following equation:

$$\rho_i = a_{dh} Q_i^2 + b_{dh} v_{sh} + c_{dh} \tag{5.9}$$

In this section we assume that the ship speed v_{sh} is constant. For the overflow density model we use the water layer model.

The hopper model has three states and the drag-head model none, so the state vector is defined as follows:

$$\boldsymbol{x}(t) = \begin{pmatrix} V_t(t) \\ m_t(t) \\ m_s(t) \end{pmatrix}$$

We consider a passive drag head where the production rate and input density is determined by the incoming flow rate Q_i. The other input is the overflow height inside the hopper h_o, so the input vector is the following:

$$\boldsymbol{u}(t) = \begin{pmatrix} u_1(t) \\ u_2(t) \end{pmatrix} = \begin{pmatrix} Q_i(t) \\ h_o(t) \end{pmatrix}$$

Hopper Process with Two Dredging Pipes

This system is the same as the system described above, but it has two dredging pipes. Two pumps, pipes and drag heads mean that the incoming flow rate Q_i will be higher. However, it is not realistic to assume that the flow rate increases twofold. If a ship is equipped with only one dredge pipe, in general the pump capacity of this one pump is larger than a single pump of a two-pipe ship with the same capacity. A small comparative study revealed that it is reasonable to assume that the total pump capacity increases with a factor 1.6. Given the model structure for this two-pipe configuration, the number of inputs is four: two incoming flow rates, the ship's speed and the overflow height. However, the models for the incoming density of the two flow rates are identical. Therefore, the incoming flow rate is considered as one input.

The drag-head model must be modified for this new configuration, which means scaling the incoming density model. Therefore, the drag-head model is given by:

$$\rho_i = a_{dh} \left(\frac{Q_i}{1.6} \right)^2 + b_{dh} v_{sh} + c_{dh} \,. \tag{5.10}$$

where the parameters a_{dh}, b_{dh} and c_{dh} are the same as for the one pipe model.

The constraints for this model are:

$$\begin{aligned} m_t &< m_{t,max} \\ 1.6 \cdot Q_{i,min} \leq & Q_i \leq 1.6 \cdot Q_{i,max} \\ h_{o,min} \leq & h_o \leq h_{o,max} \end{aligned}$$

Overall Process with One Dredging Pipe

The last configuration that is considered, is the overall process with one dredging pipe (Fig. 5.2). This system includes all the sub-processes, such as the pump, drag head, ship model, hopper and engines. With this system, all aspects of dredging are incorporated, such as power limitation, vacuum constraints and ship speed.

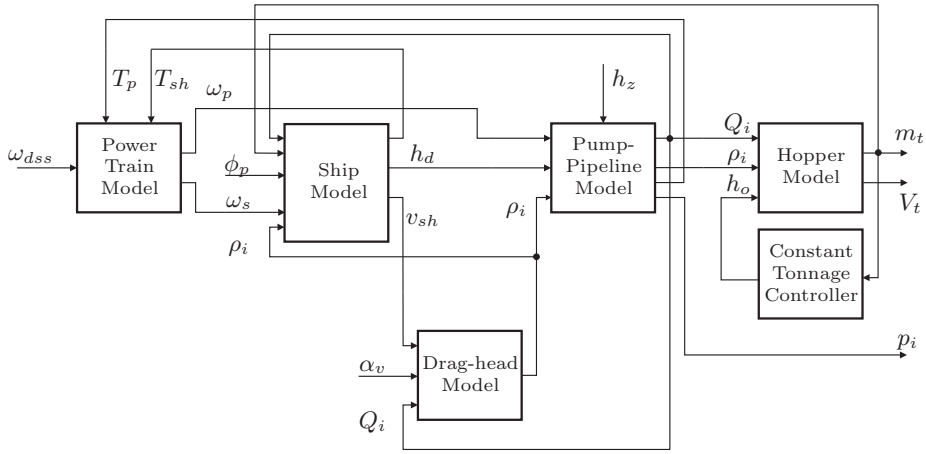

Figure 5.2: Block diagram of the overall model.

Given the model structure the following inputs can be distinguished: the diesel engine angular velocity of the port-side engine and of the starboard engine, the propeller pitch of the port-side propeller and starboard propeller, the overflow height and the water valve. We use only the port-side pitch angle to control the speed of the ship. Since the dredge pump is connected to the starboard engine, this engine speed is controlled to regulate the incoming flow rate. The port-side engine drives the port-side propeller at its nominal speed. Finally, for the overflow height a constant tonnage controller is used, because the results of the optimisation of the hopper process will show that this is the optimal strategy.

The number of inputs is now reduced to three: port-side propeller pitch ϕ_p, the starboard diesel engine angular velocity set-point ω_{dss} and the water valve α_v. Each of these inputs controls a unique variable. The port-side propeller pitch determines the ship speed v_{sh}, the starboard diesel engine angular velocity the flow rate Q_i and the water valve the input density ρ_i. The input vector $\boldsymbol{u}(t)$ is defined as:

$$\boldsymbol{u}(t) = \begin{pmatrix} u_1(t) \\ u_2(t) \\ u_3(t) \end{pmatrix} = \begin{pmatrix} \phi_p(t) \\ \omega_{dss}(t) \\ \alpha_v(t) \end{pmatrix}$$

This configuration uses all the models which are described in Chapter 3. The constraints for this system are:

$$\begin{aligned} m_t &\leq m_{t,max} \\ Q_i &\geq Q_{i,min} \\ p_i &\geq p_{imin} \\ v_{shmin} \leq v_{sh} &\leq v_{shmax} \\ Y_{is} &\leq Y_{max} \\ Y_{ip} &\leq Y_{max}\,. \end{aligned}$$

The total mass in the hopper must be less than $m_{t,max}$. The lower limit $Q_{i,min}$ for the incoming flow rate prevents settling of the sand in the suction pipe. Note, that this system does not need an upper bound of the flow rate, since the pump is explicitly modelled, so the model itself assures that the flow rate is within the pump capacity. To prevent the pump from cavitating, the absolute inlet pressure must be higher than the minimum allowed pressure p_{imin}. The ship's speed must be higher than v_{shmin}, because of safety reasons. When the ship sails too slow it might start sailing backwards due to for example the current and damage the dredging pipe and drag head. We have also defined a maximum for the ship speed v_{shmax}. A high ship speed can cause excessive trail forces and loss of contact between the drag head and the ground (bouncing). The latter effect decreases the production rate. Since this effect is not modelled in the drag-head model, we define this maximum constraint on the ship's speed to assure that the system stays within the modelled boundaries. Finally, the fuel racks of both engines (Y_{is} and Y_{ip}) are constrained by the maximum Y_{max}.

5.2.2 Optimisation Setup

Two approaches are applied to the optimisation problem of (5.4): MPC and dynamic optimisation with time discretisation (Dynopt) using a nonlinear program (NLP) solver (Biegler and Grossmann, 2004). The method used here is Dynopt with full descretisation. The details of Dynopt are given in Section 5.4. Each of the two methods is applied for a different purpose. For the on-line application, we will use MPC. The Dynopt method is used in this thesis to verify if the optimum found by the MPC is correct. The Dynopt method by itself is an off-line optimisation algorithm; however, it can also be used in the MPC as optimisation algorithm.

In this thesis, the Patternsearch algorithm, presented in Section 4.1.1, is used as nonlinear optimisation algorithm in the MPC. Patternsearch is used, because it performs more reliable and is more accurate than the Dynopt method. Dynopt is less accurate because it uses much larger step sizes for the time discretisation than the Patternsearch method. For the hopper model this is not a problem, because the dynamics have a large time constant. For the complete model the step sizes of Dynopt are too large to accurately incorporate the pump dynamics and local controller dynamics. Therefore, the comparison of MPC based on Patternsearch is only performed for the hopper sedimentation process. An overview of the optimisation setup is given in Tab. 5.1.

Table 5.1: Overview of the three configurations for the optimisation strategies in this chapter.

Name	Hopper process with one pipe	Hopper process with two pipes	Overall process
Models involved	Hopper, Drag head	Hopper, Drag head	All
System inputs	Q_i, h_o	Q_i, h_o	ϕ_p, ω_d, α_v
Optimisation Techniques	Dynopt, MPC	Dynopt	MPC
Soil Types	Fine (soil type 1), Medium/Fine (soil type 2), Coarse (soil type 5)	Medium/Fine (soil type 2)	Medium/Fine (soil type 2), Coarse (soil type 5)

We use parameters of five theoretical defined soil types in this thesis, which are defined in Appendix D, and the parameters found with the calibration of Chapter 4. The soil types range from fine (soil type 1) to coarse (soil type 5). Although the simulation is performed for al five soil types, only part of the simulations is presented here for compactness. Tab. 5.1 shows for which soil types results are presented.

5.3 Benchmark

In order to be able to make a judgement on the performance of the optimisation techniques we need to define a benchmark. Since the three configurations are different, the benchmarks will also be different. The benchmarks are optimised according to an operator philosophy, which is focussed on maximising the excavation production. This strategy makes sense, because operators cannot see what the effect of their control actions on the sedimentation process immediately is.

5.3.1 Hopper Process

For the hopper process with one pipe and the hopper process with two pipes (Tab. 5.1), the benchmark is determined as given below. The incoming flow rate Q_i is controlled such that the incoming production rate is maximal. The incoming production rate is:

$$P_{in} = \frac{\rho_i - \rho_w}{\rho_q - \rho_w} Q_i \rho_q \tag{5.11}$$

The optimum production rate is found by substituting (3.29) in (5.11) and solving:

$$\frac{\partial P_{in}}{\partial Q_i} = 0\,.$$

This maximum is given by the following equation:

$$Q_{i,max} = \sqrt{\frac{-b_{dh} v_{sh} - c_{dh} + \rho_w}{-3a_{dh}}}\,. \tag{5.12}$$

This comparison will show when the sedimentation process is important enough that it should be incorporated into the dredging strategy. The overflow height is controlled with a constant tonnage loading controller as it would be in daily practice.

5.3.2 Overall Process

For the overall process (Tab. 5.1), the benchmark is inspired by observations from the data. The data showed that the starboard diesel engine is always at its nominal speed, which means that the flow rate Q_i is not controlled. Although the ship's speed is not controlled in our data set, for this benchmark we do control the speed at the maximum constraint to increase the density as much as possible. The incoming density is maximised as long as the vacuum of the pump allows, otherwise the density is controlled such that the inlet pressure is at its minimum constraint. A constant-tonnage loading system controls the overflow height. Compared to the data set B, this benchmark performs just as well or better.

For the overall process, the performance of the MPC is also compared with the dredging performance measured in data set B, using the parameters estimated in Chapter 4.

The performance of the system is defined in terms of cycle production, see equation (5.1). This means that the time for sailing and discharging is taken into account. This performance index calculates the production rate of the hopper dredger.

5.4 Dynamic Optimisation

The dynamic optimisation problem of (5.4) can be solved analytically for simple non-linear problems. However, for complicated problems it is very hard or even impossible to find an algebraic expression for the solution. In this case, the state trajectories are calculated by numerical integration.

The dynamic optimisation problem is a Nonlinear Program (NLP) with the exception of the differential equations. To solve this NLP problem several approaches can be used (Biegler and Grossmann, 2004; Grossmann and Biegler, 2004). The first approach uses a separate numerical integrator (sequential approach, Fig. 5.3), and in the second approach the states are discretised and become equality constraints in the NLP problem (simultaneous approach).

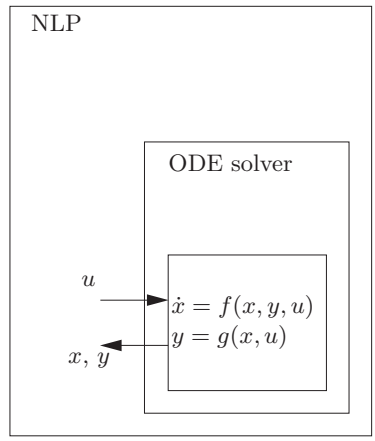

Figure 5.3: Sequential approach for solving a NLP.

The sequential approach has two main components: a NLP solver and an Ordinary Differential Equation (ODE) solver. The NLP solver feeds the decision variables (control inputs) to the ODE solver. This solver simulates the state trajectory $\boldsymbol{x}$ of the model and returns these, together with the output $\boldsymbol{y}$ to the NLP solver.

The strategy, full discretisation, discretises the objective function in time, as well as the constraints. The state trajectories are calculated by treating (5.4) as an equality constraint when solving the optimisation problem. Another strategy calculates the state trajectories with an ordinary differential equation (ODE) solver and uses these trajectories to calculate the objective function.

5.4.1 Dynopt

The dynamic optimisation problem with nonlinear state equations is in general non-convex. This section describes a method, called Dynopt, for solving the optimisation problem by discretising the control profile $\boldsymbol{u}(t)$ as well as the constraints, i.e., the state equations and the inequality constraints. This so called simultaneous approach (Biegler and Grossmann, 2004) results in a large NLP. For the discretisation, the number of discretisation steps must be chosen. The total dredging time T_d, which is also subject to optimisation, determines the step size:

$$\Delta T = \frac{T_d}{N_g - 1}\,,$$

where N_g is the number of discretisation steps. This means that the step size varies during the optimisation process. For the discretisation of the differential equation we use the implicit Euler method, because this allows large step sizes for the discretisation, without becoming numerically unstable:

$$\begin{aligned}
\dot{\boldsymbol{x}}(t) &= f(\boldsymbol{x}(t), \boldsymbol{u}(t)) \\
\frac{\boldsymbol{x}(\Delta T) - \boldsymbol{x}(0)}{\Delta T} &= f(\boldsymbol{x}(\Delta T), \boldsymbol{u}(\Delta T)) \\
\frac{\boldsymbol{x}(2\Delta T) - \boldsymbol{x}(\Delta T)}{\Delta T} &= f(\boldsymbol{x}(2\Delta T), \boldsymbol{u}(2\Delta T)) \\
&\vdots \\
\frac{\boldsymbol{x}((N_g - 1)\Delta T) - \boldsymbol{x}((N_g - 2))}{\Delta T} &= f(\boldsymbol{x}((N_g - 1)\Delta T), \boldsymbol{u}((N_g - 1)\Delta T))
\end{aligned}$$

The following notation is introduced:

$$t_k = k\Delta T\,.$$

The resulting NLP problem is:

$$\max_{\boldsymbol{u}(0),\boldsymbol{u}(t_1),\cdots,\boldsymbol{u}(t_{N_g-1}),T_d} J(\boldsymbol{x}(T_d),T_d) \tag{5.13}$$

subject to

$$\begin{aligned}
\Delta T &= \frac{T_d}{N_g-1} \qquad (5.14)\\
\frac{\boldsymbol{x}(t_1)-\boldsymbol{x}(0)}{\Delta T} &= f(\boldsymbol{x}(t_1),\boldsymbol{u}(t_1))\\
\frac{\boldsymbol{x}(t_2)-\boldsymbol{x}(t_1)}{\Delta T} &= f(\boldsymbol{x}(t_2),\boldsymbol{u}(t_2))\\
&\vdots\\
\frac{\boldsymbol{x}(t_{N_g-1})-\boldsymbol{x}(t_{N_g-2})}{\Delta T} &= f(\boldsymbol{x}(t_{N_g-1}),\boldsymbol{u}(t_{N_g-1}))\\
g(\boldsymbol{u}(t_k),t_k) &\geq 0,\forall k\\
h(\boldsymbol{x}(t_k),t_k) &\geq 0,\forall k\,,
\end{aligned}$$

where $k = 0,1,\cdots,N_g-1$, ΔT is the step size. For this algorithm the number of discretisation steps, the initial state $\boldsymbol{x}(0)$ and the model parameters must be given. An initial guess must be supplied for all the variables. The optimal stopping time T_d and the optimal input sequence $\boldsymbol{u}(0),\boldsymbol{u}(1),\cdots,\boldsymbol{u}(t_{N_g-1})$ result from the optimisation.

The method described here is an optimisation strategy which determines the optimal input trajectories and optimal dredging time T_d. The method can be used to decide on the overall dredging strategy. It predicts the possible performance improvement, based on parameters resulting from surveys, contractual constraints such as limited overflow losses and sailing distances. Given the circumstances, such as soil type and sailing distance, the method will show the optimal input strategy and whether or not an overflow phase is feasible.

Since this optimisation method is reasonably fast, it calculates the optimal strategy for a whole dredging cycle within minutes. However, computational speed comes at the cost of a large time step, which reduces the accuracy of the differential equations. Decreasing the step time increases the number of decision variables and, therefore, the complexity. With too many variables, the solver is not able to find the optimum and the computational time increases.

It can also be used to analyse the sensitivity of the strategy to the soil type dependent parameters by varying these parameters and calculate the result. This gives an answer on which parameters are most important to estimate from data.

General Algebraic Modelling System

The model is implemented in the General Algebraic Modelling System (GAMS) (Brooke et al., 1998). This is a high-level algebraic modelling language for mathematical programming and optimisation. The program has a language compiler and a variety of integrated high-performance solvers, such as Minos, Conopt and Snopt.

Which solver is best for a particular problem cannot be said beforehand. In our case we use Conopt, which is a Generalized Reduced Gradient (GRG) algorithm (Abadie

and Carpentier, 1968; Drud, 1985). It has fast convergence and is particular suitable for highly nonlinear systems. The solver takes advantage of the sparsity of the problem and copes well with large-scale systems.

Although Conopt can deal with systems that cannot be differentiated, it is designed for smooth functions. The hopper model cannot be differentiated, because of the min and max functions; see, for example, equations (3.8) and (3.10) in the hopper model. The functions are substituted by the following smooth approximations:

$$\min(f(x), g(y)) \approx \frac{1}{2}\left(f(x) + g(y) - \sqrt{(f(x) - g(y))^2 + \delta^2}\right) \tag{5.15}$$

$$\max(f(x), g(y)) \approx \frac{1}{2}\left(f(x) + g(y) + \sqrt{(f(x) - g(y))^2 + \delta^2}\right), \tag{5.16}$$

where δ is a parameter which determines the smoothness. Appropriate values are in the range $\delta = [10^{-2},\ 10^{-4}]$.

5.4.2 Model Predictive Control

MPC (Maciejowski, 2002) is a technique that calculates the control actions based on an internal model of the system. This internal model predicts the states over a prediction horizon. These predictions are then evaluated by the objective function. An optimisation algorithm searches for the best control actions that maximise the objective function over a pre-defined prediction horizon. The optimisation algorithm finds the optimal future sequence for every input. Not the whole sequence is applied to the plant, but only the first step of the input sequence. The procedure repeats itself every control step.

There are several reasons why MPC should be applied in the optimisation of the hopper dredger performance.

- It handles multivariable control problems while optimising the performance. The optimisation problem is characterized by the coupling of the subsystems. The best example of this is the excavation process versus the sedimentation process. A large incoming production rate may result in large overflow losses. MPC takes both into account and finds the trade-off.

- It can take into account the limitations of the system. As every industrial application, for safety and other reasons the operating conditions must lay within the constraints. However, it can also help the system to perform better. A cavitating pump has a poor efficiency. There are safety controllers that kick in when the pump starts cavitating. Often this is too late and the process is disturbed, leading to poor performance. MPC will avoid this situation while optimising the objective function. The operation is much smoother and undesired operation is prevented.

A general block scheme of the model predictive controller is given in Fig. 5.4. At every time step k, the MPC receives measurements of the total system. Given the state vector $\boldsymbol{x}(k)$, the optimiser simulates the internal model for various input sequences and predicts the future state evolution. The objective function calculates the performance with the objective function, which is returned to the optimiser. The optimiser searches through the solution space to find the optimal control strategy. In this thesis, it is

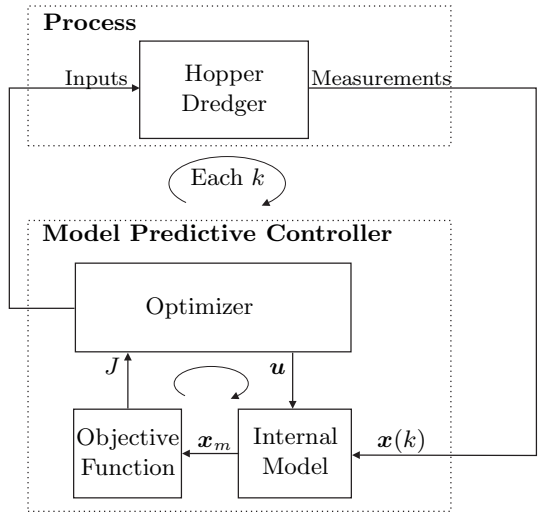

Figure 5.4: Block diagram of the model predictive controller applied to the hopper dredger.

assumed that we have full state feedback. Unfortunately, on board of the TSHD one state is not measured. This is the mass of the sand bed in the hopper m_s. This can be solved with an observer or an additional sensor. The design of the observer is not part of this study and subject for further research.

For the MPC optimisation the objective function of (5.2) must be modified. MPC works with two time horizons: a control horizon H_c and a prediction horizon H_p. The future input sequence is varied within the control horizon, but the states are predicted over the complete prediction horizon. The advantage is that the number of the decision variables is relative small, while still predicting is performed over the complete dredging cycle.

Standard MPC uses the receding horizon principle where the control horizon and the prediction horizon shift one step ahead of every control step. This is mostly used in continuous process operation. The dredging process, however, is a batch process. For a batch process the receding horizon principle must be modified. For a fixed cycle time, the prediction horizon reduces with time when the process approaches the end of the cycle. This principle is also known as the shrinking-horizon MPC and is typical for batch processes (Joseph and Hanratty, 1993; Thomas et al., 1994; Liotta et al., 1997). Usually, the prediction horizon and controller sample time are chosen by investigating how fast the system responses to a change of the inputs (time constant). The prediction horizon must be chosen such that the effect of the control input is observable, so for slower systems a longer prediction horizon should be chosen. For the TSHD the time constant of the system is not fixed and depends on the soil type. For fine sand, the sedimentation process is much slower than for coarse sand. This is also a reason to choose the shrinking horizon principle, where the end time depends on soil type.

The dredging process is more complicated, since the end-time of the cycle is not known in advance. This end-time is one of the decision variables. One possibility

is to solve the overall optimisation problem in one step (one-phase MPC). This has the following disadvantages. In the beginning of the dredging process the objective function is much more sensitive to the inputs sequence than for the T_d. This means that objective function is very flat for variations of T_d. To find the optimal T_d it is therefore necessary to use small tolerances for the termination conditions of the optimisation algorithm. This increases the computational time of the algorithm without gaining much in performance. A solution to this that balances computational time and precision is splitting up the optimisation problem in two smaller problems (two-phase MPC).

The first optimisation starts with an initial guess of the dredging time T_d. This time is used as prediction horizon in the MPC optimisation. After this optimisation, a second optimisation starts, that uses the optimal future input sequence found in the first optimisation and searches for the optimal dredging time. Then the controller supplies the input to the system and in the next iteration the newly found dredging time is used as prediction horizon. The MPC uses a fixed controller time step ΔT. Note that this a faster method it is probably at the cost of some performance compared with the one-phase MPC.

Optimisation 1

In addition to the general objective function of (5.2), the MPC penalizes large changes in the control inputs. This assures a smooth control sequence. At every control step k, the following optimisation problem is solved:

$$\max_{\boldsymbol{u}(t_k),\boldsymbol{u}(t_{k+1}),\cdots,\boldsymbol{u}(t_{k+N_c-1})} J(\boldsymbol{x}(T_d),T_d) - \sum_{i=1}^{N_u}\sum_{l=k}^{k+N_c-1} w_i \Delta u_i^2(t_l) \tag{5.17}$$

$$\text{subject to}$$

$$g(\boldsymbol{u}(t_l),t_l) \geq 0, \text{for } l = k, k+1, \cdots, k+N_c-1$$

$$h(\boldsymbol{x}(t),t) \geq 0, \text{for } t_k \leq t \leq T_d$$

where N_c is the number of future control steps, i.e., the control horizon, $\Delta u_i(t_k)$ the input increment of input i at time step t_l, w_i the weight that penalized large changes of input i and N_u the number of inputs.

The constraints on the state trajectories are not necessarily sampled with controller time step ΔT, because the ODE solver outputs the complete state trajectory with its own discretisation steps. This means that, for a large controller sample time, accurate information on the state trajectories and on whether or not the system satisfies the state constraints is still available. The patternsearch algorithm can deal with nonlinear constraints, but this slows down the computational speed so much that the algorithm becomes slower than real-time. The solution is to add the constraints to the objective function using a penalty function:

$$\max_{\boldsymbol{u}(t_k),\boldsymbol{u}(t_{k+1}),\cdots,\boldsymbol{u}(t_{k+N_c-1})} J(\boldsymbol{x}(T_d),T_d) - \sum_{i=1}^{N_u}\sum_{l=k}^{k+N_c-1} w_i \Delta u_i^2(t_l) - c(\boldsymbol{x}(t),t) \tag{5.18}$$

$$\text{subject to}$$

$$g(\boldsymbol{u}(t_l),t_l) \geq 0, \text{for } l = k, k+1, \cdots, k+N_c-1$$

where $c(\boldsymbol{x}(t), t)$ is the penalty function that outputs a large value when the constraints are violated. Usually, a smooth differential function should be chosen, but since patternsearch does not use gradient information, this is not necessary. This method may lead to constraint violation. If this is detected, the optimisation is repeated with a different initial condition until it finds a feasible solution.

Optimisation 2

The second optimisation problem must find the optimal dredging time T_d. Given the optimal future input sequence $\boldsymbol{u}(t_k), \boldsymbol{u}(t_{k+1}), \cdots, \boldsymbol{u}(t_{k+N_c-1})$ of the previous optimisation, the following optimisation problem is solved:

$$\begin{aligned} &\max_{T_d} J(\boldsymbol{x}(T_d), T_d) \\ &\text{subject to} \\ &T_d > 0 \end{aligned} \tag{5.19}$$

For this optimization also the patternsearch is used since it performs well for this problem. However, this optimization problem is relatively simple so a line search will suffice.

MPC Algorithm

The complete MPC algorithm is as follows:

1. Initialize parameters, such as initial guess T_d, k=0.
2. Repeat until $t_k > T_d$
   (a) Receive new measurements $\boldsymbol{x}(t_k)$
   (b) Update MPC model with new state $\boldsymbol{x}(t_k)$
   (c) Perform: optimisation 1, store: $\boldsymbol{u}(t_k), \boldsymbol{u}(t_{k+1}), \cdots, \boldsymbol{u}(t_{k+N_c-1})$
   (d) Perform: optimisation 2, $T_d = T_{d,new}$
   (e) Update new set-points to hopper dredger: $\boldsymbol{u}(t_k)$
   (f) $k = k + 1$
3. Stop Dredging, optimum dredging time has been reached

Step 1 is the initialisation of parameters. An initial guess for the optimal dredging time must be given; for example the optimal dredging time of the previous dredging cycle. Then, in step 2, the MPC controller starts calculating the optimal set-points for every controller step k. Once the optimal dredging time has been reached ($t_k > T_d$), the dredging stops and the cycle is finished.

5.5 Optimisation of the Hopper Process

This section discusses the simulation results of the hopper process, where the sedimentation process plays a central role in the optimisation. In the next section the

optimisation of the total process is discussed. The focus in this section is on a smaller optimisation problem where the system model consists of the hopper model of Section 3.2 and the drag-head model of Section 3.3. This gives more insight in the key elements of the optimisation. The ship speed is considered constant. The controlled variables are the input flow rate and the overflow height. This optimisation gives a good illustration of the trade-off between the excavation production rate and the sedimentation rate.

5.5.1 Dynamic Optimisation with Time Discretisation

This section describes the results of the optimisation method described in Section 5.4.1. The objective function (5.2) depends on the sailing and discharging time, unless otherwise stated we take $t_{sail} + t_{dis} = 3.5$ h, which is the average time found in the data. The larger the number of discretisation steps, the more difficult it is for the solver to converge and to find an optimum. We aim at an average sample time of 1 min for the control sample time. This means approximately 100 control steps for a dredging time of 100 min. This sailing speed v_{sh} is kept constant at 1.5 m/s.

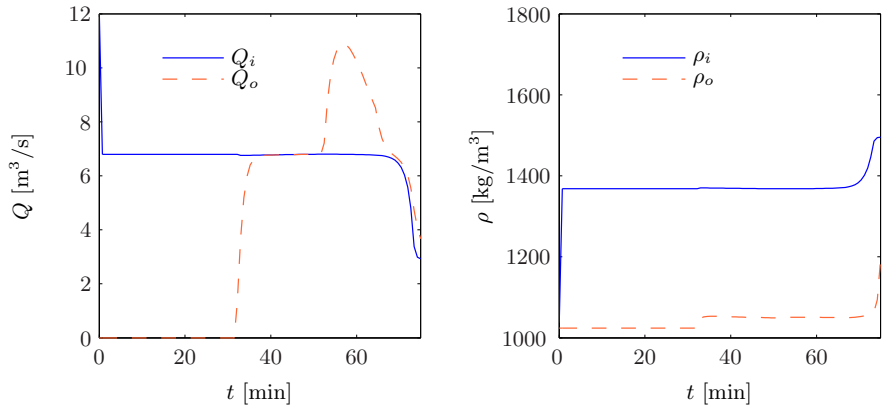

Figure 5.5: Results of dynamic optimisation for hopper process for coarse sand (soil type 5); *left*: flow-rates, *right*: densities.

In this section the results for of the theoretically defined soil types: 1, 2 and 5 are shown, see Appendix D for the derivation of the parameters. These correspond to grain sizes of 0.09, 0.12 and 0.86 mm respectively.

Soil Type 5 - Coarse Sand

The optimal flow rate Q_i is shown in the left-hand panel of Fig. 5.5 and the optimal overflow height h_o in the right-hand panel of Fig. 5.6. At $t = 31$ min the overflow phase starts and the outgoing flow-rate Q_o increases until it is equal to the incoming flow-rate. The outgoing density during the overflow phase is very low for this soil type, see the right panel of Fig. 5.5. At $t = 52$ min the overflow height is reduced to keep the hopper mass m_t within the constraint of $2.08 \cdot 10^7$ kg. In this phase the overflow

is lowered to maintain a constant mass in the hopper. The lowering of the overflow weir results in an increase of the outgoing flow rate. At the end of the dredging cycle, the incoming flow-rate is reduced. The incoming flow rate in the beginning is approximately 6.8 m^3/s. This value corresponds with the flow rate for which the incoming production rate is maximal, see (5.12).

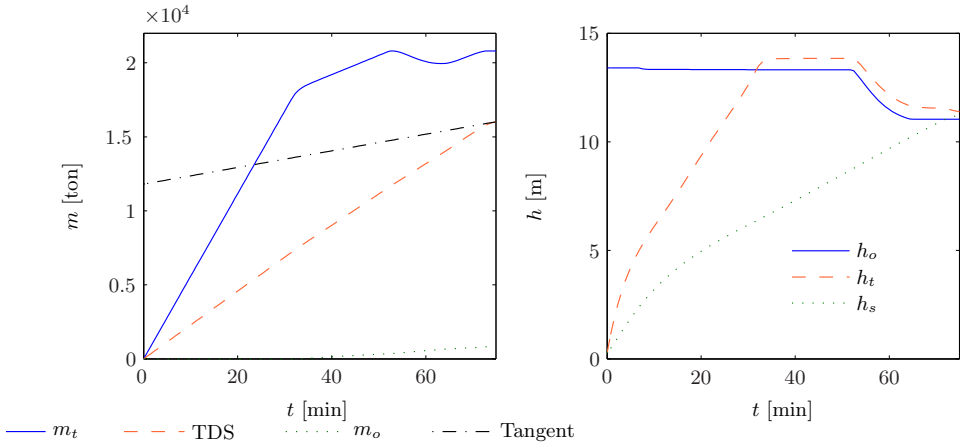

Figure 5.6: Results of Dynopt for hopper process for coarse sand (soil type 5), with $d_m = 0.86$ mm; *left*: masses, *right*: heights.

The height of the hopper content h_t and the height of sand settled in the hopper h_s, are given in the right-hand panel of Fig. 5.6. At the bottom the hopper is narrower and this causes the mixture level to increase faster in the beginning. Then, the level reaches the overflow height and stays constant. When the overflow is lowered, the height of the hopper content decreases. At first, the sand bed height quickly increases, due to the geometric shape of the hopper, and then increases linearly with time. At the end of the dredging cycle, it reaches the overflow height and the hopper is full.

The masses in the hopper are given in the left figure of Fig. 5.6. Once the level in the hopper reaches the overflow, low-density mixture is flowing out so the total mass increases with a smaller rate. Using a constant tonnage controller, this would continue until the maximal allowable draught is reached and then the total mass would stay constant.

The optimisation, however, reduces the height of the overflow much earlier and the maximum allowable draught is reached at the end of the cycle. This strategy does not lead to a higher production rate compared with the benchmark, but it does slightly reduce the cumulative overflow losses in the cycle. This can be explained as follows. If the overflow height is reduced, the flow rate Q_o increases as can be seen in Fig. 5.5. In general, at the end of the dredging cycle the overflow density ρ_o increases, see right panel of Fig. 5.5. By lowering the overflow height earlier, the increase in flow rate Q_o occurs when low-density material is flowing out instead of the high-density material at the end of the cycle.

The amount of dry solids increases linearly over time. For coarse sand the overflow

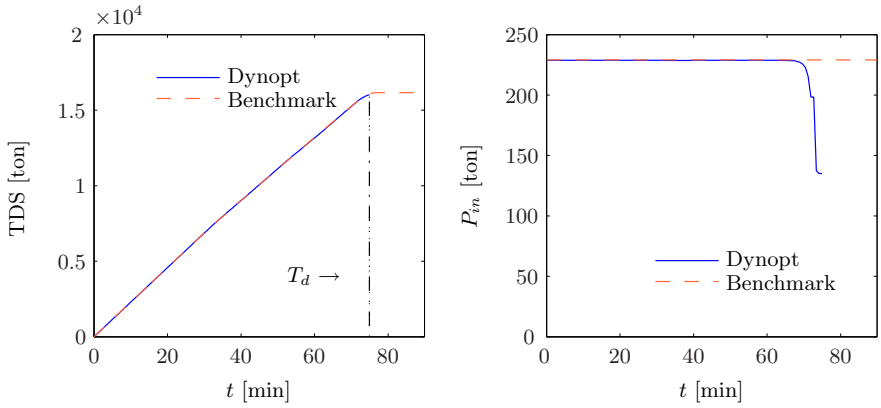

Figure 5.7: Comparison of Dynopt with the benchmark for hopper process and coarse sand (soil type 5), with $d_m = 0.86$ mm.

losses m_o are negligible. Fig. 5.6 shows a dash-dotted line to indicate the tangential method of determining the optimal stopping time (see Section 2.7). This illustrates that this method results in the same optimal T_d (75 min) as the optimisation strategy. Results for a dredger with two pipes are given in Section 5.5.1.

Fig. 5.7 shows a comparison of Dynopt with the benchmark of Section 5.3. The left-hand panel shows the tons of dry solids to illustrate that the two strategies perform almost equally well. This is expected as coarse sand settles very efficiently and, therefore, it is the production rate that dominates the performance. The right-hand panel of Fig. 5.7 shows that both strategies control the flow such that the incoming production rate is maximal in the first hour of the dredging. The strategy with Dynopt reduces the flow rate at the end of the cycle to reduce the erosion, which results in a performance improvement of 2%.

Soil Type 2 - Fine Sand

The hopper sedimentation process becomes more important when dredging finer sand. This is illustrated with an example of fine sand with a diameter of 0.12 mm. The first observation in Fig. 5.8 is that the incoming flow rate Q_i (4 m^3/s) is lower than the flow rate Q_i (6.8 m^3/s) for the benchmark. As a result, the hopper level h_t does not reach the overflow height h_o until 56 min and the constant tonnage phase starts at $t = 86$ min. The optimal dredging time T_d is 146 min. The right-hand panel of Fig. 5.8 shows the height of the overflow weir h_o, the total mixture level h_t and sand bed height h_s.

The graph of the TDS in Fig. 5.9 shows a sharp bend when the hopper content reaches the overflow. For fine sand, the overflow losses are significant, see the outgoing density in the right-hand panel of Fig. 5.8, which is also illustrated by the dotted line for accumulated overflow mass m_o. This line shows that an amount of $9.2 \cdot 10^3$ ton of dry solids is flowing overboard, i.e., 38% of the total dredged material.

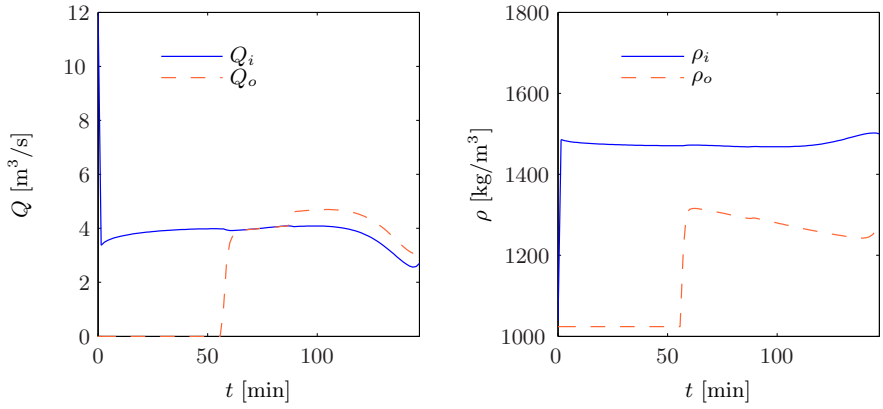

Figure 5.8: Results of Dynopt for hopper process and fine sand (soil type 2), with $d_m = 0.12$ mm; *left*: flow-rates, *right*: densities.

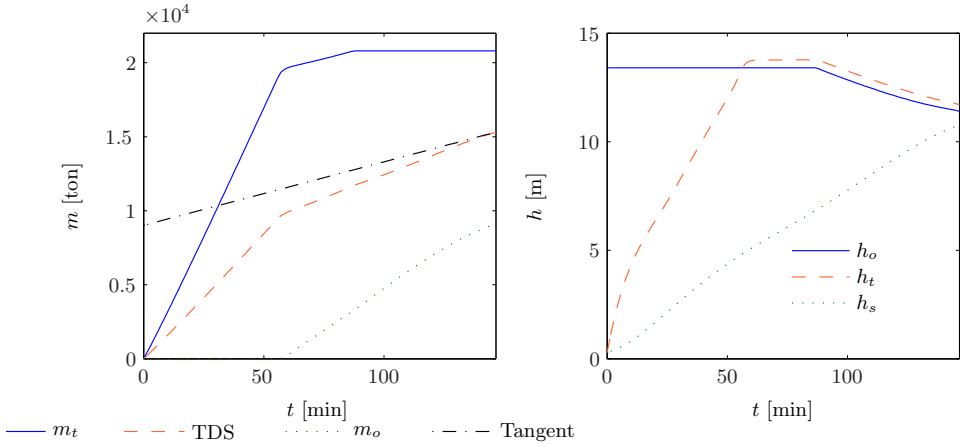

Figure 5.9: Results of Dynopt for hopper process and fine sand (soil type 2), with $d_m = 0.12$ mm; *left*: masses, *right*: heights.

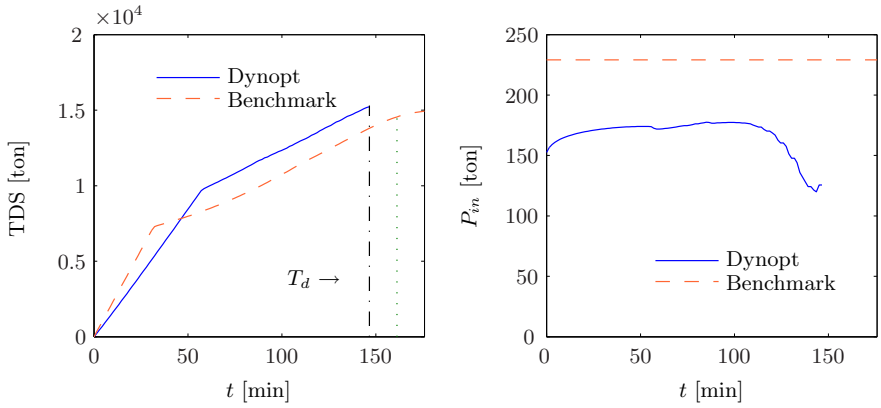

Figure 5.10: Comparison of Dynopt with benchmark for hopper process and fine sand (soil type 2), with $d_m = 0.12$ mm.

In Fig. 5.10, we compare Dynopt with the benchmark for the TDS and incoming production P_{in}. The figure shows that Dynopt performs better than the benchmark; Dynopt increases J with 8%. The MPC reduces the incoming flow-rate, which results in a higher incoming density ρ_i. So even though the incoming production rate of Dynopt is lower, see the right-hand panel of Fig. 5.10, the resulting cycle production rate is higher due to the shorter dredging time and higher TDS in the hopper (see dashed lines). In other words, although the drag head production rate is reduced, the sand sedimentation rate in the hopper is increaseb by Dynopt, which indicates that Dynopt is a much more efficient dredging process.

Soil Type 1 - Fine Sand

When the grain size is less than 0.12 mm, it is not efficient to have an overflow phase. It might be expected that in this case the optimal strategy is the one with the largest incoming production rate, but this is definitely not the case. With fine material (soil type 1), as soon as the overflow is reached the dredging should be stopped or most of the material will flow out of the hopper. The higher the flow rate, the faster this moment is reached; however, a higher flow rate means lower incoming density. This is illustrated in Fig. 5.11. The benchmark reaches the overflow height in 32 min with a production of 7300 tons of dry solids. However, the Dynopt strategy has a smaller incoming flow rate with a higher density, which results in an optimal dredge time T_d of 59 min. The final load is 9800 tons. The production rate for the complete cycle for Dynopt is 31.1 ton/min, which is 22% more than when dredging according to the benchmark. An operator should, in the case of fine sand, hold back in production for optimal process operation. The results for other grain sizes are summarised in Tab. 5.2.

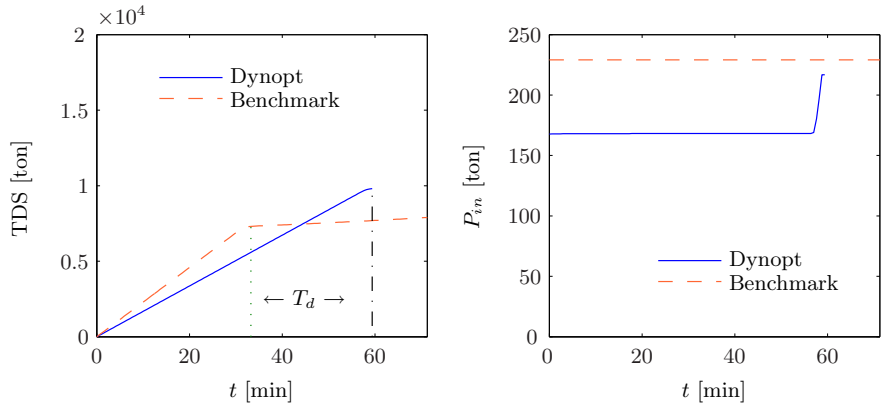

Figure 5.11: Comparison of Dynopt with benchmark for hopper process and fine sand (soil type 1), with $d_m = 0.09$ mm.

Table 5.2: Comparison of the cycle production rate J between Dynopt and the benchmark for hopper process with one pipe.

Grain size [mm]	Dynopt production rate [ton/min]	Benchmark production rate [ton/min]	Improvement [%]
0.86	53.6	52.7	2
0.31	52.0	51.1	2
0.19	48.8	47.1	4
0.12	41.9	39.0	8
0.09	31.1	25.6	22

Two Dredging Pipes

In the previous section, the results for a ship with one dredging pipe were discussed. This section discusses the results for a ship with two dredging pipes and pumps. A difference between the two ship types is that the incoming flow rate is relatively low in a one-pipe dredger. This results in a more efficient hopper process since the material is discharged with a lower velocity in the hopper. To illustrate the gain that can be achieved by optimising a two-pipe dredge, here the optimisation is performed for a configuration with two pipes and two pumps.

The total flow rate, which gives the maximum production rate divided over two dredge pumps, is 10.9 m^3/s, instead of 6.8 m^3/s. The optimisation results for fine sand with a grain size of 0.12 mm are given in Fig. 5.12. This Dynopt optimisation gives an improvement, between 3%, for coarse material, and up to 25%, for fine material (soil type 1) (see Tab. 5.3).

For a ship with two pipes the cycle production rate increases by 2 to 3% for coarse, 7% for medium and 14 to 25% for fine sand. This improvement is bigger than for a ship with one pipe (see Tab. 5.2).

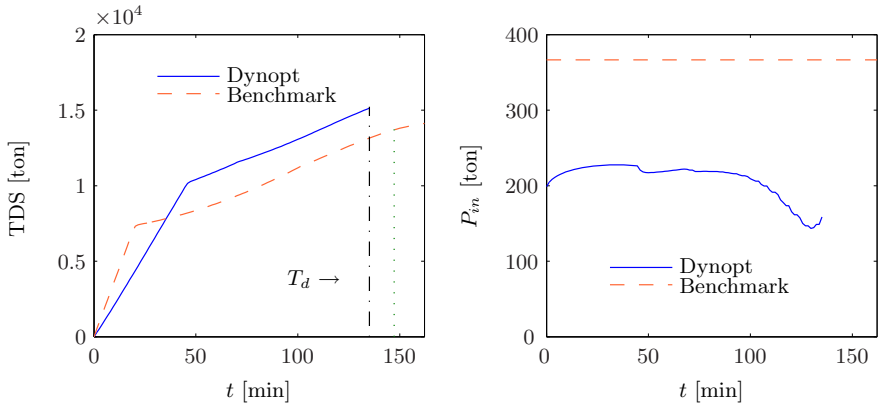

Figure 5.12: Comparison of Dynopt with benchmark for hopper process with two dredging pipes and fine sand (soil type 2), with $d_m = 0.12$ mm.

Table 5.3: Comparison of the cycle production rate between Dynopt and the benchmark for hopper process with two pipes.

Grain size [mm]	Dynopt production rate [ton/min]	Benchmark production rate [ton/min]	Improvement [%]
0.86	60.9	60.0	2
0.31	58.4	56.6	3
0.19	53.7	50.4	7
0.12	43.9	38.4	14
0.09	40.0	31.9	25

5.5.2 Model Predictive Control

This section describes the results when optimising the hopper process with the MPC method. The performance of the controller is compared with the results of constant (optimal) production rate control as in the previous section. We show only the results for soil type 2 in this section, since they are comparable with the Dynopt strategy.

Fig. 5.13 gives the results of the MPC strategy. The left-hand panel shows the incoming flow rate Q_i and outgoing flow rate Q_o; and the right-hand panel shows the incoming density ρ_i and the outgoing density ρ_o. The right-hand panel of Fig. 5.14 shows the sand bed height h_s, the overflow height h_o and the height of the total mixture h_t. The MPC strategy finds the same optimal flow rate as the Dynopt strategy of 4 m^3/s, see Fig. 5.8. The difference is that Dynopt reduces the flow rate at the end of the cycle more than the MPC.

The total mass m_t, the tons of dry solids TDS and the sand bed mass m_s are given in left-hand panel of Fig. 5.14. The sharp bend in the line for the tons of dry solids indicates that the total mixture height h_t is larger than the overflow height and that the material is flowing out, see the right-hand panel of Fig. 5.14. This occurs at 60 min, which is the same time as in the Dynopt strategy, see Fig. 5.9. At 60 min, the

mixture flows out of the hopper with an accumulated weight of m_o, see dotted line. Of this type of material a significant amount is flowing out of the hopper.

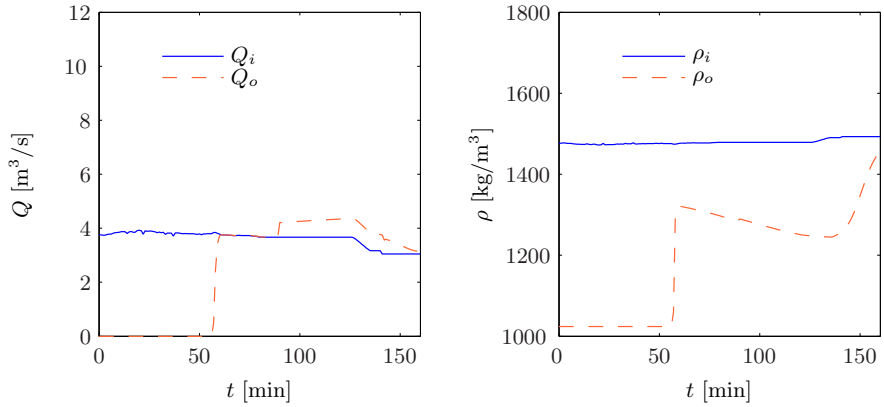

Figure 5.13: Inputs of MPC strategy for hopper process for fine sand (soil type 2); *left*: flow-rates, *right*: densities.

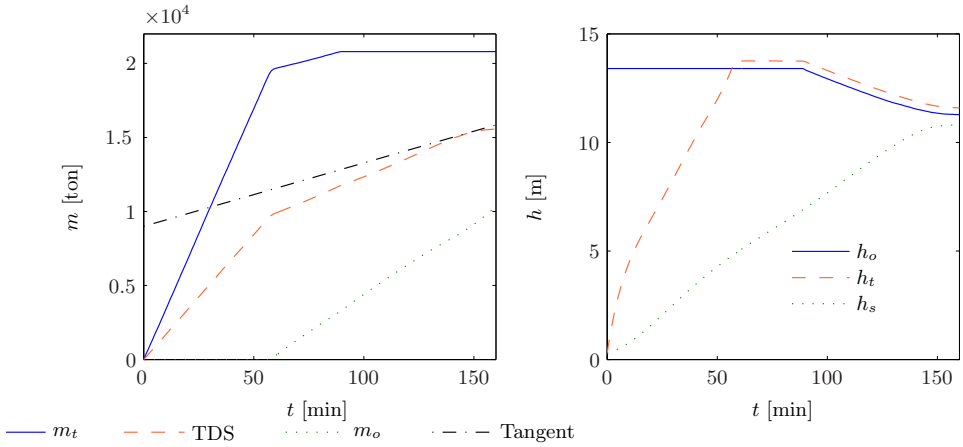

Figure 5.14: Results of MPC strategy for hopper process for fine sand (soil type 2), with $d_m = 0.12$ mm; *left*: masses, *right*: heights.

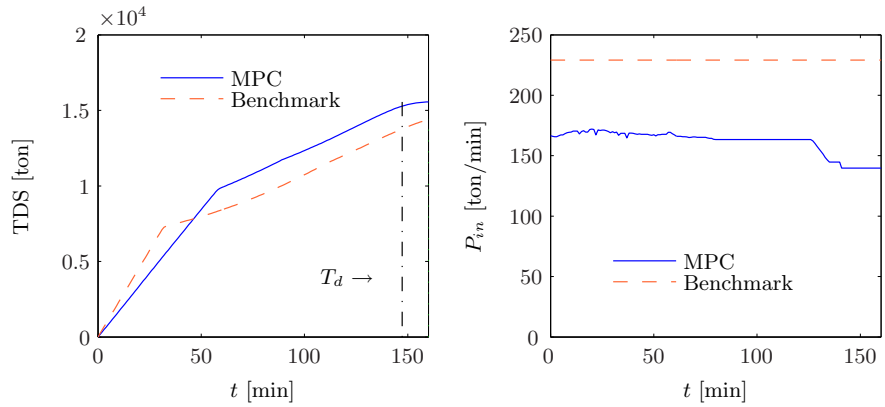

Figure 5.15: Comparison of MPC with benchmark for fine sand (soil type 2), with $d_m = 0.12$ mm.

The MPC is compared with the benchmark in Fig. 5.15. The right-hand panel shows the difference in incoming production rate. The benchmark has a larger incoming production rate, the difference is 64 ton/min, but the cycle production rate is 3.2 ton/min (8%) less than that of the MPC strategy (see Tab. 5.4). The left-hand panel shows the TDS curves of the two strategies. In the first 30 min, the benchmark has a larger amount of sand in the hopper, but for the complete cycle performance, this is not optimal. At $t = 50$ min the MPC has the same amount of sand in the hopper. Then at $t = 150$ min the optimal dredging time has been reached for the MPC, while the benchmark is not finished and needs to continue loading.

This example illustrates that for fine or medium-fine sand the TDS curve is a poor performance indicator during the first phase of the dredging. Experienced operators are aware of this and try to maximise the incoming density into the hopper instead of the production rate for this sand type. Once the overflow is reached the losses are significant.

The optimisation results of all the five soil types are summarised in Tab. 5.4. These results are comparable with those obtained by the Dynopt strategy (see Tab. 5.2). From this we can conclude that splitting the objective function into two separate optimisation steps, as is done by the MPC strategy, does not lead to a loss of performance. In fact, the performance has improved slightly. However, we cannot conclude from this that two-phase MPC performs as good as one-phase MPC.

Table 5.4: Comparison of the cycle production rate between MPC and the benchmark for hopper process with one pipe.

Grain size [mm]	MPC production rate [ton/min]	Benchmark production rate [ton/min]	Improvement [%]
0.86	54.4	52.7	3
0.31	52.7	51.1	3
0.19	49.5	47.1	5
0.12	42.2	39.0	8
0.09	31.1	25.6	22

Parameter Sensitivity

There are four soil-type-dependent parameters in the hopper model. The calibration problem is discussed in Chapter 4. Since the optimal strategy depends on these parameters, we analyse the influence of each particular parameter on the optimal strategy using Dynopt. This analysis shows which parameters are the most important ones for the dredging strategy and, therefore, must be calibrated accurately. The parameters considered are: the undisturbed settling velocity v_{s0} (equation 3.9), the sand bed density ρ_s (equation 3.9), the erosion coefficient k_e (equation 3.8) and the exponent β (eqation 3.9).

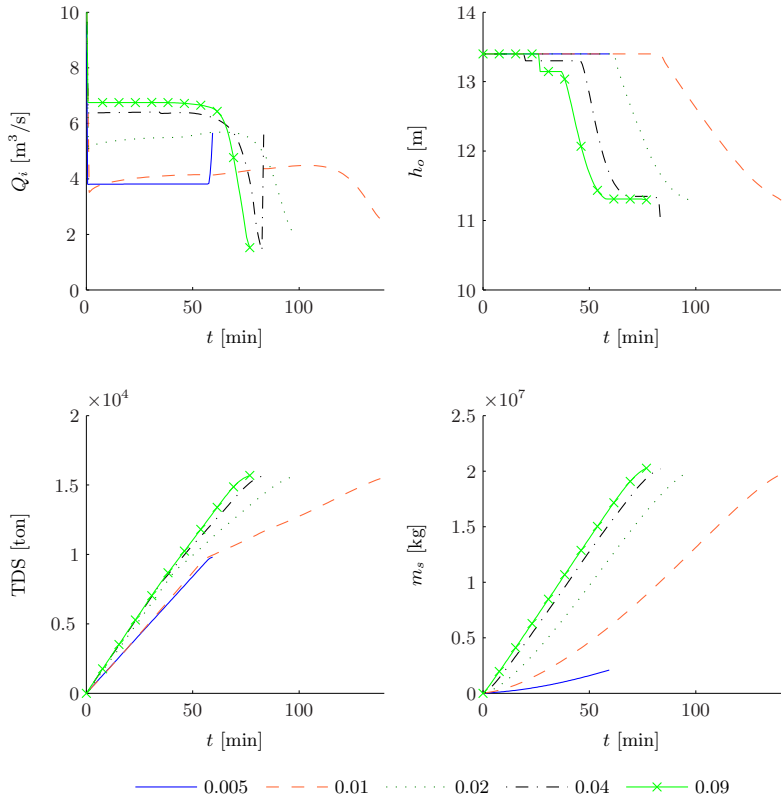

Figure 5.16: Dynopt results for hopper/drag-head model for five values of the undisturbed settling velocity v_{s0} [mm/s].

Undisturbed Settling Velocity

The undisturbed settling velocity is the settling velocity of a single particle in water. This parameter depends shape (roundness) and on the grain size; large grains settle faster then small grains. Here we assume that the quartz density is equal for all particle sizes. There are several relations for calculating the undisturbed settling velocity given

by: Stokes for grains between 0.01 mm and 0.15 mm, Budryck for grains between 0.15 mm and 1.5 mm and Rittinger for grains between 1.5 mm and 10 mm, for details see Appendix D. Tab. 5.5 gives an overview of the undisturbed settling velocities for the three types of sand.

Table 5.5: An indication of the undisturbed settling velocity for various sand types.

Type	Diameter [mm]	v_{s0} [mm/s]
Fine	0.06 - 0.2	2.8 - 24
Medium	0.2 - 0.6	24 - 70
Coarse	0.6 - 2.0	70 - 150

Here we have chosen five sand types, as defined in Appendix D: fine, v_{s0} of 5 mm/s and 9 mm/s; medium fine, 20 mm/s; medium, 38 mm/s; and coarse, 90 mm/s. Results of the optimisation for the five values of v_{s0} are given in Fig. 5.16. The figure shows that for finer sand the incoming flow rate should be lowered. Fig. 5.16 also shows that the sand-bed growth strongly depends on the undisturbed settling velocity. The optimal trajectory of the overflow height is similar to the constant tonnage loading system. Between the undisturbed settling velocity of 10 mm/s and 5 mm/s, the optimal strategy switches to a strategy without overflow phase. This is for a scenario with a sailing and discharging time of 3.5 h. This parameter is very important, because the optimal strategy heavily depends on this value.

Sand bed density

The sand bed contains grains with the quartz density (2650 kg/m^3) and water in the pores (1024 kg/m^3). The volume ratio between them determines the bed density (the wet density). This ratio is determined by a number of soil properties, such as the grain shape (roundness), grain size distribution and compactness of the soil. An overview of the density of several soil types is given in Tab. 5.6, where a distinction is made between compacted and loose. Initially, the sand in the hopper is most likely loose, while after some time it becomes more compacted. The table shows little differences between the sand types. In general, the densities of loose and compacted sand are 1891-2060 kg/m^3 and 2049-2180 kg/m^3, respectively.

To cover the whole range of sand types, we use the following five values for ρ_s: 1800, 1900, 2000, 2100 and 2200 kg/m^3. The first three values are in the range of loose sand and the last two values are in the range of compacted sand.

Table 5.6: Overview of the in situ density for several soil types (source MTI M98/277).

Soil type	Diameter [mm] (d_m)	ρ_s [kg/m^3] (compacted)	ρ_s [kg/m^3] (loose)
Fine	0.17	2049	1941
Medium	0.24	2052	1944
Medium/Coarse	0.30	2054	1946

The optimal control strategy for the several values of the sand-bed density are given in Fig. 5.17. This figure indicates that the optimal strategy in the first part of

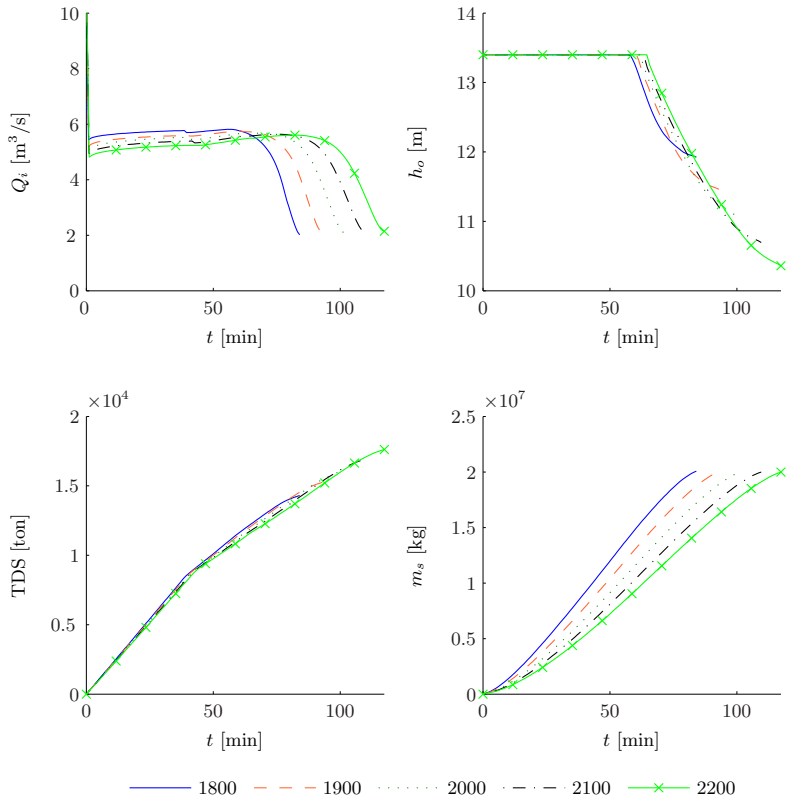

Figure 5.17: Dynopt results for hopper/drag-head model for varying ρ_s [kg/m^3].

the cycle is not sensitive to the sand-bed density. In the differential equation of the bed height, see (3.7), the sand bed density is in the denominator. Therefore, the lower the sand bed density the faster the bed height increases. However, with a higher sand bed density, more sand can be loaded in the hopper and, thus, more tons of dry solids at the end of the cycle.

The sand-bed density is less important for the optimisation strategy than the undisturbed settling velocity. It only determines when to switch from a constant flow rate to reducing the flow rate. The bed height is significantly affected by the density. With a higher sand-bed density, the cycle duration is longer and also the duration of the overflow phase. Therefore, the cumulative overflow loss increases.

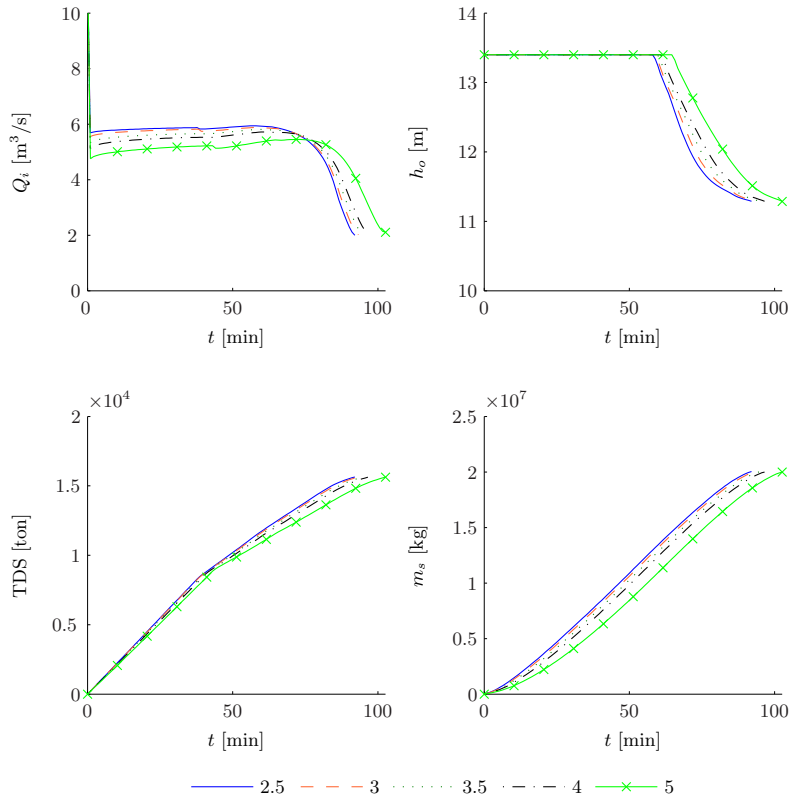

Figure 5.18: Dynopt results for hopper/drag-head model for varying β [-].

Beta parameter

The β parameter, which is the exponent in the relation found by Richardson and Zaki (1954), depends on the particle Reynolds number. The value of β varies between 2.39 and 4.65. For numerical reasons we round this off to the following test values: 2.5, 3, 3.5, 4, 4.5 and 5.

The simulation results of the Dynopt optimisation are given in Fig. 5.18. This parameter has little influence on the average flow rate in the first phase of the dredging process and influences the moment to reduce the flow rate. For the range between 2.5 and 4, the effect is negligible.

The β parameter has some influence on the important variables such as the tons of dry solids, see Fig. 5.18. Overall, we can conclude that the optimal dredging strategy is not very sensitive to this parameter. This is fortunate since this parameter is very hard to estimate, see the sensitivity analysis in Section 4.3. Fig. 5.18 illustrates that β has only a small influence on TDS and the sand bed mass m_s.

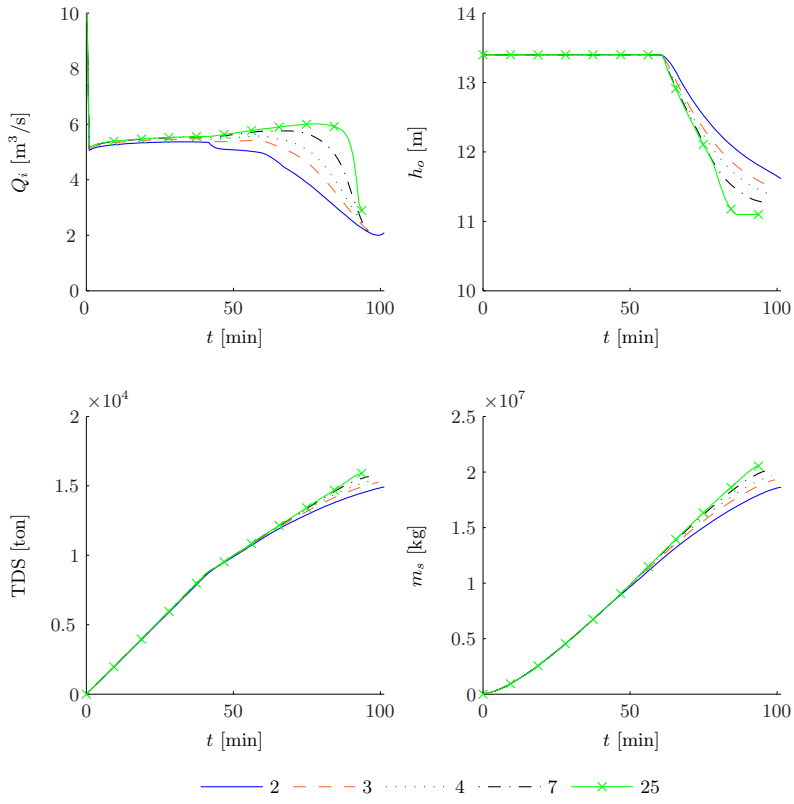

Figure 5.19: Dynopt results for hopper/drag-head model for varying k_e [m^2/s].

Erosion Parameter

The parameter k_e only influences the sedimentation rate at the end of the dredging cycle, see (3.8). The lower the value of k_e, the more erosion takes place and the sooner the erosion has its effect. It is expected that for sand with a smaller grain size the erosion increases and affects the sedimentation rate at lower flow velocities above the sand bed. The results for various values of k_e are shown in Fig. 5.19. This figure shows that the optimal flow rate in the beginning of the dredging is not affected by this parameter. For smaller values, the flow rate is reduced earlier to reduce the erosion effect.

5.6 Optimisation of the Overall Process with MPC

The previous section addressed the optimisation of the hopper process alone. Here, the optimisation of the total process is described, which now includes: the power train model, the ship model, the drag-head model, pump-pipeline model and the hopper model. The optimisation method used here is MPC. In this section, first the performance improvement is demonstrated with the use of the parameters estimated using the data set B, as described in Chapter 4. In this example, the dredging depth h_z is variable, which is a disturbance in the controlled system. For the total sailing and discharge time a value of 3.5 h has been chosen. The optimisation results are then compared with the data of data set B.

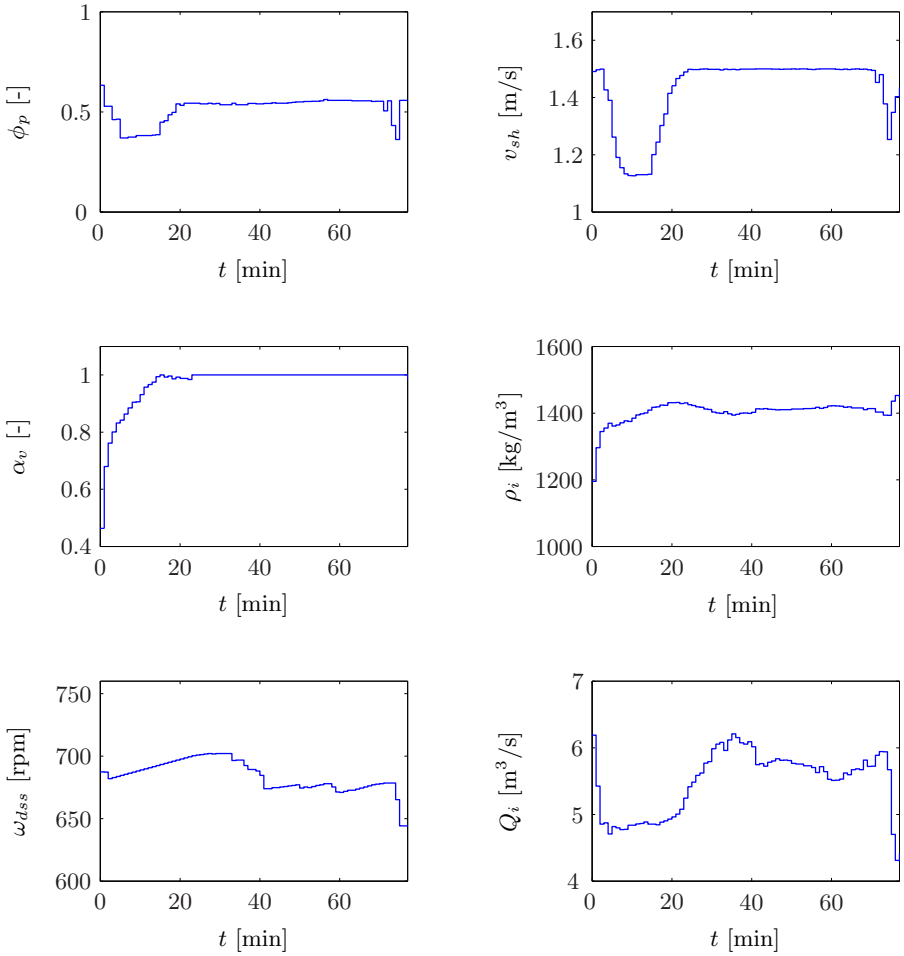

Figure 5.20: Inputs and corresponding outputs of the MPC strategy for cycle 1.

Secondly, the optimisation results of the MPC are presented for two theoretically defined soil types. These results are compared with the benchmark described in Sec-

tion 5.3. The following two types of sand have been chosen: coarse sand (soil type 5) and medium/fine (soil type 2) sand.

The dredging performance of a TSHD depends on a range of variables. Some of these variables are controlled, such as the pump speed, the ship speed or the water valve, while others are disturbances of the process, such as the dredging depth and the ship's draught. For MPC, we use three manipulated variables: the propeller blade pitch ϕ_p for adjusting the ship's speed, the diesel engine angular velocity ω_d which is connected to the pump to control the pump speed ω_p and the water valve α_v which allows water to flow into the drag head.

The constraints considered in this optimisation are the pressure limit at the inlet of the pump, to prevent cavitation, maximum draught, minimum and maximum ship speed, maximum fuel rack and the input saturations.

5.6.1 Comparison of MPC with Data

The initial sailing speed is 1.5 m/s. At $t = 0$ the dredging starts and the density into the drag head ρ_i is increased by closing the water valve α_v, see Fig. 5.20. The diesel engine speed set-point ω_{dss} starts with 680 rpm, which is at 92% compared with the nominal speed. The increase in density causes the flow rate Q_i to drop to 5 m^3/s. In the interval from 3 to 20 min the density is slowly increased by controlling the water valve as well as the ship speed, see (3.30). The speed is firstly lowered to 1.18 m/s. As soon as the water valve is closed at $t = 17$ min, the incoming density is increased further by increasing the ship's speed. At $t = 24$ min the water valve is closed and the ship's speed is maximum, meaning that the MPC cannot increase the density anymore.

It is the inlet pressure that determines the maximum incoming density ρ_i. In the first 24 min the inlet pressure is near its minimum allowed value, see Fig. 5.21. The inlet pressure depends on the position of the pump center under the water line. During loading, the mass in the hopper increases and the pump center lowers. Therefore, more pressure is available at the inlet, and this allows for a higher incoming density. This increasing trend for ρ_i is shown in Fig. 5.20, as well as in the measured data.

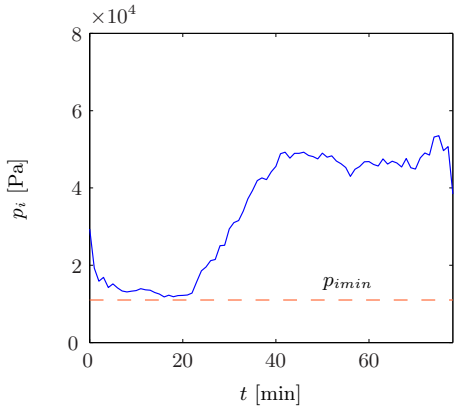

Figure 5.21: Absolute inlet pressure of the MPC strategy for cycle 1.

After $t = 24$ min, the inlet pressure is not an issue for the process anymore and the water valve on the drag head is closed. The draught is still increasing, what means that the position of the mixture inlet into the hopper is lowered relative to the water line. This reduces the static head loss of the pump-pipeline system and, therefore, the flow rate increases. To prevent the flow rate from becoming too high, the diesel engine speed is reduced at $t = 36$ min.

Fig. 5.22 shows a comparison of the data with simulated MPC. As illustration the results of two cycles are shown. One cycle shows that the performance of the MPC is comparable with the performance measured in the data (left-hand panel of Fig. 5.22) and the other cycle shows that the MPC improves the performance by 8%. The performance is expressed in J, see (5.1).

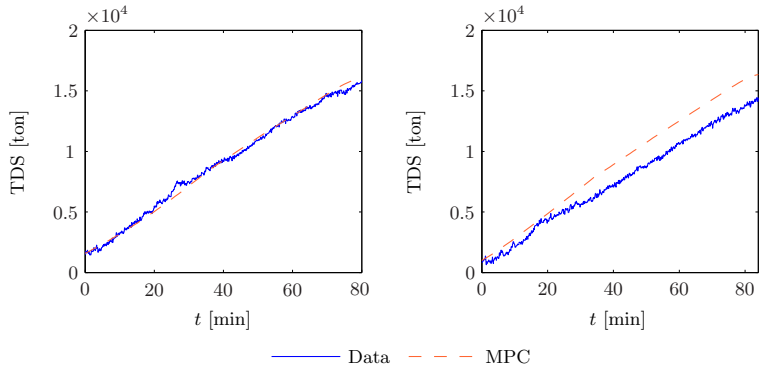

Figure 5.22: Comparison for the tons of dry solid of data and MPC simulation, left: cycle 1 and right: cycle 6.

The improvement in performance is caused by two main factors. The first factor is the ship's speed. There is a correlation between the performance and ship speed in the data set B. The ship performs better in cycles with an average ship speed around 1.5 m/s than in cycles with a lower average speed. The second reason for improvement is the reduction in incoming flow rate. The MPC uses a lower diesel engine speed, compared with the data where they use the nominal speed, to reduce the flow rate. This results in a higher incoming production rate and an improved sedimentation process.

A summary of the MPC performance compared with data set B of all other cycles is given in Tab. 5.7. The improvement ranges from 0% to 21%, with an average improvement of 6.8%. The TSHD has an average production rate of 52.2 ton/min, see Tab. 5.7, which is approximately 33 cycles for the ship which is used in this thesis. The MPC gives an improvement of 7% which is 55.7 ton/min. In a week of full time dredging this is an extra amount of 35000 ton, which is more than two hopper loads (one load is 16000 ton).

Table 5.7: Comparison between cycle production rate of data and MPC simulation.

Cycle	Data [ton/min]	MPC[ton/min]	Improvement [%]
1	54.3	54.8	1
2	53.3	55.2	4
3	49.6	54.2	9
4	52.2	55.5	6
5	54.0	55.9	4
6	51.4	55.5	8
7	53.2	56.5	6
8	51.8	55.3	7
9	52.4	57.6	10
10	55.2	55.1	0
11	46.7	56.7	21
mean	52.2	55.7	7

5.6.2 MPC for Two Soil Types

This section describes the results for the theoretically defined soil types: fine sand (soil type 2) and coarse sand (soil type 5), see Appendix D. For compactness, only the figures of two soil types are presented here. An overview of all five soil types will be given at the end of this section. In this overview also the consequences of MPC for power consumption and overflow losses are discussed.

Medium/Fine Sand

The inputs computed by the predictive controller and the outputs are shown in Fig. 5.23. The pitch ϕ_p is controlled such that the ship sails at the maximum allowed speed of 1.5 m/s. The visor is controlled such that in the first 10 min the vacuum limitation of the pump is not violated. If in this period a higher density would be excavated, the pressure drop over the pipeline would cause the pump to cavitate. After this the water valve α_v is closed. The pump speed is controlled such that the flow rate is around 4 m^3/s.

Fig. 5.24 shows the flow rate and the overflow height for a comparison with the hopper/drag-head system described in Section 5.5. Note that the input flow rate is approximately the same as for the hopper and drag-head process (Fig. 5.8 and Fig. 5.13). Only in the first 50 min the input flow rate Q_i is slightly higher than for the hopper and drag-head process. This is the influence of the pump on the optimal strategy.

The optimal dredging time T_d is 150 min. During loading of this type of sand, the cumulative overflow losses are significant (approximately 11000 ton). The comparison with the benchmark of Section 5.3.2 is given in Fig. 5.25. The left-hand panel shows the tons of dry solids and the right-hand panel the incoming production rate, see (5.11). The TDS graph illustrates several issues. The sharp bend in the lines indicates that the mixture has reached the overflow height and mixture is flowing overboard. For the local controlled case this occurs at $t = 30$ min and for the MPC at $t = 50$ min. The reason for this difference is the difference in flow rate Q_i for the two strategies.

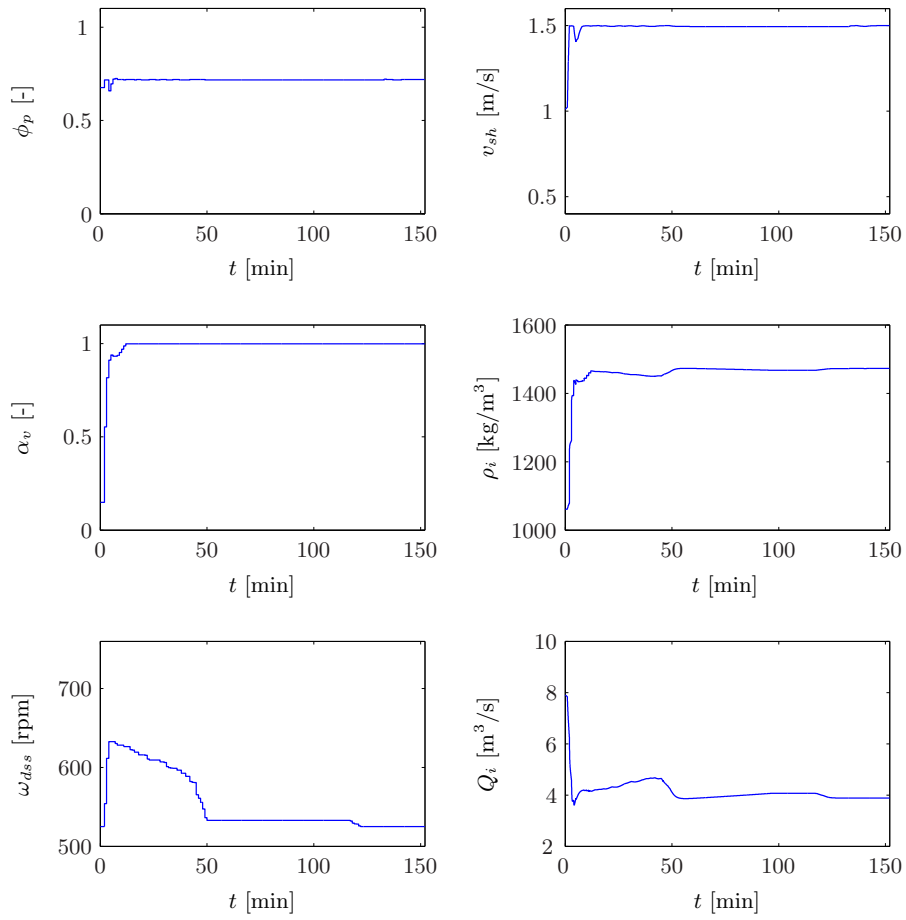

Figure 5.23: Inputs and corresponding outputs of MPC strategy for the overall process and fine sand (soil type 2), with $d_m = 0.12$ mm.

For the MPC strategy this flow rate is lower and, thus, the overflow height is reached at a later stage. This is a big advantage, because for this soil type the losses are significant. As a result the optimal loading time for the MPC is 150 min and for the local strategy 190 min.

The right-hand panel of Fig. 5.25 shows the difference in the incoming production rate. The MPC strategy has a larger incoming production rate in the beginning of the cycle, but a smaller incoming production rate after 30 min. The MPC strategy reduces the incoming flow rate and increased the incoming density to improve the sedimentation process. Therefore, the MPC outperforms the benchmark.

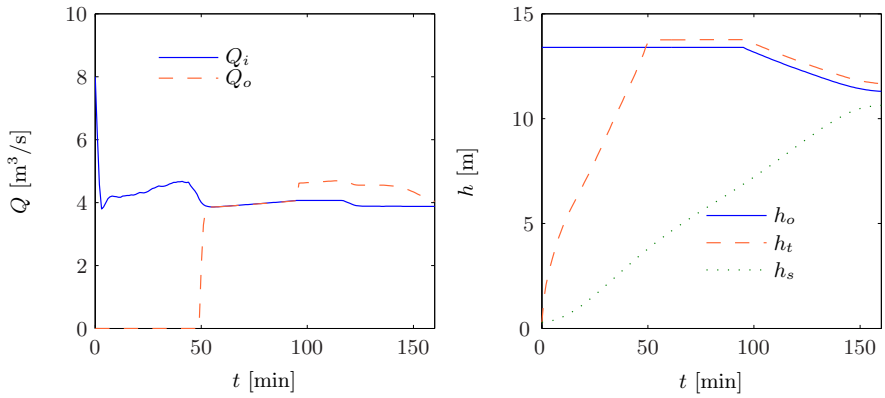

Figure 5.24: Inputs of MPC strategy for the overall process and fine sand (soil type 2), with $d_m = 0.12$ mm.

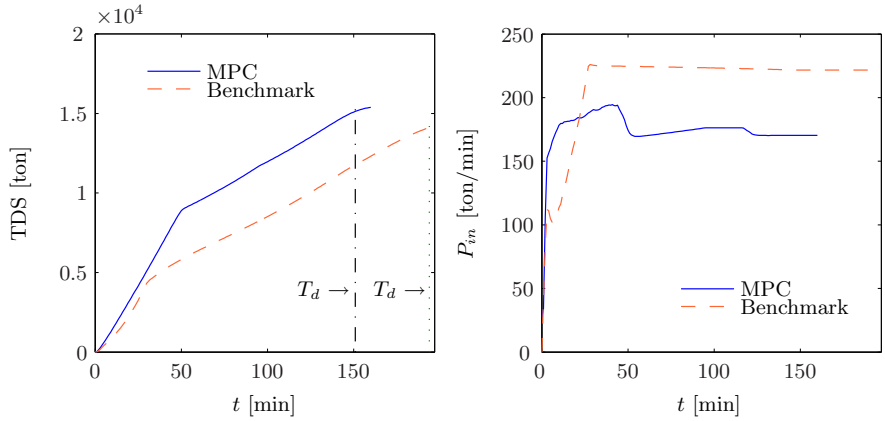

Figure 5.25: Comparison of MPC with benchmark for the overall process and fine sand (soil type 2), with $d_m = 0.12$ mm.

Coarse Sand

For coarse sand, the strategy is different than for medium/fine sand, see Fig. 5.26. The propeller pitch ϕ is controlled such that the maximum ship speed of 1.5 m/s is obtained. To prevent the pump from cavitating the water valve α_v is opened in the first 40 minutes. During this period the density is slowly increased. As before the increasing draught allows for increasing incoming density. After $t = 40$ min the incoming production rate is maximised.

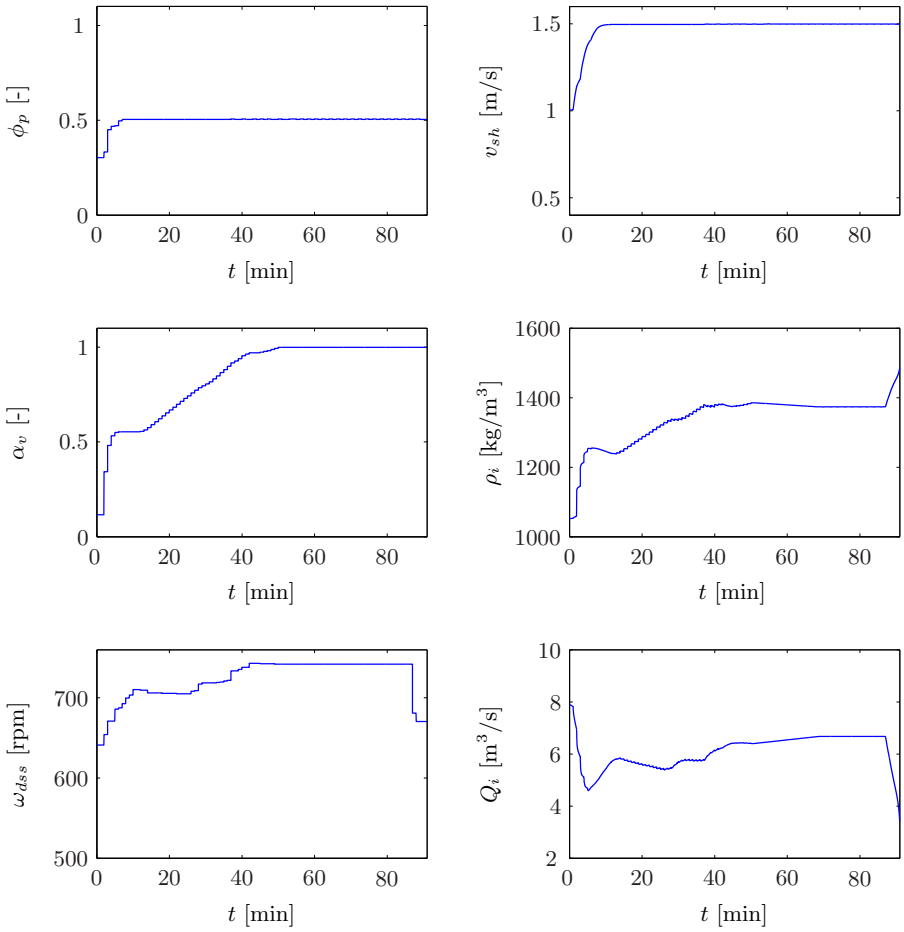

Figure 5.26: Inputs and corresponding outputs of MPC strategy for the overall process and coarse sand (soil type 5), with $d_m = 0.89$ mm.

At $t = 0$ the diesel engine set-point is 640 rpm. The MPC chooses this speed to lower the pump speed and, thus, the incoming flow rate. Lowering the flow rate reduces the pressure loss in the hydraulic pipeline system. This allows for a higher incoming density while satisfying the constraint on the inlet pressure. After $t = 40$ min the draught is large enough, so that the diesel speed is maximised to its nominal speed. The MPC tries to maximise the excavation production rate. The sedimentation

process does not play a role in the optimisation strategy for coarse sand, because the sedimentation rate is very fast and not sensitive to the incoming flow rate Q_i.

The MPC strategy is compared with the benchmark in Fig. 5.27. The left-hand panel shows the TDS, which illustrates that the two strategies perform equally well. This is not surprising, since for coarse sand the optimal strategy is maximizing the excavation production rate. The benchmark, as well as the MPC, does exactly that (see the right-hand panel of Fig. 5.27).

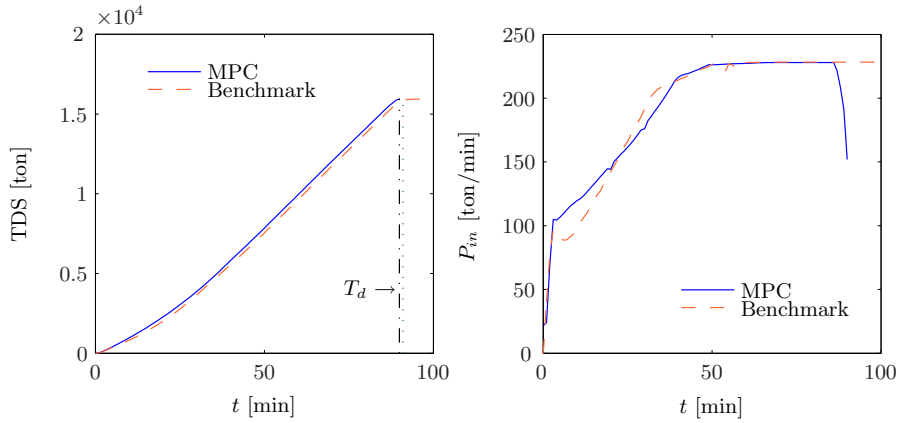

Figure 5.27: Comparison of MPC with benchmark for overall process and coarse sand (soil type 5), with $d_m = 0.89$ mm.

If we compare the optimal strategy of the overall process with the optimal strategy of the hopper process we see differences. The hopper process does not incorporate the pump process and, therefore, does not take limitations such as the inlet pressure into account. This limitation constrains the incoming production rate. Therefore, this production rate shows an increasing trend in the right-hand panel of Fig. 5.27, while this is not the case for the hopper process (see Fig. 5.7).

Overview and Comparison

The previous section describes the results for two soil types in detail. Here an overview of all five soil types and comparison of the benchmark with the MPC is given. In general, the MPC improves the cycle production rate J (see Tab. 5.8). The improvement depends strongly on the soil type. For coarse sand, only 1% improvement is expected, but for finer material the improvement is larger, up to 42%. This improvement is expected with the assumption of the benchmark, which is that the pump speed is kept at nominal speed. Clearly, these results show that it is beneficial to control the pump when optimising the performance J.

There are two other benefits when applying MPC on board of hopper dredgers. Tab. 5.9 gives a comparison of the average power during dredging between the benchmark and the MPC. This table shows that a reduction up to 25% can be achieved. For coarse sand the improvement is only 4% but for the other sand types a reduction of at least 12% is achieved. Thus, while maximising J, a beneficial side-effect is that

the average power decreases. Power reduction will become more and more important in the future, when the raw fuel prices and environmental taxes increase.

Table 5.8: Comparison of the cycle production rate (J) between MPC and the benchmark for overall process.

Grain size [mm]	MPC production rate [ton/min]	Benchmark production rate [ton/min]	Improvement [%]
0.86	53.2	52.8	1
0.31	52.6	49.4	6
0.19	50.0	44.7	12
0.12	41.9	34.9	20
0.09	34.3	24.2	42

Table 5.9: Comparison of the average power during dredging for the benchmark and the MPC.

Grain size [mm]	MPC [MW]	Benchmark [MW]	Improvement [%]
0.86	8.8	9.2	4
0.31	8.7	9.9	12
0.19	8.2	10.0	18
0.12	7.6	10.1	25
0.09	8.0	10.2	22

Table 5.10: Comparison of the cumulative overflow loss during dredging for the benchmark and the MPC.

Grain size [mm]	MPC [ton]	Benchmark [ton]	Improvement [%]
0.86	$1.1{\cdot}10^3$	$1.4{\cdot}10^3$	22
0.31	$2.5{\cdot}10^3$	$4.4{\cdot}10^3$	43
0.19	$4.9{\cdot}10^3$	$1.0{\cdot}10^4$	53
0.12	$1.1{\cdot}10^4$	$2.7{\cdot}10^4$	58
0.09	$3{\cdot}10^2$	$4.5{\cdot}10^4$	99

The other benefit is the reduction in cumulative overflow loss. Although it is not explicitly stated in the objective function, the MPC reduces the overflow loss significantly. For coarse sand the improvement in production rate was only 1% and the reduction in power 4%, but the overflow loss was reduced by 22%. The reduction of overflow loss becomes more and more important. The overflowing sediment disrupts the biological habitats of the sea animals. In vulnerable environments overflowing is often prohibited or must be minimized as much as possible. Especially for the finer sand types, a reduction of up to 58% is expected.

The improvement for the fine material with a grain size of 0.09 mm might be somewhat bigger than the actual value. The MPC strategy has no overflowing phase while the benchmark does have a very long overflowing phase. According to the tangential method, the benchmark should have an overflowing phase. Therefore, the difference is 99%.

5.7 Concluding Remarks

The objective of the optimisation problem was to maximise the production per time unit, which takes the time for sailing and discharging into account. This was first demonstrated on a smaller system: the hopper and drag head and then on the overall process. This chapter showed the results of two optimisation methods: one method for examining the optimal strategy with a large nonlinear problem, solved by a GAMS program and the Conopt solver, and the other method is MPC with the use of the Patternsearch optimisation algorithm. The two approaches were applied to the hopper process to illustrate for 5 soil types how to make a trade-off between the sedimentation process and the excavation process. Finally The whole process was optimised with the MPC method. The results of the MPC method were compared with data set B and a benchmark.

The optimisation of the hopper/drag-head process resulted in the following conclusions. This dredging strategy of the benchmark maximises the incoming production rate. Compared to this, Dynopt and MPC improved the production rate between 2% for coarse sand and 21% for fine sand. This improvement is expressed in the objective function J, which divides the tons of dry solids at the end of the dredging cycle by the total cycle time (including sailing and discharging).

For a hopper dredger with two dredging pipes an improvement of 2% for coarse sand up to 25% for fine sand is expected, compared to the benchmark defined in this chapter. This is achieved by optimal control of the flow rate. Coarse material requires the flow rate that gives the highest incoming production rate, while medium and fine sand require a lower flow rate. The improvement is not caused by a eduction of the erosion effect but by loading a mixture with a higher density, which results in its turn in an improved sedimentation rate.

The two methods, Dynopt and MPC with Patternsearch, show the same optimal strategy for the hopper process. MPC has a slightly better performance for coarse material. The Dynopt method is less suitable for optimising the overall process than MPC. The overall model is a stif system, which means that it is a combination of a slow dynamic system such as the sedimentation and a fast dynamic system such as the pump-pipeline system. For the Dynopt methods this requires a smaller discretisation step size than what is used in the hopper process. As a result the number of decision variables become too large to efficiently solve the optimisation problem. For the MPC this is not an issue, as it uses an ODE-solver with a variable step size, while keeping the number of decision variables small.

Both methods show that the optimal control strategy for the overflow height is the same as for the constant-tonnage loading system which is used onboard (see Section 2.3.3 and Section 3.2.2). Therefore, the overflow height is not used as part of the optimisation for the overall process. Instead, the constant-tonnage loading controller determines the height of the overflow weir.

The undisturbed settling velocity parameter the most important parameter for the hopper optimisation problem. This parameter has the most influence on the sedimentation process according to our model. The density of the sand bed and the erosion parameter become important near the end of the cycle. The erosion parameter influences the final height of the sand bed and the sand bed density determines the final amount of tons of dry solids in the hopper. The β value in the Richardson and

Zaki model does not influence the optimal control strategy much and this is fortunate, as it is very hard to estimate from the available measurements.

For coarse sand, the optimal control is only dependent on the incoming production rate, but for lighter sand it should be controlled between the constraints. In general, the optimal incoming flow rate is smaller, for lighter grains than for coarser grains, because this gives a higher incoming density. It also should be noted that the sedimentation process has a large impact on the optimal strategy, and erosion process has has in general a smaller impact on the optimal strategy. The erosion process becomes important near the end of the cycle.

The optimisation of the overall process shows that some cycles are operated near the optimum, but most of the cycles are not. The predictive controller improves the cycle production rate for coarse sand between 0% and 21% by reducing the cycle time. For the 11 dredging cycles an average improvement of 7% is expected.

To explore the possible improvement for other sand types, MPC was applied to five theoretically defined soil types and compared with a benchmark. This benchmark had the following dredging strategy: the diesel engine speed is at nominal speed, which is most often used in practice for a diesel-direct ship configuration. The water valve is controled such that the incoming production rate maximized, without violating the inlet pressure constraint. Finally, the propeller pitch angle is controlled such that the ship sails at the maximum speed of 1.5 m/s. Compared with this benchmark, the MPC improves the performance between 1% for coarse sand and 20% for fine sand with a grain size of 0.12 mm.

The drag head production model is only valid under the conditions stated in Section 3.3.1. In this chapter the propeller pitch, the water valve and the pump are controlled to optimise the performance. These are new conditions under which it is uncertain if the model is still valid. Therefore, once MPC is applied in practice, it must be verified if the model can be used for predicting the incoming density in the controlled situation. In the meantime it is recommended to do identification experiments on board of the hopper dredger where the conditions are similar to the strategies suggested in this chapter and verify if the models have sufficient prediction accuracy.

The calibration results in Section 4.4 showed that in some cycles the ship's speed has no influence on the incoming density. Without this correlation, the MPC is not able to find a strategy for the pitch angles, since the ship's speed has no influence on the performance of the objective function. Every propeller pitch angle is allowed as long as the power and speed constraints are not violated. In this situation it is up to the operator to decide on the ship's speed.

A beneficial side effect of MPC strategy is that it also reduces power usage by 4% for coarse sand and by up to 22% for fine sand. Moreover, the overflow loss is reduced by 22% for coarse sand and up to 58% for fine sand with a grain size of 0.12 mm. Thus, while increasing the performance based on the cycle production rate, the average power use and the overflow loss are reduced. Although we did not take environmental issues, such as fuel consumption and overflow loss, into account, they will become more important in the future and TSHD will benefit even more from this a MPC based strategy.

6

Simulation Scenarios

The previous chapter showed the improvements possible when using model predictive control (MPC). The parameters used in the MPC were based on the calibration results of Chapter 4. In this chapter we show two scenarios. One scenario is based on theoretical assumptions to show the potential of the MPC method in the case that the ship does not have sufficient power available for dredging (Section 6.1). The other scenario shows the effects of parameter uncertainty and changing soil type on the control strategy.

6.1 Power Limitation

It is observed on board of a hopper dredger that when the diesel engines of the hopper dredger are operating at maximum power and are about to enter the constant torque regime, the propeller pitch is automatically reduced. Consequently, the ship's speed reduces and the production drops. To investigate the optimal strategy in this power-limiting situation, we simulate a ship with not sufficient power for the dredge operation. The MPC solution is compared with the case in which only local controllers are used.

Various constraints depend on the characteristics of the diesel engine, centrifugal pump and the pipe characteristics. To illustrate the effect of the diesel engine on the process, we show the power characteristic of the diesel engine in Fig. 6.1. After powering up the diesel engine, the process is at operating point C. If the load increases, the fuel rack controller maintains an approximately constant speed by injecting more fuel. The load may increase until the engine supplies the maximum power (point A). If the load increases even more a controller reduces the pitch angle of the propeller. If this is not the case, the engine enters the constant torque area (between points A and B). The engine speed is now dependent on the load and drops when the load increases.

6.1.1 Ship Configuration

We consider a ship with one dredge pipe and two diesel engines as shown in Fig. 6.2. The starboard diesel engine powers the starboard propeller, the dredge pump and a generator. The other diesel engine delivers most of the trailing force and power for a

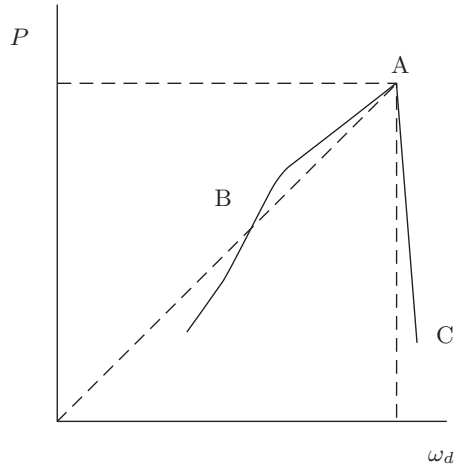

Figure 6.1: Power characteristic of a diesel engine.

generator. The generators power the jet pump installation and auxiliaries. The dredge pump is connected to the starboard engine.

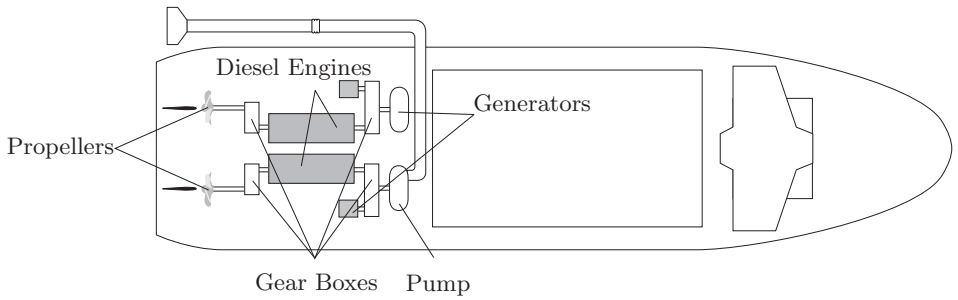

Figure 6.2: Diesel direct-driven ship with a single dredge pipe.

The control inputs are: the starboard propeller pitch ϕ_s and port-side propeller pitch ϕ_p to control the ship speed, the normalised water valve angle α_v to control the incoming density and the starboard diesel engine angular velocity ω_{dss} to control the pump speed. The port-side diesel engine is kept at its nominal speed to generate the power needed for the propulsion and the generator. To utilise all available power which is installed onboard, in this scenario both pitch angles are controlled instead of only the port side pitch as in Chapter 5.

6.1.2 Parameters and Soil Type

To create a power-demanding scenario, hard-packed sand with a grain size of 0.3 mm is chosen. Hard-packed sand causes large cutting forces and demands much power. The dredging depth is 20 m and the soil-type-dependent parameters are presented in Tab. 6.1, which have been determined by empirical correlation, see Appendix D.

Table 6.1: Soil-type-dependent parameters used in this scenario.

Parameter	Value	Unit	Parameter	Value	Unit
S_{kt}	1.2	m/s	e	0.57	-
γ	0.4	-	ρ_{si}	2054	kg/m^3
λ_f	0.010	-	ρ_s	1946	kg/m^3
v_{s0}	0.038	m/s	k_e	8	m/s
c_{hn}	0.70	-	a_{dh}	-3.38	s·kg/m^6
c_{hc}	4.2	-	b_{dh}	90.9	s·kg/m^4
k_i	$3.3{\cdot}10^{-4}$	m/s	c_{dh}	1388	kg/m^3
k_{max}	$6.7{\cdot}10^{-4}$	m/s	k_t	$6.2{\cdot}10^4$	Nm
k_m	$5.0{\cdot}10^{-4}$	m/s			

Here, it is assumed that the jet system and auxiliaries operate at a constant power level, supplied by the port-side engine. The power specification is given in Tab. 6.2.

Table 6.2: Power specifications.

Symbol	Description	Value	Unit
P_{total}	Total installed power	12	MW
P_j	Power for jetting	1.7	MW
P_{other}	Constant power demand per engine	1.4	MW

6.1.3 Comparison

To compare the performance of the MPC, a benchmark is defined. The ship of this benchmark is equipped with a local controller to assure that the simulation is within physical constraints. The controllers are comparable to controllers used on board of the hopper dredgers. Besides the physical constraints, a maximum sailing speed of 1.5 m/s has been chosen.

Benchmark

The benchmark simulates a ship as described in Section 6.1. As soon as the diesel engine reaches the maximum power, a controller regulates the pitch to maintain maximum power. This speed controller regulates the port-side propeller pitch for the ship to sail at 1.5 m/s as long as there is sufficient power. For the port-side propeller, the following controller is implemented for the propeller pitch ϕ_p:

$$\phi_p = k_{cpp}(v_{sh,s} - v_{sh}) + \phi_I - \delta_I \tag{6.1}$$

$$\dot{\phi}_I = \frac{k_{cpp}}{\tau_{cpp}}(v_{sh,s} - v_{sh}) \tag{6.2}$$

where k_{cpp} is the P-gain, $v_{sh,s}$ is set-point for the ship's speed, v_{sh} is the ship's speed and τ_{cpp} is the I-gain time constant. To maintain maximum power the following

controller, which includes an anti-windup arrangement, reduces the propeller pitch:

$$\dot{\delta} = \frac{k_{pow}}{\tau_{pl}}(Y_{ip} - Y_{max}) - k_{ap}(\delta_{Ib} - \delta_I) \tag{6.3}$$

$$\delta_{Ib} = \delta + k_{pow}(Y_{ip} - Y_{max}) \tag{6.4}$$

$$\delta_I = \min(\max(\delta_{Ib}, 0), 1) \tag{6.5}$$

where k_{pow} is the controller P-gain, k_{ap} the anti-windup gain, τ_{pl} the controller integration time constant, Y_{ip} the port-side fuel index and Y_{max} the fuel index threshold at which the pitch is reduced. As long as the power limit has not been reached the ship sails at this speed. When the engine reaches 100% of the maximum available power, the propeller pitch is automatically reduced to maintain maximum fuel injection. The power-limiting controller decreases the pitch of the port-side and the starboard engine when the engine reaches 100% of the maximum power. The starboard pitch angle set-point $\phi_{s,s}$ is chosen so high that the engine delivers 100% of the power.

$$\phi_s = \phi_{s,s} - \delta_{I,sb} \tag{6.6}$$

$$\dot{\delta}_{sb} = \frac{k_{pow}}{\tau_{pl}}(Y_{is} - Y_{max}) - k_{ap}(\delta_{Ib,sb} - \delta_{I,sb}) \tag{6.7}$$

$$\delta_{Ib,sb} = \delta_{sb} + k_{pow}(Y_{is} - Y_{max}) \tag{6.8}$$

$$\delta_{I,sb} = \min(\max(\delta_{Ib}, 0), 1), \tag{6.9}$$

where $\phi_{s,s}$ is the starboard pitch angle set-point, $\delta_{I,sb}$ the correction term when the maximum power is reached and Y_{is} the starboard fuel index.

The ship has no flow controller and the starboard diesel engine is operating at nominal speed (750 rpm). The water valve controller reduces the incoming density if the pump inlet pressure drops below the absolute pressure (11 kPa). This prevents the pump from cavitating while maximizing the incoming density. This controller is of the same PI-type with an anti-windup arrangement:

$$\dot{\nu} = \frac{k_v}{\tau_v}(p_i - p_{min,s}) - k_{av}(\nu_{Ib} - \alpha_v) \tag{6.10}$$

$$\nu_{Ib} = \nu + k_v(p_i - p_{min,s}) \tag{6.11}$$

$$\alpha_v = \min(\max(\nu_{Ib}, 0), 1), \tag{6.12}$$

where ν is the correction term to avoid cavitation, k_v is the controller P-gain, τ_v is the controller integration time constant, α_v is the normalized water valve angle. When there is enough available inlet pressure the α_v angle is 1, but when the absolute inlet pressure p_i is smaller than the minimum allowed pressure $p_{min,s}$ the water water valve is opened proportional.

6.1.4 Simulation Results

Fig. 6.3 shows the total mass m_t and the tons of dry solids TDS in the hopper for model predictive strategy and the benchmark. There is a large difference between the flow rates of the two strategies. The benchmark ship reaches the overflow phase earlier (at $t = 20$ min) since the average flow rate for this strategy is larger. However, the constant-tonnage phase is reached later, because of the larger overflow losses and less incoming production.

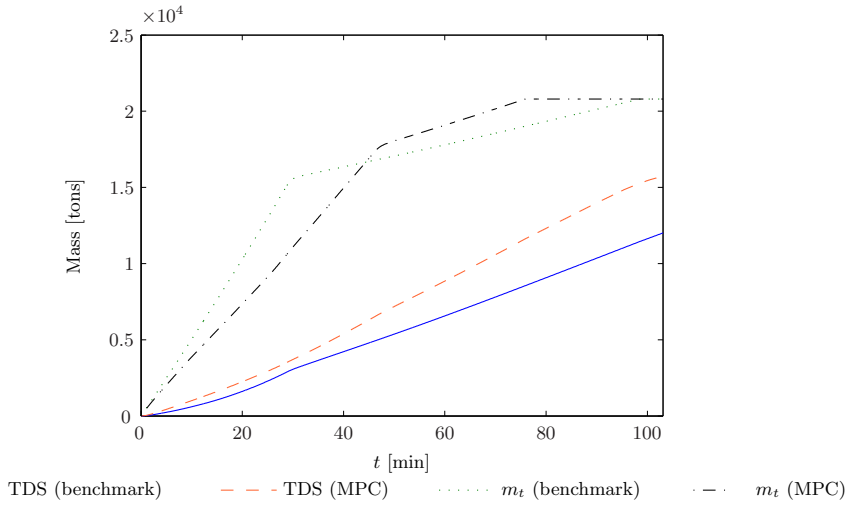

Figure 6.3: Masses in the hopper for a ship with only local controllers compared with MPC.

Optimal Input Sequences

The inputs of the two strategies differ substantially. Fig. 6.4 shows the four inputs controlled by the local controllers of the benchmark (continuous lines) and the model predictive controller (dashed lines). The top left-hand panel shows the speed of the starboard diesel engine. In the benchmark the diesel engine speed is at nominal velocity, but MPC reduces the speed to lower the flow-rate Q_i. The MPC reduces the diesel speed to approximately 660 rpm, resulting in a pump speed of 140 rpm. The top right-hand panel of Fig. 6.4 shows normalised water valve angle. A value of 1 means valve is closed and the incoming density is given by equation (3.29).

In the beginning both strategies reduce the density to prevent the pump from cavitating. Filling the hopper increases the mass and, therefore, the draught of the ship. Consequently, the pump is lowered under the waterline, which increases the available suction pressure. This allows the controllers to gradually increase the incoming density until the maximum is reached. Therefore, in both strategies the water valve is driven by the limited inlet pressure. The MPC, however, has more inlet pressure available due to the reduced flow rate, allowing the controller to increase the incoming density more than the benchmark. This lower flow rate also reduces the pressure losses in the pipe and drag head, since these depend quadratically on the flow rate. This influence is more significant than the increase in static pressure loss due to the increase in pressure loss, caused by the increasing density.

The two bottom panels show the port-side and starboard propeller pitches. For both strategies, the port-side propeller pitch is controlled such that the maximum force is supplied at the maximum fuel rack. Increasing the port-side pitch more would cause the port-side engine to enter the constant torque regime. The starboard pitch for the MPC is higher than for the benchmark. The local controller reduces the pitch at $t = 4$ min. At that moment the starboard engine reaches maximum fuel rack. To prevent

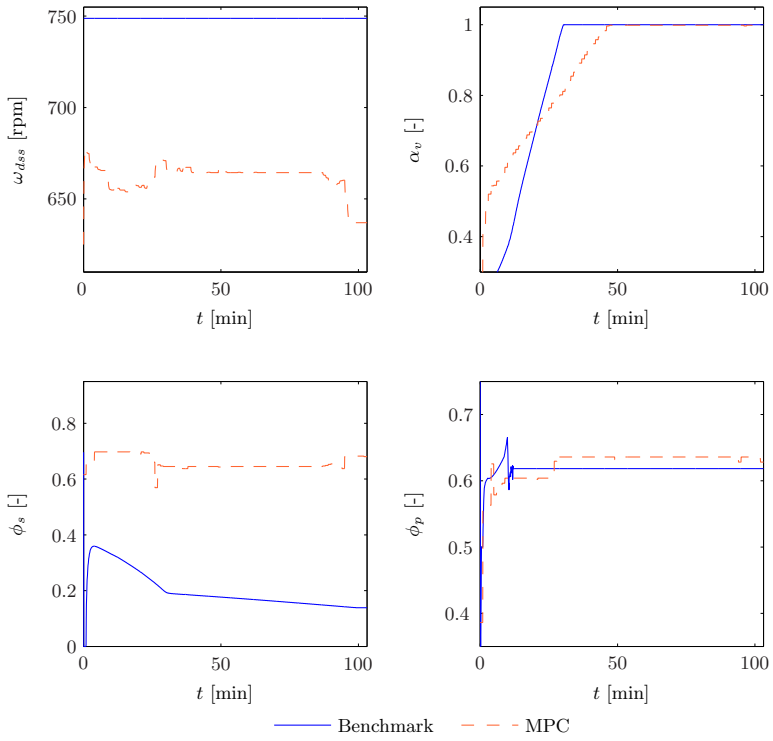

Figure 6.4: A comparison of the inputs of the benchmark and the MPC.

that this engine enters the constant torque regime the pitch is automatically reduced. In the model predictive control strategy this is not necessary. Here the pump process demands less power due to the reduced flow rate and leaves more power available for the propulsion of the propeller, although the maximum available power is lower than for the benchmark since the diesel speed is reduced. The total supplied thrust force in the MPC strategy is higher (900 kN) than for the local control strategy (560 kN). This is necessary, as the MPC excavates more material that demands more cutting force.

Comparison

The tons of dry solids increase faster in the MPC strategy than in the benchmark, resulting in 31% more sand accumulated in the hopper at the end of the loading (at $t = 99$ min). At this loading time, the predictive control strategy has loaded a mass of 15600 ton and in the benchmark has loaded only 11900 ton.

Fig. 6.5 shows the most important controlled variables. The top left-hand panel compares the flow rate of the two strategies. When the pump speed is not reduced the flow rate becomes 7.8 m^3/s (dotted line). The MPC reduces this flow rate to an average of 4.5 m^3/s. By doing so this strategy is able to increase the incoming

density by 13 to 16%. In the first 30 to 40 min, the density is increasing such that the inlet pressure does not drop below the constraint and after that the density remains approximately constant. The local strategy reaches the overflow phase earlier than the MPC strategy due to a higher incoming flow rate. Consequently, the outgoing density increases, see the bottom right-hand panel.

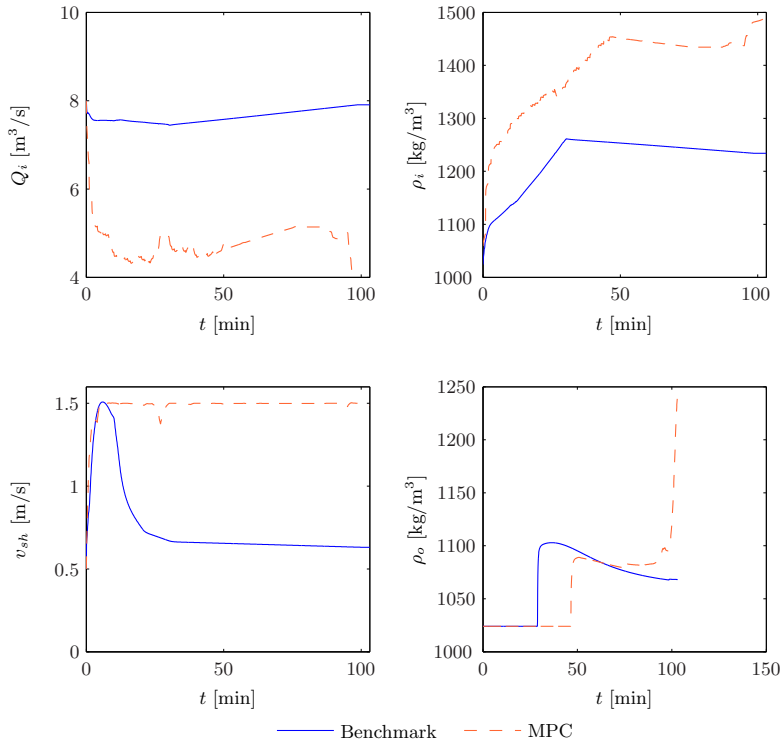

Figure 6.5: Comparison of outputs for the local controller and model predictive controller.

The MPC strategy reduces these overflow losses significantly by reaching the overflow phase later due to a lower overflow rate (but the same outgoing density). The MPC strategy reduces the cumulative overflow loss by 41% from 3310 ton of dry solids in the local strategy to 1959 tons of dry solids for the MPC strategy. This means that the MPC strategy increases the hopper efficiency.

The bottom right-hand panel shows the ship speed. The maximum speed allowed is set to 1.5 m/s to ensure that the drag head remains in contact with the bottom of the sea. Although both strategies reach a sailing speed of 1.5 m/s (3 knots) in the beginning of the dredging, as soon as the maximum fuel rack of the diesel engines for the benchmark becomes 100%, the propeller pitch is reduced. In the MPC strategy this does not happen, because it has more power available for the propulsion. The predictive controller uses an average of 1.6 MW for the pump, which is almost half of that of the benchmark (2.7 MW). The ship's speed drops to 0.65 m/s for the benchmark and remains 1.5 m/s for the MPC strategy.

The MPC has a 20% higher incoming production and 41% less overflow losses, meaning that the predictive controller is much more efficient. The high flow rate in the benchmark leads to high pressure loss, since this loss depends quadratically on the flow rate, see (3.38). Also, the benchmark starts overflowing 13 min earlier (see ρ_o in Fig. 6.5) with a much higher outgoing flow rate, leading to a significantly larger overflow loss.

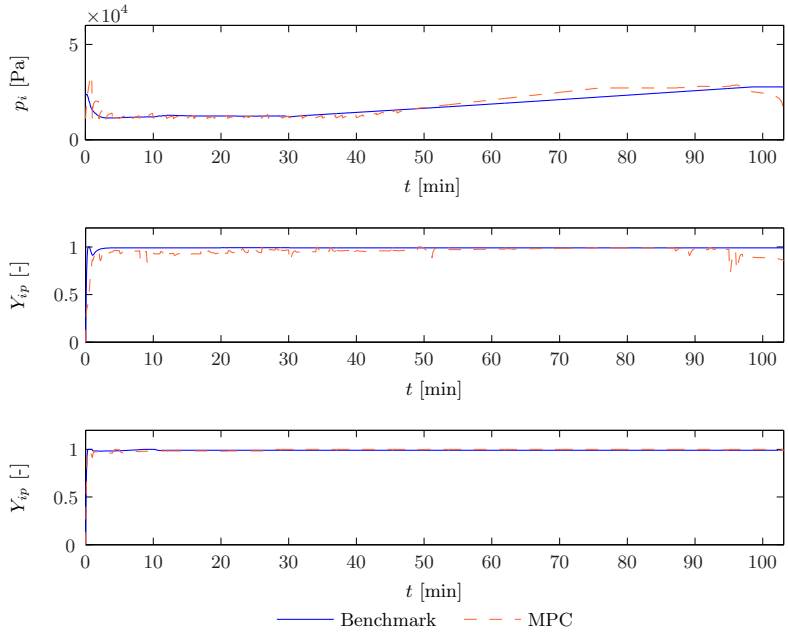

Figure 6.6: Variables that are constrained during dredging.

Constraint Handling

Fig. 6.6 shows the signals of all the important constraints, such as the pump inlet pressure to prevent cavitation and the maximum fuel rack to prevent that the engines enter the constant torque regime. The top panel shows the absolute inlet pressure for both strategies. For the MPC, the inlet pressure limits the production in the first 30 min and for the benchmark strategy in the first 40 min.

First, the MPC doses the density such that the inlet pressure constraint is not violated. After this period the process is solely controlled by the pump speed and the propeller pitches, while the visor input equals 1. Thus, by reducing the pump speed the incoming density can be increased and, although the flow rate decreases, the net result is that the total incoming production increases by 29%, which is 1200 ton of dry solids in the first 40 min. The middle and lower panel show the starboard (Y_{is}) and the port-side (Y_{ip}) fuel rack, respectively. The fuel rack of the benchmark strategy is at its maximum of 100% during the whole cycle. The fuel rack of the model predictive control strategy is slightly less than 100% for the starboard engine. This happens to

avoid crossing the 100% when the diesel speed is changed. Increasing the diesel speed set-point leads to a short increase in fuel rack. Normally one might allow these short violations of the 100% limit, but this is not implemented in the MPC.

Table 6.3: Overview parameters of plant model and the model in the model predictive controller.

Parameters	Plant	MPC	Parameters	Plant	MPC
v_{s0}	0.038	0.048 (+26%)	k_c	0.70	0.62 (-11%)
k_e	8	7 (-12%)	k_{ccav}	4.2	4.6 (+9.5%)
ρ_s	1946	1996 (+2.5%)	k_i	3.3e-5	3e-5 (-10%)
ρ_{si}	2054	2024 (-1.5%)	k_{max}	6.7e-5	7.3e-5 (+10%)
β	4	4.4 (+10%)	γ	0.4	0.36 (-10%)
a_{dh}	-3.4	-3 (+10%)	S_{kt}	1.2	1.32 (+10%)
b_{dh}	90.9	80.9 (-11%)	λ_f	0.010	0.009 (-10%)
c_{dh}	1388	1408 (+1.4%)			

6.2 Parameter Uncertainty

This section describes a simulation scenario for the effect of the uncertainty of parameters on the strategy. Until now the parameters chosen for the plant model and the MPC model are equal. In practice, however, this will hardly ever be the case. As the soil type varies during the process, consequently, the control strategy must be robust to cope with this varying behaviour and if the variation is too large the strategy must be able to adapt to the situation.

Online filtering and estimation techniques, such as recursive least squares and Kalman filtering, can be deployed to track time-varying parameters. The model parameters in the MPC are updated and new predictions based on the changed situation are made. This type of estimation will usually lag behind and, therefore, there will be a parameter mismatch in the predictive controller. The possible consequences of this are illustrated by an example in Section 6.2.1. In Section 6.2.2 the MPC control algorithm is extended with online estimation of the parameters. The scenario in this section shows how the predictive controller adapts to a step change of the soil type halfway during the dredging. Apart from adapting the control strategy, online estimation can also be used for monitoring and operator support. In Section 6.2.3 the parameter estimation is utilised to generate a 2-D plot of the grain size distribution on the bottom.

6.2.1 Parameter Mismatch

In this scenario, we use two sets of parameters: one set for the plant model and one set for the model in the predictive controller. Only the soil-type-related parameters are chosen to be different. The geometric parameters are the same for both sets. Tab. 6.3 gives an overview of the two sets. In general, a parameter mismatch of 10% is chosen, unless this will lead to unrealistic values. For example, a 10% mismatch for the sand bed will lead to densities of 2200 kg/m^3, which is not expected inside the hopper.

Fig. 6.7 shows the comparison of the tons of dry solids when the parameters in the controller are the same as in the plant model (dotted) and when the parameters are chosen as in Tab. 6.3. The figure indicates that the performance in terms of tons of dry solids is the same for the two situations. Clearly the sedimentation process is not very sensitive to the introduced uncertainty.

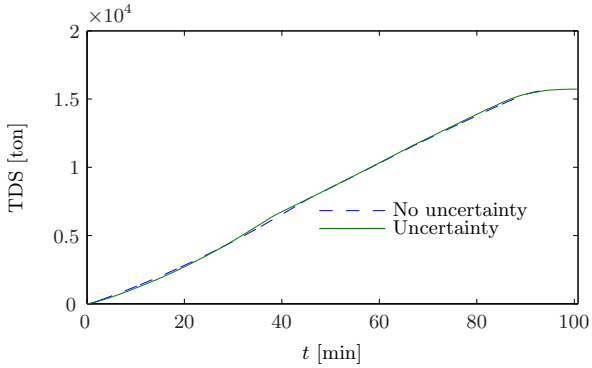

Figure 6.7: Comparison of tons of dry solids for the MPC strategy with and without parameter uncertainty

We find a small difference when comparing the inputs (Fig. 6.8). The top left-hand panel shows that the introduction of the uncertainty, on average, leads to an increase of the pump speed from 670 to 690 rpm. Therefore, the flow rate will be higher than the optimal flow rate in the case where there is no uncertainty. Not only does the average value change, but also the shape of the signal. Where in the no uncertainty situation there is a gradual decrease in speed, the uncertain case shows a more rapid decrease at the end of the cycle.

The top right-hand panel shows that introducing the uncertainty here results in a decrease of the incoming density, indicating that the strategy does not utilise the total available inlet pressure. The bottom panels show the propeller pitches, that exhibit a more restless behaviour. The parameter mismatch causes the ship to sail faster than the allowed 1.5 m/s, which is corrected in the next iteration by decreasing the pitch angles. This effect can be reduced by penalising change of inputs in the objective function.

Fig. 6.9 shows the four most important variables. The top left-hand panel shows the flow rate of the two cases. This panel shows that the flow rate is increased as a result of the higher diesel engine angular velocity for the uncertain case. Also, the incoming density is reduced (see top right-hand panel of Fig. 6.9). This density is not optimal, since the inlet pressure allows a higher incoming density.

As a result of the uncertain parameters the ship's speed varies more and sometimes drops below the maximum allowed speed. The uncertainties lead to a violation of the maximum speed, leading to a counter-measure of the controller in the next control step. The counter-measure is also based on the perturbed parameters, so that the speed drops more than actually required. Finally the outgoing density in the bottom right-hand panel shows that the uncertain case starts overflowing earlier because the

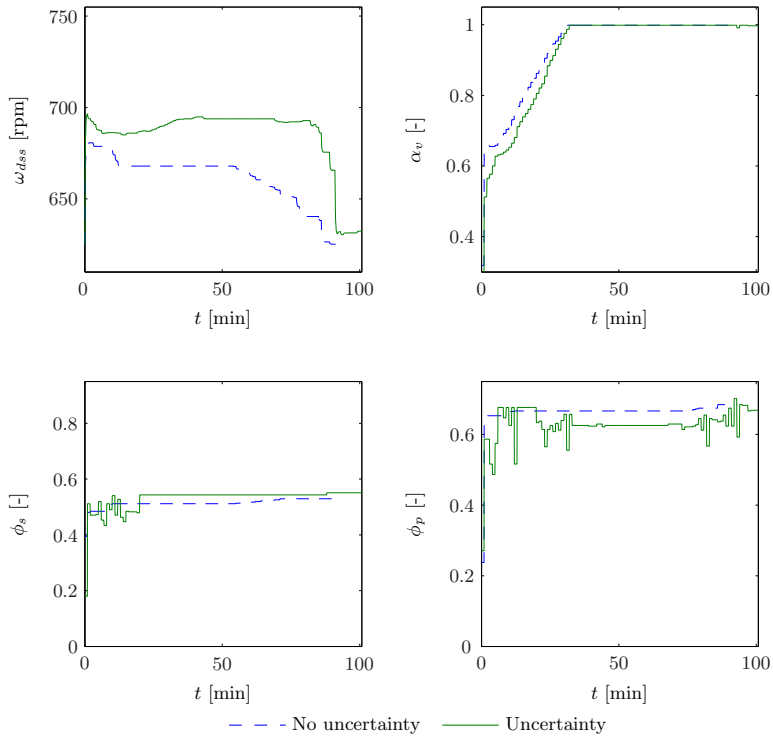

Figure 6.8: Comparison of the inputs of the MPC strategy with and without parameter uncertainty.

flow rate is higher.

Although the parameter uncertainty did not lead to a smaller value of the objective function, i.e., the TDS graphs are almost identical, the input sequences differ slightly. This is for one part caused by that fact that the objective function returns the same value for the two strategies.

The sample time of the predictive controller is 1 min, too slow to compensate for the parameter mismatch by the feedback mechanism for the faster processes such as the pump process and the sailing process. A possible solution is to increase the controller sample rate, but this is limited by the computational time of the nonlinear optimisation. Another approach is to use local controllers with fast sample rates to compensate for the fast disturbances. The MPC would then determine the set-points for these controller.

Increasing the parameter uncertainty too much, especially in the pump-pipeline process, leads to a process failure. The predictive controller in this case would increase the density in the pipeline too much, such that the pressure drop increases and the flow rate decreases. If the mixture velocity becomes lower than the critical velocity and the material starts to settle in the pipe, the pipe hydraulic friction increases even more and the flow rate collapses. This behaviour can also be prevented by the use of

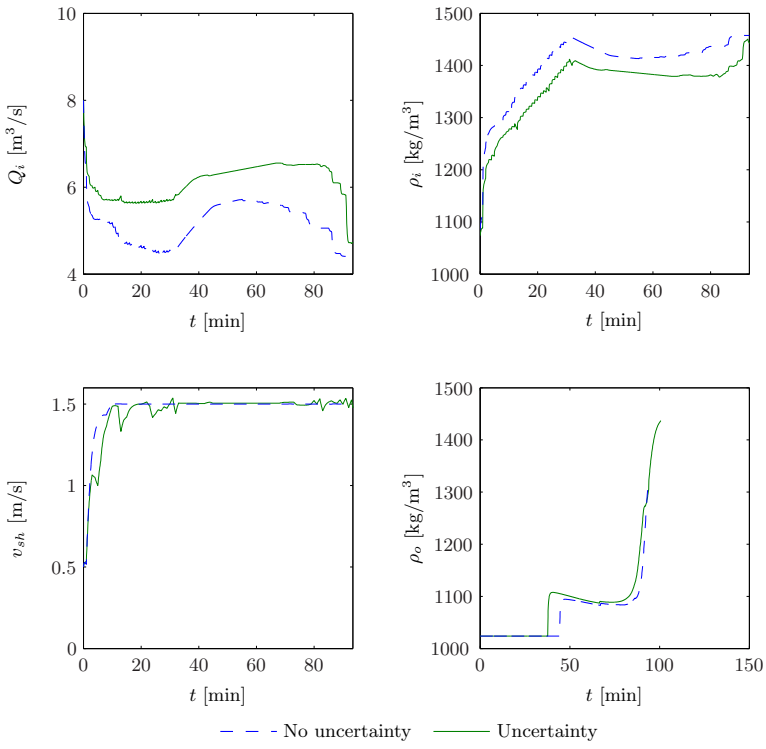

Figure 6.9: Comparison of the outputs of the MPC strategy with and without parameter uncertainty.

local controllers that would intervene in such a case.

These results underline that it is crucial to accurately estimate the soil-dependent process parameters in order to assure reliable and optimal process behaviour. This holds especially for the pump-pipeline process. In practice this means that a change in soil type must be detected and the parameters in the model of the predictive controller must be updated.

6.2.2 On-line Parameter Estimation and Adaptation

Almost all the submodels contain parameters that are dependent on the soil type as discussed in the previous two chapters. In the pump and pipeline there are two soil-dependent parameters, S_{kt} and γ. Both parameters have been made adaptive in Section 4.5.4: γ with a recursive least squares method and S_{kt} with a particle filter. This type of filter is also successfully implemented to estimate the overflow rate Q_o and overflow density ρ_o (Babuška et al., 2006). More information on particle filters can be found elsewhere (Liu and West, 2001; Arulampalam et al., 2002).

It is possible to calculate the grain size of the material in the pump and pipeline from the parameters S_{kt} or γ. The Führböter coefficient S_{kt} is correlated with the

grain size. The parameter depends on the average grain size according to the empirical correlation, see Appendix D. By inverting the relation of (D.8), d_m can be calculated. Here, d_m is used as scheduling parameter for determining the undisturbed settling velocity in the hopper model. For the undisturbed settling velocity, there are three relations that cover the whole range of sand, see Appendix D: Stokes, Budryck and Rittinger.

The other soil-dependent parameters are either kept constant or derived from the estimated pump and pipe parameters as scheduling parameters. Of course, for a successful implementation on board of a ship, all the soil-dependent parameters must be adapted automatically to changing soil conditions.

Simulation Results

In this scenario there is a change in grain size 0.27 mm to 0.64 mm at $t = 50$ min. Fig. 6.10 shows how the S_{kt} changes (continuous line). The estimated value is given as the dotted line. It follows quickly after the change but remains in the middle for some samples before estimating the correct value. The estimation is slightly biased but more accurate than the 10% parameter mismatch found in Section 6.2.1.

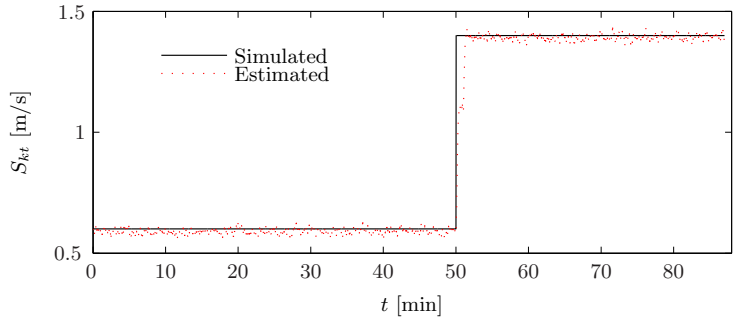

Figure 6.10: Simulation results during MPC, solid line the simulation output and dotted line the estimation by the particle filter.

The inputs resulting from the MPC of this scenario are given in Fig. 6.11. The top left-hand panel shows the starboard diesel engine set-point. The speed is first lowered to almost the minimum possible set-point and after 20 min it settles at 660 rpm. It remains constant until the step change of the grain size at $t = 50$ min. At that moment the grains become coarser and the parameter S_{kt} increases. This means that the pressure losses in the pipeline increase. The MPC responses to this by increasing the pump speed to 680 rpm. Due to the larger pressure losses the flow rate drops, which is compensated for by increasing the pump speed. Moreover, if the grain size increases, the undisturbed velocity of the grains in the hopper increases. This means less overflow loss and, therefore, the flow rate is increased to obtain a better cycle production (see Section 5.5.1).

The top right-hand panel of Fig. 6.11 shows the visor control action. In the first phase of the dredging the visor regulates the incoming density such that the pump inlet pressures does not drop below the minimum allowed inlet pressure to prevent the

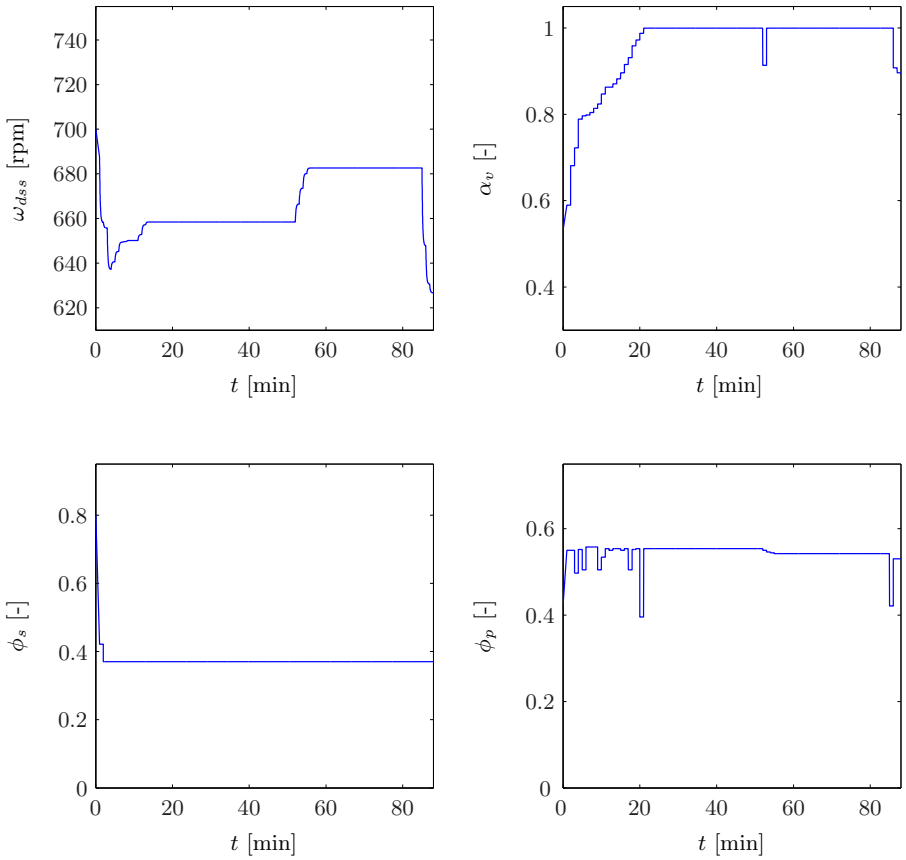

Figure 6.11: Inputs from the MPC strategy when grain size changes at $t = 50$ min.

pump from cavitating. After that the maximum density is dosed until the step change of the grain size. The predictive controller reacts to the step change by lowering the incoming density. This phenomenon can be explained as follows. The increase in pressure loss due to the coarser sand reduces the flow rate. This results in an increase of the incoming density according to the drag-head model, (3.30). A higher incoming density increases the pressure loss even more. If there is no control action and the flow velocity drops below the critical velocity, the process destabilises and the flow rate drops to zero. Thus, the predictive controller reacts by temporarily lowering the incoming density to prevent this.

Both pitch angles, given in the two bottom panels of Fig. 6.11, are hardly affected. The port-side pitch angle in the bottom right-hand panel is slightly reduced when the soil changes. The soil change reduces the incoming production and cutting height, thus reducing the cutting forces.

Fig. 6.12 shows the most important variables of the process. The top left-hand panel displays the incoming flow rate. At first it is reduced to 4 m^3/s to improve the sedimentation process, since the grain size is small in the beginning. During the

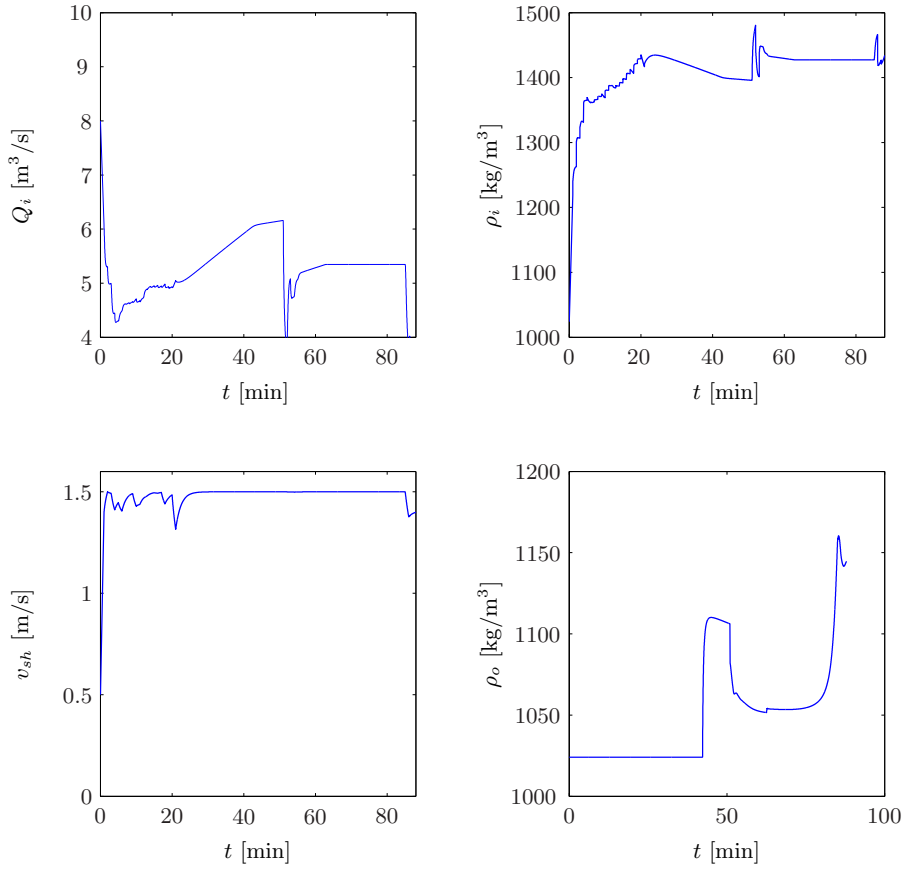

Figure 6.12: Outputs from the simulation when grain size changes at t=50 min.

loading the ship's draught increases and the static head loss decreases, because the transportation height above the sea level decreases. At $t = 50$ min the flow rate suddenly drops due to the grain size change. The flow rate recovers by increasing the pump speed and temporarily opening the water valve. The flow rate settles at 5.3 m^3/s until the end, when it decreases to 4 m^3/s. The input density (see top right-hand panel) is in the beginning determined by the constraint of the pump inlet pressure. After the first 20 min it varies because the flow rate varies. At $t = 50$ min it increases due to the reduction of the flow rate to 1430 kg/m^3, until the end of the cycle. The bottom left-hand panel shows the ship speed that is controlled such that the maximum allowed speed of 1.5 m/s is maintained. Now and then the speed drops below this value as a result of the changing inputs that disturb the sailing process. The density of the mixture flowing out of the hopper is given in the lower right-hand panel. The mixture starts flowing out of the hopper at $t = 45$ min, with a density of 1120 kg/m^3. At $t = 50$ min the soil type changes and the undisturbed settling velocity increases. Because of this the sedimentation rate increases and less material is flowing

out. As result the outgoing mixture density deceases to 1060 kg/m^3. At the end of the cycle, when the sand bed height is near the overflow height, the outgoing density increases substantially. The losses become so high that the optimal dredging time has been reached and the dredging process is stopped.

6.2.3 Soil Type Estimator

As explained in Section 6.2.2 the parameter S_{kt} can be estimated on-line. This parameter is correlated with the average grain size. During dredging this parameter changes as a result of the change in soil type. As the ship sails in the dredging area it receives GPS coordinates. The estimated grain size is mapped in a 2D plot to show the grain-size distribution at the bottom of the sea. This is useful for the following applications:

- To predict what the change in soil type will be and anticipate on the expected situation.
- Quality improvement of the sand, if the customer demands a type of sand with a specified average grain size.
- Production improvement; by avoiding areas of light sand material the overflow losses are minimised.

The dredging area is divided in equally sized boxes. Then, for every box the data of the estimated parameter are collected. Thus, if the ship sails through the same box often, a lot of data points are available. If the ship does not sail through a box, there are no data available. It is now possible to calculate the mean value for the parameter S_{kt} and determine the average grain size in every box. These results are shown in Fig. 6.13; the darker the colour, the larger the grain size.

As a reference the production is plotted in the 2D plot of Fig. 6.14. The darker areas have the highest production.

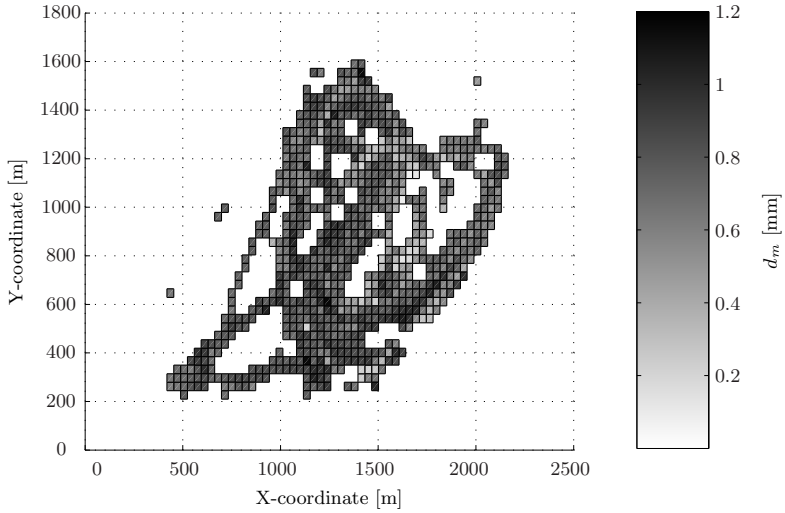

Figure 6.13: 2D plot of the grain size of the sand located on the bottom of the area to be dredged.

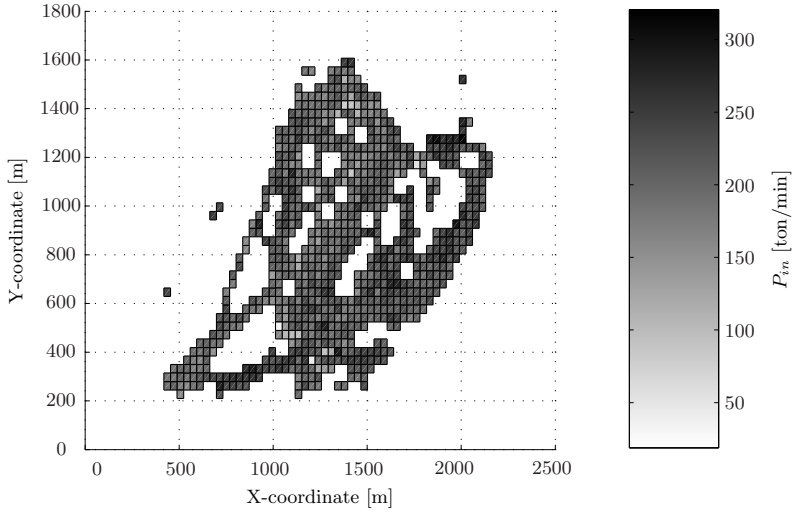

Figure 6.14: 2D plot of the production in TDS/min.

6.3 Concluding Remarks

It is clear that constraints must be taken into account when optimising the process. In each phase, different constraints can be active, depending on variables such as the dredging depth and the soil type. MPC can cope with constraints very well and has proven its potential in this example.

Controlling the pump to regulate the flow rate not only improves the incoming production by 20%, but also accomplishes this with 1.1 MW less pumping power. The predictive controller not only improves the production, but also improves the sedimentation process. The higher incoming density increases the sedimentation rate and the lower flow rate postpones the overflow phase and reduces the outgoing mass flux.

A parameter mismatch in the model for the MPC does not necessarily deteriorate the performance, but it does however have an influence on the derived control strategy. The mismatch can cause that the MPC violates the constraints. Therefore, when implementing MPC safety mechanisms should be installed that take care of the constraints in case they are violated by the MPC.

The soil-dependent parameters in the pump-pipeline model have been made adaptive. After a change in the soil type the MPC is able to adjust the strategy to the new situation. The grain size can be calculated from the estimated pump-pipeline parameters. If the result is plotted in a 2D map, the soil type can be identified during dredging. This is useful for anticipation and for quality improvement of the dredged material.

7
Conclusions

The Trailing Suction Hopper Dredger (TSHD) is irreplaceable in large-scale land reclamation projects, but also in maintenance dredging in harbours and waterways. The dredger is a complex system consisting of several components, such as a centrifugal dredge pump, propulsion and hopper. All these systems are equipped with local controllers that need set-points during operation. Usually, the set-points are determined manually by the operators. Optimal dredge operation requires constant adjustments of the set-points as the soil type changes. Due to the complexity of the system, caused by nonlinear system behaviour and interaction of all the components, it is often difficult for the operators to determine the optimal set-points. This thesis focuses on optimising the dredging behaviour using advanced control techniques.

The thesis describes four necessary steps for optimising the dredging performance: modelling, parameter estimation, model validation and model-based control. The overall performance of the TSHD plays a central role in this thesis. Integration of the sailing and discharge time, the interaction of subsystems and constraints are crucial for the global optimisation of the system. A Model Predictive Controller (MPC) is developed to optimise the overall dredging performance under various circumstances, such as different soil types.

As a benchmark for this research we use a TSHD with one pipeline and a hopper with a capacity of 13700 m^3. The ship has a diesel-driven dredge pump, two diesel engines and two pitch controlled propellers. The contributions of this thesis are summarised in Section 7.1. Consequently, the answer to the research question asked below is given in Section 7.2.

- To what degree does an integral advanced control approach improve the performance?

More detailed research objectives are:

- Development of a model of the TSHD for simulation purposes and for optimisation of the performance.
- Investigation of the model accuracy to verify if the developed models are suitable for control.
- Investigation of the improvement achievable with advanced control techniques.

- Development of a controller which optimises the performance of a TSHD under different conditions of soil types and dredging depth.

Finally, this chapter ends with recommendations for future research.

7.1 Thesis Contributions

In Chapter 3, an integral model of the total system is developed. This approach allows us to simulate the complex interaction of all important subsystems. Here, the focus is on modelling the most important mechanisms and obtaining a model requiring a short computational time. This rules out models based on partial differential equations. Instead, 1-D models with approximating functions have been formulated. Another aspect of our modelling approach is to reduce the number of soil-dependent parameters as much as possible, since the intent is to estimate these parameters from data measured on board of a hopper dredger. For on-line use of the models, the parameters are estimated from the measured data.

In Chapter 4 we show that for all models, except for the ship model, we are able to reliably estimate the parameters using measured data. We show approaches of estimating parameters using a nonlinear optimisation technique, recursive least-squares and a Kalman filter. The soil-type-related parameters are directly estimated from the data. From this approach, new opportunities, such as estimating the grain size on-line for operator feedback and control, arise. Although the models capture only the most important mechanisms, they show an accurate prediction of the system behaviour.

The computation time and accuracy of the models are the two main critical aspects for MPC as developed in Chapter 5. The simulation results show that an integral control approach improves the performance. This improvement depends on the soil type and varies between 1%, for coarse sand, and 21%, for fine sand. This improvement is given in terms of production per time unit for a complete dredging cycle. An improvement of 1% is expected in the case of coarse material and an experienced operator. MPC does not only improve the cycle production, but combines it with an improved settling process (less overflow losses) and better efficiency (less power). The effectiveness depends on the soil type. Because it takes all the important subsystems into account, it can operate under various conditions.

To evaluate the performance of the MPC, two scenarios have been presented in Chapter 6. The first scenario illustrates the ability of the predictive controller to cope with an important constraint: onboard power limitation. The current controllers onboard of the hopper dredger do not perform well in these situations. No integral system approach is used to design these controllers, which leads to suboptimal overall behaviour. The results of this scenario show that in this situation not only the propulsion power, but also the pump power must be regulated. A higher production is obtained with less power by controlling the pump speed. High flow rates cause high pressure losses, but do not necessarily lead to an optimal production.

In the second scenario, the influence of parameter uncertainties on the MPC strategy is simulated. The ability to cope with uncertainty and to adapt to a changing environment is necessary for successful implementation. The MPC is able to cope with varying soil types by using a particle filter. However, since the on-line parameter

estimation is only implemented for two of the soil-dependent parameters, there further research is necessary in this area. On-line parameter estimation also enables operator support applications. This has been illustrated with the on-line grain size estimation, based on estimation of the hydraulic friction coefficient in the pump-pipeline model.

7.2 Conclusions

7.2.1 Model and Parameter Estimation

In this thesis we combined existing models from the literature with newly developed models and a black-box model. We developed a computationally fast model which is able to predict the performance related variables such as the tons of dry solids based on the system inputs. We used dynamic models to exploit the full dynamic range of the system under various operating conditions. This model is suitable for on-line optimisation within the nonlinear MPC framework, since it is computationally fast.

Model

In this thesis there are three alternatives for the density gradient in the hopper sedimentation model are derived: the linear model, the exponential model and the water layer model. The test rig data (data set A) showed that the exponential and the water layer model predict the overflow density with the same accuracy. The validation of the models with ship data (data set B) shows that the water layer model has the best prediction of the total mass and, thus, the outgoing density, in the hopper. Moreover, the simulation time of the water layer model is the shortest.

The mixture formation in the drag head is a difficult process to model. Therefore, a black-box modelling approach has been chosen for predicting the mixture formation in the drag head. Beforehand, it was not known which variables are important for predicting the drag head process. The black-box modelling approach automatically selects the most important variables and builds a polynomial model. According to this modelling approach, the density can be predicted by the variables flow rate and the velocity of the ship. The density in the drag-head is negatively correlated with the square of the flow rate and positively correlated with the ship speed. The simulation results show high accuracy with the measurements. It is uncertain if the model will perform as well if the conditions are different from the conditions when the data were acquired.

The hydraulic transport is modelled with a pump-pipeline model. The sedimentation of sand in the suction pipeline and therefore the pressure drop depends on the inclination angle. The model takes this angle into account, which depends on the draught of the ship and the dredging depth. For the pump-pipeline model, it is very important to model the position of the pump under the water line and the position of the pipeline outlet above the water line. The first position determines the available suction pressure of the dredge pump. In the beginning of the cycle the hopper is empty and the pump centre is only a few metres below the water line. The pump inlet pressure is then the limiting factor in the production process. During filling of the hopper, the draught increases and pump centre is lowered under the water line. More pressure becomes available and it is possible to increase the production.

The position of the outlet above the water line determines the static head loss which the pump must deliver. This head loss decreases when the draught increases, because the position of the outlet above the water line decreases. The validation results show that this model is applicable to our application, since it is accurate enough and computationally fast.

The dynamic behaviour of the ship is very complex. The main components are the propeller forces, the resistance forces and the cutting forces of the drag head. During dredging the ship speed is around 1.5 m/s. This means that for cutting water-saturated sand the cutting forces are dominant over the other forces. Unfortunately, the data sets lack some important variables to fully validate our model and to derive a more accurate model. The simulation results show reasonable similarities with the data.

Parameter Estimation

The hopper is equipped with relatively few sensors. Only the total mass can be used to calibrate the soil-dependent parameters. It is possible to estimate three of the four parameters of the hopper process. This is, however, only possible after the start of the overflow phase. Before that period the parameters cannot be estimated. This statement also holds for the mass of the sand bed.

The measurements, already available, in the pump-pipeline system are sufficient to estimate the soil-dependent parameters. The influence of the soil type on the process is high, because the soil type varies from place to place; therefore, it is necessary to adapt the parameters on-line. This has been implemented with a recursive least-squares estimation algorithm for the pump coefficient γ and a particle filter for the pipeline coefficient S_{kt}.

From the estimated soil-dependent pump and pipeline parameters, it is possible to calculate the grain size. This on-line estimation method of determining the grain size can be used to derive other parameters, such as the undisturbed settling velocity in the hopper, but also to give the operators feedback on what type of soil they are dredging. GPS-position information can be used to draw a 2-D plot of the grain-size distribution at the bottom of the sea.

Sensitivity analysis shows that the undisturbed settling velocity is the most important parameter for the optimal loading strategy for the hopper model. The sand bed density and the erosion parameter only have an effect on the last interval of the dredging cycle.

7.2.2 Controller and Performance

The designed controller has been tested on a simplification of the system, the hopper model and on the overall model. The hopper model includes the black box drag-head model to restrict the incoming density. Without this model, unrealistic pairs of density and flow rate are possible. The overall model demonstrates the complexity of the optimisation problem of a hopper dredger. The interaction of the processes and the influence of the soil conditions make it a difficult process to optimise manually.

Sedimentation Process

The optimisation techniques are first applied to the hopper model to analyse the influence of the sedimentation process in the hopper on the cycle performance. The optimisation shows for a grain size equal or larger than 0.3 mm, the excavation process is most important for the optimal strategy. For smaller grain sizes, the optimal flow rate is determined by both the hopper sedimentation process and the excavation process. The improvements vary between 2% and 22% for the production per time unit. This analysis involves the whole cycle including a sailing and discharge time of 3.5 h.

Overall Process

The optimisation of the complete system with model predictive control results in better performance in terms of production, power efficiency and overflow loss. For medium and heavy sand the improvement compared with data set B is between 0.8% and 21%. For heavy material (i.e., grains larger than 0.3 mm) the MPC performs equally well as an experienced operator. However, on average for this type of sand an improvement of 7% is expected, because of inexperienced operators. This is an increase of 35280 ton during a week of fulltime dredging for a ship with a hopper capacity of 13700 m^3, in other words, an improvement of two shiploads in one week (from 32 to 34 cyles/week). It is assumed that the circumstances are comparable with our assumptions and that the dredged material is sand.

For material with a grain size less than 0.3 mm, the expected improvement is larger and varies between 7% and 21%. This improvement is caused by an improved sedimentation process which results in a shortening of the dredging time and an increase of the tons of dry solids in the hopper at the end of the cycle. For medium to fine sand, the sedimentation process becomes more important for the dredging performance. The sedimentation process is difficult for operators to incorporate because it is not visible or indicated on the instrumentation. Using MPC leads to an improved sedimentation process compared with the benchmark. An improvement of 21% is achieved for fine sand (soil type 1). It is compared to the situation with nominal diesel engine speed and maximum pump speed. In practice, an experienced operator will also reduce the flow rate for this type of sand. Therefore, 21% is an optimistic prediction of the improvement.

In case the onboard power is limited, the control of the pump to regulate the flow rate will not only improve the incoming production by 20% but accomplish this with lower pumping power (1.1 MW reduction). The predictive controller improves the production but also improves the sedimentation process. The higher incoming density increases the sedimentation rate and the lower flow rate postpones the overflow phase and reduces the overflow losses.

Estimation of the parameters in the ship model is difficult, because too little information is available from the sensors. Therefore, we must make assumptions on soil conditions, including the trail forces due to the cutting of sand. The uncertainty in this model does not have a large effect on the optimisation results, because the optimal ship speed is as fast as possible as long as there is enough power. A constraint is necessary to assure that the ship does not sail too fast and that the simulation stays within the valid model range. The maximum speed is limited to 1.5 m/s, which is the

optimal speed in all simulations.

7.3 Recommendations

In this thesis we use a centralised control and optimisation approach to directly control the system inputs. Although this is technically feasible there are practical drawbacks. The sample time (in the order of 1 min or less) of the model predictive controller is long with respect to disturbances in the order of seconds. Therefore, the model predictive controller can not adequately react to those disturbances. These disturbances must be rejected by faster low-level and local controllers. It is recommended that the best control system configuration that accomplishes fast disturbance rejection and optimal global performance is investigated. The local controllers must communicate with the centralised model predictive controller and vice versa.

A model predictive controller computes the input sequences leading to an overall improvement of the process. The sequences cannot always be interpreted directly, especially when looking at a small time portion of the sequence. Operators may incorrectly conclude from the system behaviour that the controller is malfunctioning. For successful acceptance of an advanced control system operators must be trained and educated. Moreover, the controller must not only apply the optimising control action, but also motivate these actions to the operators. It is therefore recommended to investigate what information and motivation the controller should display to the operators. Once this has been established, it should be investigated how the model predictive controller can calculate this information.

In this thesis it is assumed that all the states variables, such as the pump flow rate and the hopper mass, are measured. This is true, except for the sand bed mass in the hopper which is not measured on board of an actual hopper. The model predictive controller needs this state information at every control step. One solution is to add a sensor to measure this state, and the other solution is to estimate the state from measurements with an observer. If such a sensor system is too expensive, not reliable or technical not feasible, it should be investigated if this state can be estimated. Such a measurement could also be helpful to operators as performance feedback. It gives direct information on the settlement behaviour as result of the incoming flow rate, incoming density and overflow height.

The main focus in this thesis was on a ship with a diesel-direct configuration with one dredging pipe. This should be extended to other configurations. A diesel-direct configuration has limited controllability of the flow rate, because the diesel speed is constrained. For example, when the diesel speed is at its minimum, the flow rate cannot be reduced any more. For very fine sand, the actual optimal flow rate can be lower than the constrained flow rate. Moreover, reducing the diesel speed reduces the maximum available power. In a power limited situation reducing the diesel speed is not always desirable. The all-electric ship can flexibly divide the power over all power-demanding processes without losing performance. This is at the cost of more power losses due to all the conversions and it is more expensive. The power allocation of the all-electric ship, however, allows for a smaller amount of total installed power without losing performance.

The drag head production model is a nonlinear data driven black box model that

is only valid under comparable dredging conditions when the data set was obtained. There was no flow control or ship's speed control. However, the MPC controls the propeller pitch, the water valve and the pump speed to optimise the performance. It is therefore recommended to investigate if this model is still valid when using MPC. For this, an identification experiment can be designed, where the conditions are similar to the strategies suggested in this thesis. The results of this experiment will show if the model has sufficient prediction accuracy.

The validation results of the ship model show enough similarities with the data to conclude that this model is useful in our application. However, this model is relatively simple and needs to be improved for on-line application. The data sets B and C did not provide enough measurements for proper calibration, such as the measurements from the trail force sensors, for further development of this model.

Accurate and precise measurements on board of the hopper dredger are of vital importance for innovative research. The measurements contain much information that is necessary for controller design and improvement of efficiency and production. Operators must understand this importance and should take tasks as calibration and maintenance of sensors very seriously. Sensors that are not directly useful for the operator are often poorly maintained and, therefore, unreliable or even faulty. Although it is considered a costly activity, much effort should be made into making data available for research. For further research, new measurements are necessary. However, measurements can always be influenced by the researcher himself, but finding the correct circumstances for an interesting experiment is much harder. Making data available is an expensive and sometimes impossible task. Data reconciliation is not a research topic in this thesis, but part of the job!

This thesis showed that the integral control approach improved the operational aspects of a TSHD. A given and fixed ship design was assumed and the possible improvements for such a ship were investigated. The performance of the state-of-the-art ships leaves plenty of room for improvement. The next step, which could be breaking new grounds even further, is an integral ship design approach, which takes the mechanical, electrical and control aspects into account.

A
Pump-Pipeline Model

The pump-pipeline model describes the pressure drop due to the hydraulic friction of water or mixture with the pipeline wall. This pressure drop depends on the flow characteristics in the pipeline, which are characterized as follows:

- Flow regimes: in general, in a pipeline a carrying liquid may either flow in a laminar or a turbulent regime. When dredging sand the flow regime in the dredge pipe is turbulent (Matoušek, 2001).

- Flow patterns: when particles are present in a carrying flow, different flow patterns can occur. The flow pattern is determined by the balance between the particle settling velocity and the suspension flow rate due to the intensity of turbulence. The mixture is fully stratified when the intensity of turbulence is not sufficient to suspend any solid particle and the mixture is fully suspended when all particles are suspended. A fully suspended flow is called pseudo-homogenous when the distribution of particles is almost uniform across a cross-section. A detailed overview of the flow patterns is presented in Tab. A.1.

In this study the focus is only on the excavation of sand, which means that only models for slightly-stratified heterogeneous flow and very stratified heterogeneous flow need to be considered. The first models that were developed were empirical models predicting the basic characteristics of the slurry pipeline characteristics (Durand and Condolios, 1952; Fürböter, 1961; Jufin and Lopatin, 1966). These models are based on empirical correlations and can be easily calibrated to data.

The simplest hydraulic friction model is for a liquid such as water is determined by the Darcy-Weisbach equation:

$$I_f = \frac{\lambda_f}{d_p}\frac{|v|v}{2g},$$

where λ_f is the Darcy-Weisbach friction coefficient, d_p the pipe diameter, v the mean velocity in a cross-section of the pipe and g the gravitational acceleration.

The pressure drop over a pipeline segment for a liquid is given by the following equation:

$$-\frac{dP}{dx} = I_f g \rho_w = \frac{\lambda_f}{d_p}\frac{\rho_w |v|v}{2},$$

Table A.1: The following flow patterns occur in dredging pipelines, from Matoušek (2001)

Flow pattern	Description
Homogeneous flow of non-Newtonian mixture	Clay or silt flow in high concentrations
Pseudo-homogeneous flow of Newtonian mixtures	Coarse silt or fine sand (for sand only at high velocities)
Slightly-stratified heterogeneous flow	Medium to coarse sand mixture of which the majority is suspended and a minority travels within a granular bed
Very stratified heterogeneous flow	Medium to coarse sand of which the majority travels within granular bed and a minority is suspended
Fully-stratified flow with eroded top of bed	Fine to medium gravel of which the majority travels within a granular bed and a small portion of the particles is either sheared or moves by jumping and rolling over the top of the granular bed
Fully stratified flow	

where I_f is the frictional head loss of a liquid flow in 1 unit of pipe line length, λ_f the Darcy-Weisbach friction coefficient and v the mixture velocity. The total pressure loss over a pipeline with length L_p and diameter d_p is given by:

$$\Delta p_{loss} = I_f g \rho_w L_p = \frac{\lambda_f}{d_p} \frac{\rho_w |v| v}{2} L_p = \lambda_f \frac{8 \rho_w |Q_i| Q_i}{\pi^2 d_p^5} L_p$$

Führböter Correlation for Hydraulic Friction

In our pipeline model the Führböter model has been selected mainly because this model contains only one parameter to fit, which makes it very suitable for estimation from actual data. This parameter must cover all the effects which affect the friction inside the pipe. Online the parameter is adapted if the soil type changes. The Führböter correlation is:

$$I_m - I_f = S_{kt} \frac{C_t}{v}$$

where S_{kt} is the transport factor and C_t the transport concentration:

$$C_t = k_{tr} \frac{\rho_{pi} - \rho_w}{\rho_q - \rho_w} .$$

where k_{tr} is the slip coefficient, which equals unity in the case where there is no slip. Throughout this thesis $k_{tr} = 1$ is assumed. This slip coefficient models the effect that the liquid may travel faster than the solids. If a sliding bed has formed inside the pipe, this bed usually has a lower velocity as the liquid flowing above the bed. Then, on average, in the hopper a lower density than the density measured ($k_{tr} < 1$) is delivered.

The pressure drop over a horizontal pipeline is calculated as follows:

$$-\frac{dP}{dx} = I_m \rho_w g = \rho_w g (I_f + S_{kt} \frac{C_t}{v}) \tag{A.1}$$

$$= \frac{\lambda_f}{d_p} \frac{\rho_w |v| v}{2} + \rho_w g S_{kt} \frac{C_t}{v}\,, \tag{A.2}$$

using:

$$v = \frac{Q_i}{A_p} = \frac{4 Q_i}{\pi d_p^2}$$

gives:

$$-\frac{dP}{dx} = \lambda_f \frac{8 \rho_w |Q_i| Q_i}{\pi^2 d_p^5} + \rho_w g S_{kt} \frac{d_p^2 \pi C_t}{Q_i}$$

The pressure drop for a pipeline with length L_p is given by:

$$\Delta p_{loss} = I_m L_p = a_p \lambda_f |Q_i| Q_i + \frac{b_p C_t}{Q_i}$$

with

$$a_p = \frac{8 \rho_w L_p}{\pi^2 d_p^5}$$

and

$$b_p = \rho_w g \frac{d_p^2 \pi}{4} L_p$$

Inclination

During the dredging process a large part of the dredge pipe is under water at a certain angle. This angle affects the solids effect which is described here by the Führböter model. In a vertical pipe the grains do not settle or form a sand bed; therefore, there is no solids effect which increases the friction. On the other hand, in a horizontal pipe this effect is maximal. The angle of the suction pipe is determined by several variables:

- Dredging depth h_z, if the dredging depth increases the angle of the suction pipe decreases, which decreases the solids effect
- Draught of the ship h_d, during the dredging, if the dredging depth is constant, the draught increases due to the increasing load in the hopper. With an increasing draught the inclination angle decreases, leading to an increase in the solids effect.
- Winches: the pipe generally consists of two sections. Therefore, for a given draught and dredging depth the angles of the two sections can be determined with the intermediate winch. This also suggests that there is an optimal cable length that minimises the losses caused by the solids in the pipeline. For simplicity, in this thesis the suction pipe is considered as one section.

The consequences of the relation between the dredging depth/draught and the solids effect are large for the optimisation strategy. Dredging in shallow water might be more difficult than in deeper water due to the inclination angle, in spite of the decreased static head losses.

There are many models that describe the hydraulic friction (Durand and Condolios, 1952; Fürböter, 1961; Jufin and Lopatin, 1966; Wilson, 1976). Here, the Führböter model has been hcosen because it is easy to calibrate on data. The pipeline consists of an inclined part under water and a horizontal part above water. For a part of the pipeline which is inclined, the model of Worster and Denny (1955) is used:

$$\Delta p_{loss} = a_p \lambda_f |Q_i| Q_i + \frac{S_{kt} b_p C_t}{Q_i} \cos(\alpha_t),$$

where α_t is the angle of the suction pipe.

B

Calibrated Parameters

Hopper Model

This section gives the estimation results for the hopper model on data set B. The results of three models are presented: exponential model, linear model and water layer model.

Table B.1: Parameters estimated for hopper model of exponential model on data set B.

Cycle	v_{s0}	k_e	ρ_s	fvalmin
1	0.038	25	2e+003	0.000891
2	0.0344	25	1.94e+003	0.00269
3	0.0312	25	1.94e+003	0.0015
4	0.0373	25	1.97e+003	0.00128
5	0.0398	25	1.99e+003	0.000671
6	0.0391	25	1.94e+003	0.00117
7	0.0367	25	1.99e+003	0.000222
8	0.0381	25	1.97e+003	0.00139
9	0.041	9.98	1.98e+003	0.000666
10	0.0411	25	2e+003	0.000867
11	0.0324	25	1.9e+003	0.00108

Table B.2: Parameters estimated for hopper model of the linear model on data set B.

Cycle	v_{s0}	k_e	ρ_s	fvalmin
1	0.0369	25	1.98e+003	0.00294
2	0.0347	25	1.91e+003	0.00653
3	0.0317	25	1.9e+003	0.00495
4	0.0332	25	1.97e+003	0.00166
5	0.0389	25	1.98e+003	0.0024
6	0.0383	25	1.92e+003	0.00369
7	0.0354	25	1.98e+003	0.00107
8	0.0376	25	1.95e+003	0.0038
9	0.0383	25	1.97e+003	0.00225
10	0.041	25	1.97e+003	0.00281
11	0.0145	19.2	2e+003	0.00244

Table B.3: Parameters estimated for hopper model of the water layer model on data set B.

Cycle	v_{s0}	k_e	ρ_s	fvalmin
1	0.045	7.27	1.98e+003	0.000186
2	0.0361	25	2.02e+003	0.000665
3	0.0438	25	2.02e+003	0.000206
4	0.0319	22.5	1.93e+003	0.000799
5	0.0474	7.31	1.99e+003	0.000231
6	0.0452	19.5	2.02e+003	0.000221
7	0.0742	7.1	2e+003	0.000107
8	0.0447	5.18	2e+003	0.000301
9	0.0469	4.42	2.02e+003	0.000188
10	0.0383	9.75	1.95e+003	0.00017
11	0.0463	25	2.01e+003	0.000287

Overview Estimated Parameters

Table B.4: Overview estimated parameters on data set B.

Cycle	a_{dh}	b_{dh}	c_{dh}	S_{kt}	γ	λ_f	v_{s0}	k_e	ρ_s
1	3.38	90.90	1388	1.91	0.37	0.010	0.045	7.27	1.98e+003
2	3.09	95.86	1363	1.54	0.25	0.011	0.0361	25	2.02e+003
3	2.73	38.21	1394	2.07	0.21	0.009	0.0438	25	2.02e+003
4	4.86	101.19	1462	1.10	0.32	0.013	0.0319	22.5	1.93e+003
5	3.91	76.21	1435	1.60	0.26	0.011	0.0474	7.31	1.99e+003
6	3.05	67.00	1400	1.51	0.19	0.010	0.0452	19.5	2.02e+003
7	2.76	57.10	1405	1.61	0.10	0.009	0.0742	7.1	2e+003
8	3.13	105.35	1357	1.46	0.34	0.011	0.0447	5.18	2e+003
9	4.57	74.44	1485	1.00	0.35	0.013	0.0469	4.42	2.02e+003
10	3.50	-34.19	1609	1.07	0.27	0.013	0.0383	9.75	1.95e+003
11	3.66	102.09	1394	0.86	0.03	0.013	0.0463	25	2.01e+003

C

Automatic Black-Box Modelling for the Drag Head Process

This text is based on the work of Wangli (2006) which resulted in (Wangli et al., 2007). Mixture formation in the drag head is a complicated process for modelling. Processes such as jetting, eroding and cutting all act together in this process. It is a complex nonlinear system with many variables. It is, therefore, difficult to discover which variables play an important role in this process. Since we do not know this in advance, we propose to use a data-driven identification method. This method must find the variables with high correlation and build a nonlinear model. The method used here is an evolutionary algorithm that automatically selects the variable and builds the model (Maertens et al., 2005).

This model must predict in the incoming density ρ_i into the drag head based on operator set-points or measured disturbances. Beforehand we do not know which variables are important, but a crude selection can be made of signals that are most likely relevant. For some of the measured variables it is obvious that they do not contribute to the formation of the mixture.

Method

The method tries to find a relationship between the candidate variables x_i and the incoming density. The model structure is based on polynomial terms that are linear in the parameters. The method tries to find polynomial terms that have a significant impact on the model prediction.

The polynomial model are of the following form:

$$y = \sum_{i=1}^{n} a_i s_i + a_0 \,, \tag{C.1}$$

where a_i is one of the $n+1$ polynomial coefficients that are linked to one of the dth order polynomial terms s_i in X_p^d:

$$X_p^d \in \left\{ s | s = \prod_{0 \le j \le p}^{d} x_j \text{ with } x_0 \equiv 1 \right\} ,$$

where p is the number of selected candidate input variables ($p \leq m$ and $[a_0,\ a_1,\ \cdots,\ a_n]^T$ is a vector that determines equation (C.1). This vector is estimated using a standard least-squares technique. It is impossible to compare the prediction accuracy of all $2^m - 1$ polynomials. A genetic algorithm is used to search through the large solution space to find the optimal model.

Three main concepts need to be defined for the variable selection.

- Output variable: the variable which we wish to predict.
- Input variable set: this set contains all the candidate variables to be selected as regressors for the output variable.
- Number of qualified variables: the number of variables that remain after the selection process.

To reduce the solution space the algorithm is initialized with n_{init} to determine the maximum number of polynomial terms (d) to determine the maximum order of the polynomials and all the input variables. The genetic polynomial regression algorithm is run and the resulting polynomial structure is analysed. If one of the variables is absent in all polynomial terms, it is removed from the variable set and the procedure is repeated. This backward selection procedure is repeated until the predefined number of qualified variables is reached (Maertens et al., 2005). The selection results are expressed by means of a polynomial model for the output variable, based on the selected variables.

D

Soil-Type-Dependent Parameters

In this thesis it is proposed to estimate all the soil-dependent parameters for the purpose of on-line control. The parameters found in our data set represent only a small amount of soil types. To test our algorithms for the complete range of expected soil types, we need to define different the soil types. This appendix presents the equations and details required to calculate all soil-type-dependent parameters. Unfortunately, not all parameters can be determined with equations found in the literature. In those cases the parameters are supplied by MTI, without presenting the equations. Five theoretical soil types are defined: fine (soil type 1), fine (soil type 2), medium/fine(soil type 3), medium (soil type 4) and coarse (soil type 5).

Qualitative Description of the Soil Types

Five different soil-types have been defined, from fine material to coarse material, see Tab. D.1. Fine sand leads to high overflow loss and, thus, a long dredging time. On the other hand, for coarse sand the loss is limited and the dredging time short. The in situ soil properties determine the interaction between the drag head and sand pack on the bottom. Especially the cutting forces are influenced by the soil properties. It has been chosen to define hard-packed sand at the bottom, because this will lead to the highest cutting forces. This is the most power demanding situation for the trailing suction hopper dredger, as described in Section 6.1.

Table D.1: Qualitative definition of the five soil types.

Soil type	d_m
Fine (soil type 1)	0.09
Fine (soil type 2)	0.12
Medium-fine (soil type 3)	0.19
Medium (soil type 4)	0.30
Coarse (soil type 5)	0.86

Hopper Model

The hopper model has three soil-dependent parameters: the undisturbed settling velocity v_{s0}, the sand bed density ρ_s, β and the erosion coefficient k_e. For the undisturbed settling velocity, three different regimes can be distinguished (Stokes, Budryck, Rittinger) from Matoušek (1997):

$$v_{s0,1} = 424(\frac{\rho_q - \rho_w}{\rho_w})d_m^2 \qquad \text{for } d_m < 1 \cdot 10^{-4} \text{ m} \tag{D.1}$$

$$v_{s0,2} = \frac{8.925}{d_m}(\sqrt{1 + 95\frac{\rho_q - \rho_w}{\rho_w}d^3} - 1) \qquad \text{for } 1 \cdot 10^{-4} \leq d_m < 1 \cdot 10^{-3} \text{ m} \tag{D.2}$$

$$v_{s0,3} = 87\sqrt{\frac{\rho_q - \rho_w}{\rho_w}d} \qquad \text{for } d_m \geq 1 \cdot 10^{-3} \text{ m}\,, \tag{D.3}$$

where d_m is the grain size diameter. From these equations the undisturbed settling velocity can be computed as:

$$v_{s0} = \min(\min(v_{s0,1}, v_{s0,2}), v_{s0,3})$$

The density of the sand bed in the hopper ρ_s is calculated using correlations found by MTI. Tab. D.2 shows the minimum density of loosely settled material and the density of compacted density if it is compacted. We assume that the sand bed density

Table D.2: Loosely packed sand bed and compacted sand bed density.

Soil type	$\rho_{s,min}$	$\rho_{s,max}$
Fine (soil type 1)	1934	2020
Fine (soil type 2)	1938	2020
Medium-fine (soil type 3)	1942	2020
Medium (soil type 4)	1947	2020
Coarse (soil type 5)	1957	2040

in the hopper is loosely packed, therefore:

$$\rho_s = \rho_{s,min}$$

The exponent β in the hindered settling velocity of Richardson and Zaki (1954) is dependent on the particle Reynolds number Re_p. Based on experiments Richardson and Zaki (1954) found:

$$\beta = 4.65 \qquad \text{for } \mathrm{Re}_p < 0.2 \tag{D.4}$$

$$\beta = 4.35\mathrm{Re}_p^{-0.03} \qquad \text{for } 0.2 \leq \mathrm{Re}_p < 1 \tag{D.5}$$

$$\beta = 4.45\mathrm{Re}_p^{-0.1} \qquad \text{for } 1 \leq \mathrm{Re}_p < 200 \tag{D.6}$$

$$\beta = 2.39 \qquad \text{for } \mathrm{Re}_p \geq 200\,, \tag{D.7}$$

A more convenient representation is (van Rhee, 2002):

$$\beta = \frac{a + b\mathrm{Re}_p^{\alpha}}{1 + c\mathrm{Re}_p^{\alpha}}\,.$$

For a smoothed representation of Richardson and Zaki (1954), the coefficients are (Rowe, 1987) $a = 4.7$, $b = 0.41$, $c = 0.175$ and $\alpha = 0.75$.

Erosion takes place if the flow velocity above the sand bed is too high. For the Camp model (Camp, 1946), Vlasblom and Miedema (1995) implemented erosion by defining a threshold velocity u_s (scour velocity). If the flow velocity is below this threshold, a grain with diameter d_m will not settle:

$$u_s = \sqrt{\frac{8(1-n)\mu g d_m(\rho_q - \rho_w)}{f\rho_w}}\,,$$

where n is the porosity of the sand bed, g the gravitational acceleration, μ a coefficient dependent on the internal friction of the sediment, f a friction factor, ρ_q the density of quartz and ρ_w the density of water. The relation of u_s with k_e in our model is:

$$k_e = u_s W_{sh}\,,$$

where W_{sh} is the width of the hopper. The resulting erosion coefficients for the five soil types are given in Tab. D.3.

Table D.3: Erosion coefficient in the hopper model.

Soil type	k_e
Fine (soil type 1)	2
Fine (soil type 2)	4
Medium-fine (soil type 3)	6
Medium (soil type 4)	8
Coarse (soil type 5)	20

Drag Head

The drag-head model has two parts: the excavation model and the cutting force model. The excavation process is modelled by a black-box model. The parameters of this model do not have any physical meaning. These parameters are found by the estimation algorithm given in Section 4.4.

There are two soil-dependent parameters in the cutting force model: one parameter for cutting in the non-cavitating regime k_c and one parameter for the cavitating regime k_c. The cutting force model is based on the cutting theory of Miedema (1987). These parameters may vary in time, because they depend on varying soil conditions. In this thesis we assume that these two parameters are constant. The non-cavitating cutting coefficient is:

$$k_c = c_{hn}\rho_w g W_b N_b e/k_m\,,$$

where c_{hn} is a cutting parameter which can be determined with a lookup table in Miedema (1987), W_b is the width of one cutting blade, N_b is the number of blades, e is the volume strain and k_m is the effective permeability. The cavitating cutting coefficient is:

$$k_{ccav} = c_{hc}\rho_w g W_b N$$

where c_{hc} is a cutting parameter which can also be determined with the lookup table in (Miedema, 1987). The volume strain is given by:

$$e = \frac{n_{max} - n_{situ}}{1 - n_{max}} \qquad \text{,with} \qquad n_{max} = \frac{\rho_q - \rho_{s,min}}{\rho_q - \rho_w} \qquad n_{situ} = \frac{\rho_q - \rho_{si}}{\rho_q - \rho_w}$$

where n_{max} is the porosity after the cutting, n_{situ} is the porosity of the in situ material and ρ_{si} is the in situ density of the sand to be excavated. The effective permeability can be approximated by (Miedema, 1995):

$$k_m \approx 0.5k_i + 0.5k_{max}\,,$$

where k_i is the in situ permeability of sand and k_{max} is the permeability of the sand after cutting. The permeability is usually determined in a laboratory, but can also be determined by Kozeny-Carman equation (Verruijt, 2001). The values of the permeability used for the five theoretical defined soil types are given in Tab. D.4.

Table D.4: In situ permeability and permeability after cutting.

Soil type	k_i	k_{max}
Fine (soil type 1)	$3.68{\cdot}10^{-5}$	$6.46{\cdot}10^{-5}$
Fine (soil type 2)	$7.16{\cdot}10^{-5}$	$1.23{\cdot}10^{-4}$
Medium-fine (soil type 3)	$1.79{\cdot}10^{-4}$	$3.00{\cdot}10^{-4}$
Medium (soil type 4)	$4.47{\cdot}10^{-4}$	$7.26{\cdot}10^{-4}$
Coarse (soil type 5)	$3.2{\cdot}10^{-3}$	$5.6{\cdot}10^{-3}$

For each of the five soil types the in situ density must be defined. The higher this density is, the more compacted the sand will be. For reasons described above compacted sand is simulated, so that the cutting forces will be significant. An overview of the choices we made is given in Tab. D.5.

Table D.5: In situ density for the five soil types.

Soil type	ρ_{si}
Fine (soil type 1)	2020
Fine (soil type 2)	2020
Medium-fine (soil type 3)	2020
Medium (soil type 4)	2020
Coarse (soil type 5)	2040

Pump-Pipeline Model

In the pump-pipeline model there are three soil-dependent parameters: the Darcy-Weisbach friction coefficient λ_f, the transport factor S_{kt} and the solids effect of the pump γ. The Darcy-Weisbach friction coefficient depends on the flow regime. For a laminar flow regime this is:

$$\lambda_f = \frac{64}{\mathrm{Re}},$$

where Re is the Reynolds number of the flow:

$$\mathrm{Re} = \frac{v d_p}{\nu_f},$$

where ν_f is the kinematic viscosity of the liquid. For turbulent flow there is no simple expression, which links the velocity distribution with the pipeline shear stress. To overcome this, empirical expressions have been derived. Based on the pipe roughness, diameter and Reynolds number, the friction coefficient is obtained. This can be done by the Moody diagram (Fig. D.1) or its computational form (Churchill, 1977):

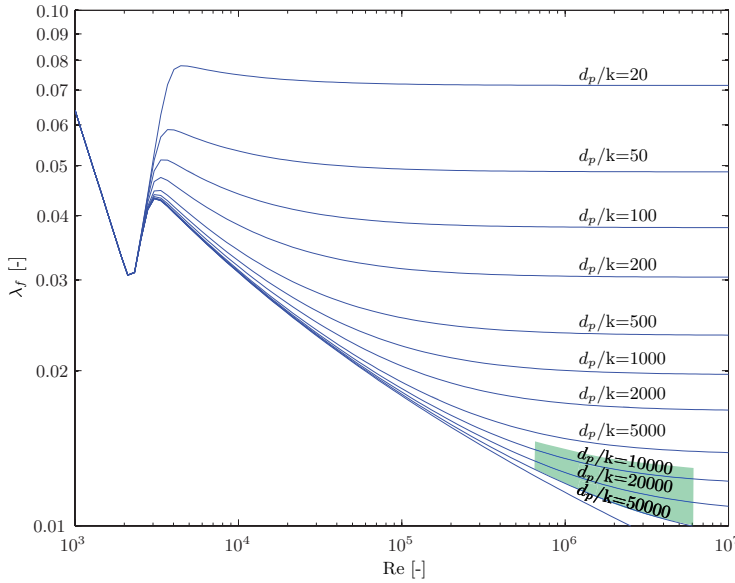

Figure D.1: Moody diagram for the determination of the Darcy-Weisbach friction coefficient. The shaded area is the working area of the dredge pipe.

The friction forces due to the solids effect are modelled by a transport factor S_{kt}. Besides that that this parameter is estimated, it can be calculated according to an empirical relation between the grain size and the transport factor is given in Fig. D.2, i.e.:

$$S_{kt} = \begin{cases} 2.59\, d_m - 0.37, & \text{for } 0.2 < d_m < 1.1 \text{ mm} \\ \text{from graph Fig. D.2} & \text{for } 1.1 \leq d_m < 3.0 \text{ mm} \\ 3.3 & \text{for } d_m \geq 3.0 \text{ mm} \end{cases} \tag{D.8}$$

The solids effect in the pump is modelled using the Stepanoff correlation (Miedema, 2002):

$$\gamma = \frac{(0.466 + \log_{10}(d_{50}))\rho_w}{(\rho_q - \rho_w) d_p)}$$

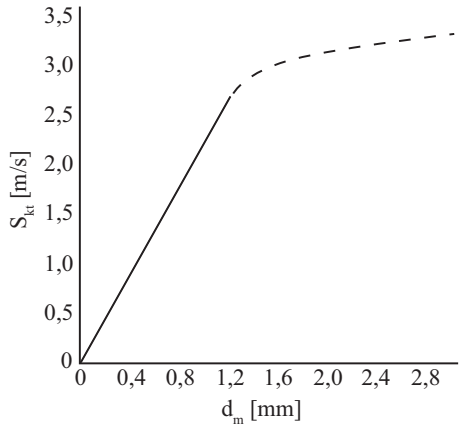

Figure D.2: Transport factor as function of the grain size.

Summary

This section summarises the parameters used for each soil type in Tab. D.6. Five soil types are used to show the performance of the model predictive controller for various soil conditions.

Table D.6: Parameters for each soil type

Soil type	1	2	3	4	5
Classification	Fine	Fine	Medium-fine	Medium	Coarse
k_e	2	4	6	8	20
d_m	0.09	0.12	0.19	0.3	0.86
γ	0.46	0.44	0.4090	0.38	0.30
S_{kt}	0.15	0.15	0.15	0.43	1.88
v_{s0}	0.005	0.009	0.020	0.038	0.09
c_{hn}	0.54	0.52	0.49	0.45	0.52
c_{hc}	3.28	3.1	2.91	2.7	3.15
ρ_{si}	2020	2020	2020	2020	2040
ρ_s	1934	1938	1942	1947	1957
k_i	$3.68{\cdot}10^{-5}$	$7.16{\cdot}10^{-5}$	$1.79{\cdot}10^{-4}$	$4.47{\cdot}10^{-4}$	$3.2{\cdot}10^{-3}$
k_{max}	$6.46{\cdot}10^{-5}$	$1.23{\cdot}10^{-4}$	$3.00{\cdot}10^{-4}$	$7.26{\cdot}10^{-4}$	$5.6{\cdot}10^{-3}$

Glossary

Notations

$\boldsymbol{a}$	Vector
$\hat{}$	Predicted
$\bar{}$	Calculated
$\tilde{}$	Average

List of symbols

α_1	Angle between horizon and excavation line	rad
α_2	Angle between excavation line and the teeth on visor	rad
α_3	Angle between teeth and visor	rad
α_4	Angle between teeth and the horizon	rad
α_p	Pipe angle	rad
α_t	Angle of the suction pipe	rad
α_v	Normalized water valve angle	-
β	Exponent in the hopper settling velocity	-
$\boldsymbol{\theta}$	Parameter vector in estimation problems	-
Δp_s	Static head loss	Pa
Δp_d	Pressure drop over the drag head	Pa
Δp_{lossw}	Pressure loss in the pipeline for water	Pa
Δp_{loss}	Pressure loss in the pipeline	Pa
Δp_{manw}	Manometric pressure head when dredging water	Pa
Δp_{man}	Manometric pressure head delivered by the pump	Pa
ϵ_k	Noise term	-
ϵ_x	The state transition noise	-
ϵ_{y_k}	The output noise	-
γ	Solid effect on the pump behavior	-
λ_f	Darcy-Weisbach friction coefficient	-
μ	Erosion grade in hopper settling	-
ν	Correction term in water valve controller	-
ν_f	Dynamic viscosity of the flow	m^2/s
ω_d	Rotational speed of diesel engine	rad/s
ω_p	Rotational pump speed	rad/s
$\omega_{d,max}$	Maximum or nominal rotational speed of diesel engine	rad/s

ω_{dps}	Set-point for the rotational speed of the port side diesel engine	rad/s
ω_{dp}	Rotational speed of port side diesel engine	rad/s
ω_{dss}	Set-point for the rotational speed of starboard diesel engine	rad/s
ω_{ds}	Rotational speed of starboard diesel engine	rad/s
ω_{pp}	Rotational velocity of port side propeller shaft	rad/s
ω_{ps}	Rotational velocity of star-board propeller shaft	rad/s
ω_s	Rotational velocity of a propeller shaft	rad/s
ϕ	Propeller pitch angle	-
ϕ_p	Propeller pitch port side	-
$\phi_{s,s}$	Setpoint for starboard propeller pitch	-
ϕ_s	Propeller pitch starboard	-
ρ	Density	kg/m^3
ρ_i	Incoming mixture density in the hopper	kg/m^3
ρ_m	Average density of mixture in hopper	kg/m^3
ρ_o	Outgoing mixture density	kg/m^3
ρ_q	Sand quartz density	kg/m^3
ρ_s	Sand bed density in hopper	kg/m^3
ρ_t	Total density of the material in the hopper	kg/m^3
ρ_w	Water density	kg/m^3
ρ_{ms}	Density of mixture soup in hopper	kg/m^3
ρ_{pi}	Density of mixture in pipe	kg/m^3
ρ_{pu}	Density of mixture in pump	kg/m^3
ρ_{si}	In situ density of sand at sea bottom	kg/m^3
τ_i	Fuel rack controller I-gain time constant	s
τ_{cpp}	Ship speed controller I-gain time constant	s
τ_c	Constant tonnage controller I-gain time constant	s
τ_{pl}	Power limitation controller I-gain time constant	s
τ_v	Visor angle controller I-gain time constant	s
υ	List of ship	m
φ	Trim of ship	m
δ	Power correction term in ship speed controller	-
τ	The time delay in samples	-
$\boldsymbol{u}$	Input vector	-
$\boldsymbol{x}$	State vector	-
$\boldsymbol{y}$	Output vector	-
A	Area of hopper	m^2
A_p	Pipe area	m^2
a_d	Coefficient in draught model	m/kg
a_{dh}	Coefficient in drag head density model	s^2kg/m^9
a_p	Coefficient in pipeline hydraulic friction model	kg/m^7
B	Magnetic field strength	T
b_d	Coefficient in draught model	m
b_{dh}	Coefficient in drag head density model	skg/m^4
b_p	Coefficient in pipeline hydraulic friction model	kgm^4/s
C_d	Volumetric concentration in the drag head	-
C_i	Incoming hopper volumetric concentration	-
C_m	Volumetric concentration of mixture in hopper	-

C_{ms}	Volumetric concentration of mixture soup in hopper	-
C_o	Outgoing overflow volumetric concentration	-
C_s	Volumetric sand bed concentration in hopper	-
C_{si}	Volumetric concentration of sand at sea bottom	-
C_t	Transport concentration of mixture in pipeline	-
c_{0n}	Pump coefficient in pump head model	$\mathrm{Pa/rad^2}$
c_{0p}	Pump coefficient in pump power model	$\mathrm{W/rad^3}$
c_{1n}	Pump coefficient in pump head model	$\mathrm{sPa/rad^2/m^3}$
c_{1p}	Pump coefficient in pump power model	$\mathrm{sW/rad^2/m^3}$
c_{2n}	Pump coefficient in pump head model	$\mathrm{s^2Pa/m^6}$
c_{2p}	Pump coefficient in pump power model	$\mathrm{s^2W/rad/m^6}$
c_{3p}	Pump coefficient in pump power model	$\mathrm{s^3W/m^9}$
c_{dh}	Coefficient in drag head density model	$\mathrm{kg/m^3}$
c_{hc}	Horizontal cutting force coefficient, cavitating	-
c_{hn}	Horizontal cutting force coefficient, not cavitating	-
d_m	Grain size diameter	m
d_p	Pipe diameter	m
d_{pi}	Pipe diameter of the inclined pipe	m
e	Volume strain	-
F_{cc}	Cutting force for cavitating regime	N
F_{cn}	Cutting force for non-cavitating regime	N
F_c	Cutting force	N
F_d	Drag friction force	N
F_{th}	Thrust force of the ship's propeller	N
g	Gravitational acceleration	$\mathrm{m/s^2}$
H_c	Control horizon	-
H_p	Prediction horizon	-
h	Height	m
h_c	Cutting height of teeth in soil	m
h_{ci}	Output of the integrator in the constant tonnage controller	m
h_{cmax}	Maximum penetration depth of teeth in soil	m
h_d	Ship's draught	m
h_e	Excavation height	m
h_i	Height of hopper inlet above keel	m
h_m	Height of the mixture layer	m
h_{mi}	Measurement position inlet pressure sensor above pump center	m
h_{mo}	Measurement position outlet pressure sensor above pump center	m
h_o	Height of the overflow in the hopper	m
$h_{o,max}$	Maximum height of the overflow in the hopper	m
$h_{o,min}$	Minimum height of the overflow in the hopper	m
h_{pd}	Height of pump above ship bottom	m
h_{ps}	Height of pump inlet above keel	m
h_s	Height of the sand bed	m
h_{s0}	Initial height of the sand bed	m
h_t	Total height of mixture in hopper	m
h_w	Height of water layer on top of mixture soup	m
h_z	Dredging depth	m

I_d	Total combined inertia in power-train model	kg/m^2
I_f	The frictional head loss of a liquid flow in a unity pipe line length	-
i	Index i	-
J	Objective function	-
j	Index j	-
k	Discrete time step	-
k_1	Constant in total pipeline pressure loss model	s^2Pa/m^6
k_2	Constant in total pipeline pressure loss model	$1/m^2$
k_3	Constant in total pipeline pressure loss model	$1/m^2$
k_{ac}	Anti-windup gain in constant tonnage controller	-
k_{ap}	Anti-windup gain in the power limitation controller	-
k_{av}	Anti-windup gain in the water valve controller	-
k_{aw}	Anti-windup constant in diesel engine 'governor'	-
k_c	Cutting force coefficient non-cavitating cutting	Ns/m^3
k_{ccav}	Cutting force coefficient cavitating cutting	N/m^2
k_{cpp}	Proportional gain in the ship speed controller	-
k_d	Friction coefficient total drag force	Ns/m^2
k_e	Erosion parameter	m^2/s
k_f	Thrust force gain of the propellers	Ns^2/rad^2
k_{fr}	Friction coefficient in power train model	Nm/rad
k_i	Permeability of the in situ material	m/s
k_{ld}	Drag head loss coefficient	s^2mPa/kg
k_m	Effective permeability	m/s
k_{max}	Permeability after cutting	m/s
k_o	Overflow coefficient	$m\sqrt{m}/s$
k_p	Proportional gain in the diesel engine controller	-
k_{pc}	Proportional gain in the constant tonnage controller	-
k_{pow}	Proportional gain in the power limitation controller	-
k_r	P-gain of fuel rack controller	-
k_{sh}	Ships resistance coefficient	Ns/m^2
k_T	Torque gain of the propellers	Nm/rad^2
k_t	Torque gain of diesel engine model	Nm
k_{tr}	Transport coefficient	-
k_v	Proportional gain in the water valve controller	-
k_{ρ_e}	Density decay factor in exponential model	1/m
k_{ρ_l}	Density slope in linear model	kg/m^4
L_d	Distance from the visor rotation point to the teeth connection point	m
L_{ex}	Distance from the visor rotation point to the tips of the teeth	m
L_{pi}	Length of inclined pipe	m
L_{ps}	Suction pipe length	m
L_p	Pipe length	m
L_{sh}	Ship length	m
L_{th}	Length of teeth on drag head	m
m_b	Mass of water in the ballast tanks	kg
m_{b0}	Mass of water in ballast tanks when calibrating	kg
m_o	cumulative mass of overflowing mixture in dry solids	kg
m_s	Mass of sand bed	kg

m_{se}	Mass of empty ship	kg
m_{sh0}	Mass of ship when calibrating	kg
m_{sh}	Total mass of the ship	kg
m_t	Total hopper mass	kg
$m_{t,max}$	Maximum total hopper mass	kg
N	Total number	-
N_b	Number of blades	-
N_p	Gear ratio from the diesel engine to the pump axis	-
N_s	Gear ratio from the diesel engine to the propeller axis	-
P_{cyc}	Production rate for the complete dredging cycle	kg/min
P_d	Excavated production of sand measured in dry solids	kg/min
P_p	Power demand of dredge pump	W
p	Pressure	Pa
p_{atm}	Atmospheric pressure	Pa
p_h	Pressure measurement for draught calculation	Pa
p_i	Absolute inlet pressure	Pa
p_{imin}	Minimum allowed inlet pressure	Pa
P_{in}	Incoming production of sand measured in dry solidse	kg/min
$P_{max,full}$	Maximum available power of diesel engine by full speed	W
$p_{min,s}$	Set-point minimum absolute inlet pressure for water valve controller	Pa
p_{mi}	Pressure measurement inlet pump pressure	Pa
p_{mo}	Pressure measurement outlet pump pressure	Pa
Q_i	Incoming mixture flow-rate in hopper	m^3/s
$Q_{i,max}$	Maximum incoming mixture flow-rate in hopper	m^3/s
$Q_{i,min}$	Minimum incoming mixture flow-rate in hopper	m^3/s
Q_{ms}	Mixture soup flow-rate	m^3/s
Q_o	Outgoing mixture flow-rate of hopper	m^3/s
Q_s	Settling sand flow-rate	m^3/s
Q_w	Water flow rate	m^3/s
Re	Reynolds number of the pipeline flow	-
Re_p	Particle Reynolds number	-
s_0	Horizontal flow velocity above the sand bed	m/s
S_{kt}	Transport factor in Führböter pipeline hydraulic friction model	m/s
T_{auxps}	Torque of port side auxiliaries	Nm
T_{auxsb}	Torque of starboard auxiliaries	Nm
T_d	Torque of diesel engine	Nm
T_{dps}	Torque of port side diesel engine	Nm
TDS	Tons of dry solids	ton
T_{dsb}	Torque of starboard diesel engine	Nm
T_p	Torque of pump shaft	Nm
T_{shp}	Torque of port side propeller shaft	Nm
T_{shs}	Torque of starboard propeller shaft	Nm
T_{sh}	Torque of propeller shaft	Nm
t	Time	s
t_d	Time for dredging	s
t_{dis}	Time for discharging	s
t_s	Sample time	s

t_{sail}	Time for sailing	s
U	Voltage	V
u	Input	-
V	Volume	m^3
V_t	Total hopper volume	m^3
VAF	Variance-accounted-for	-
v	Mixture velocity	m/s
var	Variance	-
v_h	Horizontal mixture velocity in hopper	m/s
v_s	Settling velocity	m/s
v_{s0}	Undisturbed settling velocity	m/s
$v_{sh,s}$	Ships speed set-point for ship speed controller	m/s
v_{shmax}	Maximum allowed ships speed	m/s
v_{shmin}	Minimum allowed ships speed	m/s
v_{sh}	Ships speed	m/s
W_b	Width of cutting tooth on drag head	m
W_d	Width of drag head	m
W_{sh}	Width of hopper	m
x	State	-
Y	Fuel rack of diesel engine fuel pump	-
Y_{ip}	Output of integrator in port side fuel rack controller	-
Y_{is}	Output of integrator in starboard fuel rack controller	-
Y_{lb}	Fuel rack lower bound	-
Y_{max}	Maximum fuel rack when propeller pitch is lowered	-
Y_p	Fuel rack of diesel engine fuel pump	-
Y_s	Fuel rack of diesel engine fuel pump	-
Y_{ub}	Fuel rack upper bound	-
y	Output	-

List of abbreviations

ADWC	Automatic Drag head Winch Control
ALMO	Automatic Light Mixture Overboard
CCMs	Conductivity Concentration Meters
Dynopt	Dynamic optimisation with time discretisation
EMF	Electromagnetic Flow meters
MPC	Model Predictive Control
TDS	Tons of Dry Solids
TSHD	Trailing Suction Hopper Dredger

Bibliography

Abadie, J. and Carpentier, J. (1968). Generalization of the Wolfe Reduced Gradient Method to the case of Nonlinear Constraints, *Optimization* pp. 37–47. 107

Arulampalam, S., Maskell, S., Gordon, N. J. and Clapp, T. (2002). A tutorial on particle filters for on-line nonlinear/non-Gaussian Bayesian tracking, *IEEE Transactions on Signal Processing* **50**: 174–188. 148

Babuška, R., Lendek, Z., Braaksma, J. and de Keizer, C. (2006). Particle filtering for on-line estimation of overflow losses in a hopper dredger, *Proceedings of the 2006 American Control Conference, Minneapolis*, pp. 5751–5756. 62, 148

Bellman, R. E. (1957). *Dynamic Programming*, Princeton University Press. 97

Biegler, L. T. and Grossmann, I. E. (2004). Retrospective on optimization, *Computers & Chemical Engineering* **28**(8): 1169–1192. 103, 105, 106

Bos, W. (1974). *Van Baggerbeugel tot Sleepzuiger*, Van Wijngaarden, Scheepvaartuitgaven, Sliedrecht (Holland). 2

Box, G. E. P. (1957). Evolutionary Operation: A Method for Increasing Industrial Productivity, *Applied Statistics* **6**(2): 81–101. 60

Braaksma, J., Klaassens, J. B., Babuška, R. and de Keizer, C. (2007a). A computationally efficient model for predicting overflow mixture density in a hopper dredger, *Terra et Aqua* **106**: 16–25. 27, 58

Braaksma, J., Klaassens, J. B., Babuška, R. and de Keizer, C. (2007b). Model predictive control for optimizing the overall dredging performance of a trailing suction hopper dredger, *Proceedings of the Eighteenth World Dredging Congress (WODCON XVIII)*, pp. 1263–1274. 97

Braaksma, J., Osnabrugge, J., Babuška, R., de Keizer, C. and Klaassens, J. B. (2007). Artificial intelligence on board of dredgers for optimal land reclamation, *CEDA Dredging Days 2007*, pp. 1–14. 48, 97

Brooke, A., Kendrick, D., Meeraus, A. and Raman, R. (1998). *GAMS-A User's Guide*, www.gams.com. 107

Camp, T. R. (1946). Sedimentation and the design of settling tanks, *Trans. ASCE* pp. 895–936. 27, 31, 173

Canon, M. D. and Eaton, J. H. (1966). A new algorithm for a class of quadratic programming problems with application to control, *SIAM Journal on Control* **4**(1): 34–45. 97

Churchill, S. W. (1977). Friction-factor equation spans all fluid-flow regimes, *Chemical Engineering* **84**(24): 91–92. 175

Corless, R. M., Gonnet, G. H., Hare, D. E. G., Jeffrey, D. J. and Knuth, D. E. (1996). On the Lambert W function, *Advances in Computational Mathematics* **5**: 329–359. 36

Davidon, W. C. (1991). Variable metric method for minimization, *SIAM Journal on Optimization* **1**(1): 1–17. 60

de Bree, S. E. M. (1977). Centrifugal dredgepumps, *Ports and Dredging* . 2, 27, 45

de Jong, R., van Gelderen, P., Lindo, M. and Fernandez, J. (2005). Dubai's extreme reclamations, *CEDA Dredging Days*. 1

de Koning, J. (1978). Denken met de handen, Intreerede T.H. Delft. 2

Drud, A. (1985). CONOPT: A GRG code for large sparse dynamic nonlinear optimization problems., *Mathematical Programming* **31**(2): 153–191. 107

Durand, R. and Condolios, E. (1952). Transport hydraulique et decantation des materiaux solides, *Deuxiemes Journees de l'Hydraulique* pp. 27–55. 45, 163, 166

Franzini, J. B. (1997). *Fluid Mechanics with Engineering Applications*, The McGraw-Hill Companies, Inc. 33

Fürböter, A. (1961). Über die Förderung von Sand-Wasser-Germischen in Rohrleitungen, *Mitteilungen des Franzius-Instituts* **19**. 45, 163, 166

Grossmann, I. E. and Biegler, L. T. (2004). Part ii. future perspective on optimization, *Computers & Chemical Engineering* **28**(8): 1193–1218. 105

Hahlbrock, U. and Freese, I. (1998). Hopper load measurement; some recent experiences with a remote-operated data acquisition and analysing system, *Terra et Aqua* **72**: 18–26. 6

Hooke, R. and Jeeves, T. A. (1961). "direct search" solution of numerical and statistical problems, *Journal of the Association for Computer Machinery* **8**: 212–229. 60

IHC Holland (1991). Optimal loading of trailing dredgers, *Ports and Dredging* **137**. 5, 6, 25

Ikeda, T., Kato, H., Tomoi, T., Yano, S. and Nakamura, Y. (1995). Artificial intelligence for dredging control of the trailing suction hopper dredger, *Dredging benefits; proceedings of the 14th World Dredging Congress (WODCON XIV). Vol. 1*, pp. 203–217. 6

Izadi-Zamanabadi, R. and Blanke, M. (1999). A ship propulsion system as a benchmark for fault-tolerant control, *Control Engineering Practice* **7**(2): 227–239. 52, 53

Joseph, B. and Hanratty, F. W. (1993). Predictive control of quality in a batch manufacturing process using artificial neural network models, *Industrial & Engineering Chemistry Research* **32**: 1951 – 1961. 109

Jufin, A. P. and Lopatin, N. A. (1966). O projekte TUiN na gidrotransport zernistych materialov po stalnym truboprovodam, *Gidrotechniceskoe Strojitelstvo* pp. 49–52. 45, 163, 166

Knust, J. (1973). Analogous computers to optimize hopper fillings in hopper suction dredgers, *Proceedings of WODCON V World Dredging Conference*. 5

Kurita, I., Okayama, Y., Tomoi, T. and Nakamura, Y. (1992). Automatic operation system for drag suction hopper dredger, *13th World Dredging Congress*. 6

Lay, D. C. (1997). *Linear Algebra and its Applications*, Addison-Wesley. 61

Lewis, R. M. and Torczon, V. (1999). Pattern search algorithms for bound constrained minimization, *SIAM Journal on Optimization* **9**(4): 1082–1099. 60

Liotta, V., Georgakisa, C. and El-Aasser, M. S. (1997). Real-time estimation and control of particle size in semi-batchemulsion polymerization, *Proceedings of the American Control Conference*. 109

Liu, J. and West, M. (2001). *In Sequential Monte Carlo Methods in Practice*, New York: Springer. 148

Ljung, L. (1987). *System identification - theory for the user*, Prentice Hall, inc. 41

Maciejowski, J. M. (2002). *Predictive Control with Constraints*, Pearson Education. 108

Maertens, K., Babuška, R. and Baerdemaeker, J. D. (2005). Evolutionary input selection for the non-linear identification of complex processes, *Computers and Electronics in Agriculture* **49**(3): 441–451. 41, 169, 170

Matoušek, V. (1997). *Flow Mechanism of Sand-Water Mixtures in Pipelines*, PhD thesis, TU Delft. 2, 27, 28, 45, 172

Matoušek, V. (2001). *Lecture Notes: Hydraulic Transport as one of the Dredging Processes*, TU Delft. 48, 163, 164

Miedema, S. A. (1987). *Calculation of the Cutting Forces when Cutting Water Saturated Sand*, PhD thesis, TU Delft. 2, 3, 27, 28, 39, 42, 43, 173, 174

Miedema, S. A. (1994). On the snow-plough effect when cutting water saturated sand with inclined straight blades, *ASCE Proc. Dredging 94*, Orlando, Florida. 39

Miedema, S. A. (1995). Production estimation based on cutting theories for cutting water saturated sand, *Proc. WODCON XIV*, Amsterdam, The Netherlands. 41, 174

Miedema, S. A. (1996). Modeling and simulation of the dynamic behavior of a pump/pipeline system, *17th Annual Meeting & Technical Conference of the Western Dredging Association*. 45, 48

Miedema, S. A. (2002). The dynamic behavior of a diesel engine, *Proc. WEDA XXII Technical Conference & 34th Texas A&M Dredging Seminar, June 12-15, Denver, Colorado, USA*. 175

Morita, H., Nakamura, H. and Shimazaki, M. (2002). Control of large dredger with oil recovery equipment, *IHI Engineering Review* **35**(2): 53–58. 6

Ooijens, S. C. (1999). Adding dynamics to the camp model for the calculation of overflow losses, *Terra et Aqua* **76**: 12–21. 31, 37

Ooijens, S. C., de Gruijter, A., Nieuwenhuijzen, A. A. H. and Vandycke, S. (2001). Research on hopper settlement using large-scale modelling, *Proceedings of the CEDA Dredging days 2001*, pp. 1–11. 16, 17

Pontryagin, L. S., Boltyanskii, V. G., Gamkrelidze, R. V. and Mishchenko, E. F. (1962). *The mathematical theory of optimal processes*, New York, Interscience Publishers. 97

Richardson, J. F. and Zaki, W. N. (1954). Sedimentation and fluidisation: Part I, *Transactions of the Institution of Chemical Engineers* **32**: 35–53. 32, 124, 172, 173

Rowe, P. N. (1987). A convenient empirical equation of the richardson-zaki exponent, *Chemical Engineering Science* **42**(11): 2796–2796. 173

Sjoberg, J., Zhang, Q., Ljung, L., Benveniste, A., Delyon, B., Glorennec, P. Y., Hjalmarsson, H. and Juditsky, A. (1995). Nonlinear black-box modeling in system identification: a unified overview, *Automatica* **31**(12): 1691–1724. 41

Slotta, L. S. and Heydarpour, J. (1989). Computer simulation of draghead excavation, *World Dredging Congress*, pp. 454–462. 41

Sørensen, A. J. and Ådnanes, A. K. (1997). High performance thrust allocation scheme in positioning of ships based on power and torque control, *Dynamic Positioning Conference*, pp. 1–17. 55

Spendley, W., Hext, G. R. and Himsworth, F. R. (1962). Sequential Application of Simplex Designs in Optimisation and Evolutionary Operation, *Technometrics* **4**(4): 441–461. 60

Tabak, D. and Kuo, B. C. (1969). Application of mathematical programming in the design of optimal control systems, *International Journal of Control* **10**(5): 546–552. 97

Thomas, M. M., Kardos, J. L. and Joseph, B. (1994). Shrinking horizon model predictive control applied to autoclave curing of composite laminate materials, *Proceedings of the American Control Conference*. 109

van Groesen, E. W. C. and Molenaar, J. (2007). *Continuum Modeling in the Physical Sciences*, SIAM publishers. 32

van Rhee, C. (2002). *On the sedimentation process in a Trailing Suction Hopper Dredger*, PhD thesis, TU Delft. 2, 27, 28, 31, 33, 37, 39, 172

Vandewalle, J. and Suykens, J. A. K. (1998). *Nonlinear Modeling: Advanced Black-Box Techniques*, Kluwer Academic Publishers. 41

Vandycke, S., Van den Broeck, M. and Thomas, K. (2005). The DRACULA-system pushes the limits of hopper dredgers in cemented sand, *CEDA Dredging Days*. 3

Vercruijsse, P. M., Versteeg, G. J. P., Ooijens, S. C., Hofstra, C. F., Lin, F. and Kramers, C. H. M. (2005). Wild dragon developing a draghead for dredging extreme fine, hard packed aquatic soils, *CEDA Dredging Days*. 3

Verruijt, A. (2001). *Soil Mechanics*, TU Delft. 174

Vlasblom, W. J. (2003). *Lecture notes, Designing Dredging Equipment, WB3408*, TU Delft. 2

Vlasblom, W. J. and Miedema, S. A. (1995). A theory for determining sedimentation and overflow losses in hoppers, *Proc. of the 14th World Dredging Congress, Amsterdam*, pp. 183–202. 28, 173

Wangli, D. (2006). *Intelligent data analysis and control of a hopper dredger*, Master's thesis, Delft University of Technology. 42, 79, 169

Wangli, D., Braaksma, J., Klaassens, J. B., Babuška, R. and de Keizer, C. (2007). Evaluation of dredging performance in a trailing suction hopper dredger, *Proceedings of the Eighteenth World Dredging Congress (WODCON XVIII)*, pp. 1275–1284. 169

Wilson, K. C. (1976). A unified physically-based analysis of solid-liquid pipeline flow, *Proceedings Hydrotransport 4*, BHRA, Cranfield, UK, pp. 1–12. 166

Wilson, K. C. (1992). Influence of particle properties on solids effect, *Proceedings 10. Int. Kol. Massenguttransport durch Rohrleitungen*, Univ. GH Paderborn, Meschede, Germany. 45

Worster, R. C. and Denny, D. F. (1955). Hydraulic transport of solids materials in pipelines, *Proceedings of Institute of Mechanical Engineering*. 49, 166

Wright, M. H. (1996). *Numerical Analysis 1995*, Addison Wesley Longman Limited, chapter Direct search methods: Once scorned, now respectable, pp. 191–208. 59

Yagi, T. (1970). Sedimentation effects of soil in hopper, *Proceedings of WODCON III World Dredging Conference*. 31

Yagi, T. and Okayama, Y. (1975). Dredging effects of water-jet and teeth with the drag head, *First International Symposium on Dredging Technology*, pp. F4–39–F4–50. 41

Young, P. (1984). *Recursive Estimation and Time-Series Analysis*, Springer-Verlag. 62

Curriculum Vitae

Jelmer Braaksma was born in Harlingen, the Netherlands, in 1979. He finished his secondary school (Atheneum) in 1997 at the RSG Simon Vestdijk in Harlingen. In 1997 he started with his study Electrical Engineering at the Delft University of Technology. From 2002 until 2003, Jelmer Braaksma fulfilled the position of chair in the board of the student society 'Verstelregel'. He graduated in June 2003 with a major in control system engineering with the M.Sc. thesis entitled 'A manipulator for a shield tunnelling machine'. The subject of his master thesis project was the modelling and control of an industrial robot for a shield tunnelling machine. From July 2003, Jelmer Braaksma has been working on his Ph.D. project at the Delft Center for Systems and Control of the Delft University of Technology. He did his Ph.D research on model-based optimisation of hopper dredgers. This research was in close cooperation with IHC Systems B.V., Sliedrecht. Since September 2007, Jelmer Braaksma is employed at IHC Systems B.V., where he continues the research on model-based optimisation of hopper dredgers. The goal of this research is to implement the techniques which have been derived during his Ph.D. research in practice.